# Development of hard/soft magnetic composite ferrite for microwave application

**A**

**Thesis**

**Submitted for the partial fulfilment**

**of the requirements for the award of degree of**

## Doctor of Philosophy

**By**

**Chhavi Pahwa**

**(Registration No. 901412016)**

**Under the supervision of**

**Dr. Puneet Sharma**
**(Professor)**

THAPAR INSTITUTE
OF ENGINEERING & TECHNOLOGY
(Deemed to be University)

**School of Physics & Materials Science**
**Thapar Institute of Engineering & Technology,**
**Patiala -147004 (Punjab), India**
***(Deemed to be University)***

**(December-2020)**

**Contents**

Dedicated to my Parents

# CERTIFICATE

This is to certify that the thesis entitled **"Development of hard/soft magnetic composite ferrite for microwave application"** which is being submitted by Chhavi Pahwa in the fulfilment of the requirement for the award of the degree Doctor of Philosophy in the School of Physics & Materials Science, Thapar Institute of Engineering & Technology (TIET), is an authentic record of candidate's own work carried out by her under my supervision and guidance. The matter presented in this thesis has not been submitted in part or full for the award of any degree in any other University or Institute.

Date:

Place: Patiala


**Dr. Puneet Sharma**
(Professor)
School of Physics & Materials Science
Thapar Institute of Engineering & Technology
(TIET), Patiala (147004) Punjab.

# Acknowledgement

"We must find time to stop and thank the people who make a difference in our lives".

In my journey towards this degree; I have found a teacher, an inspiration and a pillar of support in my supervisor (the person I admire a most), **Dr. Puneet Sharma**, Professor, Thapar Institute of Engineering & Technology (TIET) Patiala, Punjab. I would like to express my deep and sincere gratitude for giving me opportunity to carry out the research work under his supervision. He has been there providing his heartfelt support, invaluable guidance, inspiration, constant encouragement and valuable suggestion throughout the journey without whom the work would not have been crowned with success. Without his able guidance, this thesis would not be possible and I shall be eternally grateful to him for his assistance.

I offer my special thanks to **Dr. O. P. Pandey**, Head, School of Physics & Materials Science, Thapar Institute of Engineering & Technology (TIET), Patiala, for providing all the necessary facilities in the department. I extend my gratitude to my doctoral committee members and all faculty members of the SPMS who supported and encouraged me especially, **Dr. B.N Chudasama** and **Dr. Chandini Khurana.**

I am thankful to my labmates **Santhoshkumar Mahadevan**, **Anoop Pratap Singh, Shivani Jindal** and **Parminder Singh.** My special thank to **Santhoshkumar Mahadevan** for his kind support in experimental activities during my research.

I would like to thank SAI Lab, Thapar Institute of Engineering & Technology for SEM and XRD facility.

I am grateful to all non-teaching staff of School of Physics and Materials Science who never turn me down whenever I approached for any help.

I gratefully acknowledge the Council of Scientific and Industrial Research (CSIR)( grant no. 03(1449)/18/EMR-II and SRF 09/677(0032)/2018-EMR-I.) for the financial support in the form of Senior Research Fellow.

I gratefully acknowledge DST-FIST for providing magnetic measurement facility.

I would like to convey my sincere gratitude to my friends **Ishita Sharma, Mir Rameez Ahmed and Piyush Sharma** for creating cheerful atmosphere during my stay. Special thank to my friend, **Chetan Sharma** for kind and moral support he provided me during the stay. He always supported and courage me in my bad time. I express my deep gratitude to **Shivani Jindal** for the joyful company during my work.

Most of all, I would like to thank my parents my power booster; for their love, moral support and inconvenience experienced by them during my study. Words fail to express my gratitude from the depth of my heart for my loving brother and loving sister and all other family members who provided me relentless encouragement, prayers, pure love, an unmatched affection that made this work to reach its destination. Special thank to my brother **Alok Pahwa** and Sister **Aditi** who have always been a source of incessant support.

And above all, I pay my profound gratitude to The Almighty GOD for giving me strength, love and blessings.


**Chhavi Pahwa**

## List of Publications

1. **Chhavi Pahwa**, Sukhleen Bindra Narang, Puneet Sharma, "Composition dependent magnetic and microwave properties of exchange-coupled hard/soft nanocomposite ferrite", Journal of Alloys and Compounds 815 (2020) 152391-152397.

2. **Chhavi Pahwa**, Sukhleen Bindra Narang, Puneet Sharma, "Interfacial exchange coupling driven magnetic and microwave properties of $BaFe_{12}O_{19}/Ni_{0.5}Zn_{0.5}Fe_2O_4$ nanocomposites", Journal of Magnetism and Magnetic Materials 484 (2019) 61–66.

3. **Chhavi Pahwa**, Santhoshkumar Mahadevan, Sukhleen Bindra Narang, Puneet Sharma, "Structural magnetic and microwave properties of exchange coupled and non-exchange coupled $BaFe_{12}O_{19}/NiFe_2O_4$ nanocomposites", Journal of Alloys and Compounds 725 (2017) 1175-1181.

4. **Chhavi Pahwa**, Santhoshkumar Mahadevan, Sukhleen Bindra Narang, Puneet Sharma**,** "Studies on exchange-coupled magnetodielectric ceramics for microwave application in $K_u$-band"(IEEE Transactions on magnetic) (Revision Submitted).

## Other publications

1. Santhoshkumar Mahadevan, **Chhavi Pahwa**, Sukhleen Bindra Narang, Puneet Sharma, "Structural, dielectric and magnetic properties of $BaFe_{12-x}Al_xO_{19}$ hexaferrite thick films", Journal of Magnetism and Magnetic Materials 441 (2017) 465–474.

2. Samiksha Verma, Santhoshkumar Mahadevan, **Chhavi Pahwa**, Sukhleen Bindra Narang, Puneet Sharma, "Improved magnetic and microwave properties of La-substituted barium hexaferrite screen printed thick films", Journal of Superconductivity and Novel magnetism 33 (2020) 2507-2512.

# List of conferences and workshop

1. **Chhavi Pahwa**, Puneet Sharma, "Effect of processing method on exchange coupling and magnetic properties of hard ($BaFe_{12}O_{19}$)/ soft ($Ni_{0.5}Zn_{0.5}Fe_2O_4$) nanocomposite ferrites", 1st National Conference on Innovations in Applied Science and Engineering **(NCIASE-2019)** April 27-28, 2019.

2. **Chhavi Pahwa**, Puneet Sharma, "Composition dependent tunable magnetic properties of exchange coupled $BaFe_{12}O_{19}/CoFe_2O_4$ nanocomposites" International Conference on Magnetism and Magnetic Materials **(ICMAGMA- 2018)** December 09-13, 2018.

3. **Chhavi Pahwa**, Puneet Sharma, "Effect of calcination temperature on the exchange coupling of hard ($BaFe_{12}O_{19}$)/ soft ($Ni_{0.5}Zn_{0.5}Fe_2O_4$) nanocomposite ferrites", International Conference on Nanomaterials: Synthesis, Characterization and Applications **(ICN -2018)** May 11-13, 2018.

4. **Chhavi Pahwa**, Puneet Sharma, "Studies of exchange spring behavior of hard/soft ferrite nanocomposite prepared by different processing methods" International Conference on Magnetism and Magnetic Materials **(ICMAGMA- 2017)** February 01-03, 2017.

5. National Workshop on Advanced Techniques for surface characterization, Thapar University, Oct 28-30, 2015.

6. Summer School on Magnetism **(SSM-2016)** July 11-15, 2016, Thapar University, Patiala.

# List of Figures

# List of Tables

# List of Symbols

| | |
|---|---|
| $M_s$ | Saturation magnetization |
| $M$ | Magnetization |
| $H_c$ | Coercivity |
| $M_r$ | Remanent magnetization |
| $H_A$ | Magnetocrystalline anisotropy |
| $H_N$ | Nucleation field |
| $\Delta H$ | FMR linewidth |
| $T_c$ | Curie Temperature |
| $f_r$ | FMR frequency |
| $C.S$ | Crystallite size |
| $\mathcal{E}$ | Permittivity |
| $\mu$ | Permeability |
| $\tan \delta_\mu$ | Magnetic loss tangent |
| **Z** | Impedance |
| **RL** | Reflection loss |
| **T** | Tesla |
| **Oe** | Oerested |

# Abbreviations used

| | |
|---|---|
| BaM | Barium Hexaferrite($BaFe_{12}O_{19}$) |
| NiF | Nickel Ferrite($NiFe_2O_4$) |
| NZFO | Nickel Zinc Ferrite($Ni_{0.5}Zn_{0.5}Fe_2O_4$) |
| CFO | Cobalt Ferrite($CoFe_2O_4$) |
| CZFO | Cobalt Zinc Ferrite($Co_{0.5}Zn_{0.5}Fe_2O_4$) |
| FMR | Ferromagnetic resonance |
| EM | Electromagnetic |
| *M-H* | Magnetic hysteresis loop |
| *M-T* | Magnetization *vs*. Temperature |
| *RT* | Room temperature |
| *dM/dH* | Switching field distribution |
| XRD | X-ray diffraction |
| PM | Physical mixing |
| SS | Single step |
| SEM | Scanning Electron Microscopy |
| TEM | Transmission Electron Microscopy |
| VSM | Vibrating Sample Magnetometer |
| VNA | Vector Network Analyzer |
| $K_u$-band | 12.4-18 GHz |
| nm | Nanometre |
| GHz | Gigahertz |
| dB | Decibel |

# Preface

Exchange coupling between hard and soft magnetic phases at nanometric scale has gained considerable attention due to associated intriguing physics in the system and their application in high energy product magnets. Recently, such exchange-coupled hard/soft ferrite nanocomposite has gained attention in microwave device applications due to large composition flexibility and wide variation in magnetic properties. Therefore, the main focus of this work is systematically investigates the processing and properties of various hard/soft exchange-coupled ferrite composite. In the present work, various series of exchange-coupled nanocomposites of $BaFe_{12}O_{19}/AFe_2O_4$, (A = Ni, Zn, Co) were prepared by sol-gel autocombustion method. The effect of various process parameters; processing methodology, annealing temperature, soft phase magnetization and weight fraction of soft phase on structural, magnetic and microwave properties has been investigated and compared. The carried out work is organized into five chapters. The content of each chapter is given below.

**Chapter 1 (Introduction):** This chapter gives general introduction of exchange coupling and exchange-spring mechanism. The classification of different exchange-coupled system with reference to rare earth based, ferrites based and other composites are shown. A brief description of hexagonal and spinel ferrites are given and their respective magnetic and microwave properties are compared. Important applications of exchange-coupled composites are mentioned. The chapter is concluded with motivation and objectives of the present work.

**Chapter 2 (Literature review):** In this chapter a brief preamble related to origin of exchange coupling, its development and various experimental and theoretical studies carried out on different nanocomposite systems are reviewed. The review is divided into rare earth alloys and ferrites based composites in bulk and thin films form. Effect of various processing methods and conditions on exchange coupling between hard and soft phase has been discussed. The emphasis are given to magnetic and microwave properties of hexagonal/spinels ferrite nanocomposites. A few other exchange-coupled systems are also mentioned in the end of the chapter.

**Chapter 3 (Experimental procedure & characterization techniques):** In this chapter, details of processing method adopted for hard magnetic hexagonal ferrite ($BaFe_{12}O_{19}$), soft magnetic spinels ($NiFe_2O_4$, $Ni_{0.5}Zn_{0.5}Fe_2O_4$, $CoFe_2O_4$, $Co_{0.5}Zn_{0.5}Fe_2O_4$) and their composites are explained. A brief description of thin film deposition technique by RF-sputtering is given. Various techniques, such as X-ray diffraction (XRD), scanning electron microscopy (SEM), transmission electron microscopy (TEM), vibrating sample magnetometer (VSM) and vector network analyzer (VNA) used to examine the structural, magnetic and microwave characterization, are briefly explained.

**Chapter 4 (Results and discussions):** In this chapter, the structural, magnetic and microwave properties of hard/soft magnetic exchange-coupled composites are presented. The results are divided in five sections. In the first section, optimal conditions for preparation of pure hard and soft magnetic ferrites are discussed. Second section describes the effect of different processing methodology i.e. physical mixing and single-step method on exchange coupling. The variation in exchange coupling with annealing temperature is discussed in third section. In fourth subsection effect of weight fraction of soft phase on magnetic and microwave properties of composites are discussed. In fifth section effect of soft phase magnetization on exchange coupling and their respective change in magnetic and microwave properties are given. In the last, exchange coupling also shown in bilayer.

**Chapter 5 (Conclusions):** This chapter summarizes the outcomes of the various experiments described in the previous chapter. The effect of various process parameters on exchange coupling is outlined. The influence of weight fraction and magnetization of soft phase on magnetic and microwave properties are discussed and tabulated. The exchange coupling exist in bilayer $NiFe_2O_4/BaFe_{12}O_{19}$ thin film is also showcased. Future scope of the work is presented at the end of this chapter.

# *Chapter 1*

# Introduction

**Overview**

This chapter gives general introduction of exchange coupling and exchange-spring mechanism. The classification of different exchange-coupled system with reference to rare earth based, ferrites based and other composites are shown. A brief description of hexagonal and spinel ferrites are given and their respective magnetic and microwave properties are compared. Important applications of exchange-coupled composites are mentioned. The chapter is concluded with motivation and objectives of the present work.

## 1. Introduction

Interfacial exchange coupling between hard and soft magnetic phases at nano-metric scale has gained considerable attention due to associated intriguing physics in the system and their application in high energy product ($(BH)_{max}$) magnets. In 1989 Coehoorn [1] reported the first experimental evidence of exchange interaction between the phases in melt spun rapidly quenched NdFeB-$Fe_3B$ flakes. In early 1990s, Kneller and Hawing [2] first proposed the concept of exchange-spring magnets in suitably dispersed hard and soft magnetic materials. Later in 1993, Skomski and Coey [3,4] interpreted interfacial interaction with different analytical expressions and micromagnetic modelling. Over a decade (1990-2000), interfacial coupling were largely investigated for rare earth based nanocomposite magnets and thin films such as SmCo/Co, SmCo/Fe, Fe/Nd-Fe-B, and FeNi/FePt [5–8] etc. The exchange mechanism in composites was largely explained for granular, bilayer/multilayer thin films, where spin switching behavior with different soft magnetic film thickness was the primary consideration. In late 1990s, Skomski and others groups [9,10] experimentally verified that exchange-coupled magnets posses high coercivity($H_c$) and $(BH)_{max}$. They have calculated effective anisotropy ($K_{eff}$), remanence ($M_r$) and nucleation field ($H_N$) using following equations:

$$K_{eff} = \int \Psi^*(r) K_1(r) \Psi(r) dr = \langle K_1(r) \rangle = f_s K_S + f_h K_h \quad (1.1)$$

$$M_r = f_s M_S + f_h M_h \quad (1.2)$$

$$\mu_0 H_N = 2 \frac{f_s K_S + f_h K_h}{f_s M_S + f_h M_h} \quad (1.3)$$

where, ψ is eigen value calculated using 3-D potential wall model for particular thickness. *f*, *M*, and *K* are volume fraction, magnetization and magnetic anisotropy respectively. The subscripts *s* and *h* corresponds to soft and hard magnetic phases.

Using equation 1.2 and 1.3, expression for $(BH)_{max}$ was obtained as:

$$(BH)_{max} = \frac{1}{4}\mu_0 M_s^2 \left[1 - \frac{\mu_0 (M_s - M_h) M_s}{2K_h}\right] \quad (1.4)$$

It is clear from the equations that $(BH)_{max}$ significantly depends upon $M_s$ of soft phase.
In early 2000, it was observed that exchange coupling is not limited to rare earth based composite magnets but ferrite based composites also exhibit similar phenomenon. Table

1.1 shows the general classification of exchange-coupled magnets based on respective hard and soft magnetic phases.

Table 1.1 General classification of exchange-coupled system.

| Type | Composites |
|---|---|
| Rare-earth based composite systems | $Nd_2Fe_{14}B/\alpha$-Fe, $Nd_2Fe_{14}B/Fe_3B$, $Sm_2Fe_{17}N_3/Fe_{16}Co_{35}$, $Y_2Fe_{14}B/Fe_3B$, $SmCo_5/Fe$, SmCo/Co, SmCo/Fe, $Sm_2Co_7/Co$, $Sm_{22}Co_{78}/Fe/Sm_{22}Co_{78}$ |
| Ferrite based composite systems | $SrFe_{12}O_{19}/AFe_2O_4$, , $BaFe_{12}O_{19}/AFe_2O_4$, $BaFe_{12}O_{19}/Y_3Fe_5O_{12}$ $Ba_ySr_{1-y}Fe_{12}O_{19}$/ $Ni_{0.7}Co_{0.9}(MnZr)_xFe_{2-2x}O_4$, $BaCa_2Fe_{16}O_{27}$/ $Fe_3O_4$, $BaFe_{12}O_{19}/Fe_3O_4$, $CoFe_2O_4/Fe_3O_4$ $MnFe_2O_4/CoFe_2O_4$, $CoFe_2O_4/ZnFe_2O_4$, $SrFe_{12}O_{19}/Fe_2O_3$,$SrFe_{12}O_{19}$/FeCo, $CoFe_2O_4$/FeCo,$CoFe_2O_4/CoFe_2$, ferrite/$Sm_2Fe_{17}N_3$ (A: Mn, Zn, Ni, Co) |
| Other composite systems | $FePt/Fe_3Pt$, Fe/FePt, $Fe_{55}Pt_{45}/Fe_{49}Rh_{51}$, FePt/FeNi, FeRh/FePt, $DyFe_2/YFe_2$, MnGa(Bi)/FeCo, PrFeB/NdFeB and $Co_3C$-$Co_{0.35}Fe_{0.65}$ |

## 1.1 Exchange-spring mechanism

The exchange-spring phenomenon is considered as interaction of soft and hard magnetic spins at the interface. These interactions can be understand by demagnetization curves, and explained considering two types of spin reversal mechanism by V. M Chakka *et al.* [11]. If soft and hard magnetic spins coherently switches with reverse magnetic field and shows smooth hysteresis loop, referred as type-1 reversal mechanism. However, in type-2 soft and hard magnetic spins switch individually and results a kinked demagnetization curve. The schematic of type-1 and type-2 reversal mechanism are shown in Fig. 1.1. The existence of coherent and non-coherent demagnetization behaviors are the interplay of three types of spin interactions i.e. between soft-soft, hard-hard and hard-soft spin interactions. In type-1 reversal mechanism; hard-soft spin interactions are most dominant and results a coherent rotation of spins. However, in type-2, swift demagnetization of uncoupled soft magnetic spins at lower field provides a kink in demagnetization curve.

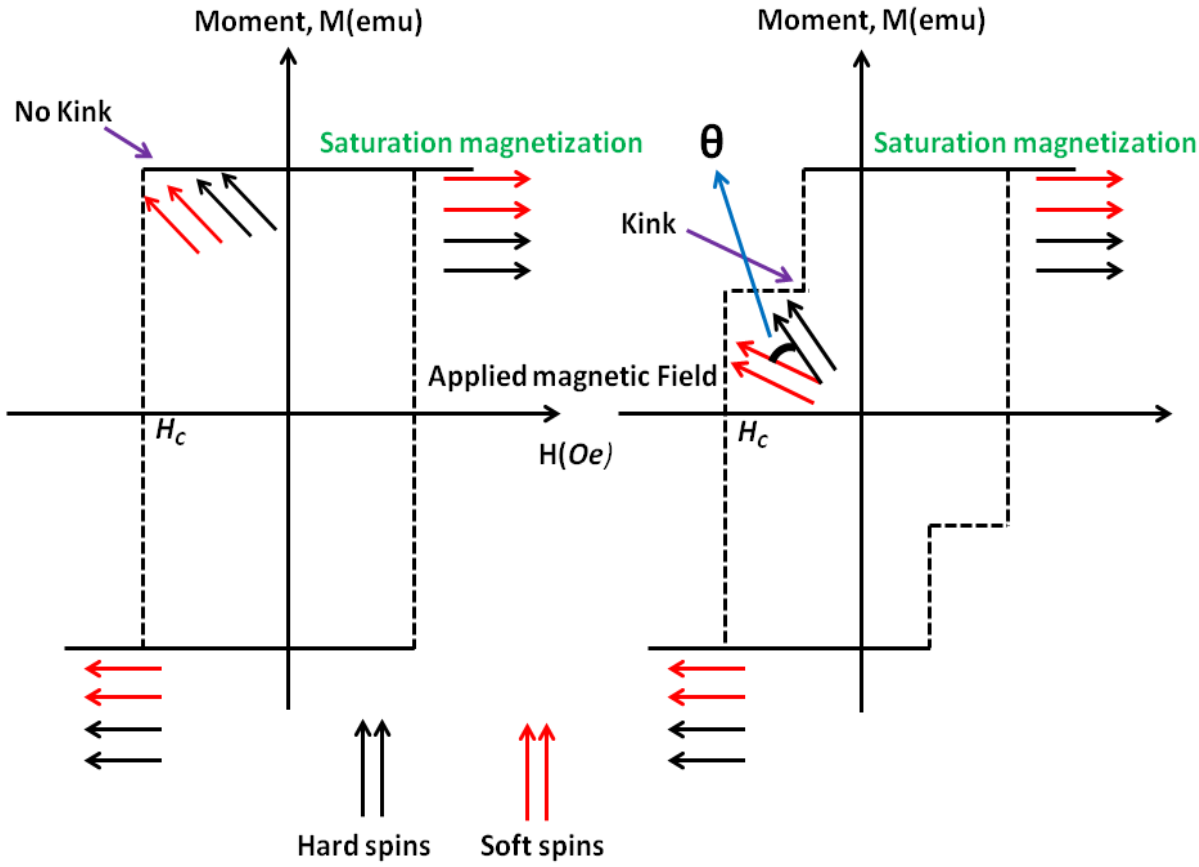


Fig. 1.1 Representative hysteresis (*M-H*) loops (a) Type-1 coherent rotation and (b) Type-2 non-coherent rotation.

Such kind of spin reversal mechanism was also explained by S.D. Bader *et al.* [12,13] for SmCo/Fe system using spin interaction model for hard and soft magnetic spins. As exchange coupling is interfacial in nature, hence maximum at the interface and gradually decrease with distance away from the interface. The distance up to which exchange coupling dominates is called as exchange length. With the applied field, soft magnetic spins far from interface are uncoupled and flip independently in the direction of magnetic field. However, spins which are coupled across the interface switch coherently, whereas distant spins causes non-coherent reversal. In another way, the angular difference between hard and soft magnetic spins increases from 0° (at interface) to 180° with field which causes a spring type spin structure (Fig. 1.2).

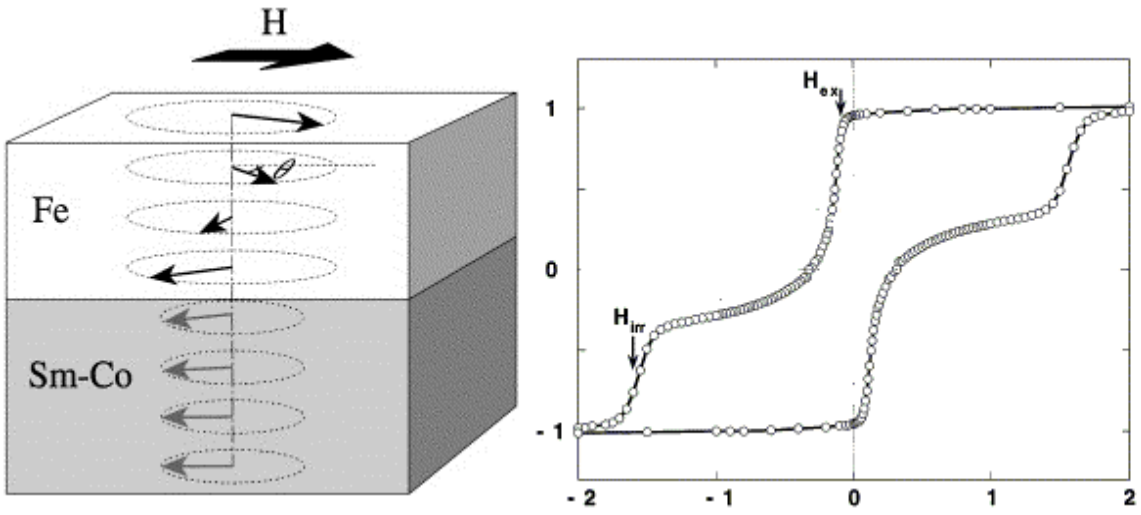


Fig. 1.2 Schematic of hard-soft spin interaction in SmCo/Fe system [12].

Since interfacial exchange coupling is not an intrinsic property, therefore being a structure sensitive property it can be controlled by effective particle size, film thickness, relative weight fraction of magnetic phases, and their distribution. In a system, coherent and non-coherent demagnetization can be obtained subjected to size of the phases. Hysteresis loop of nanocomposite with particle size/film thickness below the exchange length will show a smooth demagnetization while higher result in kinked or shouldered one.

In 1990-2000, studies were mainly focused on rare earth based composite magnets, thin films and nanopowders as they provide high $(BH)_{max}$ and gives broad pathway for permanent magnets. In late 2000, exchange-coupled hard/soft ferrite nanocomposite has gained attention in permanent magnet and microwave device application due to their chemical stability and magnetodielectric properties in microwave region. In last few years, tremendous work has been done to investigate the magnetic behavior of such exchange-coupled ferrites adopting different processing methodologies. However, role of exchange coupling in the view of its magnetic and microwave properties needs an attention.

### 1.2 Exchange-coupled ferrite composite as a new microwave material

Magnetic ferrites includes hexagonal, spinel and garnet were extensively studied for microwave frequency applications due to their inherited magnetic, dielectric and

microwave properties [14–16]. General classification of commonly used ferrites is given in Table 1.2.

Table 1.2 Classification of ferrites.

| Structure | Type | General formula | Examples |
|---|---|---|---|
| Cubic | Spinel | $AFe_2O_4$ | A = Mn, Zn, Ni, Mg, Co |
| | Garnet | $Ln_3Fe_5O_{12}$ | Ln = Y, Sm, Eu, Gd, Tb, Dy, Ho, Er, Tm |
| Hexagonal | M-type | $MFe_{12}O_{19}$ | M= Ba, Sr<br>Me=$Fe^{+2}$, $Ni^{+2}$, $Mn^{+2}$ |
| | X type | $M_4Me_2Fe_{36}O_{60}$ | |
| | W-type | $MMe_2Fe_{16}O_{27}$ | |
| | Y-Type | $M_2Me_2Fe_{12}O_{22}$ | |
| | Z type | $M_3Me_2Fe_{24}O_{41}$ | |

Ferrites are known to mankind since many centuries, but their application as microwave material comes into existence in late 1930s. The ferrite were first systematically studied by Snoek *et al.* [17,18] for application in devices that send, receive and manipulate electromagnetic signal at radio frequency, microwave and millimetre wave frequencies. Till 1990's ferrites were used as permanent magnets only and later their microwave absorbing character were explained [19,20].

Spinel and garnets have been investigated for decades due to their useful electromagnetic properties and their very high specific resistance ( $10^8$ -$10^{10}$ ohm-meter) makes them suitable for microwave frequency applications [15,21,22]. However, their cubic spinel structure (Fig. 1.3); in which divalent metal ions occupy tetravalent sites and trivalent metal ions distributed over octahedral and tetrahedral sites leads to small magnetocrystalline anisotropy. Resultant low $H_A$ restricts their operational frequency below 3 GHz [15,23]. However, operational frequencies can further be increased to X-band with external biased field with an implication of large device size.

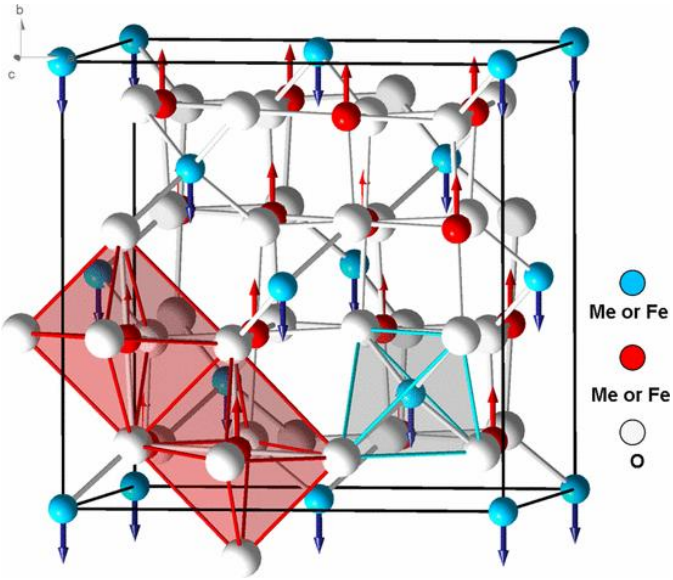


Fig. 1.3 Unit cell of spinel ferrite (adapted from [14]).

On the other hand, crystal symmetry of hexaferrites leads to high $H_A$, and FMR frequency [24]. Among the family of hexaferrite, M-type Ba(Sr)$Fe_{12}O_{19}$ ferrite is hard magnetic and received great attention due to their technological applications in permanent magnet, high density magnetic recording media and microwave devices [25–28]. It's large uniaxial $H_A$(~17 KOe), self-biased nature, low microwave losses i.e. narrow FMR line width ~500 Oe upto K-band and less than 25 Oe above 50 GHz, makes possible material for microwave and millimetre devices [14,24,29]. Their characteristic magnetic properties lies in its hexagonal crystal structure in which 24 $Fe^{3+}$ ions distributed among five different crystallographic sites i.e. one tetrahedral ($4f_1$), three octahedral ($12k$, $4f_2$, $2a$) and one trigonal bipyramidal site ($2b$) as shown in Fig 1.4.

The FMR ($f_r$) and operational frequency of ferrite materials directly depends on the intrinsic magnetic parameters ($H_a$ and $M_s$) and can be further tuned by external magnetic field evaluated by the relation:

$$f_r = \gamma(H_o + H_a + 4\Pi M_s) \qquad (1.5)$$

where γ (2.8 MHzOe) is gyromagnetic ratio, $H_o$ is external applied magnetic field and $H_a$ is anisotropic field.

Due to self bias nature of M-type ferrite; minimum external biased field is required, which greatly reduces the size of device [14,30]. Apart this, suitable cations substitution

for $Fe^{3+}$ ion, remarkably affect it's $H_a$ with a subsequent shift in it's FMR, and hence the operational frequency band [31–34]. For example, the substitution of $Sc^{3+}$ or $In^{3+}$ for $Fe^{3+}$ ions reduces its operable frequency to X-band [35,36], while the substitution of $Al^{3+}$, $Cr^{3+}$ and $Ga^{3+}$ increase the device operational frequency up to W-band [37–40]. Devices based on BaM and its substitution systems can be operable from 1 to 100 GHz. Magnetic and microwave properties of different ferrites are tabulated in Table 1.3.

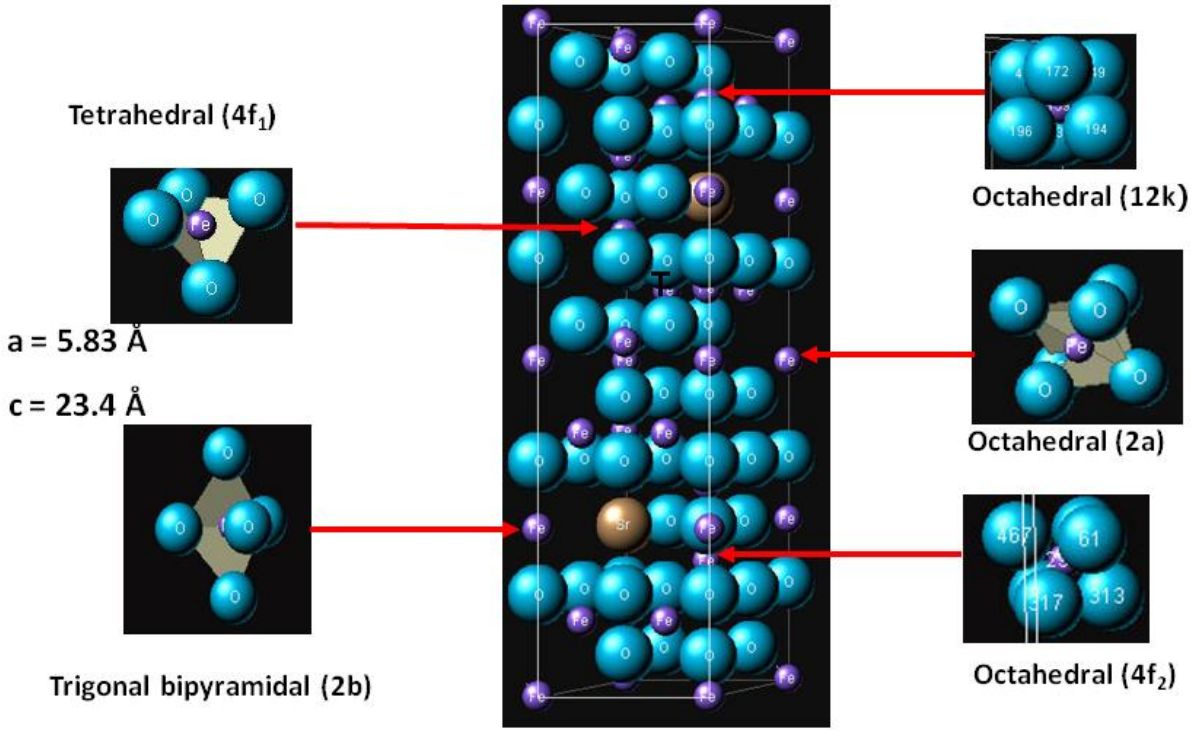


Fig. 1.4. Unit cell and different crystallographic sites of M-type hexaferrite.

The magnetism in a system is originated due to Kramers-Anderson superexchange. In complex oxide systems such as ferrites; superexchange interactions occurs through oxygen ions in which spins of the neighboring metallic ions are linked via intermediate oxygen ion (Me-O-Me). The magnitude of exchange interaction depends upon the distance and angle formed by Me-O-Me bond. A semi-empirical rule based on the symmetry relations and electron occupancy referred as Goodenough-Kanamori rule is used to measure magnetic properties of ferrite materials on the quantitative level.

Table 1.3 Properties of different type of ferrites and composites commonly used at microwave frequencies.

| Type | Example | Operable Microwave frequency ($f_r$) | $M_s$ (G) | $H_c$ (Oe) | $H_a$ (Oe) | ΔH (Oe) |
|---|---|---|---|---|---|---|
| Cubic [16] | $NiFe_2O_4$ $CoFe_2O_4$ | ~750MHz | 3200 | | | 350 |
| | | | 5300[41] | 1566[42] | 6800[41] | 2509 |
| | $MgFe_2O_4$ | <1MHz | 2150 [43] | | 173[44] | 648 |
| | $Y_3Fe_5O_{12}$[45] | <1GHz | 1750 | | 82 | 0.6 |
| Hexaferrites [19,20] | M | Upto 36GHz | 4000(BaM)[46] 4320(SrM) [47] | 3187[48] 3193[49] | 17460[48] 20000[50] | 530 (X & K band) 16 (60GHz) |
| | X[51,52] | 3GHz | 3400 | 50 | 9500 | ---- |
| | Z[53] | 1.3 GHz | 3300 | 23 | 12000 | 750 |
| | W[54] | 3GHz | 4800 | 80 | 21000 | 42 |
| | Y[55] | Upto14GHz | 2300 | 60 | 9500 | 18(at 9GHz) |
| Hard/soft Composite | $BaFe_{12}O_{19}/NiFe_2O_4$ $BaFe_{12}O_{19}/CoFe_2O_4$ $SrFe_{12}O_{19}/$ $Mn_{0.5}Zn_{0.35}Co_{0.15}Fe_2O_4$ | 1-100GHz | --- | --- | --- | ---- |

It can be seen that there is a vast difference in the properties of spinels, garnets and hexaferrites. This difference in the properties is suitably exploited for wide variety of application from microwave absorbers to non reciprocal devices and as magnetodielectric substrate material for antenna miniaturization [15,16]. For an ideal shielding material broad band width (ΔH), high saturation magnetization ($M_s$), high permittivity ($\varepsilon_r$) and permeability ($\mu_r$) is required. Also for antenna miniaturization at microwave frequencies; high $\varepsilon_r$ with high $\mu_r$ of magnetodielectric material is required. A single ferrite material cannot fulfill the demands for application in wider frequency band. Hence, along with suitably substituted ferrite, a composite of hard (high $H_A$) and soft (low $H_A$) ferrites could be an alternative material. Presence of effective interfacial coupling between high $M_s$ soft phase and high $H_A$ hard phase composite may modify the magnetic and microwave properties for high frequency microwave applications [56]. The few studies on exchange-coupled nanocomposite ferrites with modified magnetic properties for microwave absorbers have already reported [57,58].

## 1.3 Applications of exchange-coupled composites

The application of exchange-coupled composites depends upon the magnetic properties of constituent materials. The Exchange-coupled rare earth based composite of hard-soft phase **(**$Sm_2Co_7$/FeCo) [59] gives $(BH)_{max}$ of 17.6 MGOe which is much higher than the single-phase $Sm_2Co_7$ (4 MGOe). These magnets has larger share in permanent magnets market. On other hand, the exchange-coupled ferrite composite are largely exploited as magnetodielectric materials. These ferrites have also shown good shielding characteristic, and used as microwave absorber above X-band. The co-existence of high $\mu_r$ and $\varepsilon_r$ in exchange coupled ferrite can be potentially used for antenna miniaturization [60]. Also both rare earth and ferrites based exchange-coupled composites provide a new pathway to electronic industry. Apart from the electronic industry, magnetic nanoparticles of composite ferrites always have drawn their attention in biomedical applications as a biosensor and in hyperthermia. Recently, composite system of $SrFe_{12}O_{19}$ coupled with γ-$Fe_2O_3$ and $CoFe_2O_4$-$NiFe_2O_4$ have been proposed as a possible hyperthermia agent because of their large magnetic losses.

## 1.5 Motivation

Magnetic ferrites includes hexagonal, spinel and garnet has gained attention for microwave frequency applications due to their inherited magnetic, dielectric and microwave properties such as moderate magnetization, high permeability, high permittivity and low losses. However, large difference in their anisotropic field and FMR frequency restricts application of individual ferrite in wide frequency range. Alternatively, the composites of hard and soft ferrite may cater to high frequency device application with a large band width from 1-100 GHz. Large amount of work has been varied out with individual soft and hard ferrites. However studies based on soft/hard ferrite composites for high frequency application is very limited. Only a few reports investigated their microwave absorbing properties in X- and K- band. Therefore, the main focus of this work systematically investigates the processing and properties of various hard/soft exchange-coupled ferrites.

## 1.6 Objectives

1. Preparation of M-type hexaferrite-spinel nano/micro composite by sol-gel and solid state synthesis method.
2. To investigate the effect of various structural and compositional parameters on magnetic and microwave properties of composite ferrites.
3. Processing of composite $NiFe_2O_4/BaFe_{12}O_{19}$ thin films by sputtering and its magnetic characterization.

# *Chapter 2*

# Literature review

**Overview**

In this chapter, a brief preamble related to origin of exchange coupling, its development and various experimental and theoretical studies carried out on different nanocomposite systems are reviewed. The review is divided into rare earth alloys and ferrites based composites in bulk and thin films form. Effect of various processing methods and conditions on exchange coupling between hard and soft phase has been discussed. The emphasis are given to magnetic and microwave properties of hexagonal/spinels ferrite nanocomposites. A few other exchange-coupled systems are also mentioned in the end of the chapter.

## 2.1 Preamble

The interfacial interaction in composites comprises of hard magnetic and soft magnetic phase was first introduced by Kneller and Hawing in early 1990 [2] and referred as "*exchange-spring system*" or "*exchange-hardened system*". The purpose was to develop exchange-coupled permanent magnets with high energy product ($(BH)_{max}$) by exploiting high saturation magnetization ($M_s$) of soft phase and high anisotropy of hard phase simultaneously. Such exchange-coupled magnet gives choice of different soft and hard magnetic material and large compositional flexibility as well. The exchange-spring mechanism between the phases was further explained by Skomski and Coey [3,9,61] using several theoretical models and experimental studies with an emphasis on structure property relationship. Over a decade (1990-2000); studies were mainly focused on development of novel rare earth based alloys nanocomposite magnets with high $(BH)_{max}$ and provided a new paradigm to permanent magnets. The exchange-spring phenomenon was also studied for thin film composites structures for better understanding of inherited mechanism [7,12,62]. In 2004, exchange coupling in ferrite based nanocomposite system has gained attention and investigated. Such exchange-coupled ferrites showed promising properties for microwave absorbers and other high frequency applications.

Large number of studies was conducted to verify the understanding with different soft and hard magnetic phases. Apart from choice of materials, researchers have also done considerable work on microstructural aspects of interfacial coupling in nanopowders and thin films. It was found that interfacial coupling strongly depends upon film thickness, and powder/grain size, which vanishes above a critical size. Hence, different processing methodologies were adopted to investigate the role of optimizing particle size, film thickness and relative weight fraction of soft and hard magnetic phase.

The following section provides a summary of research carried out for different exchange-coupled systems classified as rare earth alloy composite and ferrites based composites in bulk and thin films form.

## 2.2 Rare earth based composite magnets

Since 1990's various research groups were actively involved on processing of rare earth based exchange-coupled nanocomposite permanent magnets with enhanced $(BH)_{max}$. Most of the theoretical and experimental studies were focused on $Nd_2Fe_{14}B/\alpha$-Fe, $Sm_2Fe_{17}N_3/Fe_{16}Co_{35}$, $Y_2Fe_{14}B/Fe_3B$, $Sm_2Co_7/FeCo$, and $SmCo_5/\alpha$-Fe magnets. The primary aim was to increase interfacial coupling by structural and compositional modifications, which consequently enhances the magnetic properties. The important research studies and their findings in mentioned system are summarized below.

After the introduction of exchange coupling phenomenon, extensive theoretical and numerical calculations on magnetization reversal mechanism in two phase permanent magnet were given by T. Schrift [63–66]**,** and showed that size of soft magnetic grain should be smaller or twice the domain wall width of hard magnetic grain for maximum exchange interaction. In other numerical calculations proved that reducing the grain size of soft phase by half the domain wall width of hard phase can help in significant reduction of coercivity ($H_c$). Ralph Skomski and Coey *et al.* [3,4,9] have calculated nucleation field ($H_N$) and $(BH)_{max}$ of exchange-coupled $Sm_2Fe_{17}N_3/Fe_{16}Co_{35}$ with different particle size of soft phase. E. H. Feutrill *et al.* [67], have done the theoretical simulation for exchange-coupled mixture and showed $H_c$, $M_s$ and $(BH)_{max}$ directly depends on the size of soft magnetic phases which significantly enhanced by size optimization. R. Fischer *et al.* [68] given another analytical treatment using a simulation model to explain relation between magnetic properties and microstructure of $Nd_2Fe_{14}B/\alpha$-Fe permanent magnet composite. The maximum $(BH)_{max}$ of 400 kJ/m$^3$ with 10 nm size of α-Fe was simulated. W. C. Feng *et al.* [69] showed the effect of phase distribution and grain size on $H_c$, exchange coupling and effective anisotropy using theoretical modelling. The results showed that when the size of soft grain is larger than exchange coupling length, the presence of uncoupled soft magnetic spins are evidenced as a shoulder in demagnetization curve. Apart from the grain size; magnetic phase distribution also affects the exchange coupling interaction between the phases.

With various theoretical studies, the dependence of exchange coupling on grain size was simultaneously verified experimentally for similar systems. Choong Jin Yang *et al.* [70] prepared the composite of $Nd_2Fe_{14}B$ with soft magnetic $Fe_3B$ and α-Fe phase. The results showed that decreasing grain size of soft magnetic phase by 20%, coupling increases and

resulted in enhanced remanence ($M_r$) (12.5 kG) and $(BH)_{max}$ (15.8 MGOe) by 30%. Also, Youhui Gao *et al.* [5,6], studied the effect of Hf and Ga on crystallization and coupling of nanocomposite $Nd_2Fe_{14}B/Fe_3B$ magnet. In the presence of Hf and Ga; composite annealed at 680 °C and 700 °C showed maximum exchange coupling with $(BH)_{max}$ of 15.3 MGOe and 14.6 MGOe respectively.

D.H. Ping *et al.* [71] studied the magnetic and microstructural properties of α-$Fe/Nd_2Fe_{14}B$ composite with Nb, Zr, Cu and Ga addition. The results showed that Ga and Zr improved the magnetic properties and provide a fine structure by controlling the grain growth of α-Fe particles. With Zr addition high $H_c$ (496l A/m) and $(BH)_{max}$ (134 $kJ/m^3$) were obtained due to large interfacial interaction between α-Fe and $Nd_2Fe_{14}B$ phase. Later Zhao-hua Cheng *et al.* [72] observed similar effect of Zr on $Sm_2Fe_{15}Ga_2C_x$/α-Fe nanocomposite.

R. W. Gao *et al.* [73] studied the effect of intergrain exchange coupling on anisotropy and $H_c$ in $Nd_2Fe_{14}B$/α-Fe composite. The anisotropy of the composite was calculated statistically between hard-hard, soft-soft and hard-soft grains. Anisotropy found to decrease with decrease in grain size and increase in weight fraction of soft phase. They concluded that grain size in the range of 10-15 nm and soft phase weight fraction below 0.50 gives higher $(BH)_{max}$. Later F.T. Parker *et al.* [74,75] prepared $Nd_2(FeCo)_{14}B$/α-Fe and $Pr_{6.93}Fe_{85.7}Nb_{1.39}$/α-Fe nanocomposite and showed that exchange-spring coupling directly depends on the size of soft magnetic phases. L. H. Lewis *et al.* [10], V. Neu *et al.* [76] and T. Hopfinger *et al.* [77] also observed similar results for $Fe_{14}Nd_2B$/α-Fe composite magnets.

Toru Maeda *et al.* [78] showed the effect of annealing temperature on hard $Y_2Fe_{14}B$ and soft $Fe_3B$ magnet on the microwave properties and resonance frequency. The composite annealed at 1003 K and 1123 K showed single phase behavior with relative high $H_c$ compared to annealed at 973 K. Excellent microwave properties (reflection loss (*RL)* = -32 dB; permeability ($\mu$") = 0.38) at higher frequencies (39.5 GHz and 44 GHz) were observed and justified as microwave absorber material.

N.V. Rama Rao *et al.* [79] and Yanglong Hou *et al.* [80], investigated the exchange-spring interaction in mechanically milled $SmCo_5$ with different weight percent of soft magnetic Fe. The exchange coupling was observed for 5% of Fe content, with a

maximum $H_c$ of 8.9 kOe. X.Y. Xiong *et al.* [81] studied the distribution of α-Fe particles in SmCo/Fe permanent magnet. Different distribution of α-Fe particle with constant weight fraction was induced by varying ball milling time. The result showed that $M_s$ and $(BH)_{max}$ increases with milling time as consequence of better coupling in well distributed phases. Narayan Poudyal *et al.* [59] has prepared SmCo/Fe and SmCo/Co nanocomposite with different weight ratio by high energy ball mill method. Maximum interfacial coupling was observed for $Sm_2Co_7$(60%)/Fe(40%) nanocomposite which was larger than theoretical calculated using Stoner-Wohlfarth model. Much larger $(BH)_{max}$ (17.6 MGOe) compared to single-phase $Sm_2Co_7$ (4 MGOe) were observed. These studies on rare earth based composite revealed that well exchange-coupled composites are promising way to produce high performance permanent magnet.

### 2.3 Rare earth based composite thin films

Apart from the exchange-coupled composite permanent magnets; the exchange-spring mechanism in thin film system were also extensively investigated. S.D Bader *et al.*[12,13] first revealed detailed systematic understanding of exchange interaction in thin film layered composite structure. A theoretical explanation on magnetic reversal and role of critical thickness of soft layer were explained. Using his theoretical model, alloy based thin films was also grown and their behaviour was experimentally studied. A brief summary of important findings are given below:

M. Shindo *et al.* [82] fabricated α-Fe/Nd-Fe-B multilayer by radio frequency magnetron sputtering. The effect of α-Fe film thickness on intralayer and interlayer coupling were investigated and supported by micromagnetic calculations. It was observed that $H_c$ strongly depends upon film thickness whereas interlayer coupling strength is independent of thickness. J.S. Jiang *et al.* [83] investigated the exchange coupling behaviour with Fe film thickness and annealing temperature on magnetron sputtered Sm-Co/Fe bilayers. Their results showed that films annealed below 400 °C and thickness less than 10 nm are not optimum for interfacial exchange-spring mechanism. Bilayer of Sm-Co (20 nm) and Fe (10 nm) annealed at 400 °C gives single phase like behavior with the maximum $H_c$ (6 kOe) and $(BH)_{max}$ (27.7 MGOe). Joseph E. Davies *et al.* [84] studied the magnetization reversal behavior in Fe/SmCo and compared it with non rare earth based FeNi/FePt systems using theoretical first order reversal curves (FORC) technique and vector magnetometry. A single sharp drop in $M_s$ and simultaneous switching in FORC was

observed in FeNi/FePt films. Single onset found to be more gradual and prominent for thin soft (Fe & FeNi) phase layer. Their FORC and experimental results showed that exchange coupling and magnetic parameters can be controlled by thickness of soft phase. Daniel R. Cornejo *et al.* [85] deposited bilayer of SmCo/Fe on Si substrate by magnetron sputtering and studied the effect of Fe film thickness. Preisach model was used to evaluate reversible and irreversible magnetization component of the composite. The obtained Henkel plots and Preisach parameter ($k_m$) confirmed that demagnetization interaction between SmCo and Fe depends on Fe layer thickness. X. H. Liu *et al.* [86] deposited trilayer of $Sm_{22}Co_{78}$/Fe/$Sm_{22}Co_{78}$ on Cr/glass substrate using multiple gun sputtering. All the samples showed in-plane anisotropy and single phase magnetization behavior irrespective of Fe thickness. From magnetic interactions studies, they proved that exchange coupling are thickness dependent and magnetostatic interaction are dominant above coercive field. T. Schrefl *et al.* [8] calculated the magnetic properties of SmCo/Fe and SmCo/Co systems for different soft layer thickness using Landau Lifshitz Gilbert equation. It was observed that magnetization reversal strongly depends on soft magnetic layer thickness. SmCo/Co system with 10 nm thick Co film showed maximum $(BH)_{max}$ of 389 kJ/m$^3$ and was comparable to theoretical calculated (396 kJ/m$^3$).

V Neu *et al.* [87] deposited epitaxial $SmCo_{25}$(25 nm)/Fe/$SmCo_{25}$(25 nm) trilayer on MgO substrate using pulse laser deposition (PLD) system and showed the effect of soft Fe film thickness on exchange coupling. When thickness of Fe layer (6 nm) was twice of Bloch wall of $SmCo_{25}$ (2-3 nm), the coupling found to be dominant. The maximum $H_c$ of 1.5 T and $(BH)_{max}$ of 224 kJm$^{-3}$ (28 MGOe) was observed with 16 nm thick Fe film. To understand the interfacial profile between Sm-Co and Fe layers, Y. Choi *et al.* [88] deposited Sm–Co/Fe bilayers of different thickness on MgO substrate by magnetron sputtering. Their results concluded that interfacial profile and exchange coupling can also be tailored by alternating sublayer deposition. In later [89] recoil loop for SmCo/Fe system were measured and compared with micromagnetic simulated data. The results showed that recoil loops of the composite system are strongly dependent on anisotropy of hard phase as well as interphase coupling.

Yuzi Liu *et al.* [90] has given the microstructural analysis of SmCo/Fe bilayer system. STEM micrograph showed that Fe layer diffused into textured SmCo layer and responsible for exchange-spring coupling and high $(BH)_{max}$. S. Sawatzki *et al.* [91]

deposited a trilayer of $SmCo_5/Fe/SmCo_5$ with different Fe film thickness using PLD and reported maximum energy density of 312 $kJm^{-3}$. Wei-Bin Cui *et al.* [92] deposited the anisotropic thin films of $Nd_2Fe_{14}B/FeCo$ by magnetron sputtering. Their results showed that by controlling distribution of Nd and Fe, the $(BH)_{max}$ can be enhanced to 480 $kJm^{-3}$ which was close to the theoretical calculated (486 $kJm^{-3}$) value. J. Zhang *et al.* [93] also obtained maximum $(BH)_{max}$ of 32 MGOe for exchange-coupled $Sm(Co,Cu)_5/Fe$ multilayer.

Recently, X. J. Weng *et al.* [94] and Wenjing Si *et al.* [95] given the theoretical interpretation on coercivity mechanism in hard/soft bilayer system by changing the thickness of soft layer. They used 1-D and 3-D micromagnetic methods to understand spin distribution and showed that larger thickness of soft phase widen spin angle difference that weakens the exchange-coupling.

### 2.4 Ferrite based exchange-coupled nanocomposite

After extensive research on rare earth based high $(BH)_{max}$ composite magnets, the focus of researchers was shifted to explore the similar exchange mechanism in hard/soft ferrite based composite. They have prepared a large variety of composite ferrites and established that exchange phenomenon also exists at nanoscale. Their chemical stability, ease of processing, magnetodielectric nature and wide variety of application were the key driven force to explore magnetic and microwave properties of such ferrites. Among the choices of hard and soft magnetic phases; the hexagonal M-type hard ferrite and soft spinel ferrites are the primary one. However, a few works on different kind of ferrites were also reported. In the present section, various works pertaining to hard/soft exchange-coupled ferrites are discussed. The emphasis is laid on their processing, properties and applications.

In 2006, Han Zhidong *et al.* [96] successfully synthesized the exchange-coupled nanocomposite of $BaFe_{12}O_{19}/MFe_2O_4$(M=Co, Mn) by sol-gel method. Their structural measurements by XRD and SEM confirmed that both the phases coexist independently without any intermediate phase. Followed by its work, the magnetic studies on these composite ferrites confirmed the exchange coupling among the phases, which are predominantly processing dependent. K. W. Moon *et al.* [97] prepared $BaFe_{12}O_{19}/NiZnFe_2O_4$ nanocomposite by two different processing techniques and

studied the change in interfacial coupling. Their results showed that self propagation method was an adequate way to obtain exchange-coupled composite.

Effect of particle size and volume fraction of soft phase on exchange coupling was investigated by Debangsu Roy *et al*. [98] for $BaFe_{12}O_{19}/Ni_{0.8}Zn_{0.2}Fe_2O_4$ system. It was found that suitable particle size and composition give rise to exchange-spring mechanism and enhances $(BH)_{max}$ of composite magnet. Single phase magnetization behavior of composite corresponds to exchange-coupled system. Similar studies were extended for $BaCa_2Fe_{16}O_{27}$-$Fe_3O_4$ system and identical behaviour was observed [99]. Later, theoretical calculations [100] were performed to understand magnetization reversal behavior in $Ni_{0.8}Zn_{0.2}Fe_2O_4/BaFe_{12}O_{19}$ composite. Results showed that pinning mechanism and interfacial spin interaction plays a dominant role in magnetization reversal. Further, reversible and irreversible magnetization mechanisms of exchange-coupled and non-exchange coupled $CoFe_2O_4/SrFe_{12}O_{19}$ composite with fixed weight ratio (1:8) were investigated by FORC. The studies showed single maxima for exchange-coupled system whereas non exchange system gives two maxima as confirmed from FORC. Obtained two maxima in non exchange-coupled composite proved that ferromagnetic interactions between hard and soft phases were more prominent in exchange-coupled system compared to non-exchange coupled system [101]. Later V. Harikrishnan *et al*. [102,103] extended experimental studies on $Ba_{0.5}Sr_{0.5}Fe_{12}O_{19}/CoFe_2O_4$ system and showed that exchange coupling and structural properties of the composites can be controlled by adequate processing, annealing temperature and soft phase content.

Subhenjit Hazra *et al.* [104] prepared $(NiFe_2O_4)_x$–$(BaFe_{12}O_{19})_{1-x}$ composites by one-pot and physical mixing method to understand exchange-spring mechanism. The one-pot composite showed maximum interfacial coupling and gives high $M_s$ and $H_c$. Later, Rui Xiong *et al*. [105] studied the exchange-spring behavior in $BaFe_{12}O_{19}/Ni_{0.5}Zn_{0.5}Fe_2O_4$ composites. The presence of exchange-spring interaction between hard and soft phases was confirmed by *M-H* loops and their respective Henkel plots. They showed that magnetic properties can be tailored by adopting adequate technique and controlling dipolar as well as interfacial interactions.

Fuzhan Song *et al.* [106,107] prepared hollow nanofibers of $SrFe_{12}O_{19}/Ni_{0.5}Zn_{0.5}Fe_2O_4$ by sol-gel process and size dependent coupling were observed. In similar system, exchange coupling was also verified with enhanced $M_r$ and $H_c$ for certain composition. Shahab

Torkian *et al.* [108] studied the magnetic properties of sol-gel synthesized $SrFe_{10}Al_2O_{19}/Ni_{0.2}Co_{0.8}Fe_2O_4$ composites and showed that exchange coupling and magnetic parameters can also be controlled by weight fraction of individual phases. Recently, they also showed [109] an enhancement in $(BH)_{max}$ by 10.5% compared to pure hard phase. Jiuyang Xia *et al.* [110,111] studied the exchange-spring behavior in $Mn_{0.6}Zn_{0.4}Fe_2O_4/Sr_{0.85}Ba_{0.15}Fe_{12}O_{19}$ and $Ni_{0.5}Zn_{0.5}Fe_2O_4/SrFe_{12}O_{19}$ composites synthesized by ball milling method. Their results showed that two step ball milling method was suitable to obtain exchange-coupled magnets. Wen Chen *et al.* [112] carried out similar studies on $Li_{0.3}Co_{0.5}Zn_{0.2}Fe_2O_4/SrFe_{12}O_{19}$ core/shell composite system. Their results also supported that interfacial coupling and $M_s$ can be enhanced by adopted suitable processing.

M. A. Almesseire *et al.* [113] also synthesized the exchange-coupled $CuFe_2O_4/Sr_{0.3}Ba_{0.4}Pb_{0.3}Fe_{12}O_{19}$ composite with enhanced magnetic properties. J. N. Dahal *et al.* [114] successfully prepared the exchange-coupled composite of $SrFe_{12}O_{19}/La_{(1-x)}Sr_{(x)}MnO_3$ and studied their magnetic properties. Higher $M_r/M_s$ ratio (0.58) and $H_c$ (6.29 kOe) were observed for composite with 60/40 weight ratio. Their results showed that by controlling the magnetization of soft ferrite; $(BH)_{max}$ and exchange coupling can be tailored. Dongyun Li *et al.* [115] studied the effect of grinding time and soft phase weight content on exchange coupling in $SrFe_{12}O_{19}/CoFe_2O_4$ and $SrFe_{12}O_{19}$/Fe-B composite. Their results showed that grinding time as well as magnetic properties of soft phases simultaneously helps to control the interfacial interaction and magnetic properties of composite system.

Li Zhao *et al.* [116] showed the effect of soft phase weight fraction on magnetic properties of $(1-x)CoFe_2O_4/xSrFe_{12}O_{19}$ composites. The interfacial coupling and magnetic properties found to depend on composition. Faezeh Tavakolinia *et al.* [117] also studied the magnetic properties for $SrFe_{12}O_{19}/Co_{0.5}Zn_{0.5}Fe_2O_4$ system. Results showed that exchange coupling and magnetic properties depends on soft phase content and processing method. Composite showed maximum $M_s$ (91 emu/g) and $H_c$ in one-pot assisted method for 60/40 weight ratio. S. Manjura Hoque *et al.* [118] studied the effect of calcination temperature on exchange coupling and magnetic properties of $BaFe_{12}O_{19}/CoFe_2O_4/MgFe_2O_4$ composite. Exchange coupling and $M_s$ both found to be temperature dependent. Composite calcined at 1000 °C and 1100 °C showed high $(BH)_{max}$

as a result of interfacial coupling. Haibo yang *et al.* [119,120] prepared exchange-coupled $BaFe_{12}O_{19}/CoFe_2O_4/CaFe_2O_4$ and $BaFe_{12}O_{19}/Y_3Fe_5O_{12}$ composites with enhanced $(BH)_{max}$ by 15% and 107% respectively. The existing interfacial coupling found to be responsible for this giant enhancement.

Yan Wang *et al.* [121] studied the effect of calcination temperature and presintering on exchange coupling of $BaFe_{12}O_{19}/Ni_{0.8}Zn_{0.2}Fe_2O_4$ composite. The composite calcined at 1100 °C with 3 hour presintering at 400 °C showed increased $M_s$ (63 emu/g), $H_c$ (2750 G) and $M_r$ (36 emu/g) compared to pure hard and soft phases. Their results suggested that interfacial interaction can be increased by presintering. Ailin Xia *et al.* [122] studied the exchange coupling behavior in $SrFe_{12}O_{19}/(Ni,Zn)Fe_2O_4$ composites. Effect of different mass ratio (2:1, 1:1 and 1:2) and sintering temperature (700 °C & 900 °C) on magnetic properties were investigated. Their results showed that grain size influence the exchange coupling interaction and magnetization. In later studies [123,124], exchange interaction in $SrFe_{12}O_{19}/(Ni,Zn)Fe_2O_4$, $SrFe_{12}O_{19}/CoFe_2O_4$ and $SrFe_{12}O_{19}$/Fe-B composites were also confirmed by single peak in Henkel ($\delta M$-$H$) plots. Miao Liu *et al.* [125] successfully synthesized exchange-coupled composites of $BaFe_{12}O_{19}/CoFe_2O_4$ and reported 10% enhancement in $(BH)_{max}$. Recently, N. A. Algarou *et al.* [126,127] studied the effect of various soft phases $MFe_2O_4$ (M= Co, Ni, Cu, Zn, Mn) with $SrCo_{0.02}Zr_{0.02}Fe_{11.96}O_{19}$ and $SrTb_{0.01}Tm_{0.01}Fe_{11.98}O_{19}$ hard phases on exchange coupling for fixed weight fraction. It was observed that different soft phase remarkably affect interfacial coupling and magnetic properties.

Later, few research groups also studied the dielectric behaviour along with magnetic properties of such exchange-coupled composites. Andzrej Hilczer *et al.* [128] studied the dielectric behavior in exchange-coupled $SrFe_{12}O_{19}/CoFe_2O_4$ composites. Their results were explained on the basis of Koop's theory based on Maxwell-Wagner model. Later, R. K. Kotnala *et al.* [129] investigated the effect of interfacial coupling on magnetic and dielectric properties of $x BaFe_{12}O_{19}/(1-x)Mn_{0.2}Ni_{0.4}Zn_{0.4}Fe_2O_4$ composite. Change in dielectric behavior with hard phase weight fraction was also explained by Maxwell-Wagner model. Obtained high $H_c$ and $M_s$ corresponded to existence of interfacial coupling. It was showed that dielectric losses directly depend on weight fraction of hard phase and interfacial coupling. The similar dielectric studies were reported on exchange-coupled $BaFe_{11.7}Al_{0.15}Zn_{0.15}O_{19}/Mn_{0.8}Mg_{0.2}Fe_2O_4$ composite by S. F. Mansour *et al.* [130].

The dielectric studies on exchange-coupled composites were not only limited to low frequency. Ferrites as a good microwave absorber and a magnetodielectric material; studies on high frequency microwave applications were also investigated. *Na Chen et al.* [131] first investigated the microwave absorption properties of exchange-coupled $SrFe_{12}O_{19}/ZnFe_2O_4$ composite system. The effect of soft phase weight fraction on permittivity ($\varepsilon$), permeability ($\mu$) and microwave absorption were reported in the frequency range of 5-15 GHz. The results showed that $\mu$ increases with $ZnFe_2O_4$ content as a consequence of interfacial coupling. *RL* shift toward lower frequency band and a minimum of -37 dB was observed for 15 wt% $ZnFe_2O_4$. Liuyang Zhang *et al.* [132] studied the microwave absorption behavior of $SrFe_{12}O_{19}/CoFe_2O_4$ nanocomposite. Core shell nanoparticles of composites showed maximum *RL* at 14.5 GHz compared $SrFe_{12}O_{19}$. M. Mehdipour *et al.* [133] compared the magnetic and microwave properties of $SrFe_{12}O_{19}$, $NiFe_2O_4$ with exchange-coupled $SrFe_{12}O_{19}/NiFe_2O_4$ composites. Results showed that magnetic and microwave properties can be modified with the exchange coupling. Maximum loss of -18 dB at 11 GHz was obtained for the composite sintered at 1200 °C.

Silvia E. Jacobo *et al.* [56] prepared $Sr_{0.5}Cr_{0.5}Nd_{0.5}Fe_{10.5}O_{19}/NiFe_2O_4$ composites in different weigh ratio and compared their microwave properties in X-band. Strong exchange coupling were observed for 30:70 and 50:50 composition with single phase magnetization behavior. Loss dip of -34.4 dB at 11.1GHz with the bandwidth of 3.5 GHz was observed for 50:50 compositions. Sachin Tyagi *et al.* [134] prepared nanocomposite of $SrFe_{12}O_{19}$ with $NiFe_2O_4$ and $ZnFe_2O_4$ by coprecipitation method. Obtained high $M_s$ (59.79 emu/g) and *RL* dip of -29.36 dB at 10.21 GHz of composites showed that such exchange-coupled systems are suitable for RADAR absorbing materials.

Subhenjit Hazra *et al.* [135,136] studied microwave absorption properties for $(NiFe_2O_4)_x$-$(SrFe_{12}O_{19})_{1-x}$ and $(Ni_{0.65}Zn_{0.35}Fe_2O_4)_x$-$(SrFe_{12}O_{19})_{1-x}$ systems and maximum loss dip of -17 dB and -21 dB were observed respectively. S.R. Saeedi Afshar *et al.* [137] studied the microwave properties for $SrFe_{12}O_{19}/Ni_{0.6}Zn_{0.4}Fe_2O_4$ composite system and showed absorption of -23.5 dB at 9.9 GHz. Later, Vipul Sharma *et al.* [138] measured the microwave properties of $BaFe_{12}O_{19}/Y_3Fe_5O_{12}$ in 8-35 GHz frequency range for microwave patch antenna substrate. Maximum absorption of -26 dB at 28 GHz and high operational frequency of the notch filter (35 GHz) at the applied field of 1 T was reported.

FMR linewidth (ΔH) found to be varied between 2 kOe to 0.2 kOe with the composition. Haibo yang *et al.* [139] compared the microwave absorption properties of $BaFe_{12}O_{19}/CoFe_2O_4$ and $PANI/BaFe_{12}O_{19}/CoFe_2O_4$ composites. Enhanced microwave properties in $PANI/ BaFe_{12}O_{19}/CoFe_2O_4$ with *RL* of -36.4 dB at 9.8GHz in broad frequency range (7-14 GHz) were observed. Yin Liu *et al.* [140] also obtained maximum *RL* of -31.6 dB at 12.7 GHz for $(0.3)SrFe_{12}O_{19}/(0.7)NiFe_2O_4$ composite. Kunal Pubby *et al.* [141] observed *RL* of -42.02 dB for $Ni_{0.7}Co_{0.9}(MnZr)_xFe_{2-2x}O_4/Ba_ySr_{1-y}Fe_{12}O_{19}$ composite synthesized by physically mixing method. Ying Lin *et al.* [142] analysed the microwave absorption properties of $BaFe_{12}O_{19}/Fe_3O_4$ core-shell nanocomposites prepared by hydrothermal method. Maximum absorbance of -33.6 dB at 11.6 GHz frequency was obtained for the composite which was twice as compared to BaM in the studied frequency band (2-18 GHz).

Besides microwave properties, such ferrite could also be used as antenna substrates due to its magnetodielectric nature. The simultaneous existence of high permeable soft phase and high $\varepsilon$ hard phase in exchange-coupled composites can reduce the antenna size. Ashish Saini *et al.* [58] group prepared $Ni_{0.5}Zn_{0.3}Co_{0.2}Fe_2O_4/BaFe_{12}O_{19}$ and $Mn_{0.5}Zn_{0.35}Co_{0.15}Fe_2O_4/SrFe_{12}O_{19}$ [60] composites and showed that size of patch antenna can be reduced by suitable adjustment of $\mu$ and $\varepsilon$ below 1 GHz.

### 2.5 Ferrite based bilayer system

Apart from powder composite; few studies were also conducted on hard/soft ferrite bilayer system to understand the exchange-spring mechanism. $CoFe_2O_4/ZnFe_2O_4$, $MnFe_2O_4/CoFe_2O_4$, $ZnFe_2O_4/CoFe_2O_4$, and $CoFe_2O_4/Fe_3O_4$ bilayers films were deposited by different deposition techniques. The role of annealing temperature and film thickness on magnetization reversal behavior were explained [143–146].

Last but not least, the other ferrite based systems that includes $SrFe_{12}O_{19}/Fe_2O_3$, $SrFe_{12}O_{19}/FeCo$ [147–150], $CoFe_2O_4/FeCo$ [151–160] and $ferrite/Sm_2Fe_{17}N_7$ [161] were also investigated with an aim to understand exchange-spring mechanism between the two different magnetization phases. The studies on such systems give the systematic understanding of geometrical shape and particle size on exchange coupling and magnetic properties.

The important work carried out on exchange-coupled ferrite composite and their respective microwave properties in last decade are summarized in Table 2.1.

Table 2.1 Summarized microwave properties of hard/soft ferrite composites.

| **Exchange-coupled hard/soft ferrite composite** | **Processing method** | **Microwave properties** |
|---|---|---|
| $SrFe_{12}O_{19}/ZnFe_2O_4$ | Sol-gel | *RL*= -31 dB at 8.7 GHz<br>$\varepsilon'$= 3.8, $\varepsilon''$=1.5, $\mu'$=1.5, $\mu''$=3 |
| $SrFe_{12}O_{19}/NiFe_2O_4$ | Co-precipitation | *RL*= -11 dB at 11GHz |
| $SrFe_{12}O_{19}/NiFe_2O_4$ | Solid state route | *RL*=-31.6dB at 12.7GHz, tan$\delta_\mu$=1<br>Absorber thickness=2.5 mm |
| $Sr_{0.5}Co_{0.5}Nd_{0.5}Fe_{11.5}O_{19}$/ $NiFe_2O_4$ | Self combustion | *RL*= -34.4 dB at 11GHz<br>ΔH= 3.5 GHz |
| $SrFe_{12}O_{19}/NiFe_2O_4$ | Co-precipitation | *RL*= -29.36 dB at 10.21GHz |
| $SrFe_{12}O_{19}/NiFe_2O_4$ | Sol-gel | *RL*= -17 dB at 8.2GHz<br>Absorber thickness=3.2mm |
| $BaFe_{12}O_{19}/Ni_{0.65}Zn_{0.35}Fe_2O_4$ | Sol-gel | *RL*= -21 dB at 9.86 GHz<br>$\varepsilon'$= 7.1, $\varepsilon''$=0.2, $\mu'$=0.9, $\mu''$=0.31<br>Absorber thickness=3.05 mm |
| $BaFe_{12}O_{19}/Ni_{0.65}Zn_{0.35}Fe_2O_4$ | Physical mixing | *RL*= -6.65dB at 9.67 GHz<br>$\varepsilon'$= 7, $\varepsilon$"=0.8, $\mu'$=1.5, $\mu$"=0.35 |
| $SrFe_{12}O_{19}/Ni_{0.6}Zn_{0.4}Fe_2O_4$ | Self propagation combustion | *RL*= -23.5 dB at 9.9GHz<br>$\varepsilon'$= 3.3, $\varepsilon''$=0.5, $\mu'$=1.1, $\mu''$=0.5<br>Absorber thickness=3.5 mm |
| $BaFe_{12}O_{19}/Y_3Fe_5O_{12}$ | Sol-gel | *RL*= -26 dB at 28 GHz |
| $BaFe_{12}O_{19}/CoFe_2O_4$ | Sol-gel | *RL*= -36.4 dB at 9.8 GHz<br>$\varepsilon'$=8, $\varepsilon''$=4, $\mu'$=1, $\mu''$=0.8 |
| $Ni_{0.7}Co_{0.9}(MnZr)_xFe_{2-2x}O_4/Ba_ySr_{1-y}Fe_{12}O_{19}$ | Physical mixing | *RL*= -42.4 dB at 31.63 GHz<br>$\varepsilon'$=7, $\varepsilon''$=2, $\mu'$=1.6, $\mu''$=1<br>Absorber thickness=2.3 mm |
| $BaFe_{12}O_{19}/Fe_3O_4$ | Hydrothermal | *RL*= -33.6 dB at 11.6 GHz |

## 2.6 Other composite system

Few alloy based nanocomposite and bilayer system such as $FePt/Fe_3Pt$ [162], $Fe/FePt$, $Fe_{55}Pt_{45}/Fe_{49}Rh_{51}$, $FeRh/FePt$ [163–165], $DyFe_2/YFe_2$ [166], MnGa(Bi)/FeCo [167,168] and PrFeB/NdFeB [169] etc. were also studied by different researchers. In these composite systems role of processing method, annealing/calcination temperature, film thickness, particle size and distribution of phases on exchange coupling were reported. Their results also suggested that particle size and film thickness of soft phase greatly affect the magnetization reversal behavior and magnetic properties of the composite system.

# *Chapter 3*

## Experimental procedure & characterization techniques

**Overview**

In this chapter, details of processing method adopted for hard magnetic hexagonal ferrite ($BaFe_{12}O_{19}$), soft magnetic spinels ($NiFe_2O_4$, $Ni_{0.5}Zn_{0.5}Fe_2O_4$, $CoFe_2O_4$, $Co_{0.5}Zn_{0.5}Fe_2O_4$) and their composites are explained. A brief description of thin film deposition technique by RF-sputtering is given. Various characterization techniques used to study structural, morphological, magnetic and microwave properties are briefly explained.

### 3.1 Synthesis of nanopowders

Nanopowders of barium hexaferrite ($BaFe_{12}O_{19}$), spinel ferrite ($AFe_2O_4$; A = Ni, Co, Zn) and their composite ferrites were synthesized by sol-gel autocombustion method. Analytical grade (<99%, Sigma Aldrich) metal nitrates; iron nitrate nonahydrate ($Fe(NO_3)_3.9H_2O$, barium nitrate ($Ba(NO_3)_2$, nickel(II) nitrate hexahydrate ($Ni(NO_3)_2.6H_2O$, zinc nitrate hexahydrate ($Zn(NO_3)_2.6H_2O$, cobalt(II) nitrate hexahydrate ($Co(NO_3)_2.6H_2O$, and citric acid anhydrous ($C_6H_8O_7$) were used as precursors. The stoichiometric amount of desired metal nitrates and citric acid were dissolved in deionized water. The mixture was stirred continuously at room temperature (*RT*) till a homogeneous reddish brown transparent solution was obtained. Further $NH_3$ (25%) solution was added drop by drop during stirring to maintain pH ~7 of the solution. The solution was continuously stirred and heated at 70-80 °C until it turns into viscous gel. The as-prepared gel was kept on heating till its combustion and formation of grayish black powder. As-obtained powders were annealed at different temperatures (900 °C - 1200 °C) for 3 hours in the muffle furnace. During annealing; heating as well cooling rate were kept constant to 5 °C/min. Process flowchart of sol-gel autocombustion method are shown in the Fig. 3.1.

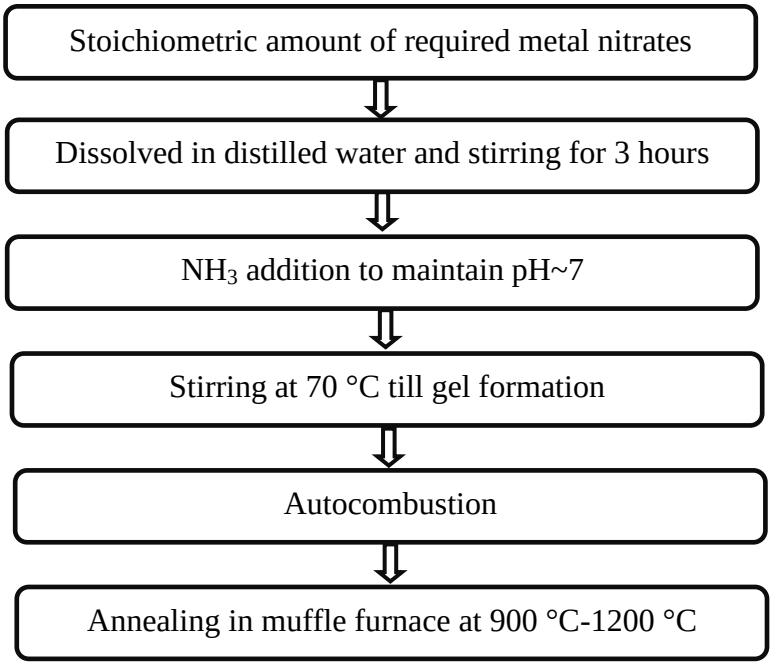


Fig. 3.1 Process flowchart of sol-gel autocombustion method.

## 3.2 Preparation of composites

The composite of $BaFe_{12}O_{19}$ (BaM) and spinel ferrites were prepared by adopting two different methodologies i.e. physical mixing and single-step method.

In physical mixing method; individually prepared $BaFe_{12}O_{19}$ and spinel ferrites by sol-gel autocombustion method (as described above) were weighed in the desired weight ratio and wet mixed for 1 hour in acetone media using planetary ball mill. The ball to charge ratio and RPM were kept constant to 1:10 and 150 respectively. The as-mixed powders were dried at *RT* and named as physically mixed (PM) composites. Further, the powder were mixed with 5% aqueous of polyvinyl alcohol (PVA) binder and dried. The dried lumps were pulverized, sieved and pelletized in desired shape (cylindrical and rectangular) using hydraulic press at a pressure of 50 MPa. As pressed powder were sintered at different temperature ranging from 1100 °C – 1200 °C for one hour in muffle furnace. Heating and cooling rate were kept constant to 5 °C/min during sintering. Fig. 3.2 shows the flow chart of PM method. The composite series prepared by PM method are:

1. $(1-x)\ BaFe_{12}O_{19} - x NiFe_2O_4$ ( $x$ = 0.1, 0.2, 0.3, 0.4, 0.5)
2. $(1-x)\ BaFe_{12}O_{19} - x Ni_{0.5}Zn_{0.5}Fe_2O_4$ ( $x$ = 0.1, 0.2, 0.3, 0.4, 0.5)

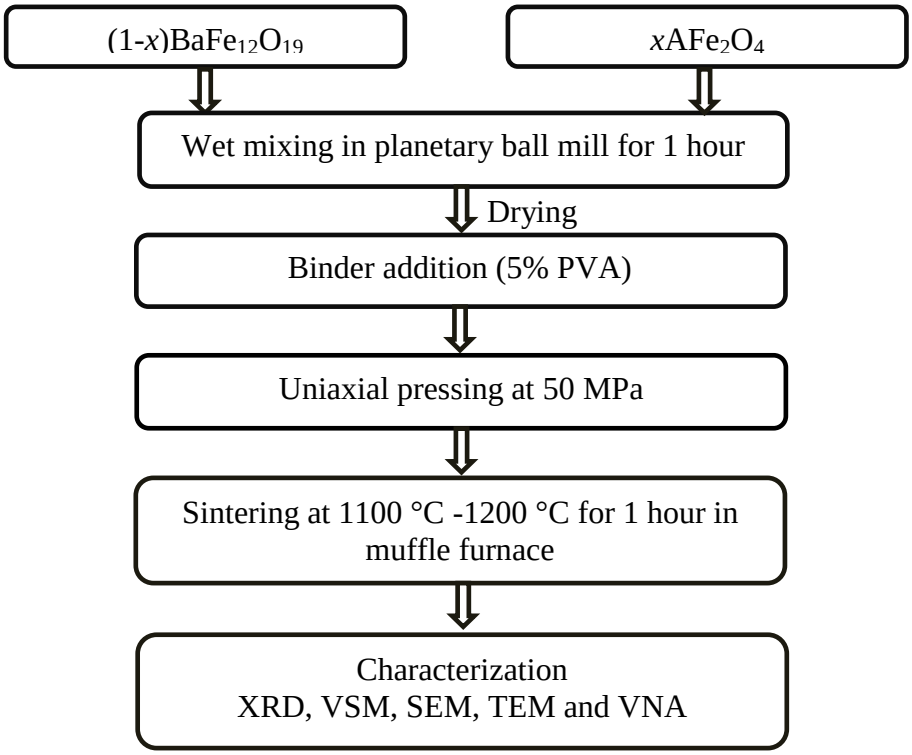


Fig. 3.2 Process flowchart of physical mixing method.

In single-step method, stoichiometric composition of metal nitrates solutions for BaM and spinel were individually prepared. The as-prepared solution of BaM and spinel were mixed in desired composition and stirred together for 3 hours to obtain homogeneous solution. The solution was then subjected to sol-gel autocombustion method as explained earlier. The autocombusted powders were calcined, pressed into pellets and sintered in the conditions mentioned above. Fig. 3.3 shows the flow chart of single-step method. The composite series prepared by single-step method are:

1. (1-$x$) $BaFe_{12}O_{19}$-$x$$NiFe_2O_4$ ( $x$ = 0.1, 0.2, 0.3, 0.4, 0.5)
2. (1-$x$) $BaFe_{12}O_{19}$-$x$$Ni_{0.5}Zn_{0.5}Fe_2O_4$ ( $x$ = 0.1, 0.2, 0.3, 0.4, 0.5)
3. 0.7 $BaFe_{12}O_{19}$-0.3$Ni_xZn_{1-x}Fe_2O_4$ ($x$ = 0.0, 0.1, 0.2, 0.3, 0.4, 0.5)
4. (1-$x$) $BaFe_{12}O_{19}$-$x$$CoFe_2O_4$ ( $x$ = 0.1, 0.2, 0.3, 0.4, 0.5)
5. (1-$x$) $BaFe_{12}O_{19}$-$x$$Co_{0.5}Zn_{0.5}Fe_2O_4$ ( $x$ = 0.1, 0.2, 0.3, 0.4, 0.5)

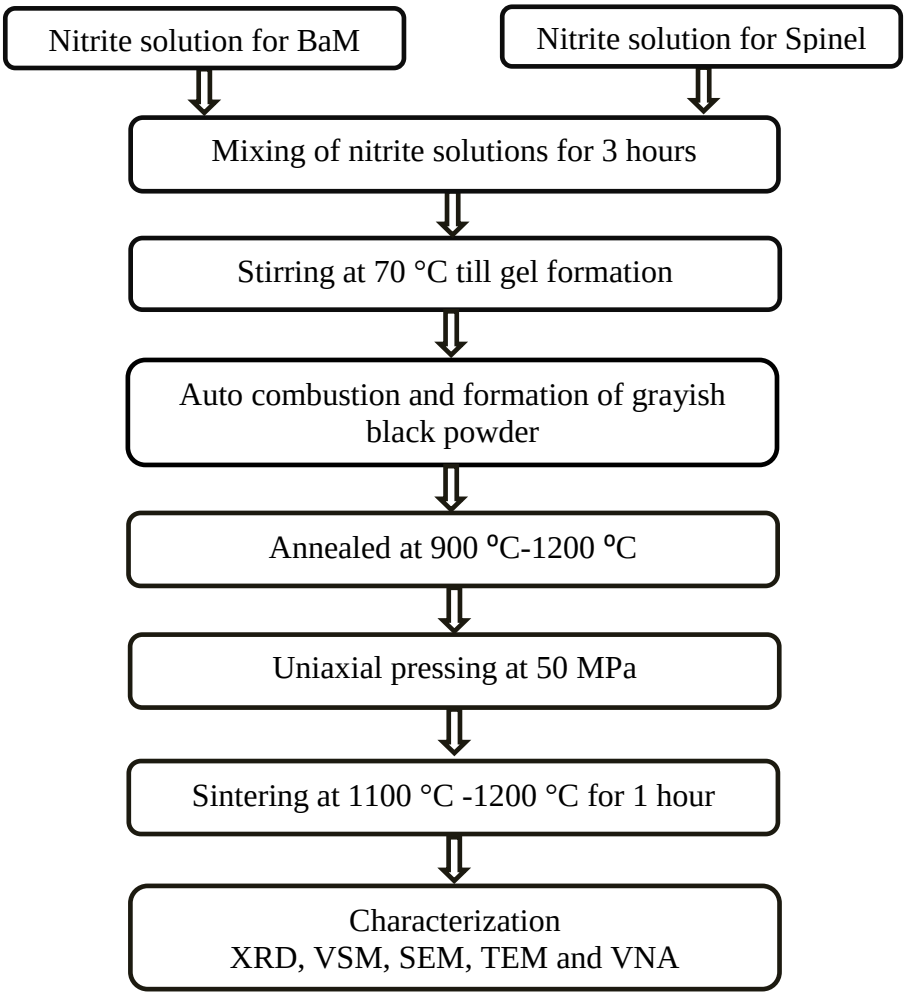


Fig. 3.3 Process flowchart of single-step method.

### 3.3 Processing of exchange-coupled thin films

First, sputtering targets (two inch dia.) of $BaFe_{12}O_{19}$ and $NiFe_2O_4$ were prepared by solid-state synthesis method. As prepared target were used for deposition of $BaFe_{12}O_{19}$, $NiFe_2O_4$, and $BaFe_{12}O_{19}/NiFe_2O_4$ thin film. Films on $Al_2O_3$ substrate were deposited by RF sputtering. Prior to film deposition base pressure was maintain better than $5.5*10^{-5}$ mbar. Pure and bilayer films were deposited at sputter pressure of $4.2*10^{-2}$ mbar in argon atmosphere for 60 minutes. Post deposition annealing of the films were carried out at 800 °C.

### 3.4 Material Characterization

The structural characterization of powders and composites were carried out by X-ray diffractometer (XRD), scanning electron microscope (SEM) and transmission electron microscope (TEM). To confirm the exchange coupling in composite ferrite room temperature **(***RT)* and high temperature (*HT*) magnetic studies were performed by vibrating sample magnetometer (VSM). *RT* microwave properties of composites were measured by vector network analyzer (VNA). The brief details for adopted characterization measurement are described below:

#### 3.4.1 X-ray Diffractometer (XRD)

The phase analysis of hexagonal, spinels and composites were carried out by X-ray diffractometer (XRD) model X'PERT Pro-Panalytical (PANalytical), using Cu-$K_{\alpha 1}$ radiation. The diffraction patterns were recorded at room temperature in 2θ range from 20° to 80° with a step size of 0.013°. The obtained diffraction peaks were matched with standard ICDD card no. 84-0757, 78-0133, 39-1433, 72-0738 for hexagonal $BaFe_{12}O_{19}$ (space group $P6_3/mmc$) and 74-2081, 44-1485, 74-1913, 52-0278, 52-0277 for spinel (space group Fd3m) phase. To calculate crystallite size (C.S); peak position 2θ (Bragg's angle) and full width at half maxima (FWHM) of the peaks were measured by X-ray line profile fitting technique using Gaussian function method. The average crystallite size of the samples was calculated from Scherrer formula [170] and define as:

$$C.S = \frac{k\lambda}{\beta\, Cos\theta} \tag{3.1}$$

where, k is dimensionless shape factor taken as 0.92 , λ is the wavelength (1.54 Å) , θ is

Bragg's angle in degree and β is FWHM of 2θ *vs.* intensity profile.

### 3.4.2 Scanning Electron Microscope (SEM)

The morphological and microstructural features of the fractured surfaces of the sintered sample were examined by scanning electron microscope (SEM) model JSM-1T100 at different magnification. Prior to SEM measurement, thin Au layer (< 5 nm) was deposited on sample surface by sputtering to avoid charging. Elemental compositions of composites were verified with energy dispersive spectroscopy (EDS) attached with SEM. To measure the grain size axio vision software was used.

### 3.4.3 Transmission electron microscope (TEM)

Transmission electron microscope (TEM) model (Tecnai G3, F30) was used to confirm the existence of hexagonal and spinel phases in the composite nanopowders. Prior to measurements, sonicate the sample for 20 minutes to disperse the particles in ethanol media. The dispersed particles were spread on copper coated TEM grid (200 mesh and 3 mm diameter).

### 3.4.4 Vibrating Sample Magnetometer (VSM)

Magnetic hysteresis (*M-H*) loops of the powders and composite were measured by (VSM) using Lake Shore model 7404 with maximum applied field of +10 kOe to -10 kOe. From the *M-H* loops; $M_s$, $H_c$, and $M_r$ of the composites were measured. The nature of exchange coupling in the composite was characterized by plotting switching field distribution (SFD) curves (d*M*/d*H vs* H) for second quadrant of *M-H* loop. Temperature dependent magnetization (*M-T*) measurements (300 K to 850 K) were carried out at 1000 Oe field. The Curie temperature ($T_c$) of composites were measured by plotting d*M*/d*T vs*. *T* curves. The sharp peak in the curve corresponded to $T_c$ of the respective material.

The in-plane magnetic measurement of the thin films was performed with maximum applied field of 1T.

### 3.4.5 Vector Network Analyzer (VNA)

Vector network analyzer (VNA) is widely used for high frequency dielectric measurements. VNA generally gives the frequency dependent scattering (S) parameters i.e. reflection ($S_{11}$) and transmission ($S_{21}$) coefficients.

VNA measurements in $K_u$-band (12.4 - 18 GHz) of sintered rectangular pellet (15.74 mm × 7.96 mm) were carried out by Agilent model N5225A PNA series. Prior to measurement two port calibrations was done on the test setup to eliminate error due to source/load mismatch and isolation [171]. The complex permittivity ($\mu_r = \mu' - j\mu''$) and permeability ($\varepsilon_r = \varepsilon' - j\varepsilon''$) was calculated by Agilent software module 85071 using obtained S parameters. Further, dielectric loss (tan $\delta_\varepsilon$) and magnetic loss tangent (tan $\delta_\mu$) were calculated from obtained $\mu$ and $\varepsilon$ using following equation:

$$\text{dielectric loss tangent}(\tan\delta_\varepsilon) = \frac{\varepsilon''}{\varepsilon'} \tag{3.2}$$

$$\text{magnetic loss tangent } (\tan\delta_\mu) = \frac{\mu''}{\mu'} \tag{3.3}$$

Frequency dependent reflection losses (*RL*) were also measured from *S*-parameters using following equations:

$$\text{Reflection loss (dB)} = 20\log_{10}|S_{11}| \tag{3.4}$$

$$\text{Transmission loss (dB)} = 20\log_{10}|S_{12}| \tag{3.5}$$

Reflection losses were simulated for different thickness by following equations:

$$\text{RL} = 20\log\left|\frac{(Z_{in} - Z_0)}{(Z_{in} + Z_0)}\right| \tag{3.6}$$

$Z_{in}$ is given by

$$Z_{\text{in}} = Z_0\sqrt{\frac{\mu_r}{\varepsilon_r}}\tanh\left\{j\left(\frac{2\pi f t}{c}\right)\sqrt{\mu_r\varepsilon_r}\right\} \tag{3.7}$$

where, $f$ is the frequency, $t$ is the thickness of sample, $c$ is the velocity of the light, $Z_0$ is the impedance of air and $Z_{in}$ is the input impedance at the absorber surface**.**

# *Chapter 4*

# Results and discussion

**Overview**

In this chapter, the structural, magnetic and microwave properties of hard/soft magnetic exchange-coupled composites are presented. The results are divided in five sections. In the first section, optimal conditions for preparation of pure hard and soft magnetic ferrites are discussed. Second section describes the effect of different processing methodology i.e. physical mixing and single-step method on exchange coupling. The variation in exchange coupling with annealing temperature is discussed in third section. In fourth subsection effect of weight fraction of soft phase on magnetic and microwave properties of composites are discussed. In fifth section effect of soft phase magnetization on exchange coupling and their respective change in magnetic and microwave properties are given. Finally, an attempt has also been made to deposit exchange-coupled $BaFe_{12}O_{19}/NiFe_2O_4$ bilayer thin films.

The obtained results from various studies are divided and discussed in the following section:

1. Preparation of single phase $BaFe_{12}O_{19}$ and spinel phase.
2. Effect of processing method.
3. Effect of annealing temperature.
4. Effect of soft phase weight fraction.
5. Effect of soft phase magnetization.

## 4.1 Preparation of single phase $BaFe_{12}O_{19}$ and spinel ferrite

To prepare hexagonal $BaFe_{12}O_{19}$ (BaM) and spinel phases, respective autocombusted powders were annealed at different temperature (950 °C - 1150 °C). Fig. 4.1 shows the XRD patterns of BaM and representative spinel phase annealed at 950 °C, 1050 °C and 1150 °C. It is observed that single hexagonal and spinel phase are formed for all studied temperature and average crystallite size were lie in the range of 25 nm to 45 nm. To select the appropriate temperature, the *M-H* loops of all annealed powders were measured and analyzed their magnetic properties. Fig. 4.2 shows the *M-H* loops of BaM, and representative spinel phases i.e. $NiFe_2O_4$ (NiF) and $Ni_{0.5}Zn_{0.5}F_2O_4$ (NZFO) powders. It is clear from the graphs that BaM shows characteristic feature of hard magnetic phase while NiF and NZFO shows the soft magnetic behaviour. Table 4.1 lists the magnetic properties of all annealed powders. From the table, it is well evident that within the studied temperature range maximum magnetization (*M*) of both ferrites were achieved at 1050 °C and selected as suitable annealing temperature for composite processing. Hence, remaining set of experiments were performed at 1050 °C by considering it optimal annealing temperature.

Table 4.1 Magnetization of BaM, NiF and NZFO powders.

| | **Magnetization (*M*) at 1T (emu/g)** | | | | |
|---|---|---|---|---|---|
| | 950 °C | 1000 °C | 1050 °C | 1100 °C | 1150 °C |
| BaM | 53.2 | 53.71 | 54.69 | 54.12 | 53.96 |
| NiF | 46.02 | 45.18 | 46.18 | 46.12 | 46.07 |
| NZFO | 73.15 | 73.55 | 74.41 | 73.74 | 71.36 |

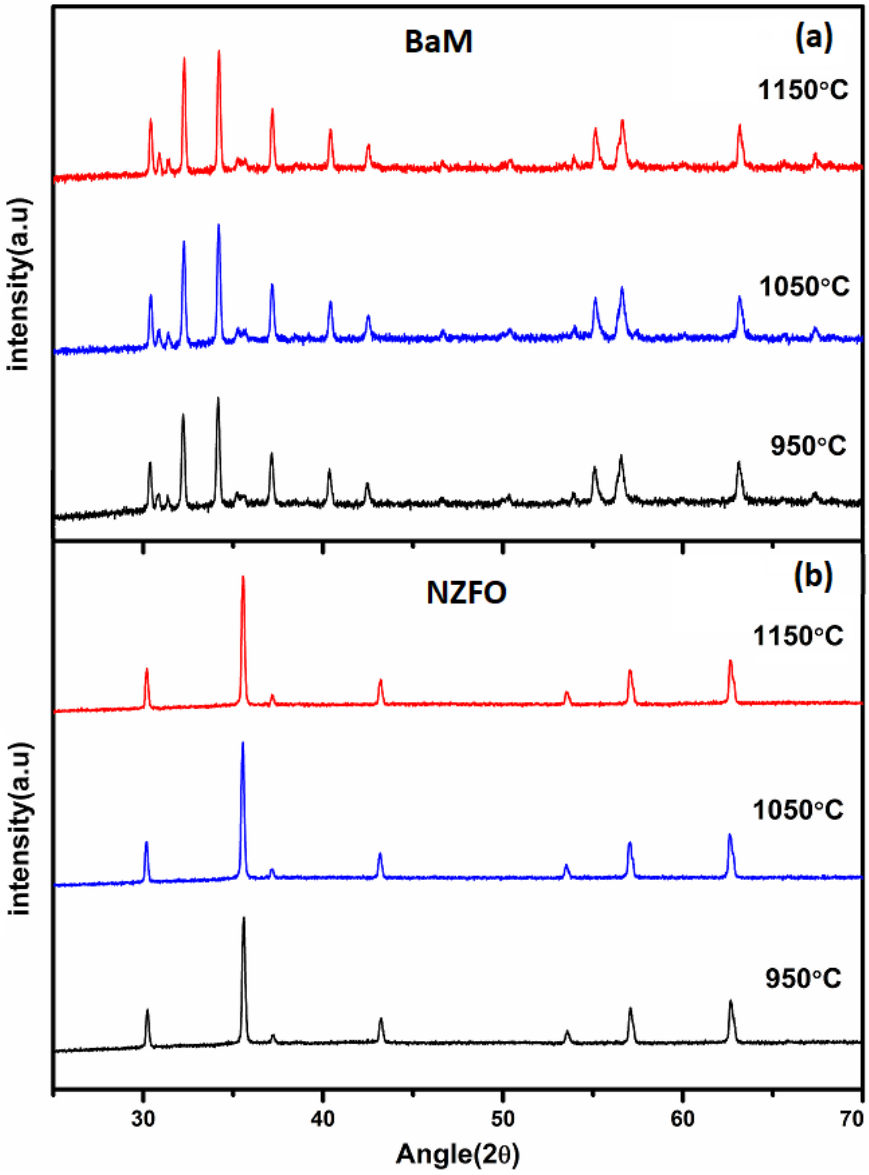


Fig.4.1. X-ray diffraction patterns of (a) BaM and (b) Spinel (NZFO) annealed at different temperature.

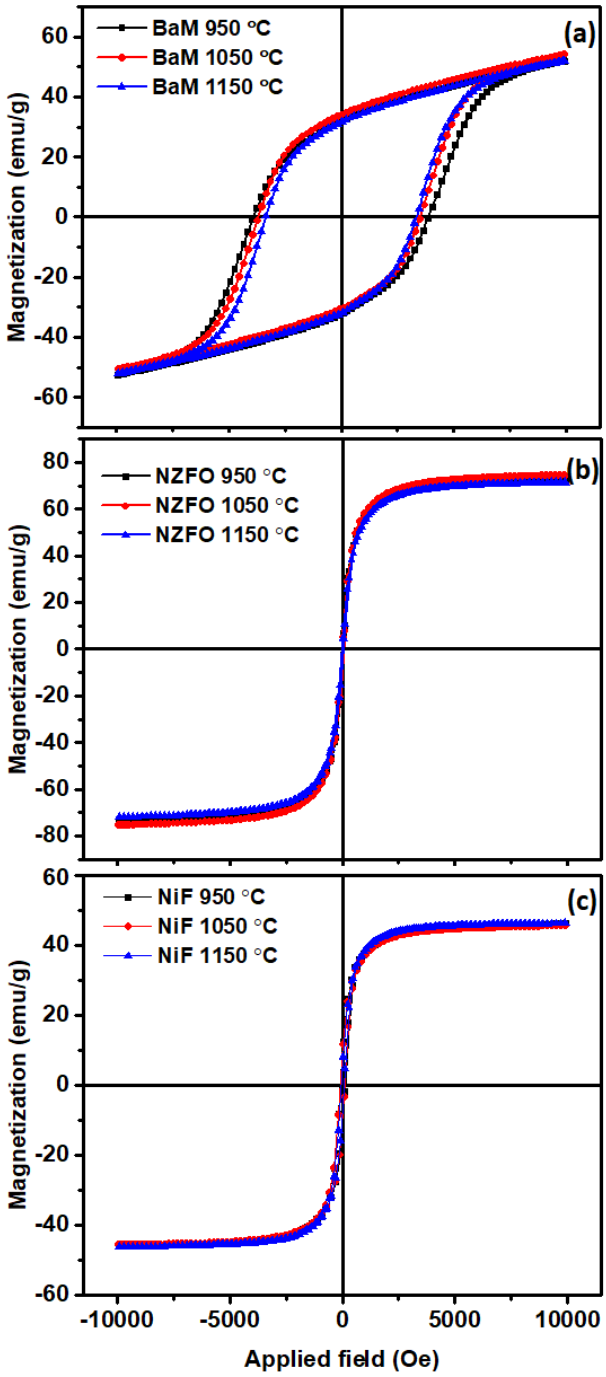


Fig. 4.2 Representative *M-H* loops of (a) BaM, (b) NZFO and (c) NiF nanopowders.

### 4.2 Effect of processing method

To understand the role of processing methodology on exchange coupling; series of BaM/NiF nanocomposites were prepared by physically mixing (PM) and single-step (SS) method. All composite powders were calcined at 1050 °C and sintered at 1100 °C in ambient atmosphere. Effect of processing method on structural, magnetic and microwave properties are systematically compared and shown in below section.

### 4.2.1 XRD analysis

Fig. 4.3 (a-c) shows the XRD patterns of pure BaM, NiF and BaM/NiF nanocomposites prepared by SS and PM methods. In pure BaM and NiF, all the diffraction peaks correspond to hexagonal (space group $P6_3/mmc$) and cubic (space group Fd3m) phases respectively without any impurity. Representative XRD patterns of composite confirmed the co-existence of BaM and NiF phases. From the figure, it is clear that the intensity of the NiF increases with the NiF content. All individual peaks of BaM and NiF in composites were considered for crystallite size (*C.S*) calculations. Average *C.S* for BaM (~45 nm) and NiF (~38 nm) phase in pure and composite samples found nearly same irrespective to processing method. Since *C.S* primarily depends upon the annealing temperatures, which are kept same (1050 °C) for both the methods.

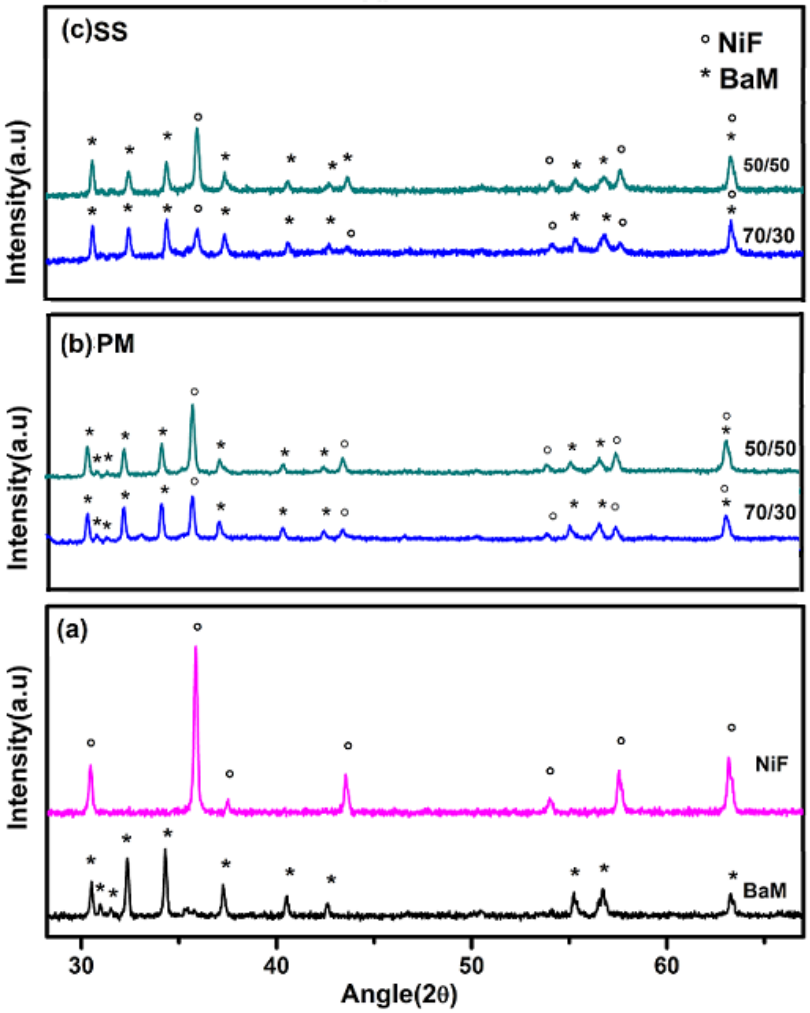


Fig. 4.3 X-ray diffraction patterns of (a) BaM and NiF (b) PM, & (c) SS nanocomposites with different composition.

### 4.2.2 Microstructure analysis

Fig. 4.4 (a-d) shows the SEM micrographs of pure BaM, NiF and SS 70/30, PM 70/30 composites sintered at 1100 °C. Microstructure of pure BaM shows large elongated grains with an aspect ratio ~ 3.0. Elongated grains are characteristic property of sintered BaM as observed earlier [172]. NiF grains are nearly spherical in shape with an average size of ~2 µm. On comparing the microstructural features of SS 70/30 and PM 70/30 composites (Fig. 4.4 (c-d)); the SS 70/30 shows the well distinguished grains of BaM and NiF. The larger grain corresponds to the BaM, while smaller represents the NiF phase. On other hand no well distinguished particles are observed in PM 70/30 composite. This shows that the processing method plays an important role in defining the microstructure of composite. The *C.S* of BaM and NiF in sintered composites are also calculated and found ~50 nm and ~45 nm respectively. A slight increase in *C.S*, as compared to powder, is due to the higher sintering temperature (1100 °C). Hence, the larger grains as observed by SEM in sintered samples are basically the agglomerates of several nanosize crystallites.

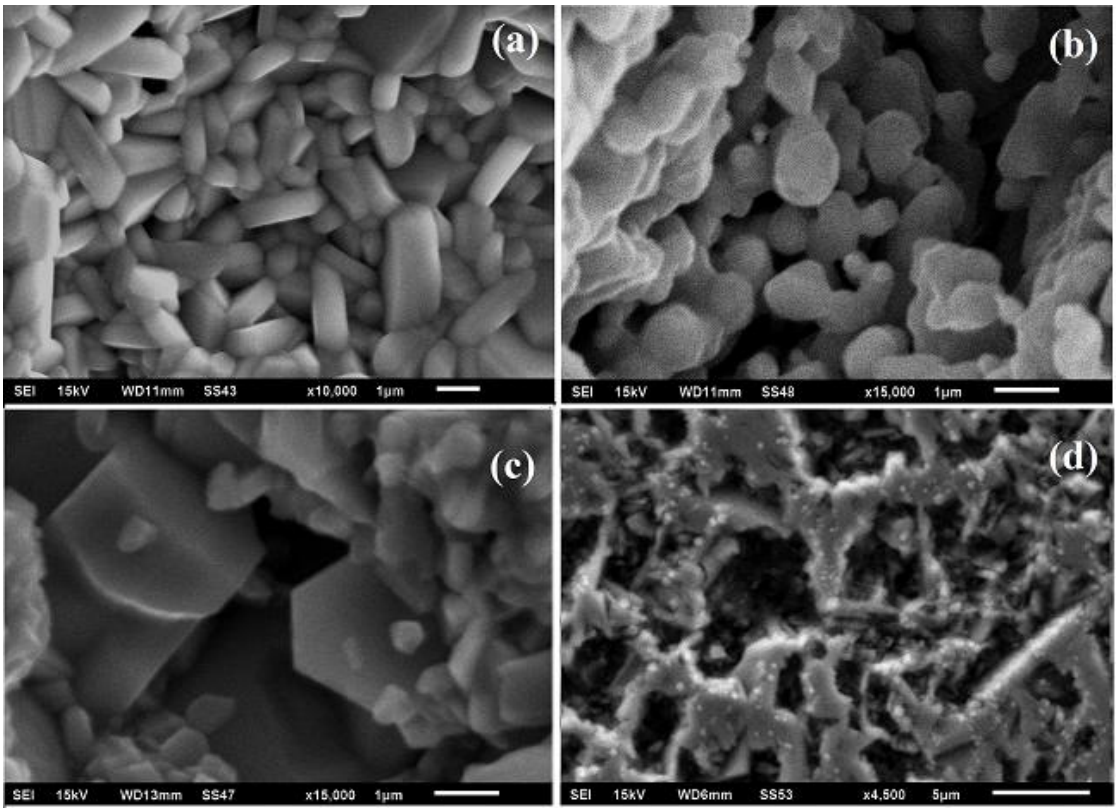


Fig. 4.4 SEM micrographs of (a) BaM , (b) NiF (c) SS 70/30 composite, and (d) PM 70/30 composite.

### 4.2.3 Magnetic measurements

Fig. 4.5 (a-f) shows the *M-H* behavior of pure BaM, NiF and nanocomposite samples prepared by SS and PM methods. BaM phase shows higher *M* compared to NiF and in agreement with the previously reported one [172,173]. *M-H* behavior of nanocomposites prepared by SS and PM methods are well distinct. In PM samples, stepped *M-H* loops were observed while SS composite shows a smooth curve without any step. Stepped *M-H* loops corresponds to the individual switching of hard and soft phases which is a characteristic behavior of uncoupled hard and soft phases. While the simultaneously switching of BaM and NiF suggest the existence of exchange coupling among the phases. The difference in the demagnetization behavior is interplay of three types of spin interactions in the composites i.e. between soft-soft phase, hard-hard phase and hard-soft phases. For exchange-couple systems, the interfacial interaction between hard and soft phases should be dominating. and grain size of soft phase should not be larger than the domain wall width of the hard phase [63,98]. If the spin interactions of individual phases are stronger than interfacial interaction, the independent switching of soft phase occurs at relatively lower field than that of hard phase. The observed step in demagnetization curve is consequence of spin torque effect of the soft phase on to hard phase [12]. The step is more pronounced in the composite with higher NiF content.

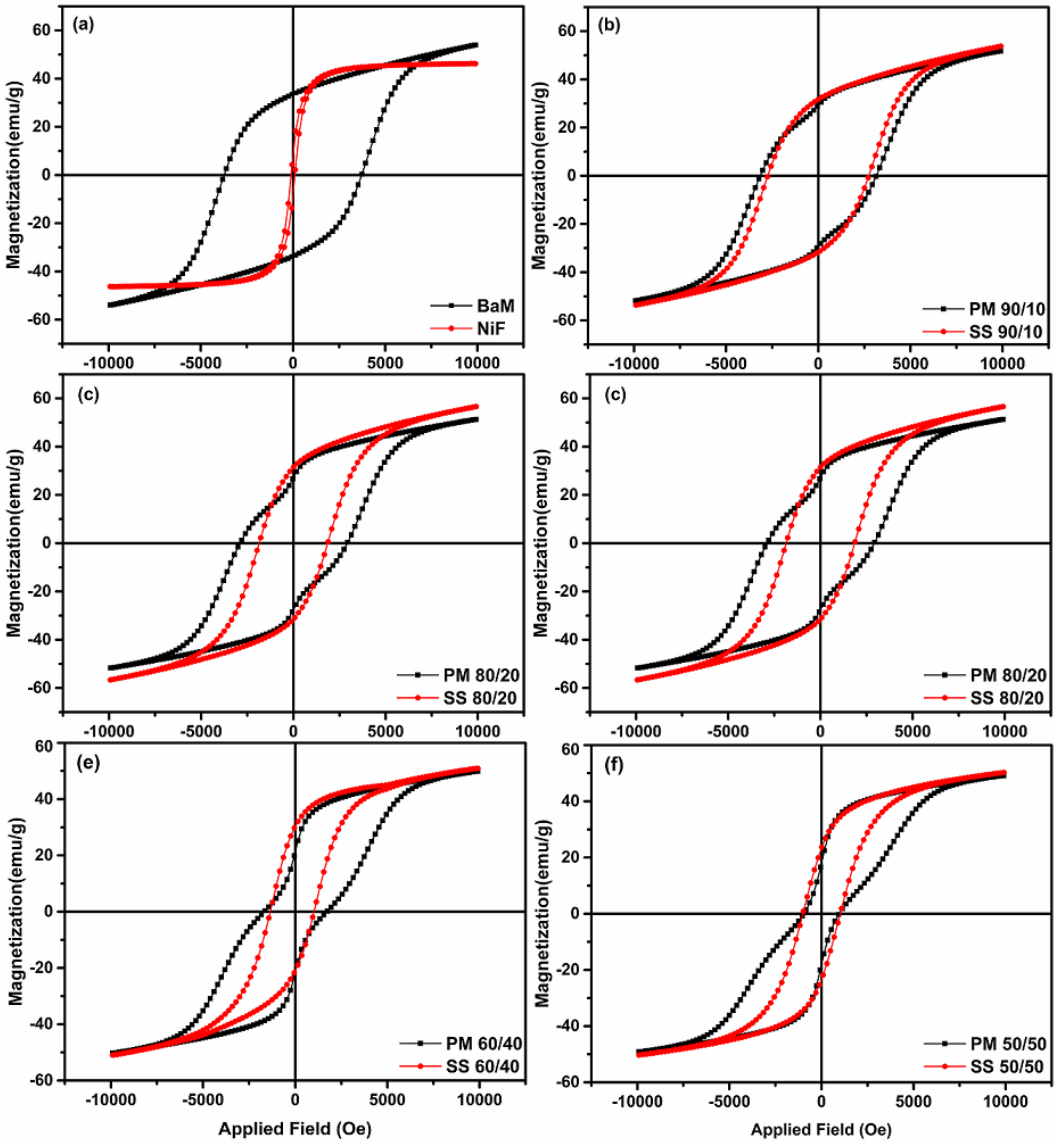


Fig. 4.5 Comparative *M-H* loops of (a) BaM & NiF, (b-f) SS & PM nanocomposites with different composition.

To confirm exchange coupling between hard and soft phases, switching field distribution (SFD) curves i.e. d*M*/d*H* *vs.* applied field of second quadrant were plotted for SS and PM nanocomposites (Fig. 4.6 (a & b)). Single peak in d*M*/d*H* for SS nanocomposites irrespective of composition indicates the strong exchange coupling between hard and soft phases. The SFD curves of PM composite shows two distinct peaks, which corresponds to individual switching of hard and soft magnetic spins.

Further, composites prepared by SS and PM were sintered, and their magnetic behavior was observed. Fig. 4.7 shows the representative *M-H* loops of PM 70/30 and SS 70/30 with a confirmation of distinct loop in the sintered composite magnets.

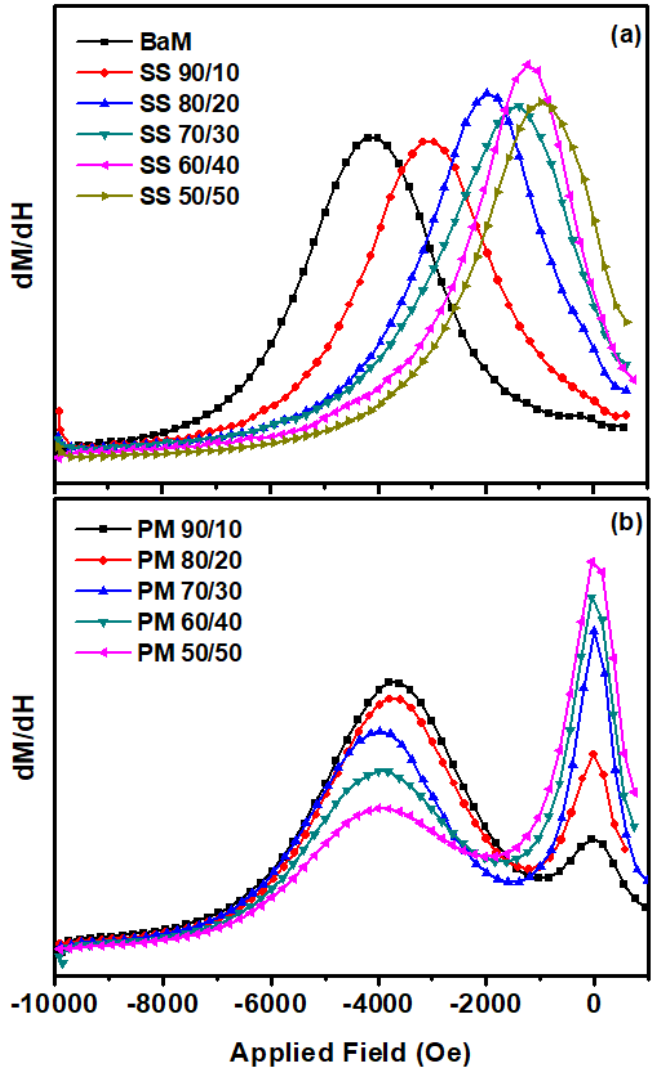


Fig. 4.6 d*M*/d*H vs.* applied field curves of (a) SS and (b) PM nanocomposites**.**

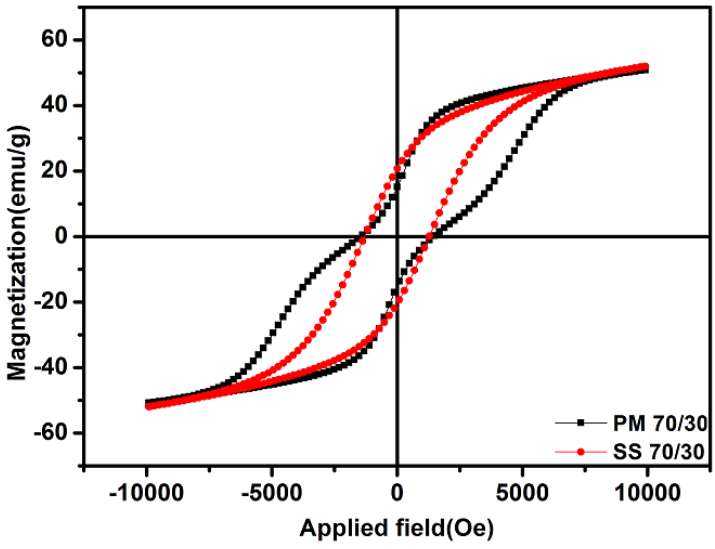


Fig. 4.7 *M-H* loops of PM 70/30 & SS 70/30 sintered composite magnets

Variation in magnetization ($M$), residual magnetization ($M_r$) and coercivity ($H_c$) with NiF content in SS and PM composites is shown in Fig. 4.8 (a-c)**.** It is well evident that $M$ and $M_r$ behavior are different for SS and PM samples. $M$ found to increase initially with the NiF content and then decrease, while a continuous decrease is observed for PM samples. For 70/30 composition, the $M$ and $M_r$ for SS composites are 57.7 emu/g and 30.1 emu/g respectively. While for PM composites low values of $M$ (50.6 emu/g) and $M_r$ (23.5 emu/g) are obtained. The high $M$ and $M_r$ of SS composites is a consequence of interfacial coupling driven alignment of more magnetic moments. Further, decrease in $M$ and $M_r$ is due to the higher NiF content which dominates over the exchange coupling dependent magnetization enhancement. On other hand, a linear decrease in $M$ and $M_r$ is observed in PM composites as it is well reported that non-exchange coupled system follows the rule of mixture [3]. Employing it in a present system, $M$ of composite can be expressed as:

$$M_C = (1 - x)M_{BaM} + xM_{NiF} \tag{4.1}$$

where, $M_{BaM}$ and $M_{NiF}$ are the measured $M$ of BaM and NiF respectively and $x$ is the weight fraction of NiF. Similarly, the $M_r$ and $H_c$ of composites can also be calculated. Therefore, the decrease in magnetic parameters ($M$, $M_r$) of PM composites is merely due to the low $M$ of NiF and decreases linearly with its content. $H_c$ is found to decrease with NiF content in both the samples due to its soft magnetic nature. However, exchange-coupled sample shows an asymptotic decrease in $H_c$ compared to linear decrease in non-coupled samples. This depicts that SS method is more appropriate for well exchange coupled system [136].

Fig. 4.8 (a-c) represents the experimentally observed and theoretically calculated values of $M$, $M_r$ and $H_c$. It is clear that experimentally observed magnetic properties for non-coupled composites are very close to theoretically calculated values while wide deviation is observed in exchange-coupled samples. In summary, exchange coupling among the BaM and NiF, strongly affect the magnetic properties of nanocomposite.

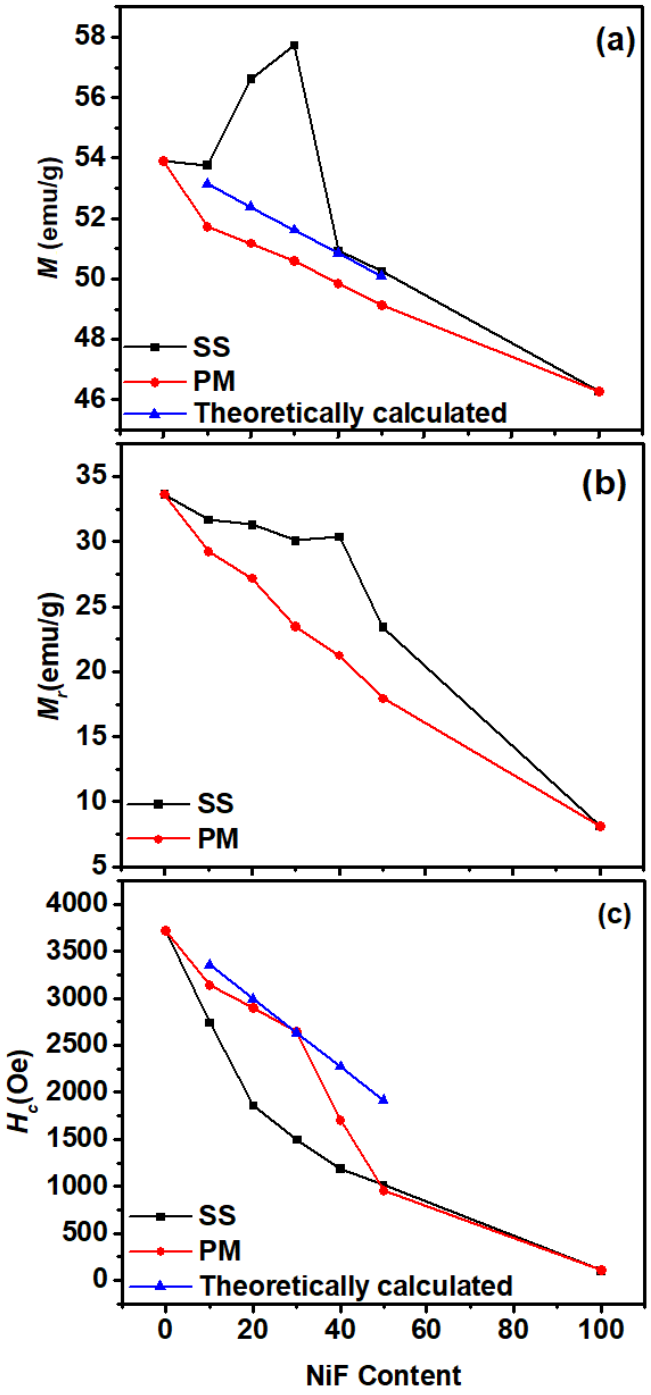


Fig. 4.8 (a-c) Variation in $M$, $M_r$ and $H_c$ with NiF content in SS and PM nanocomposites.

Fig. 4.9 shows the magnetization *vs* temperature ($M$-$T$) behavior of pure BaM, SS 70/30 and SS 50/50 at 1000 Oe. The decrease in $M$ with temperature is due to thermal effect. Curie temperature ($T_c$) is measured by plotting derivative of $M$ ($dM/dT$) with respect to $T$ (Fig 5(b)). The $T_c$ was also found to increase from 497 °C to 517 °C which also confirms the existence of exchange coupling between hard and soft phases.

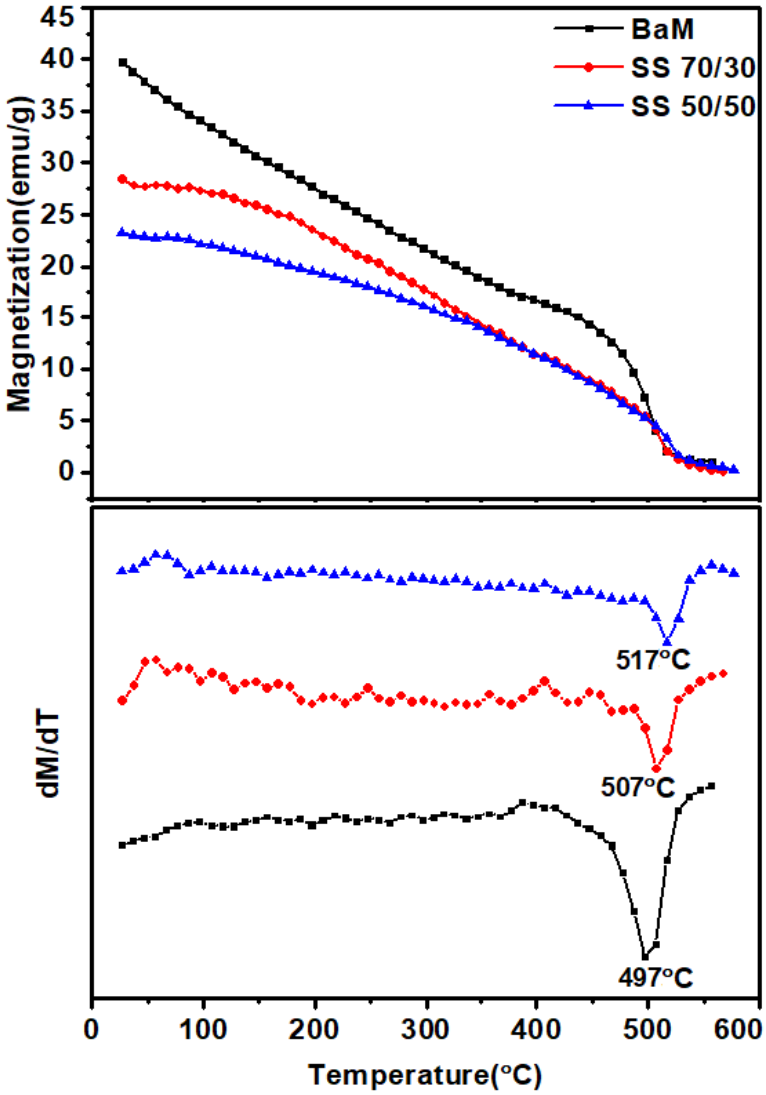


Fig. 4.9 High temperature *M-T* plots for BaM and SS 70/30 & SS 50/50 nanocomposites.

### 4.2.4 Microwave studies

*RT* microwave absorption properties of BaM, SS 70/30, SS 50/50, PM 70/30 and PM 50/50 were investigated by VNA in the frequency range of $K_u$-band (12.4-18 GHz). Complex permittivity ($\varepsilon$) and permeability ($\mu$) were calculated using Nicolson and Ross technique [174]. The variation of $\varepsilon$ and $\mu$ with frequency are shown in Fig. 4.10 (a-b)**.** From Fig. 4.10 (a) it is clear that the $\varepsilon$ of pure BaM is high as compared to the nanocomposites because of high uniaxial anisotropy and large $H_c$ of hexaferrites [175]. Nearly constant $\varepsilon$ is observed for PM composites in the measured frequency range and found to decreases with NiF content. On other hand, the large fluctuations in $\varepsilon$ spectra are observed in the SS composites. The SS 50/50 composition shows more variation in $\varepsilon$

between 13-16 GHz frequency range. As in exchange-coupled system, the spin-spin interaction or interfacial dipoles may exist and in phase at a particular applied field frequency, which are responsible for the observed peaks in permittivity spectra. Fig. 4.10 (b) shows the permeability spectra of BaM and nanocomposite samples. It is clear from the figure that permeability spectrum of BaM, PM 70/30 and SS 70/30 are nearly same (1.18 to 1.25 at 12.4 GHz) and shows the similar behavior with frequency. However, a slight variation in $\mu$ with composition and processing is ascribed to different magnetization behaviour of PM and SS composites.

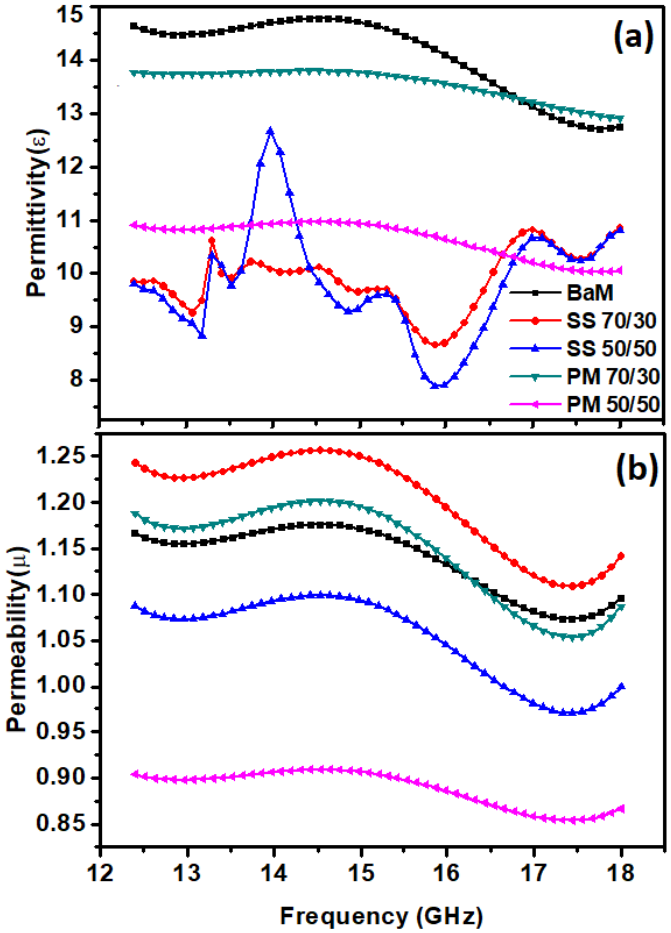


Fig. 4.10 (a) Complex permittivity ($\varepsilon$) & (b) Complex permeability ($\mu$) of BaM, SS 70/30, SS 50/50, PM 70/30 & PM 50/50 nanocomposite.

Reflection loss *vs.* frequency plots for BaM and nanocomposites are shown in Fig. 4.11. The dip of the plots demonstrates the minimum reflection loss (*RL*) and maximum absorption. It was observed that with increasing the NiF content, microwave absorption properties were decreased in the studied frequency range. The observed minimum *RL* of pure BaM was -27.6 dB at 13.2 GHz frequency. For composite SS 70/30, *RL* are found at

5.3 GHz and 16.3 GHz, whereas PM 70/30 shows loss at only 13.2 GHz. The SS 50/50 composite exhibits losses at 13.9 GHz, 16.7 GHz and 17.5 GHz. PM 50/50 composites exhibits *RL* at 17 GHz. The observed loss peaks for the SS composites gets shifted to the higher frequency bands as compared to the pure BaM and PM nanocomposites. This enhancement in matching frequency in nanocomposites prepared by SS method might be due to the exchange coupling between hard and soft ferrite. The reflection and absorption loss can further be improved by varying the thickness of the sample [135].

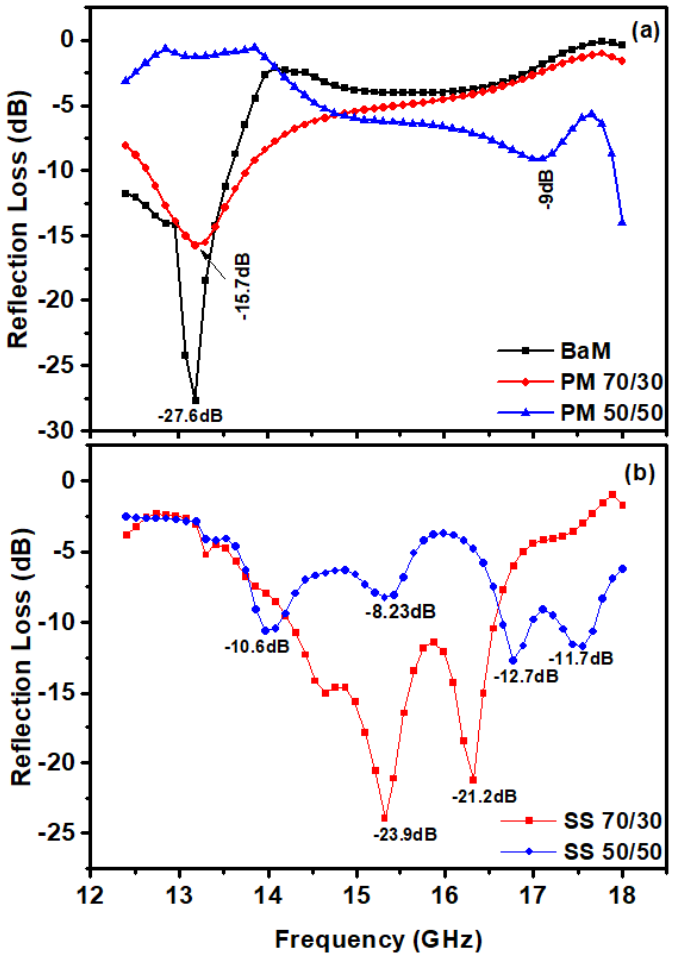


Fig. 4.11 Reflection loss *vs.* frequency plots for (a) BaM, PM 70/30, PM 50/50 & (b) SS 70/30, SS 50/50 nanocomposites.

The obtained magnetization behaviour, magnetic and microwave properties evidence that single-step sol gel method is appropriate methodology to obtain exchange–coupled composite. To verify the role of processing method, BaM/$Ni_{0.5}Zn_{0.5}Fe_2O_4$ (NZFO) series were also prepared by PM method. *M-H* loops and respective SFD curves (Fig. 4.12) also confirmed that PM method is not an adequate way to obtain exchange-coupled composite

and is independent of soft magnetic phase.

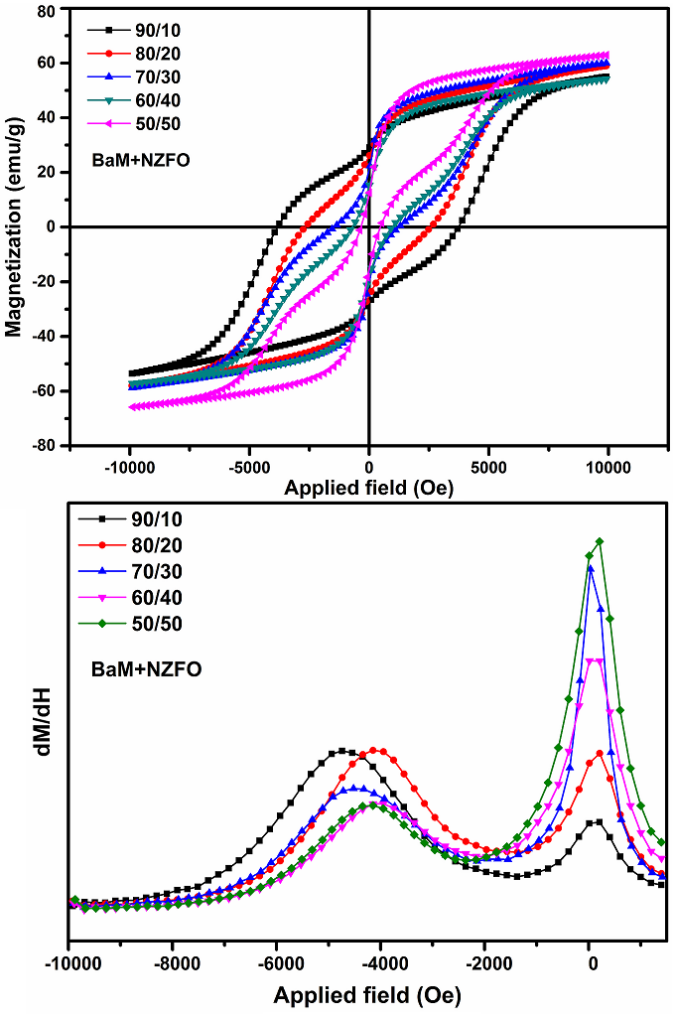


Fig. 4.12 *M-H* loops and SFD curves of physically mixed BaM/NZFO nanocomposite.

### 4.3 Effect of annealing temperature

Apart from the adopted processing methodology; annealing temperature of ferrite nanopowders is also one of the process parameter to influence their structural, magnetic and microwave properties. To study the effect of annealing temperature on exchange coupling; BaM/NZFO nanocomposite in the weight ratio of 70/30 were prepared by single-step sol-gel method and annealed at 950 °C, 1000 °C, 1050 °C, 1100 °C, 1150 °C and 1200 °C. Their structral, magnetic and microwave properties have been compared and described in the given section.

### 4.3.1 XRD analysis

XRD patterns of BaM/NZFO nanocomposites annealed at 950 °C, 1050 °C and 1150 °C are shown in Fig. 4.13. The XRD peaks confirm co-existence of both BaM and NZFO phases. The average *C.S* for BaM & NZFO peaks in composites was calculated and shown in Table 4.2. The minimum *C.S* of NZFO and BaM in the nanocomposite was 29 nm and 21 nm at 1050 °C respectively.

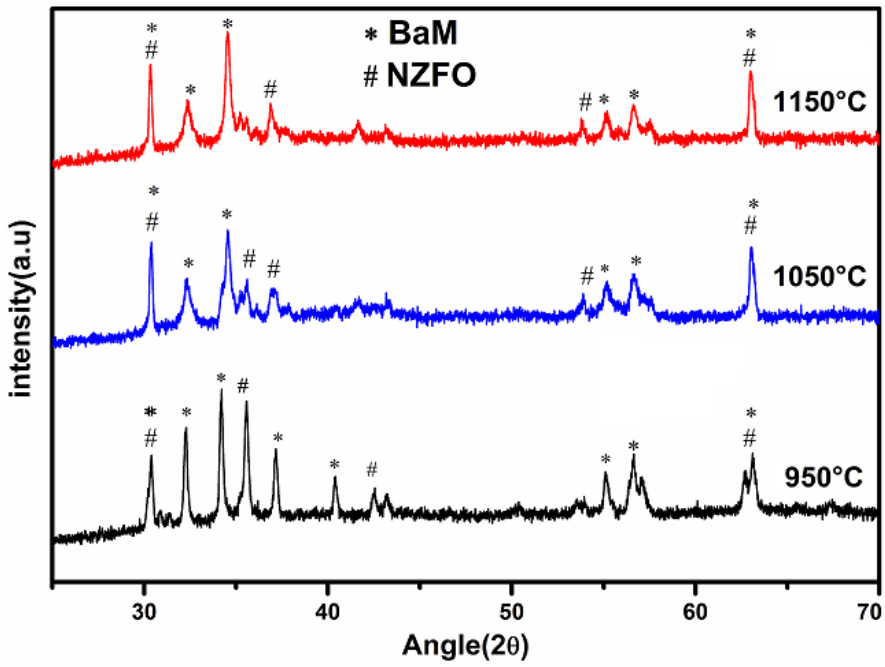


Fig. 4.13 X-ray diffraction patterns of BaM/NZFO nanocomposite annealed at 950 ºC, 1050 ºC and 1150 ºC.

Table 4.2 Crystallite size of BaM and NZFO in composite with annealing temperature

| **Temperature**(°C) | **Crystallite Size(nm)** | |
|---|---|---|
| | NZFO | BaM |
| 950 | 36.7 | 40.1 |
| 1050 | 29.4 | 20.7 |
| 1150 | 34.0 | 29.3 |

### 4.3.2 Microstructure analysis

Fig. 4.14 (a & b) shows TEM micrographs of BaM and BaM/NZFO nanocomposite powders. In BaM; all particle shows hexagonal morphology. In composite (Fig. 4.14(b)) smaller NZFO particles are coagulated with larger BaM particles. The stacking of particles is due to their mutual magnetic attraction [176].

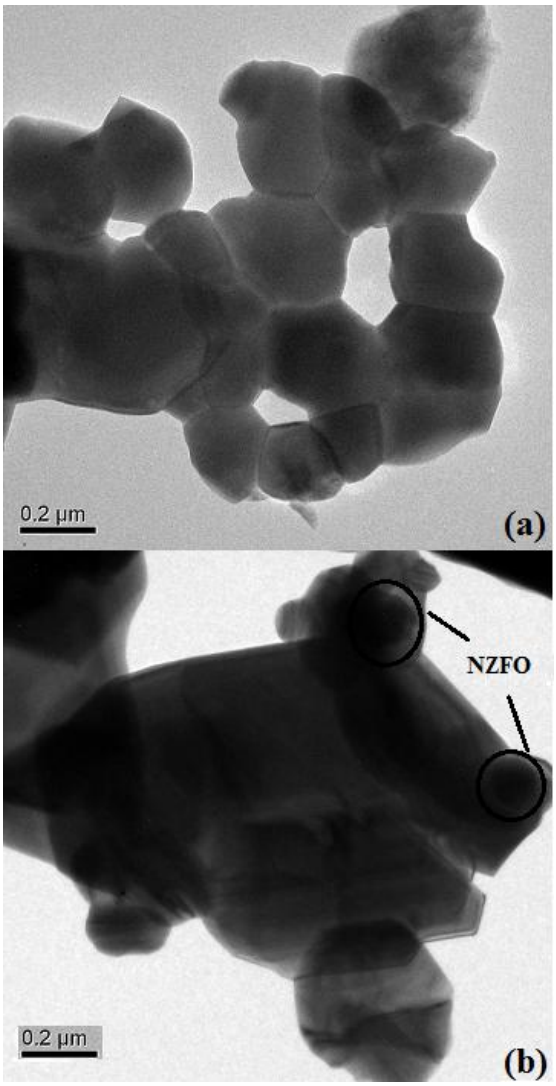


Fig. 4.14 TEM micrographs of (a) BaM (b) BaM/NZFO nanocomposite powders annealed at 1050 ºC.

Fig. 4.15 (a-c) shows the fractured surface micrographs of NZFO, BaM and BaM/NZFO composite sintered at 1200 ºC. Microstructure of NZFO shows well distinguished equiaxed grains whereas, BaM shows randomly oriented elongated grains. The microstructure of composite shows distinct feature from BaM and NZFO with cleavage fracture and smaller grains. All microstructure shows dense morphology without any measurable porosity.

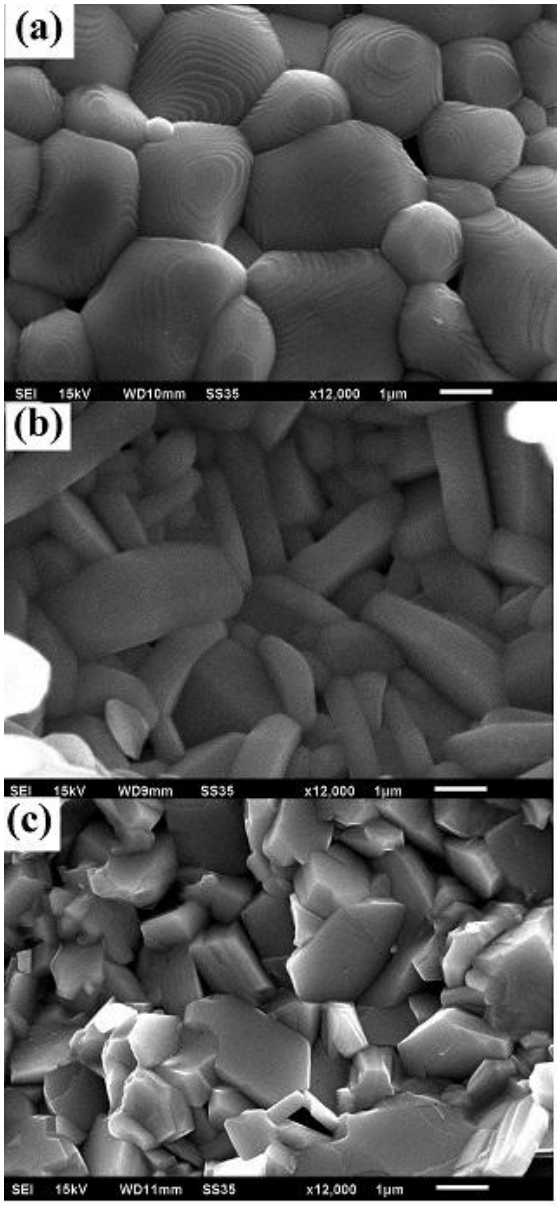


Fig. 4.15 SEM micrographs of (a) NZFO, (b) BaM and (c) BaM/NZFO nanocomposite annealed at 1050 ℃ and sintered at 1200 ℃.

### 4.3.3 Magnetic measurements

Fig. 4.16 (a-c) shows the representative *M-H* plots of NZFO, BaM and BaM/NZFO composite powders annealed at different temperature ranging from 950 °C - 1200 °C. Higher *M* of NZFO compared to BaM is in agreement with previous studies [177,178].

*M-H* loops of nanocomposites showed coherent demagnetization due to simultaneous switching of NZFO and BaM spins. The observed switching suggests that the system is well exchange-coupled in the studied temperature range. It is well reported that non-exchange coupled system shows a kink or shoulder in demagnetization curve[101].

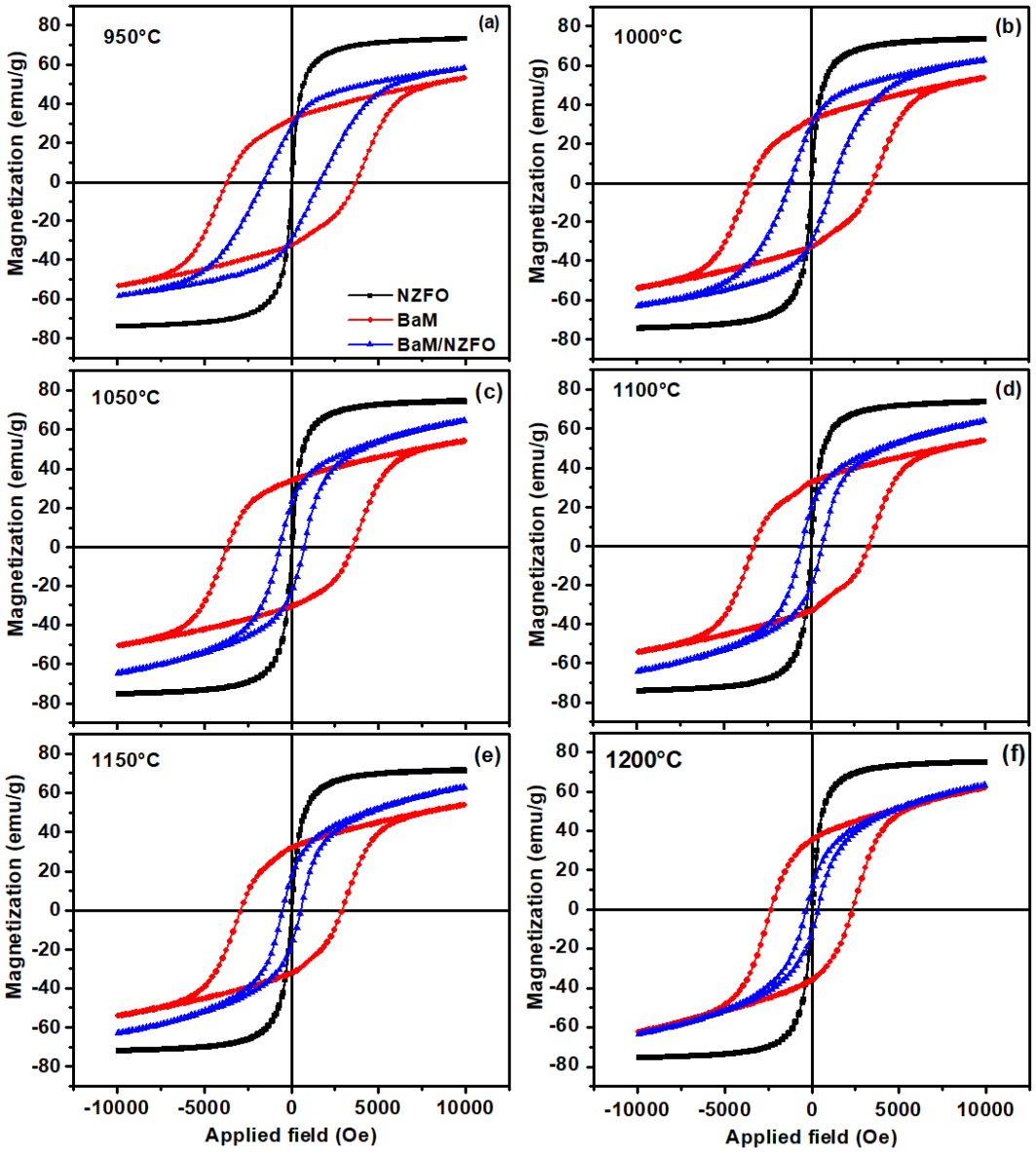


Fig. 4.16 Comparative *M-H* loops of BaM, NZFO and BaM/NZFO nanocomposite powders annealed at different temperature.

Variation in $M$ and $H_c$ for BaM, NZFO and BaM/NZFO nanocomposite as a function of annealing temperature are shown in Fig. 4.17 (a & b). $M$ and $H_c$ were also theoretically calculated using equation 4.2 [3].

$$M = 0.7M_{BaM} + 0.3M_{NZFO} \quad (4.2)$$

where, $M_{BaM}$ and $M_{NZFO}$ are the measured $M$ of BaM and NZFO respectively. Similarly, theoretical $H_c$ was calculated and compared to experimental values.

The $M$ of BaM and NZFO increase with annealing temperature and then decrease (Fig.

4.17 (a)). The maximum observed values for BaM and NZFO at 1050 °C is 54.7 emu/g and 74.4 emu/g respectively. The increase in *M* with temperature is due to the distribution of cations at ferromagnetically favourable sites. A drastic increase in *M* of BaM/NZFO nanocomposite has been observed with temperature from 950 °C to 1050 °C (58 emu/g to 65 emu/g) followed by slight decrease. At 1150 °C and 1200 °C no change in *M* was observed. It is well evident that experimentally observed *M* of nanocomposites are higher than theoretically calculated, which suggests that system is well exchange- coupled. Also, the variation in *M* with temperature reflects that extent of exchange coupling is temperature dependent. Since the coupling between phases is interfacial in nature; therefore powders with optimum crystallite size may prevail higher exchange coupling. The high *M* of nanocomposite at 1050 °C is ascribed to higher coupling associated with minimum crystallite size of BaM and NZFO phase (Table 4.2).

Contrary to magnetization behavior, the $H_c$ values of nanocomposite are well below the theoretically calculated values for studied temperatures. The $H_c$ is primarily governed by crystal anisotropy and particle/crystallite size of magnetic phases. Since the composition of BaM/NZFO is constant, hence the role of crystal anisotropy of the composite on $H_c$ can be ignored. A sharp decrease in $H_c$ of nanocomposite with temperature may ascribe to variation in crystallite size (Table 4.2). However, a minimum $H_c$ value is observed for the composite with lower crystallite size suggests the dominance of exchange coupling over structural parameters. Therefore, low $H_c$ of nanocomposites than the theoretically calculated values may due to strong intervening coupling between the phases where switching of soft magnetic spins at low nucleation field drive away the hard magnetic spins.

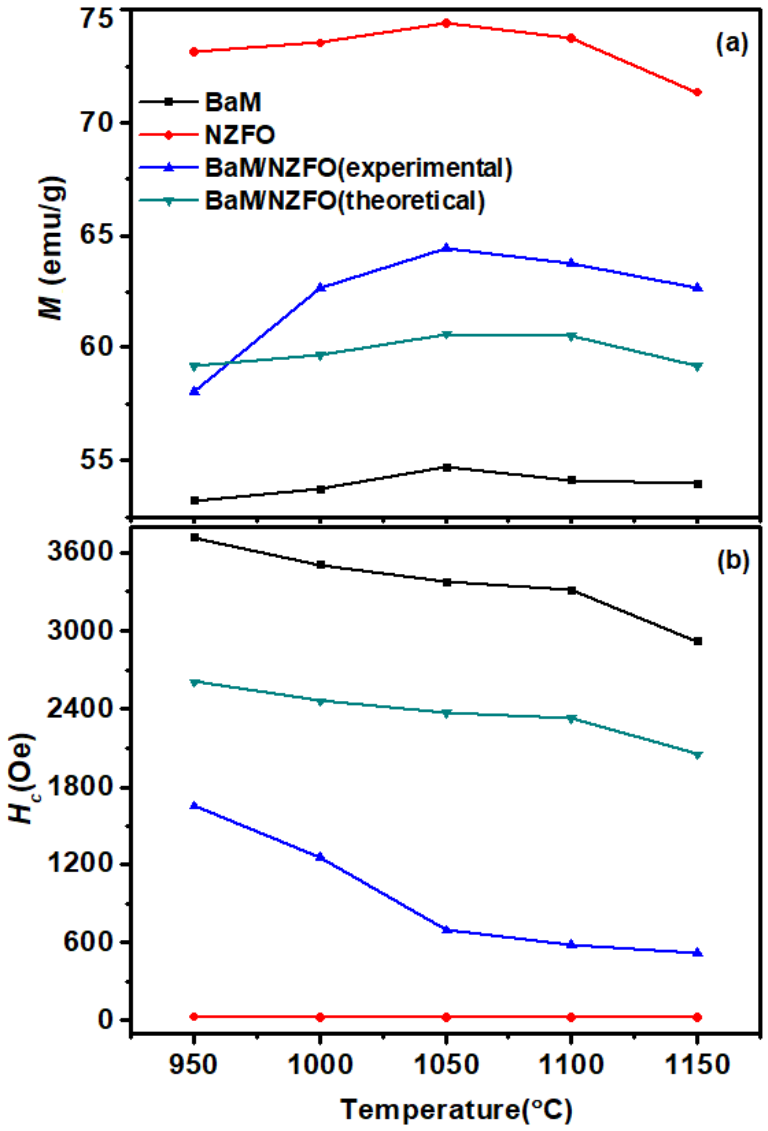


Fig. 4.17 Variation in theoretical and experimentally observed (a) *M* and (b) $H_c$ of BaM. NZFO and BaM/NZFO powders with annealing temperature.

The *M*-*T* plots of BaM, NZFO and BaM/NZFO nanopowders annealed at 1050 °C are shown in Fig. 4.18 (a). The sharp dip represents the $T_c$ of respective phases. The $T_c$ for BaM and NZFO was found to be 497 °C and 337 °C respectively. The observed $T_c$ for exchange-coupled nanocomposite is 473 °C which is close to BaM due to its higher weight fraction. For non-exchange coupled system independent values of $T_c$ for NZFO (347 °C) and BaM (527 °C) were observed as shown in Fig. 4.18 (b). A single $T_c$ value for BaM/NZFO nanocomposite also demonstrates that the phases are well exchange-coupled.

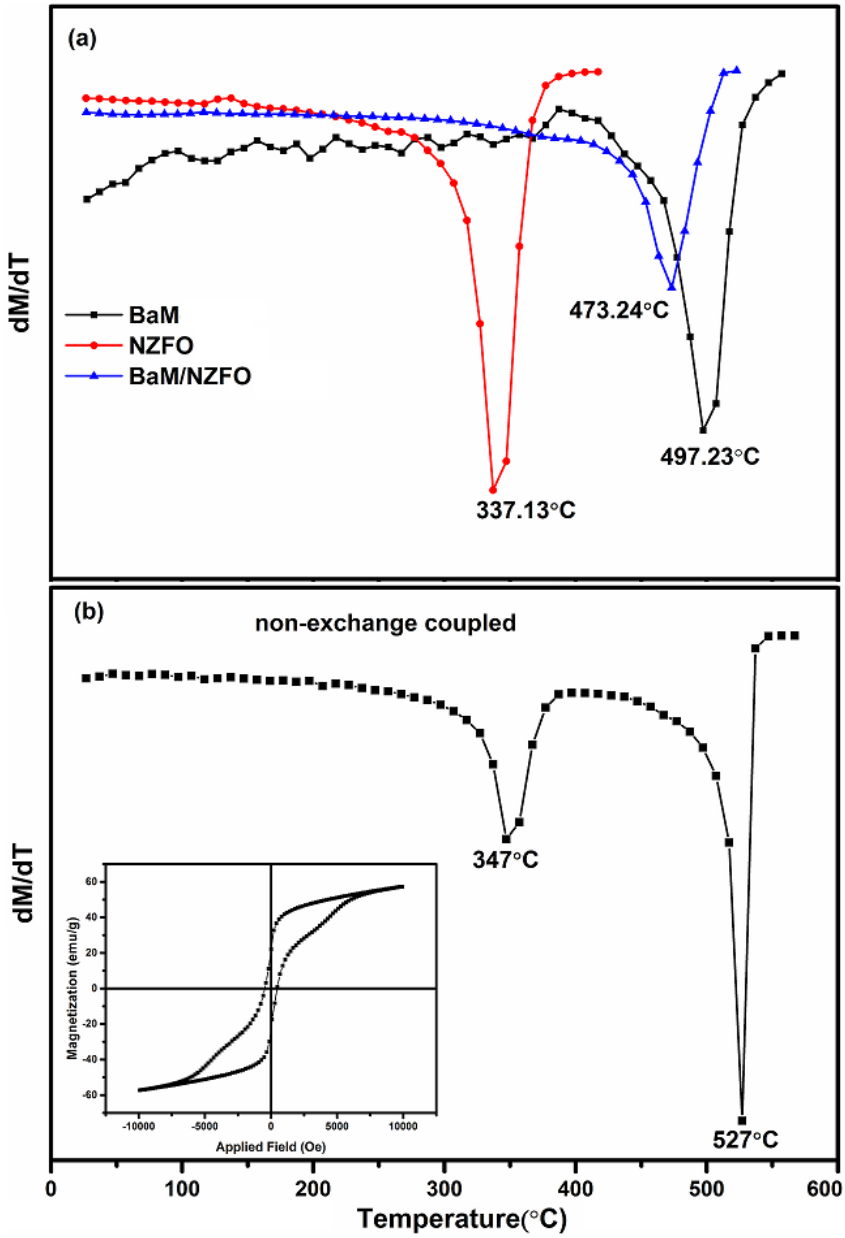


Fig. 4.18 (a) High temperature *M-T* plots for BaM, NZFO and BaM/NZFO annealed at 1050 °C, (b) *M-T* plot and *M-H* loop (inset) for non-exchange coupled BaM/NZFO.

Similar, temperature dependent magnetic properties were also studied for BaM/NiF and BaM/$CoFe_2O_4$(CFO) composite system. The representative *M-H* plots for BaM/NiF, BaM/CFO composite are shown in Fig. 4.19 (a & b) and obtained magnetic parameters are tabulated in Table 4.3. The high magnetization of 1050 °C annealed BaM/NiF and BaM/CFO nanocomposites was also ascribed to higher coupling as observed in BaM/NZFO.

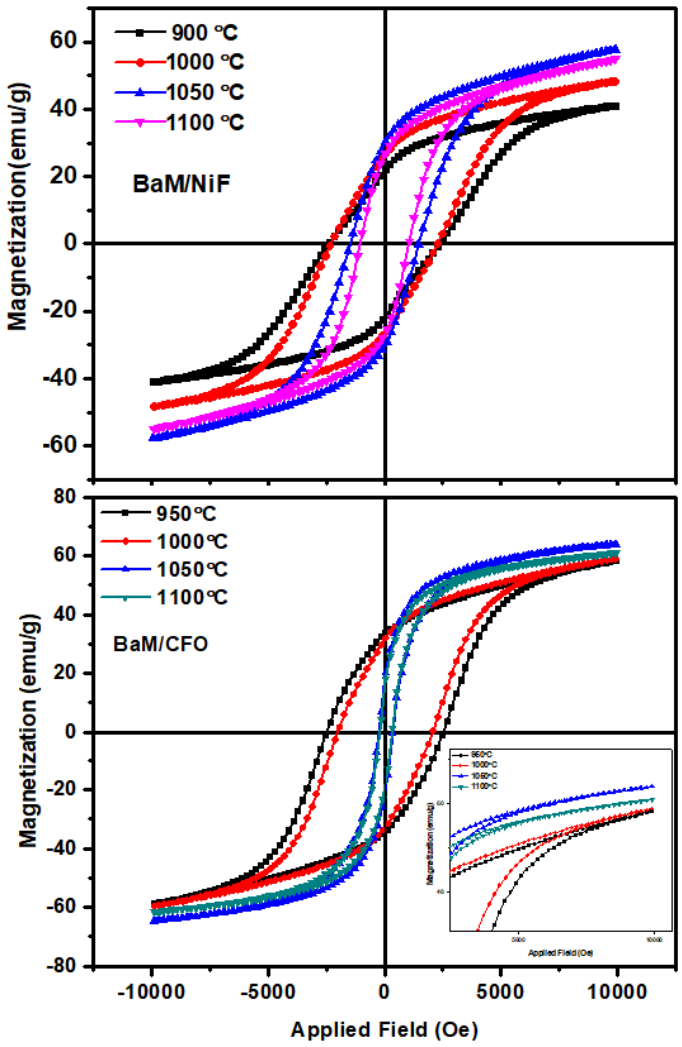


Fig. 4.19 *M-H* loops of (a) BaM/NiF (70/30) and (b) BaM/CFO (70/30) composites annealed at 950 °C, 1000 °C, 1050 °C and 1100 °C.

Table 4.3 Magnetic properties of BaM/NiF and BaM/CFO composites.

| **BaM/NiF** | | | | |
|---|---|---|---|---|
| | 950 °C | 1000 °C | 1050 °C | 1100 °C |
| $M$ (emu/g) | 41.10 | 48.40 | 57.74 | 54.91 |
| $H_c$ (Oe) | 2395 | 2303 | 1493 | 1077 |
| $M_r$ (emu/g) | 21.96 | 26.53 | 29.93 | 26.53 |
| **BaM/$CoFe_2O_4$** | | | | |
| | 950 °C | 1000 °C | 1050 °C | 1100 °C |
| $M$ (emu/g) | 58.36 | 58.90 | 64.01 | 60.94 |
| $H_c$ (Oe) | 2518 | 2058 | 287 | 256 |
| $M_r$ (emu/g) | 33.82 | 32.03 | 19.41 | 16.90 |

### 4.3.4 Microwave studies

Microwave properties for BaM and BaM/NZFO composite annealed at 950 °C, 1050 °C and 1150 °C were measured in $K_u$-band. Fig. 4.20 shows the variation of magnetic loss tangent (tan $\delta_\mu$) with frequency. For BaM, tan $\delta_\mu$ remains constant in studied frequency range, however, low losses were observed for the samples annealed at higher temperature. For BaM/NZFO composite; variation in tan $\delta_\mu$ along with resonance peaks at different frequency were observed. Sample annealed at 950 °C showed a sharp resonance peak at 16 GHz. However, composites annealed at 1050 °C and 1150 °C showed resonance peaks in broad frequency range. In the composite system, spin-spin interaction and interfacial dipole may exist and are in phase at a particular applied field, which are responsible for peaks in loss tangent. Also, resonance peaks found to shift towards lower frequency with annealing temperature. The observed variation in tan $\delta_\mu$ may arise due to varied exchange coupling between hard/soft phases.

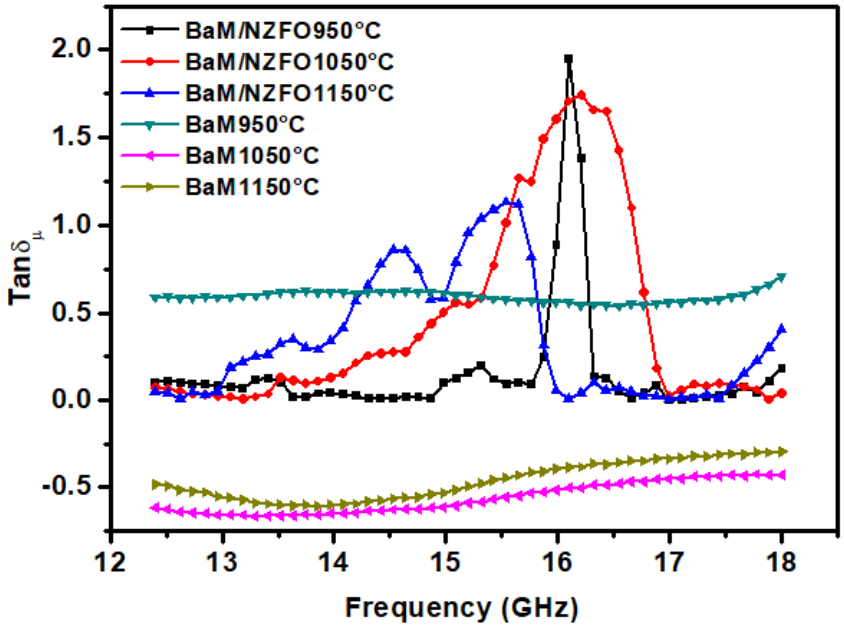


Fig. 4.20 Frequency dependent magnetic losses of BaM and BaM/NZFO nanocomposites annealed at 950 ºC, 1050 ºC and 1150 ºC.

Fig. 4.21 shows the reflection loss plots for sintered BaM and BaM/NZFO. For BaM, no losses were observed in the studied frequency band (12.4-18 GHz) irrespective to annealing temperature. The absence of reflection dip may ascribe to higher FMR frequency of BaM (36-43 GHz) [30,179]. The composites annealed at 950 °C, 1050 °C and 1150 °C showed well defined *RL* dips at 16.9 GHz, 15.8 GHz and 16.3 GHz

respectively. The *RL* are well above -10 dB (absorption more than 90%) with a maximum value of -38 dB for composite annealed at 1050 °C. It is also evident that the *RL* frequency depends upon the coupling, since sample with higher exchange coupling (annealed at 1050 °C) shows losses at lower frequency. The results suggest that the extent of exchange coupling depends on annealing temperature and hence affect absorption losses. Compared to BaM, the loss peaks for composites system observed at lower frequencies as a consequence of lower ferromagnetic frequency of NZFO. Such composite could play a dominant role in microwave device application with tunable frequency.

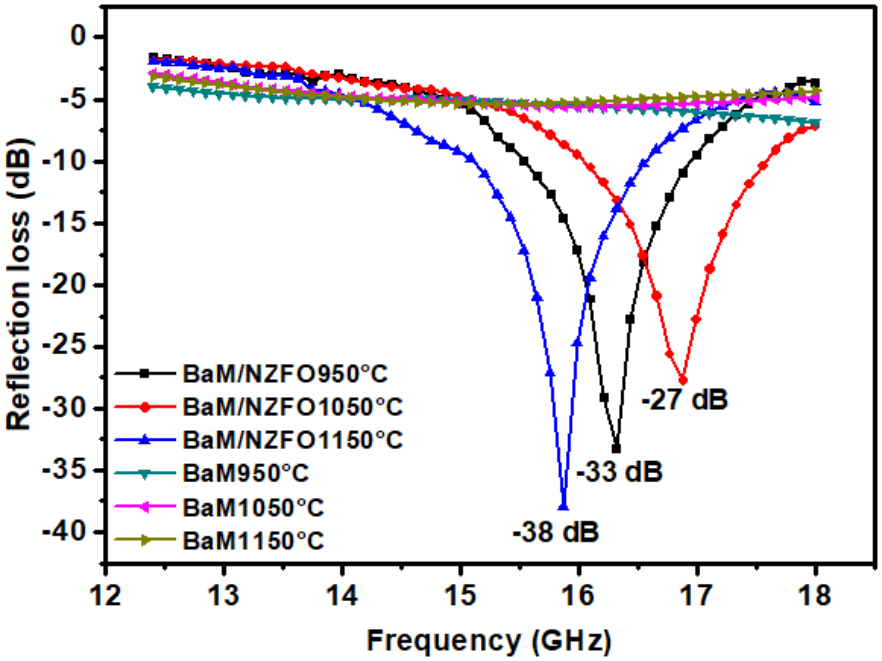


Fig. 4.21 Reflection loss *vs.* frequency plots for BaM and BaM/NZFO nanocomposites annealed at 950 ºC, 1050 ºC and 1150 ºC.

### 4.4 Effect of soft phase weight fraction

To understand the effect of soft phase weight fraction, three series of exchange-coupled composites BaM/NZFO, BaM/$CoFe_2O_4$(CFO) and BaM/$Co_{0.5}Zn_{0.5}Fe_2O_4$ (CZFO) with different soft phase content were prepared. The effect of weight fraction of soft phase on structural, morphological, magnetic and microwave properties were investigated.

### 4.4. 1 BaM/NZFO series

#### 4.4.1.1 XRD analysis

Fig. 4.22 shows the representative XRD patterns of BaM/NZFO composite powders for the 70/30 and 50/50 weight ratio. XRD patterns confirmed the co-existence hexagonal and spinel phases in the composites. No intermediate phase was formed during annealing and sintering of composites. The NZFO peak intensity found to increase with its content. All individual peaks of BaM and NZFO were considered for *C.S* calculations. Table 4.4 shows the average *C.S* calculated for different composition. It is clear that the *C.S* is independent to the relative weight ratio. Since the annealing temperature is constant (1050 °C), therefore no obvious changes in *C.S* were on expected lines.

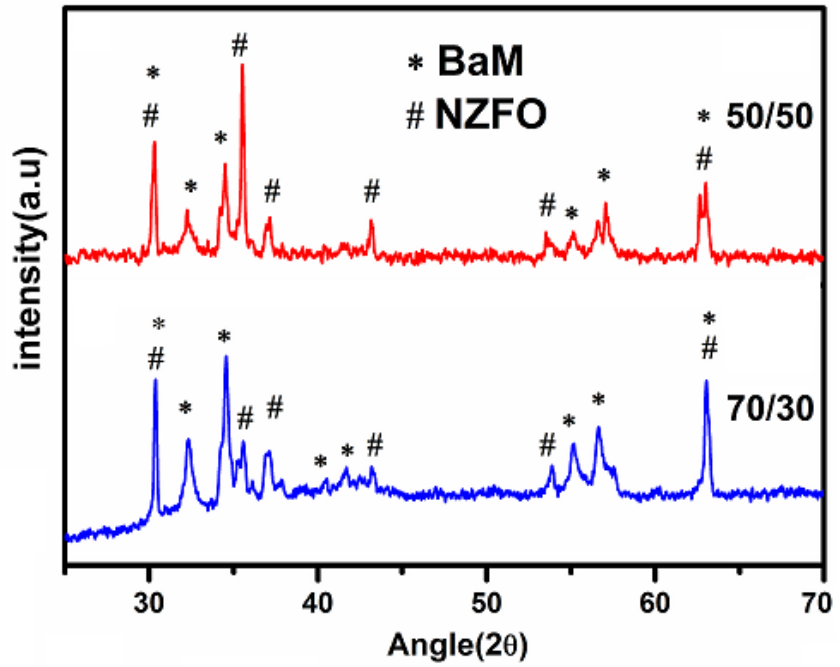


Fig. 4.22 X- ray diffraction patterns of 70/30 and 50/50 BaM/CFO nanocomposite powders.

Table 4.4 Crystallite size of BaM and NZFO in the composite samples.

| **Composition** (BaM/NZFO) | **Crystallite Size(nm)** NZFO | BaM |
|---|---|---|
| 100/0 | - | 37.4 |
| 70/30 | 37.6 | 38.5 |
| 50/50 | 39.5 | 38.6 |
| 0/100 | 38.0 | - |

### 4.4.1.2 Microstructure analysis

Fig. 4.23 (a-c) shows the fractured surface micrographs of BaM, NZFO and BaM/NZFO (70/30) composite sintered at 1200 ºC. Randomly oriented elongated grains were observed in BaM whereas; NZFO grains posses equiaxed morphology. In BaM/NZFO composite; well distinguished hexagonal BaM platelets along with small NZFO grains were observed. The corresponding EDS spectrum (Fig. 4.23 (d)) confirms the presence of all elements (Ba, O, Fe, Ni and Zn) in the composite.

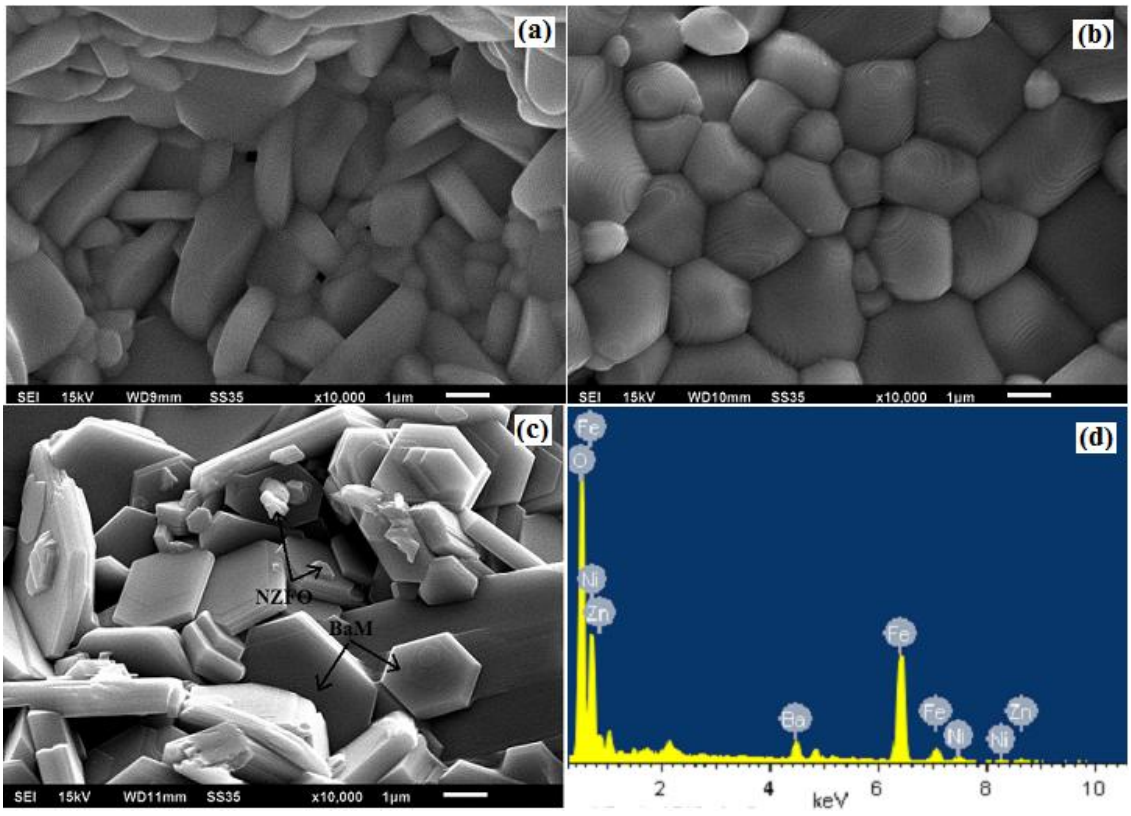


Fig. 4.23 SEM micrographs of (a) BaM, (b) NZFO, (c) BaM/NZFO (70/30), and (d) EDS of sintered composite.

### 4.4.1.3 Magnetic measurements

Fig. 4.24 (a & b) shows *M-H* loop of BaM, NZFO and their nanocomposite (90/10, 80/20, 70/30, 60/40, 50/50) powders respectively. Smooth demagnetization curve without any kink (Fig. 4.24(b)) suggests that BaM/NZFO phases are well exchange-coupled in composites. This smooth demagnetization of composite system is a consequence of coherent rotation of hard and soft spins with applied magnetic field.

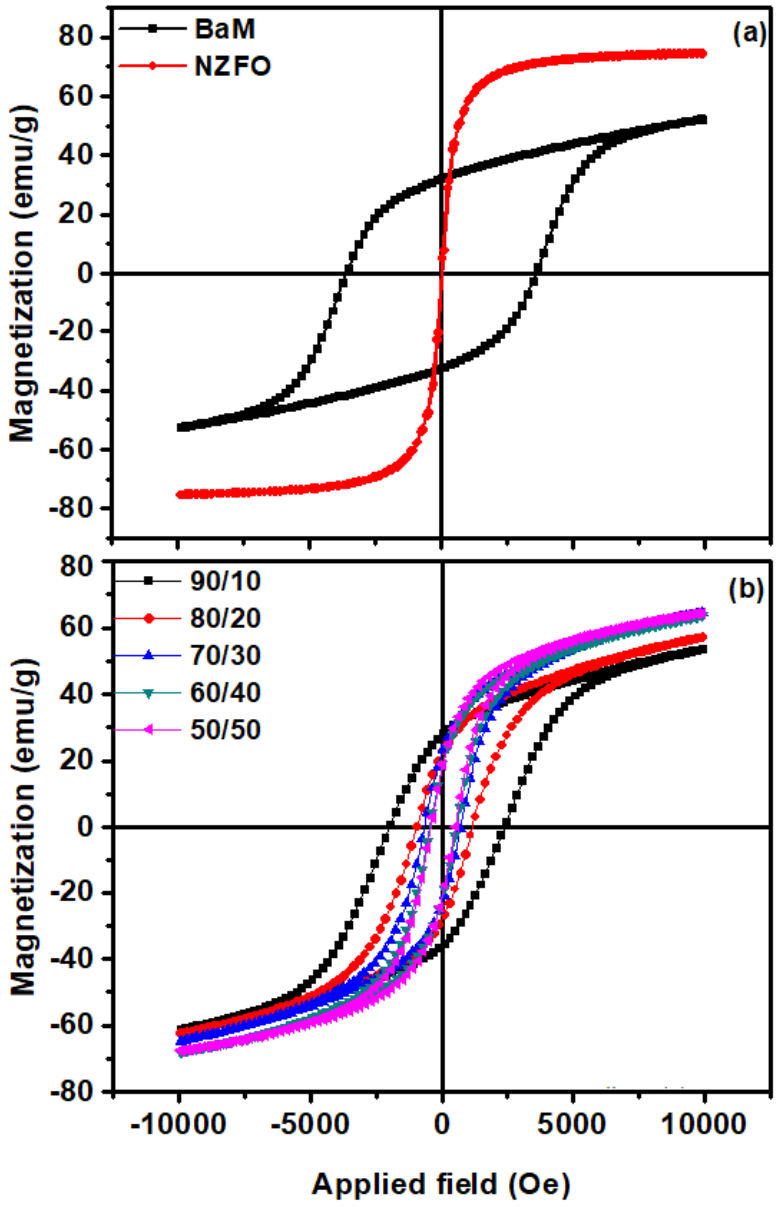


Fig. 4.24 Comparative *M-H* loops of (a) BaM & NZFO and (b) BaM/NZFO nanocomposites with different weight ratio.

The measured $M$ and $H_c$ of BaM, NZFO and their respective composites are shown in Table 4.5. The $M$ and $H_c$ of composites lies between their constituents magnetic properties. Fig. 4.25 (a & b) shows the variation in measured and theoretical calculated $M$ and $H_c$ of composites with NZFO content. The theoretical $M$ and $H_c$ were calculated using rule of mixture.

Table 4.5 Magnetic properties of BaM, NZFO and BaM/NZFO nanocomposites

| Magnetic properties | **BaM/NZFO weight ratio** | | | | | | |
|---|---|---|---|---|---|---|---|
| | BaM | 90/10 | 80/20 | 70/30 | 60/40 | 50/50 | NZFO |
| *M*(emu/g) | 52.14 | 53.63 | 57.21 | 64.44 | 63.62 | 64.31 | 74.40 |
| $H_c$ (Oe) | 3615.38 | 2204.9 | 1079 | 691.18 | 522.3 | 481.6 | 22.5 |
| $M_r$(emu/g) | 32.16 | 27.97 | 22.79 | 22.81 | 17.98 | 18.39 | 3.3 |

The *M* of nanocomposites drastically increased from 53.63 emu/g ($x$ = 10) to 64.44 emu/g ($x$ = 30). Further, *M* found to be nearly constant for higher NZFO content (Fig. 4.25(a)). Contrary to magnetization behavior, sharp decrease in $H_c$ was observed for $x$ = 30 (Fig. 4.25(b)) followed by marginal decrease. It is to be noted that, the change in *M* and $H_c$ is nonlinear and vastly deviates from theoretical calculated values. This anomalous behaviour suggest that spin interactions between hard-soft phases were maximum for certain composition ($x$ = 30). Reportedly, any change in *M* and $H_c$ of the composite is a consequence of three types of spin interactions i.e. between soft-soft phase, hard-hard phase and hard-soft phases [73]. In the present case, enhancement in magnetization was dominated by interfacial spin interaction of soft and hard phase.

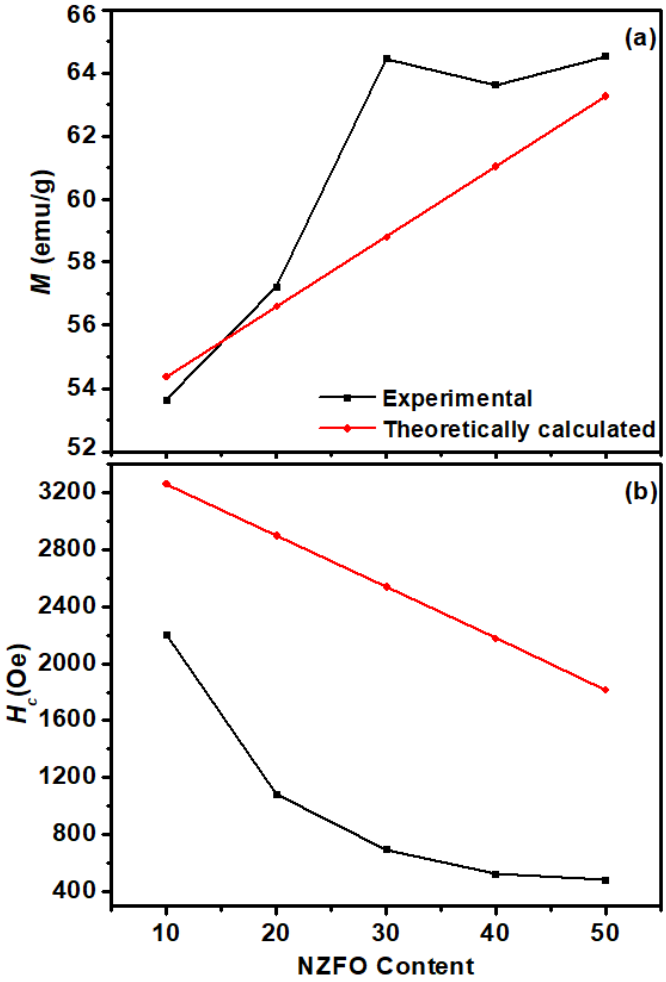


Fig. 4.25 Variation in theoretical and experimentally observed (a) $M$, and (b) $H_c$ of BaM/NZFO composite with NZFO content.

To understand the anomalous increase in $M$, the spin alignment behaviour of BaM in exchange-coupled composites with different NZFO content was compared. The schematic (Fig. 4.26) represents interfacial surface spins of composites with and without magnetic field. In the absence of field, both hard and soft magnetic spins are randomly oriented. At H=10 KOe, it is shown that the fraction of aligned spins in BaM are increasing with NZFO content.

Schematic represents that in pure BaM; major fraction of spins is aligned in the field direction. The remaining spins are not able to align (hindered spins) due to grain boundary hindrance to spin alignment in polycrystalline materials. Such hindered spins may require larger field or an additional driving force to align. With addition of NZFO, the interfacial spin interactions between hard/soft phases occurs, which increases with its content. Owing to soft magnetic nature of NZFO, spins get swiftly align at much lower

magnetic field and provide a torque to hard hindered spins. As a result, higher fraction of spin alignment increases the magnetization (53.6 emu/g to 64.5 emu/g). In schematic, it is also depicted that interfacial interactions are optimal for 70/30 weight ratio where all possible spins of BaM are aligned. As a consequence of optimum spins orientation causes an abrupt increase in magnetization. However, further increase in NZFO content magnetization remains nearly same, which suggests that hard/soft interfacial interactions reached to its saturation. The torque due to soft magnetic spins and coherent demagnetization caused a corresponding sharp decrease in $H_c$ of composites (Fig. 4.25(b).

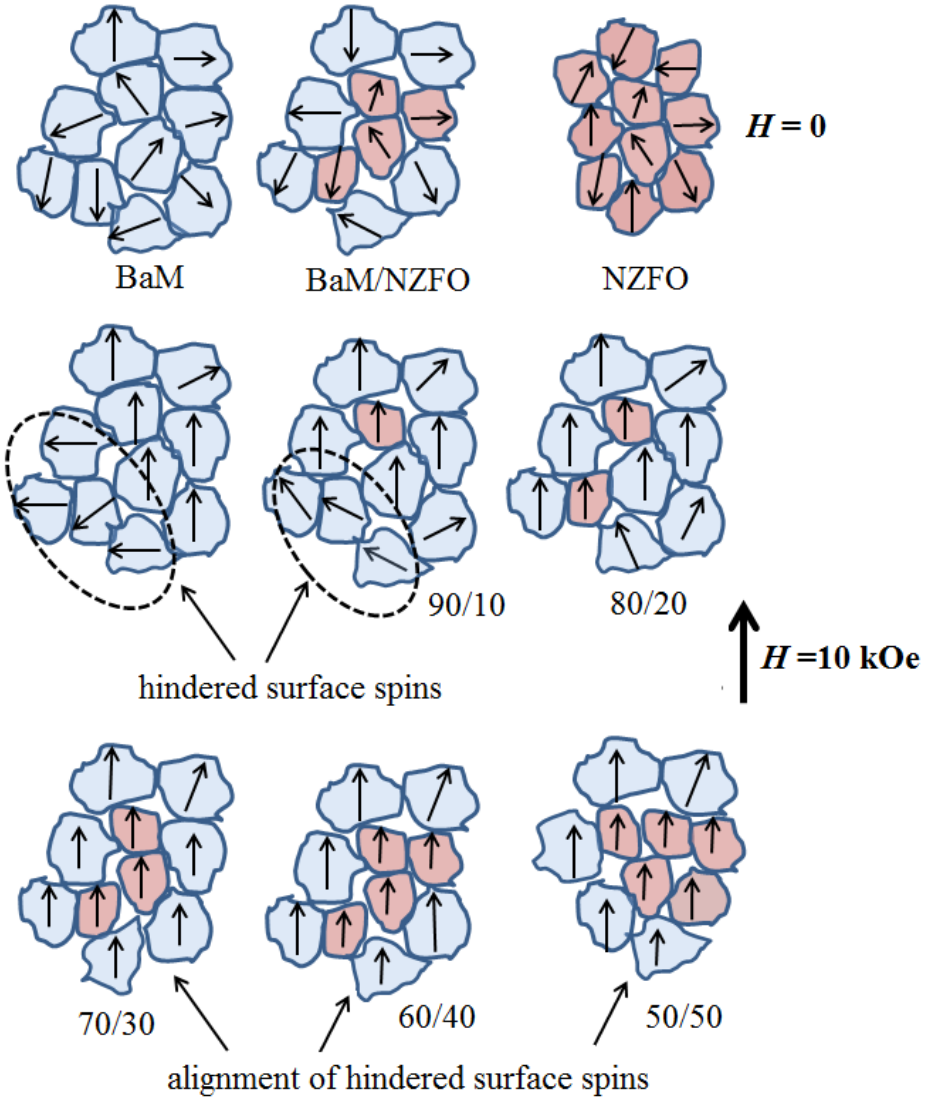


Fig. 4.26 Schematic representation of surface spins interactions of exchange-coupled BaM/NZFO composites.

### 4.4.1.4 Microwave studies

Fig. 4.27 (a-d) shows the real and imaginary parts of complex permittivity ($\varepsilon = \varepsilon' - j\varepsilon''$) and permeability($\mu = \mu' - j\mu''$) of BaM, NZFO and BaM/NZFO composites in $K_u$-band (12.4-18 GHz). The real part ($\varepsilon'$ and $\mu'$) shows the storage capacity and imaginary part ($\varepsilon''$ and $\mu''$) represents the loss of electric and magnetic energy respectively. It is clear that $\varepsilon'$ and $\mu'$ found to increase initially with the NZFO content and then decreases. For higher NZFO content large fluctuations were observed. The similar variation was also observed for $\varepsilon''$ and $\mu''$. To understand the effective loss mechanism in the composite; complex permittivity ($\varepsilon$) and permeability ($\mu$) of BaM, NZFO and BaM/NZFO composites were plotted as shown in Fig. 4.28 (a & b).

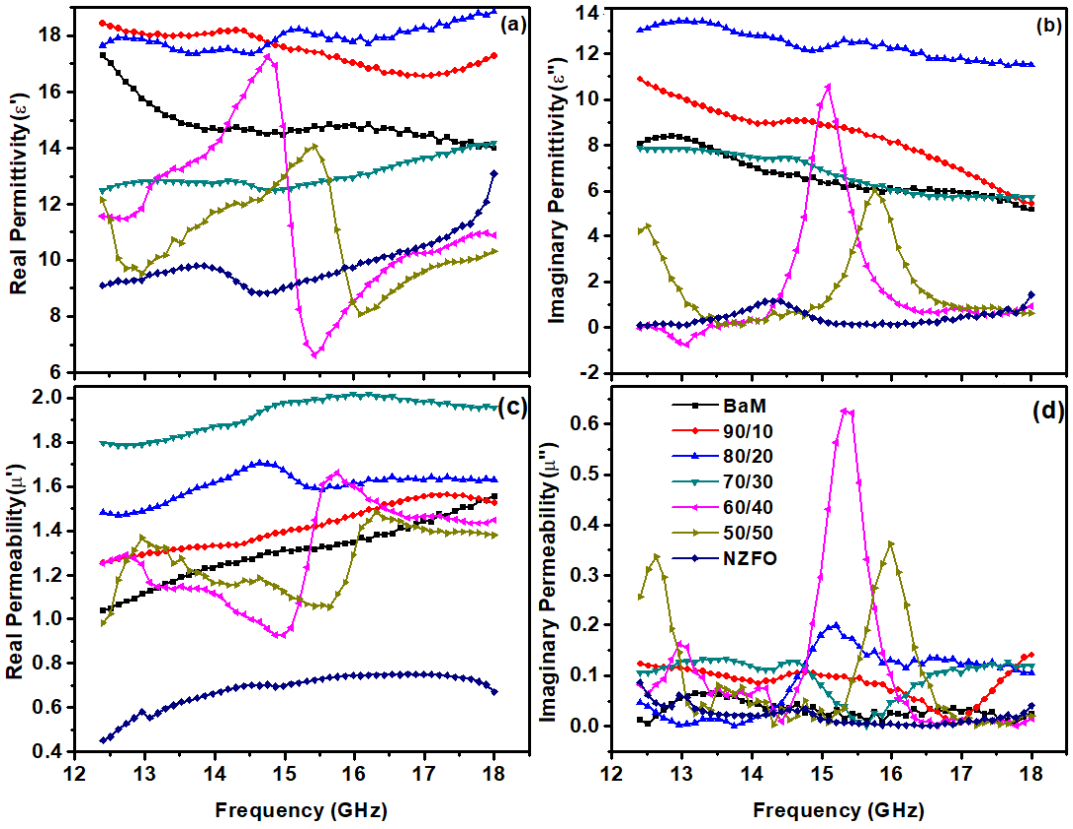


Fig. 4.27 (a) Real ($\varepsilon'$), (b) imaginary ($\varepsilon''$) part of complex permittivity and (c) real ($\mu'$), (d) imaginary ($\mu''$) part of complex permeability of BaM, NZFO & BaM/NZFO composite.

It is clear that $\varepsilon$ and $\mu$ remains constant for BaM, NZFO and 90/10, 80/20 & 70/30 composites. However, oscillatory behaviour of $\varepsilon$ and $\mu$ were observed for higher weight ratio of NZFO as in real and imaginary part. The large variations in $\varepsilon$ between 13 to 16 GHz frequency range may ascribe to the resonance of interfacial dipolar interaction with

applied field frequency (14.8 GHz and 15.4 GHz). For low NZFO content, the $\mu$ found to be nearly constant. This may due to the overlapping of precession motion of different magnetization vector. However, fluctuation in $\mu$ may correspond to individual precession of the magnetic vectors of hard and soft phases, which dominates for higher NZFO content.

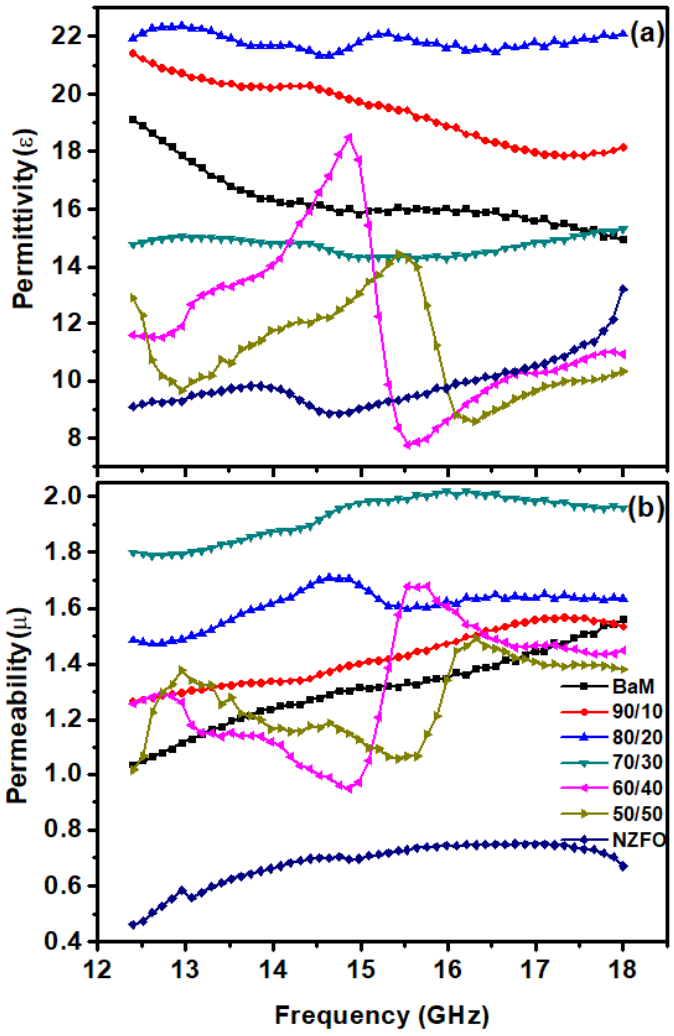


Fig. 4.28 Frequency dependent (a) Complex permittivity ($\varepsilon$) & (b) Complex permeability ($\mu$) of BaM, NZFO & BaM/NZFO composite.

The variation in $\varepsilon$ and $\mu$ with the NZFO content at 12.5 GHz frequency is shown in Fig. 4.29. Both $\varepsilon$ and $\mu$ found to increase initially with the NZFO content. The initial increase in $\varepsilon$ of the composite is due to the hindrance to charge motion caused by NZFO particles. Also, capacitive action caused by low resistive NZFO phase separated by high resistive BaM; results in higher $\varepsilon$. At higher NZFO content, low resistive continuous channels forms that facilitate charge conduction with a subsequent decrease in $\varepsilon$.

The measured $\mu$ of NZFO and BaM at 12.5 GHz are 0.6 and 1.5 respectively which are in agreement with the previously reported data [136,180]. The maximum value of $\mu$ is observed for 70/30 weight ratio. Strong exchange coupling between high and low permeable phases might be the reason for high $\mu$ of composite.

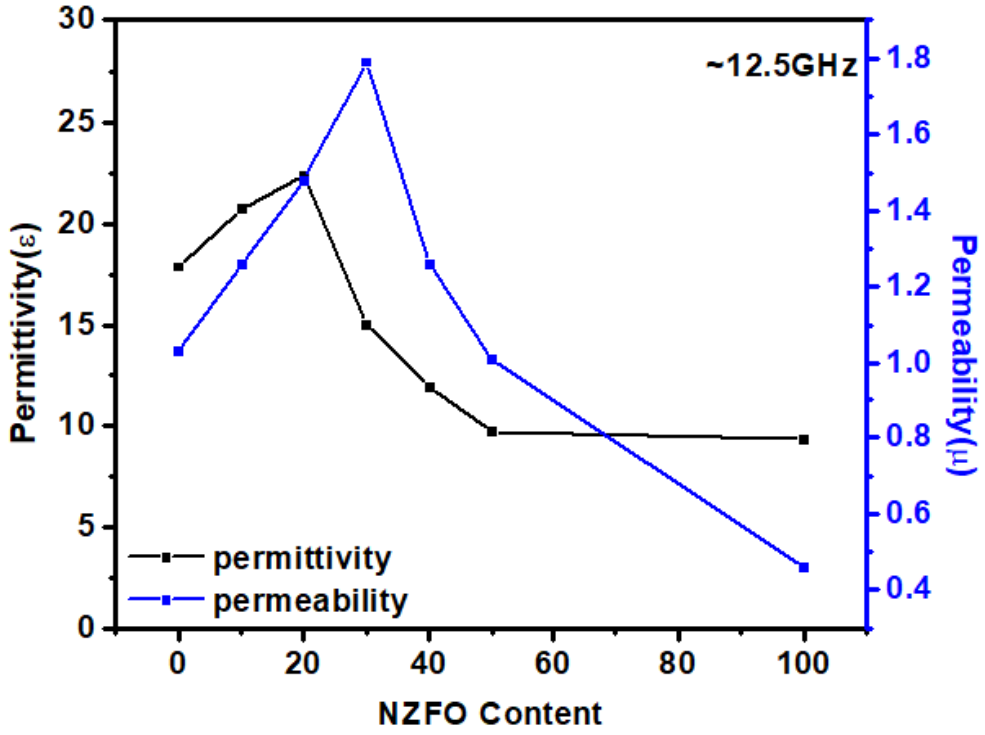


Fig. 4.29 Permittivity and permeability of the composite with NZFO content.

Fig. 4.30 shows the reflection loss plots for BaM/NZFO composites and compared with individual BaM and NZFO phases. For BaM, *RL* of -27 dB was observed at 13 GHz, whereas no losses were seen for NZFO due to its low FMR [15]. In the composite, *RL* were observed at higher frequencies. The maximum *RL* of - 41 dB (absorption > 99%) was obtained for 70/30 weight ratio. The results suggest that *RL* and their loss frequency strongly depend upon the exchange coupling.

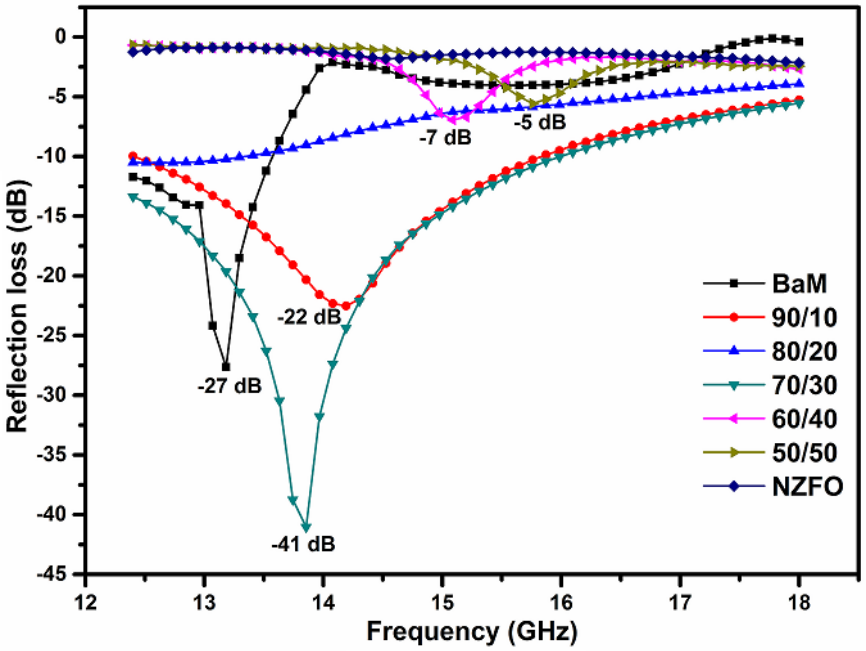


Fig. 4.30 Reflection loss *vs.* frequency plots for BaM, NZFO and BaM/NZFO nanocomposites for different NZFO content.

### 4.4.2 BaM/CFO and BaM/CZFO series

#### 4.4.2.1 Phase Analysis

Fig. 4.31 (a-e) shows the representative XRD patterns of pure and composites powders calcined at 1050 °C. Single BaM and CFO/CZFO phase were observed for pure powders whereas nanocomposites showed co-existence of both the phases. No evidence of any intermediate phase was found. Calculated average *C.S* size for both the phases is shown in Table 4.6. It is evident that crystallite size of CFO and CZFO were suppressed in composites despite similar annealing temperature (1050 °C). The lower *C.S* may ascribe to the pinning force by hexagonal phase.

Table 4.6 Average crystallite size of pure and composite nanopowders.

| Sample | Crystallite Size (nm) |
|---|---|
| BaM | 35.5 |
| CFO | 58.3 |
| CZFO | 62.9 |
| BaM/CFO | 31.5/30.5 |
| BaM/CZFO | 30.7/30.4 |

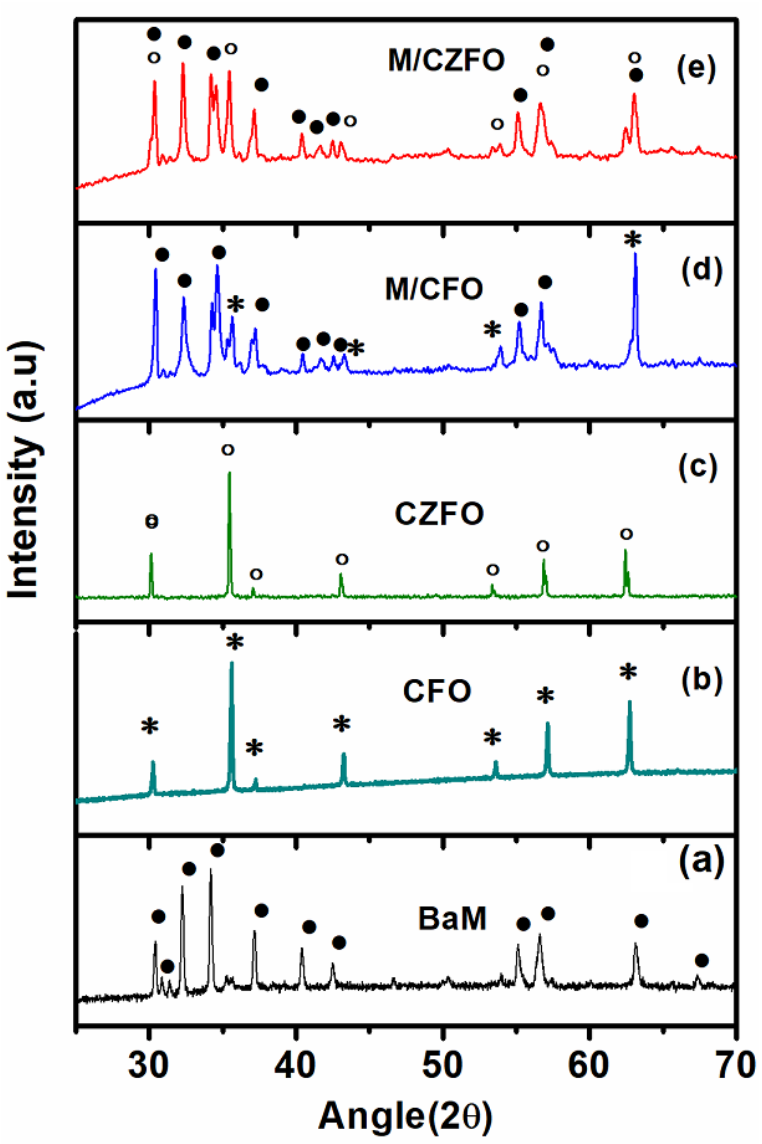


Fig. 4.31 X-ray diffraction patterns of (a) BaM, (b) CFO, (c) CZFO, (d) BaM/CFO(70/30) and (e) BaM/CZFO(70/30).

#### 4.4.2.2 Microstructure analysis

The representative microstructure of sintered BaM, CFO, CZFO and their composites are shown in Fig. 4.32 (a - e). Well distinguished equiaxed grains were observed for CFO and CZFO whereas; BaM showed signature isotropic elongated grains with random orientation. In composites, large hexagonal platelets correspond to BaM while smaller grains represent the CFO/CZFO. The respective EDS analysis (Fig. 4.33(a & b)) showed the presence of Ba, O, Fe, Co and Zn elements in the system.

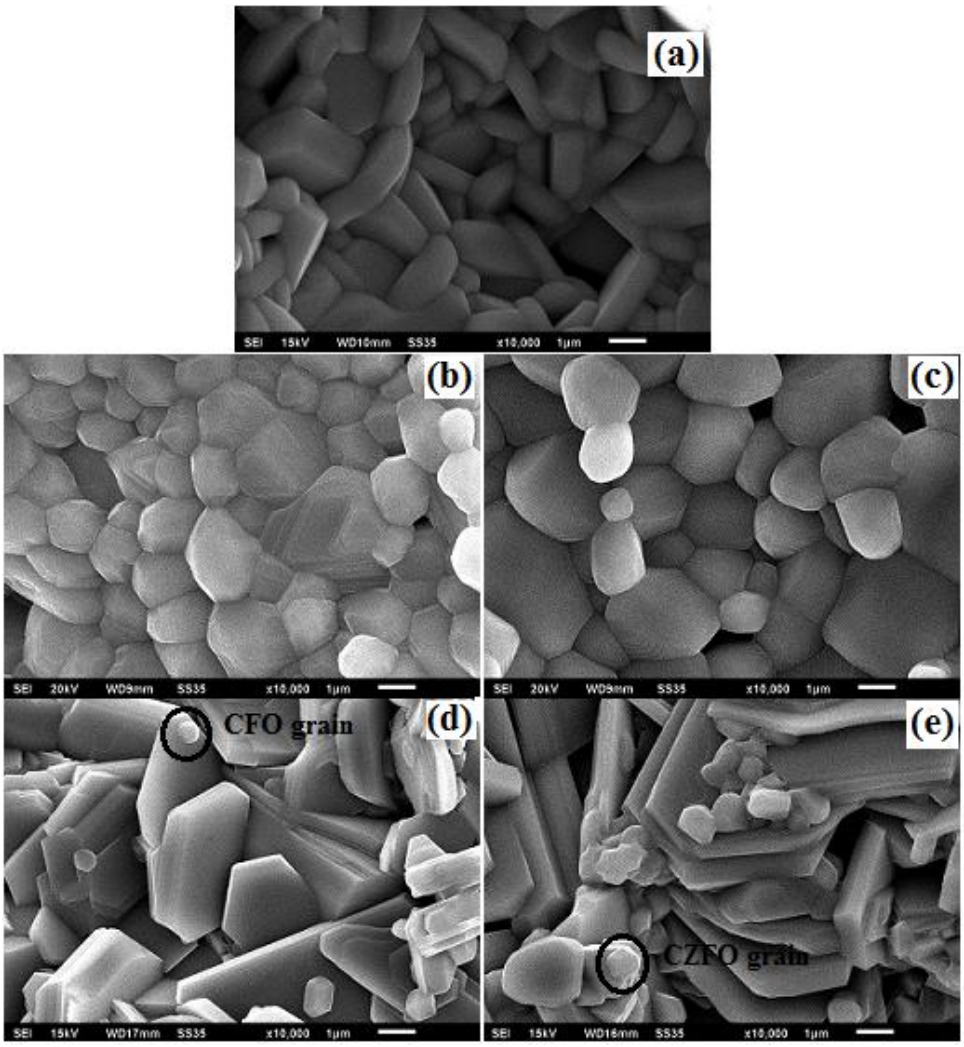


Fig. 4.32 SEM micrographs of (a) BaM, (b) CFO, (c) CZFO, (d) BaM/CFO (70/30) & (e) BaM/CZFO (70/30).

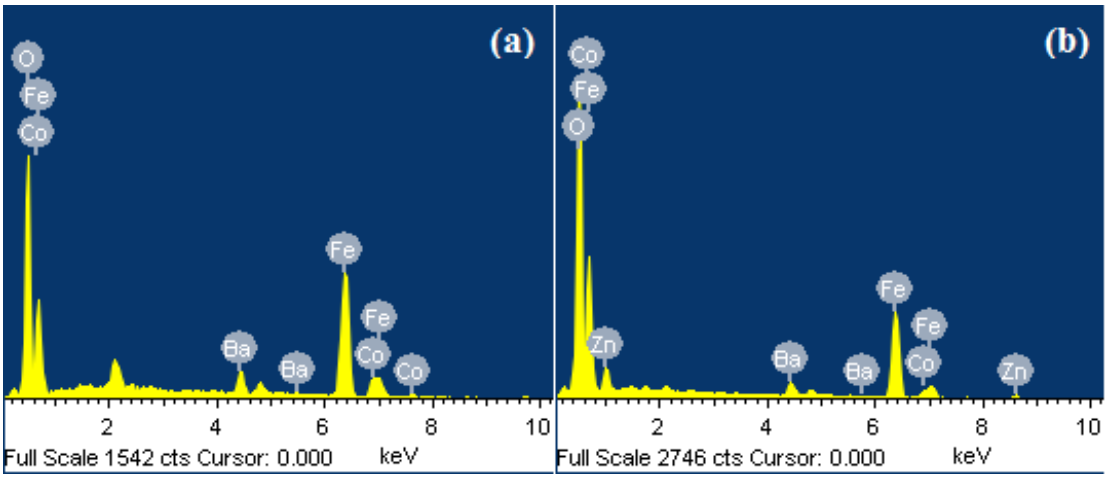


Fig. 4.33 EDS spectra of (a) BaM/CFO and (b) BaM/CZFO composites.

### 4.4.2.3 Magnetic measurements

Fig. 4.34 (a-f) shows the *M-H* loops of CFO, CZFO, BaM and their nanocomposites at maximum field of 10 kOe. An obvious higher *M* of soft(CFO/CZFO) phase were observed and in agreement with the previously reported data [172,181]. The obtained smaller $H_c$ (55 Oe) of CZFO compared to CFO is due to the presence of non-magnetic $Zn^{2+}$ ions [181]. The smooth demagnetization behavior of composites demonstrates coherent switching of hard and soft magnetic spins as a consequence of interfacial coupling.

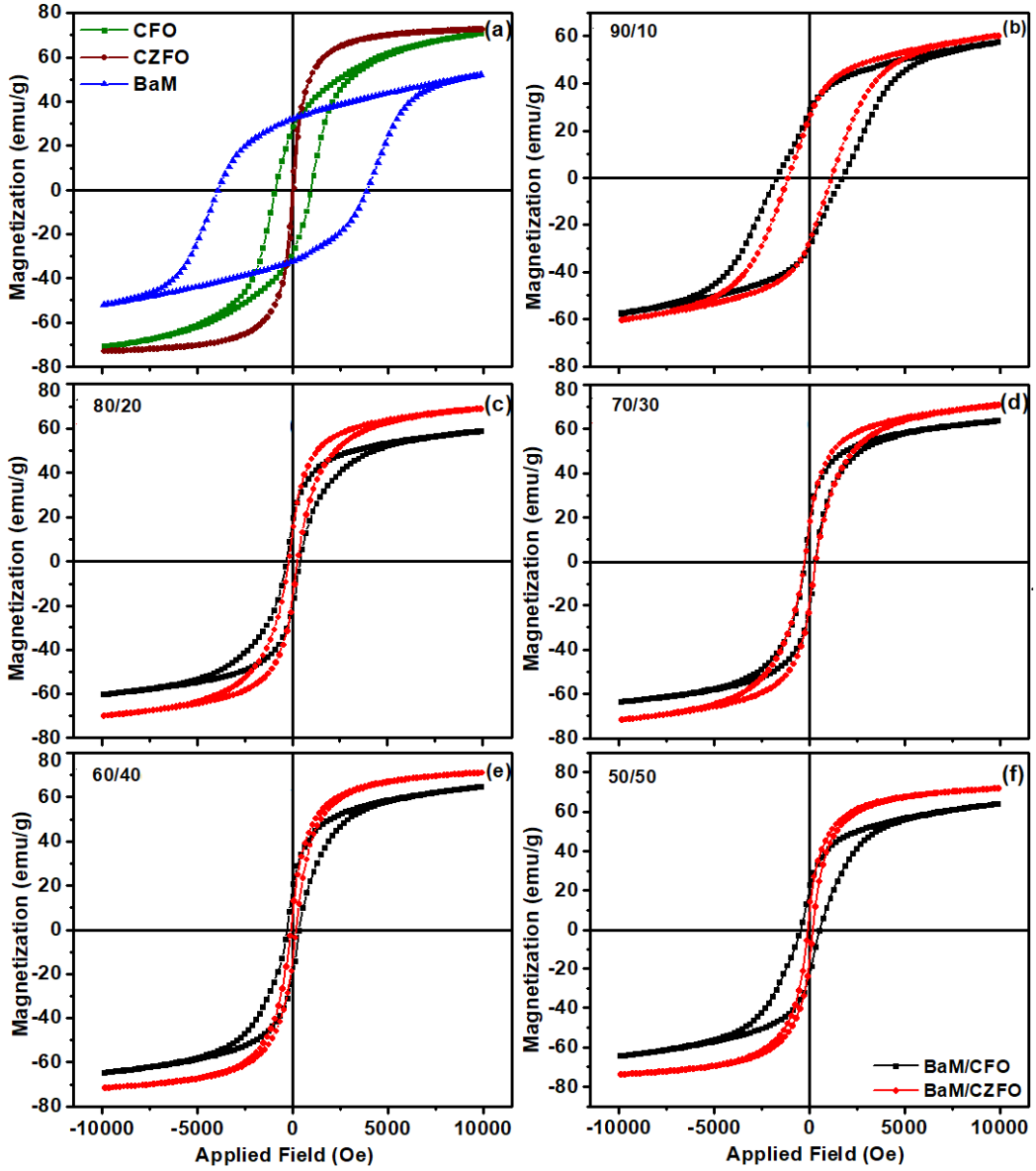


Fig. 4.34 Comparative *M-H* loops of (a) BaM, CFO & CZFO, (b-f) BaM/CFO & BaM/CZFO nanocomposites with different composition.

The measured magnetic properties of pure and composite powders are given in Table 4.7. It is evident that $M$ and $H_c$ of the exchange-coupled composites lies in between their constituent properties. Obtained high $M$ and low $H_c$ in comparison to theoretical values suggest that exchange length is comparable to their $C.S$ which is a prerequisite condition for interfacial coupling.

Table 4.7 Magnetic properties of pure (BaM, CFO, CZFO) and nanocomposite (BaM/CFO & BaM/CZFO) powder.

| **Magnetic properties** | | **CFO weight content (wt%)** | | | | | | |
|---|---|---|---|---|---|---|---|---|
| | | 0 | 10 | 20 | 30 | 40 | 50 | 100 |
| $M$ (emu/g) | Experimental | 52.05 | 57.52 | 58.95 | 63.66 | 64.40 | 63.9 | 70.74 |
| | Calculated | 52.05 | 53.91 | 55.78 | 57.65 | 59.52 | 61.39 | 70.74 |
| $H_c$ (Oe) | Experimental | 3920 | 1734 | 361 | 272 | 316 | 498 | 949 |
| | Calculated | 3920 | 3623 | 3326 | 3029 | 2732 | 2435 | 949 |
| | | **CZFO weight content (wt%)** | | | | | | |
| $M$ (emu/g) | Experimental | 52.05 | 60.23 | 69.17 | 70.73 | 70.97 | 71.85 | 72.58 |
| | Calculated | 52.05 | 54.1 | 56.15 | 58.21 | 60.26 | 62.31 | 72.58 |
| $H_c$ (Oe) | Experimental | 3920 | 1152 | 237 | 272 | 140 | 146 | 55 |
| | Calculated | 3920 | 3533 | 3164 | 2759 | 2373 | 1986 | 55 |

Fig. 4.35 (a & b) shows the relative percent change in $M$ and $H_c$ with CFO/CZFO phase content. A non-linear change in $M$ and $H_c$ showed their strong dependence on relative weight fraction. The initial enhancement in $M$ is due to the interfacial spin interaction where swift alignment of soft magnetic spins in the direction with field releases the hindered hard magnetic spins. Above a certain composition, nearly constant $M$ is due to spin interaction saturation and dominance of soft phase magnetization.

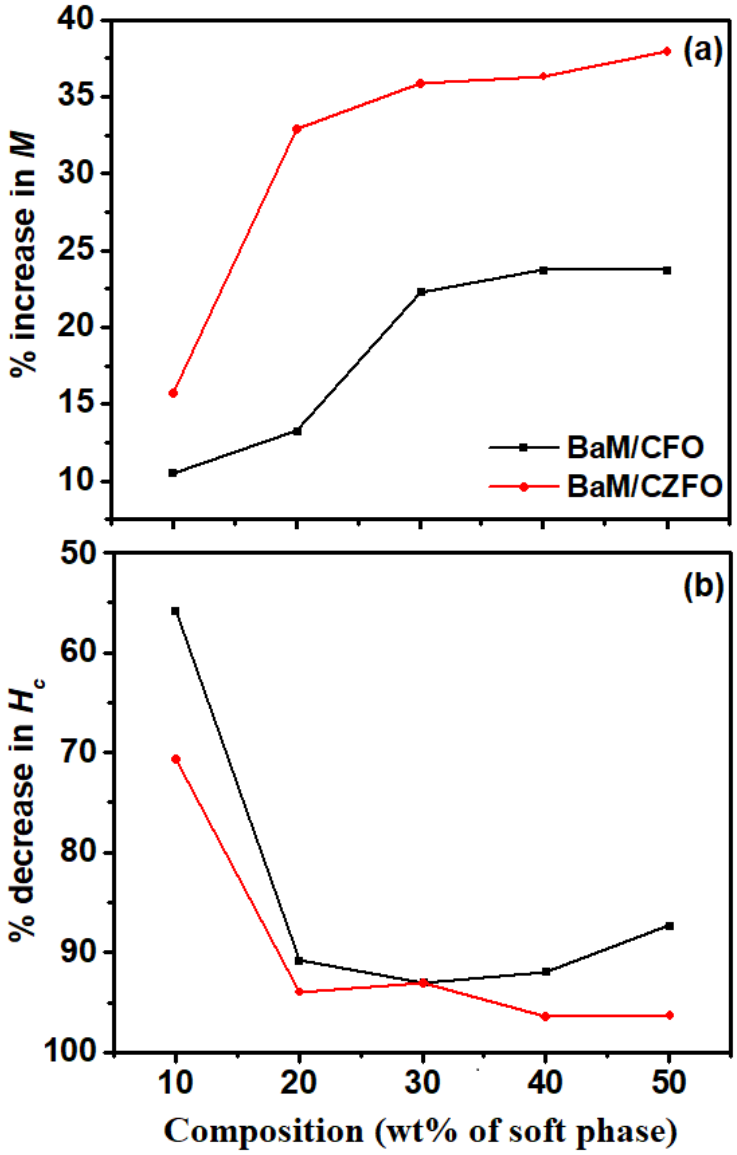


Fig. 4.35 Percentage change in (a) *M* and (b) $H_c$ of BaM/CFO and BaM/CZFO composite with soft phase content.

One of the interesting feature to note that *M* of composite strongly depends upon the nature of soft magnetic phase. The marginal difference (2.6%) in *M* of CFO (70.74 emu/g) and CZFO (72.58 emu/g) shows notable changes in composite magnetization. The composite with CZFO shows 19.6 % higher magnetization compared to CFO for 80/20 weight fraction. It is also evident that an abrupt increase in *M* was observed for 20 wt % of CZFO, whereas similar trend was observed for 30 wt % of CFO. The presence of $Zn^{2+}$ ions in CZFO provide large number of uncoupled surface spins and promote interfacial coupling which activate hard hindered spins at much lower weight fraction compared to CFO. On contrary to *M*; a sharp percentage decrease in $H_c$ (Fig. 4.35(b)) were observed

for 20 wt % soft phase content followed by a marginal change. Obtained higher percentage decrement (> 90%) in $H_c$ values is due to switching of hard magnetic coupled spins at much low nucleation field. Obtained variations in $M$ and $H_c$ of the composite suggest that the spin interactions strongly depend upon magnetic behaviour of soft phase and their relative composition.

#### 4.4.2.4 Microwave studies

To understand the magnetodielectric behavior of the composites; the frequency dependent complex permeability ($\mu$) and permittivity ($\varepsilon$) behavior of BaM, BaM/CFO and BaM/CZFO composite is shown in Fig. 4.36 (a & b). The $\varepsilon$ found to decrease while a slight increase in $\mu$ was observed with the frequency. Large variation in $\varepsilon$ and $\mu$ were observed in two exchange coupled-composite system. In BaM/CFO; both $\varepsilon$ and $\mu$ found to increase despite the presence of low anisotropic soft phase. Increase in $\varepsilon$ is due to the capacitive actions caused by low resistive soft magnetic (CFO/CZFO) grains separated by high resistive BaM grains. The higher CFO content, promotes more capacitive action that results in higher $\varepsilon$. In BaM/CZFO composite, similar capacitive mechanism with low CZFO content (30 wt %) responsible for enhancement in $\varepsilon$ of the material. However, at higher CZFO content the decrease in $\varepsilon$ is ascribed to higher conduction losses due to presence of non-magnetic $Zn^{2+}$ ions. The $\mu$ of the composites is also found to be composition dependent. It can be seen from the figure that high $\varepsilon$ and $\mu$ are parallelly achieved in BaM/CFO composites.

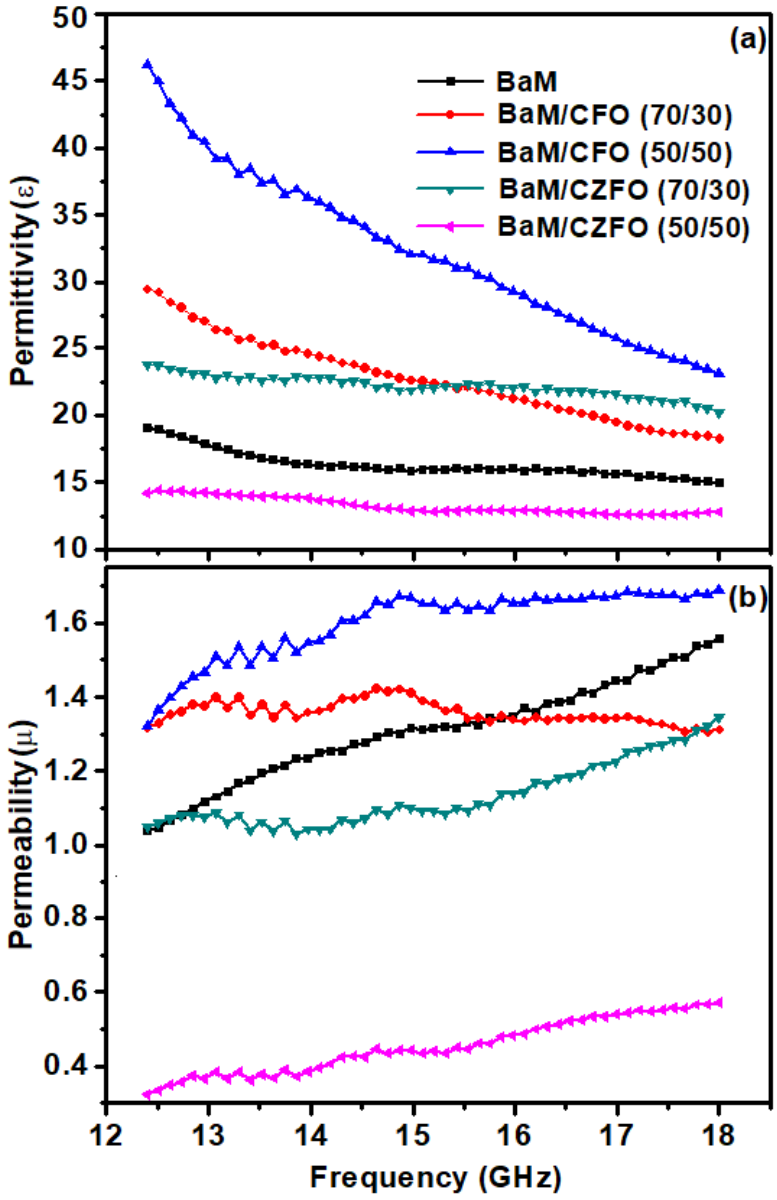


Fig. 4.36 Frequency dependent (a) Complex permittivity ($\varepsilon$) & (b) Complex permeability ($\mu$) of pure and composite systems.

Fig. 4.37 shows the comparative reflection loss *vs*. frequency plot of BaM, BaM/CFO and BaM/CZFO systems. For pure BaM; the maximum *RL* of -40 dB (absorption >99%) was observed at 15.9 GHz frequency. A small dip of -13 dB at 17.5 GHz frequency has also been obtained for BaM/CFO (50/50) composite. The composites without reflection dip may show losses either in high or low frequency band. The observed changes in the loss behavior may ascribe to different FMR frequency and interfacial exchange coupling.

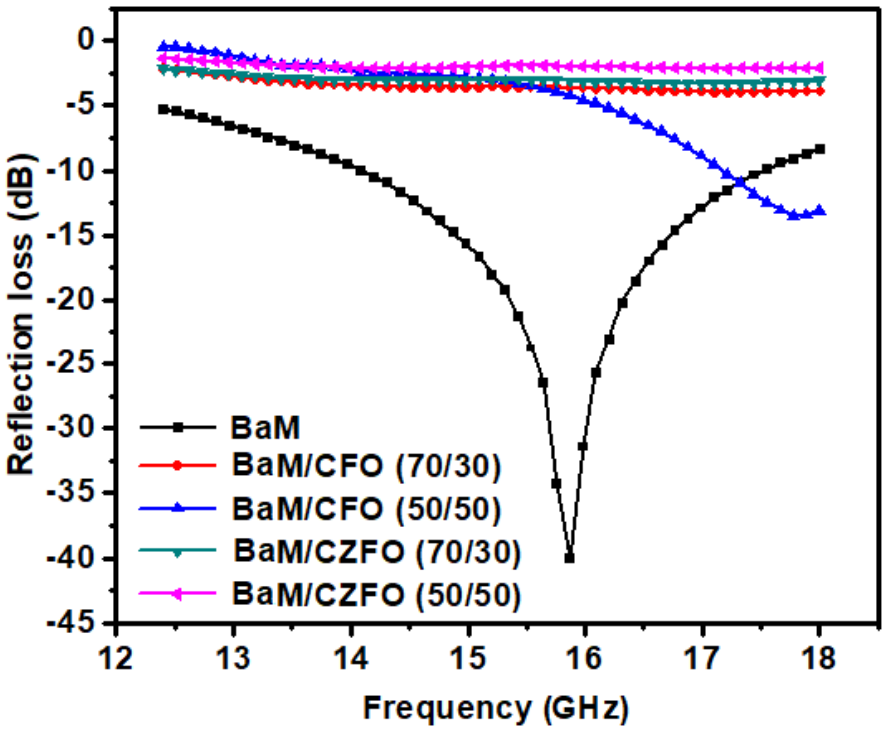


Fig. 4.37 Reflection loss *vs.* frequency plots for BaM BaM/CFO and BaM/CZFO systems.

### 4.5 Effect of soft phase magnetization

To understand the role of soft phase magnetization on exchange coupling; composite of BaM and $Ni_{1-x}Zn_xFe_2O_4$ in the weight ratio of 70/30 were prepared by sol-gel autocombustion method. Different values of soft phase magnetization were induced by substituting ($x$ = 0.0, 0.1, 0.2, 0.3, 0.4, 0.5) non magnetic $Zn^{2+}$ ions. The effect of different soft phase magnetization on magnetic and microwaves properties was investigated.

#### 4.5.1 XRD analysis

Fig. 4.38 shows the representative XRD patterns of BaM/$Ni_{1-x}Zn_xFe_2O_4$ ($x$ = 0.0, 0.1, 0.2, 0.3, 0.4, 0.5) nanocomposites. The diffraction patterns confirmed the coexistence of hexagonal (BaM) and spinel ($Ni_{1-x}Zn_xFe_2O_4$) phases in all the composites. No secondary and impurity phase was formed during annealing of powders. The average *C.S* for hexagonal and spinel phases in the composite were calculated and are shown in Table 4.8.

Table 4.8 Average crystallite size of BaM and $Ni_{1-x}Zn_xFe_2O_4$ in the composite system

| Composite | Crysatallite size (nm) |
|---|---|
| BaM/NiF | 45/38 |
| $BaM/Ni_{0.9}Zn_{0.1}Fe_2O_4$ | 37.03/32.9 |
| $BaM/Ni_{0.8}Zn_{0.2}Fe_2O_4$ | 33.1/32.62 |
| $BaM/Ni_{0.7}Zn_{0.3}Fe_2O_4$ | 27.18/23.16 |
| $BaM/Ni_{0.6}Zn_{0.4}Fe_2O_4$ | 28.13/27.1 |
| $BaM/Ni_{0.5}Zn_{0.5}Fe_2O_4$ | 38.8/37.6 |

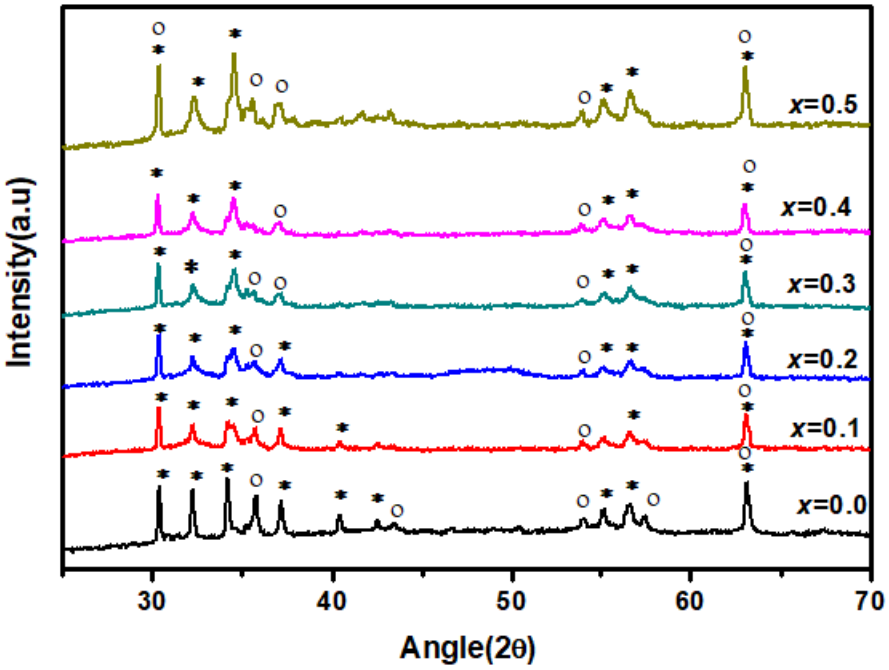


Fig. 4.38 X-ray diffraction patterns of $BaM/Ni_{1-x}Zn_xFe_2O_4$ ($x$ = 0.0, 0.1, 0.2, 0.3, 0.4, 0.5) nanopowders.

### 4.5.2 Magnetic measurements

*M-H* loops of $Ni_{1-x}Zn_xFe_2O_4$ and $BaM/Ni_{1-x}Zn_xFe_2O_4$ (70/30) nanopowders are shown in Fig. 4.39 (a & b). The *M-H* plots of $Ni_{1-x}Zn_xFe_2O_4$ showed the soft magnetic nature, however, *M* found to increase with the Zn substitution and maximum of 75 emu/g was obtained for $x$ = 0.4 and 0.5. Increase in *M* is might be due to the preferential occupation of non magnetic $Zn^{2+}$ ions at antiparallel sites of $Ni^{2+}$ ions [182]. The representative *M-H* loops of $BaM/Ni_{1-x}Zn_xFe_2O_4$ composites are shown in Fig. 4.39 (b). Obtained smooth demagnetization curve without any kink (Fig. 4(b)) suggests that hard/soft phases were well exchange-coupled. The measured *M* and $H_c$ of $Ni_{1-x}Zn_xFe_2O_4$ and $BaM/Ni_{1-}$

$_x$Zn$_x$Fe$_2$O$_4$ composites are shown in Table 4.9.

Table 4.9 Magnetic properties of $Ni_{1-x}Zn_xFe_2O_4$ and $BaM/Ni_{1-x}Zn_xFe_2O_4$ nanopowders.

| **$Ni_{1-x}Zn_xFe_2O_4$** | | | | | | |
|---|---|---|---|---|---|---|
| *x* | 0.0 | 0.1 | 0.2 | 0.3 | 0.4 | 0.5 |
| *M* (emu/g) | 46.3 | 56.8 | 67 | 71 | 74.4 | 75 |
| $H_c$ (Oe) | *102* | 67 | 57 | 40 | 32 | 22.5 |
| **$BaM/Ni_{1-x}Zn_xFe_2O_4$** | | | | | | |
| *x* | 0.0 | 0.1 | 0.2 | 0.3 | 0.4 | 0.5 |
| *M*(emu/g) | 57.7 | 54 | 57 | 60 | 62 | 64 |
| $H_c$ (Oe) | 1068 | 869 | 720 | 679 | 665 | 690 |

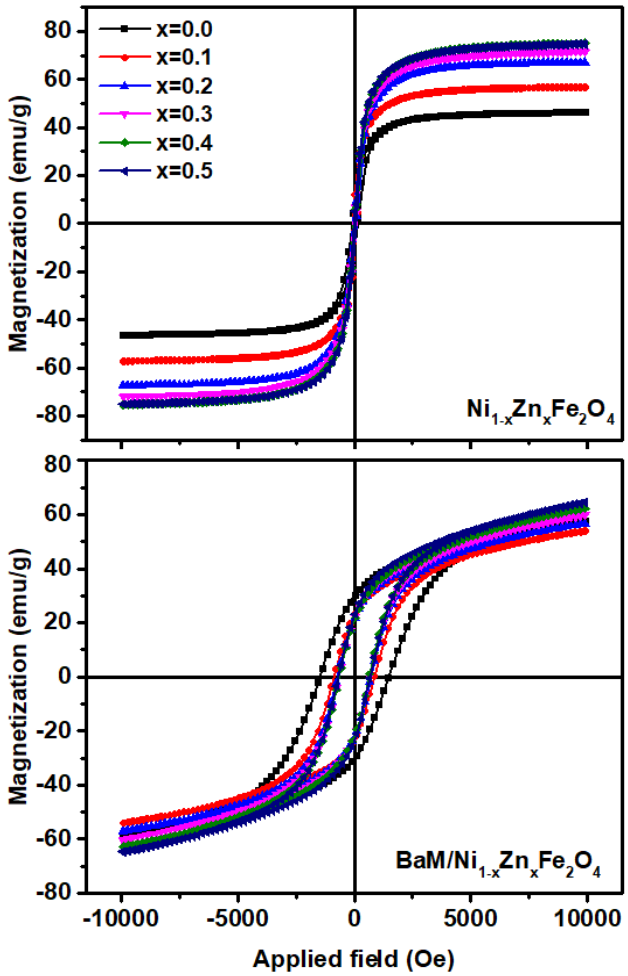


Fig. 4.39 *M-H* loops of $Ni_{1-x}Zn_xFO$ and $BaM/Ni_{1-x}Zn_xFe_2O_4$ nanopowders.

The variation in magnetization of composites with the soft phase magnetization is shown

in Fig. 4.40. Magnetization was also theoretically calculated by rule of mixture and compared to experimental value. The relative high experimental *M* compared to calculated one is the consequence of interfacial coupling. From the graph it is clear that *M* of soft phase increases linearly with the Zn substitution. On contrary, *M* of the composite varied non linearly with the magnetization of soft phase. Since the weight ratio of the composite was kept constant to 70/30 hence, obtained variation in *M* of composite is due to the change in interfacial magnetic spin interaction in the presence of $Zn^{2+}$ ions. From the figure it is clear that, when the difference between the magnetization of hard (53 emu/g) and soft (46 emu/g) phases is large; increase in *M* of composite (57.7 emu/g) was observed. Further, when *M* of hard-soft phase are comparable i.e. 53 & 57 emu/g; *M* of composite found to decrease (53 emu/g). Further, a linear increase in *M* was observed with relative high *M* soft phase ($x$=0.3-0.5) as magnetization of hard-soft phases are largely deviated. This anomalous behaviour suggests that interfacial spin interactions between hard and soft phases are soft phase magnetization dependent. The interfacial spin interactions are maximum if the difference in the *M* of hard and soft phases is large that further results an enhancement in *M* of the composite.

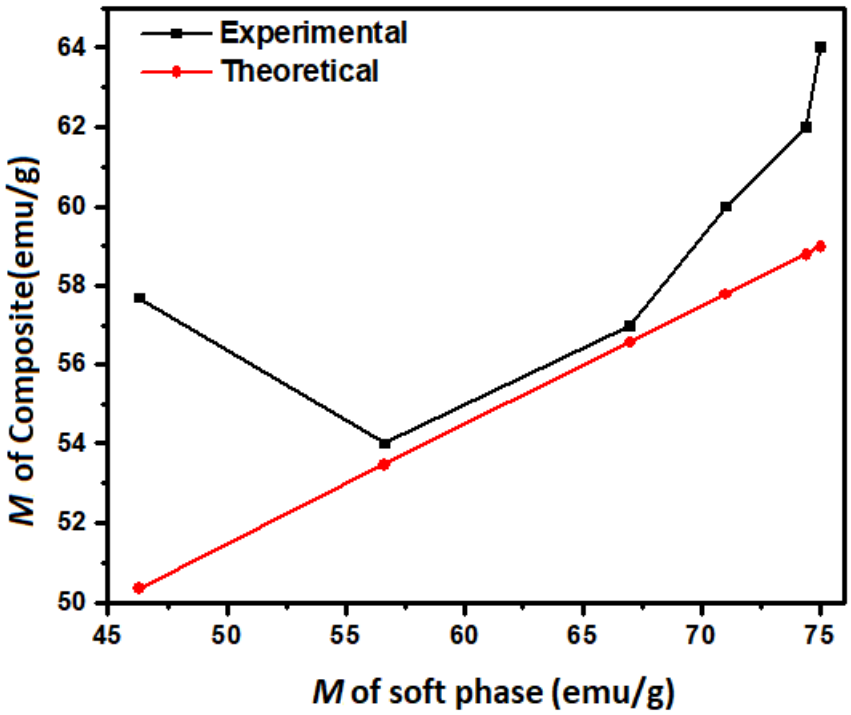


Fig. 4.40 Variation in *M* of composite with soft phase magnetization.

### 4.5.3 Microwave studies

Fig. 4.41 shows the complex permeability ($\mu$) and permittivity ($\varepsilon$) spectra of BaM and BaM/$Ni_{1-x}Zn_xFe_2O_4$ composites. It is clear that $\varepsilon$ and $\mu$ remains constant for BaM and BaM/NiF composites. However, oscillatory behaviour in $\varepsilon$ and $\mu$ were observed for Zn substituted soft phase composite. The large variations in $\varepsilon$ and $\mu$ spectra are observed between 13.5-16.5 GHz frequency range. In exchange-coupled system presence of spin-spin interactions or interfacial dipoles is the cause of observed peak in $\varepsilon$ spectra as described in earlier sections. For BaM/NiF composite, $\mu$ found to be nearly constant, however, large fluctuation in $\mu$ spectra for Zn substituted soft phase composite is observed. In these composites; the presence of non magnetic $Zn^{2+}$ ions decrease the ferromagnetic coupling and results a change in precession motion of magnetic spins and resultant fluctuations in $\mu$. The observed variation in $\mu$ may arise due to varied exchange coupling between hard/soft phases as a result of different magnetization vector of soft phase.

Both $\varepsilon$ and $\mu$ of the composites found to be relative high compared to BaM. The increases in $\varepsilon$ of the composite is due to the capacitive actions caused by low resistive soft magnetic grains and create hindrance to charge motion. However, decrease in $\varepsilon$ for $x$ = 0.4 & 0.5 composite is ascribed to higher conduction losses due to presence of large non-magnetic $Zn^{2+}$ ions. The relative high $\mu$ of the composite is due to the strong exchange coupling between high and low permeable phases.

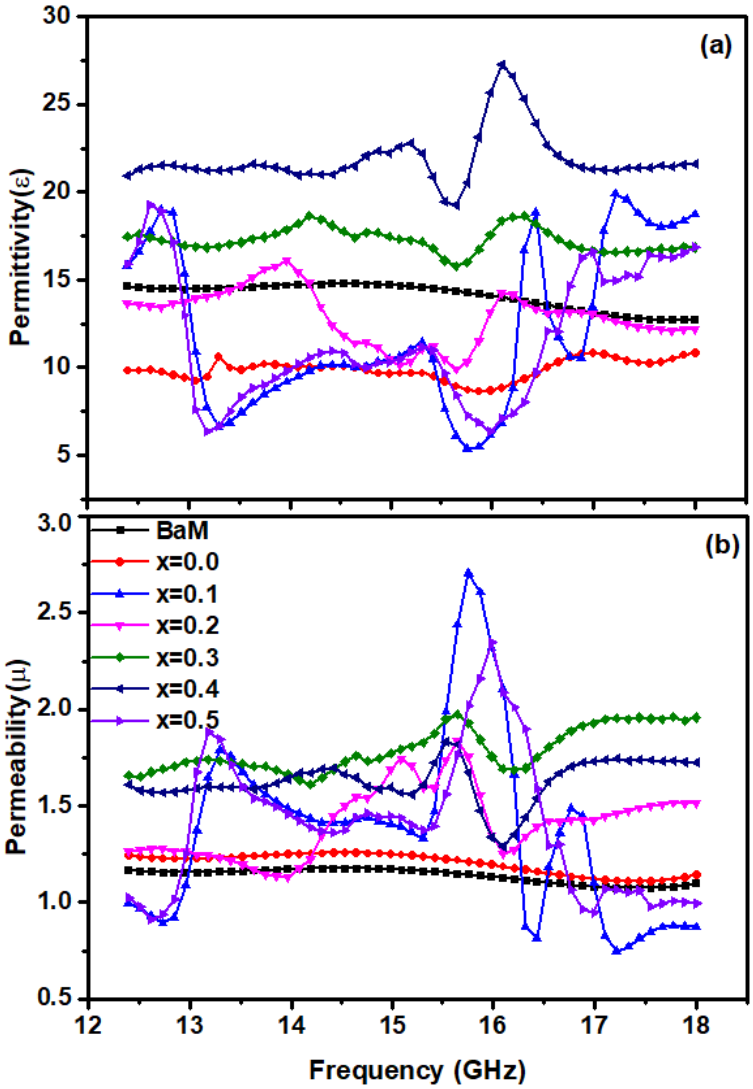


Fig. 4.41 Frequency dependent complex (a) permittivity ($\varepsilon$) & (b) permeability ($\mu$) of BaM/$Ni_{1-x}Zn_xFe_2O_4$ ($x$ = 0.0, 0.1, 0.2, 0.3, 0.4, 0.5) composite.

Reflection loss *vs.* frequency plots for pure BaM and BaM/$Ni_{1-x}Zn_xFe_2O_4$ composites are shown in Fig. 4.42. For BaM, *RL* dip of -27.6 dB was obtained at 13.2 GHz, whereas exchange-coupled composite shows losses at multiple frequencies. The *RL* peak of the composites gets shifted to the higher frequencies. In BaM/NiF, loss dips were found at 5.3 GHz and 16.3 GHz where BaM/$Ni_{0.9}Zn_{0.1}Fe_2O_4$ composite showed loss dips at 13.3 GHz, 15.5 GHz, 16 GHz and 16.8 GHz frequencies. Composite BaM/$Ni_{0.5}Zn_{0.5}Fe_2O_4$ shows maximum *RL* of -12 dB and -25 dB at 15.9 GHz and 16.4 GHz frequencies respectively. Since, the composite BaM/NiF and BaM/$Ni_{0.5}Zn_{0.5}Fe_2O_4$ showed maximum *RL* (< - 20 dB) which confirms that their absorbance is > 99% and can be considered as good microwave absorbing material. These results suggest that *RL* and loss frequency of

composites strongly depend upon nature of soft phase material that further affects the absorption losses.

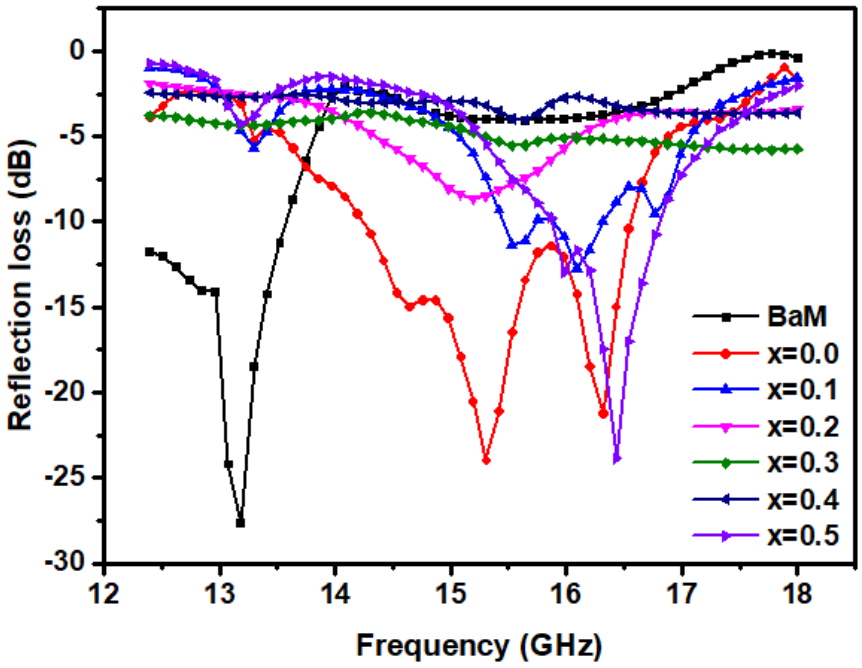


Fig. 4.42 Reflection loss *vs.* frequency plots for BaM and BaM/$Ni_{1-x}Zn_xFe_2O_4$ ($x$ = 0.0, 0.1, 0.2, 0.3, 0.4, 0.5) composite.

### 4.6 Magnetic studies of $BaFe_{12}O_{19}/NiFe_2O_4$ bilayer thin film

To investigate the exchange coupling in ferrite thin films; an attempt has been made to deposit bilayer thin film of $NiFe_2O_4$ /$BaFe_{12}O_{19}$ and its magnetic behavior was compared with pure $BaFe_{12}O_{19}$, and $NiFe_2O_4$ thin films. Fig. 4.43(a) shows the hysteresis loops of pure and bilayer films annealed at 800 °C. The obtained smooth demagnetization and single peak in respective SFD curve confirms the exchange coupling between $NiFe_2O_4$ and $BaFe_{12}O_{19}$ layer. This observation of exchange coupling in hexagonal/spinel ferrite bilayer system paved the way for future investigation.

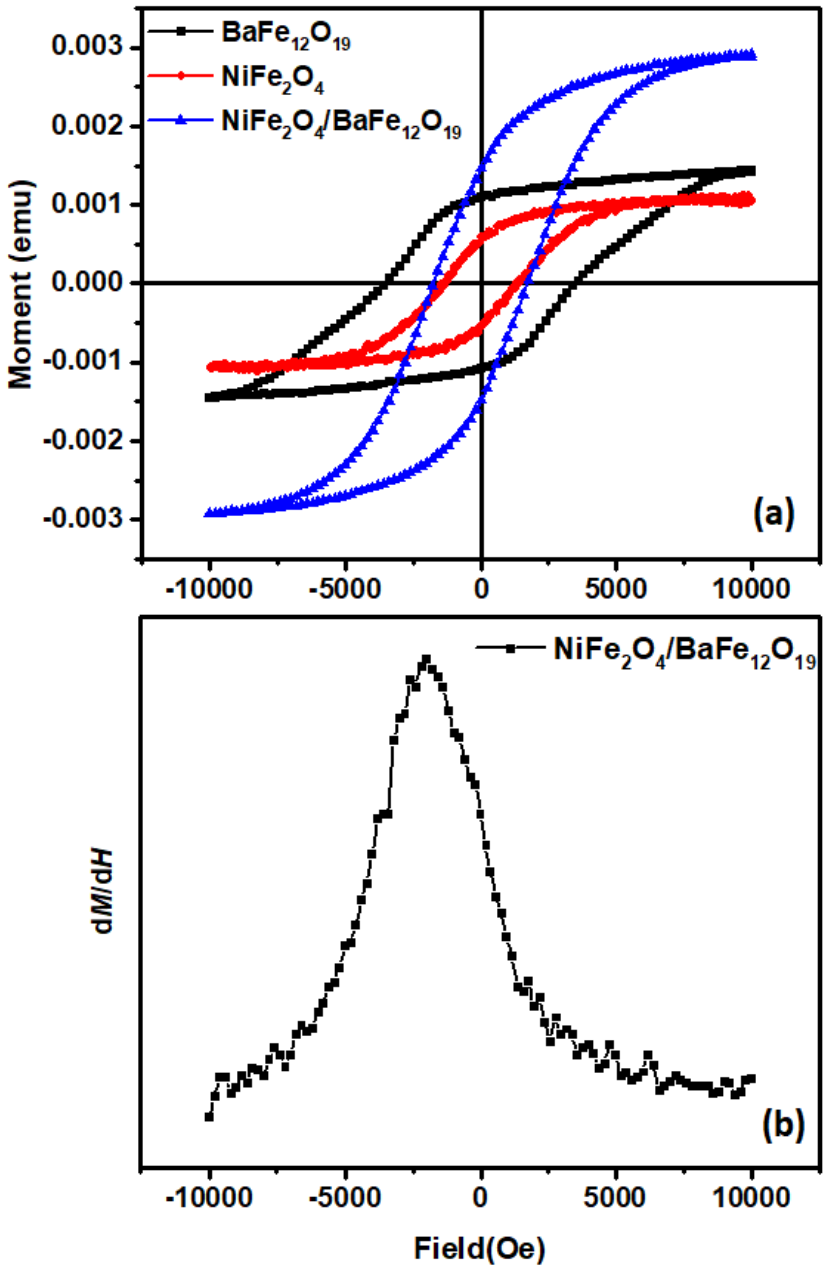


Fig. 4.43 (a) Hysteresis loops of $BaFe_{12}O_{19}$, $NiFe_2O_4$ and bilayer $BaFe_{12}O_{19}/NiFe_2O_4$ thin films, (b) SFD curve of bilayer system.

# *Chapter 5*

# Conclusions

**Overview**

This chapter summarizes the outcomes of the various experiments described in the previous chapter. The effect of various process parameters on exchange coupling is outlined. The influence of weight fraction and magnetization of soft phase on magnetic and microwave properties are concluded and tabulated. The exchange coupling are exist in bilayer $NiFe_2O_4/BaFe_{12}O_{19}$ thin film is also showcased. Future scope of the work is presented at the end of this chapter.

In the present work, exchange-coupled composites of $BaFe_{12}O_{19}/NiFe_2O_4$, $BaFe_{12}O_{19}/Ni_{0.5}Zn_{0.5}Fe_2O_4$, $BaFe_{12}O_{19}/CoFe_2O_4$ and $BaFe_{12}O_{19}/Co_{0.5}Zn_{0.5}Fe_2O_4$ in different weight ratio (90/10, 80/20, 70/30, 60/40 & 50/50) were prepared by sol-gel autocombustion method. The effect of various process parameters, annealing temperature, soft phase magnetization and weight fraction of soft phase on structural, magnetic and microwave properties has been investigated and compared. The important findings and conclusions drawn from the work are as follows:

- Firstly, exchange-coupled and non-exchange coupled BaM/NiF nanocomposites were prepared by adopting two different processing methods i.e. single-step (SS) and physical mixing (PM) and to describe the role of processing methodology. XRD patterns confirmed the co-existence of BaM and NiF phases in composites without any secondary phase. SEM micrographs showed the well distinguished BaM and NiF grains in exchange-coupled composites. Smooth hysteresis loops were observed for exchange-coupled composites in contrast to non-exchanged coupled, which showed stepped-loops for all studied compositions. *M-H* loops confirm that interfacial interaction is predominant in exchange-coupled nanocomposites. Higher *M* was found in exchange-coupled composites. Whereas, *M* showed a linear decrease with NiF content in non-coupled composites. $H_c$ found to decrease with NiF content with distinct trend among the two systems. $T_c$ also found to increase with the soft NiF content, which confirms the exchange coupling. Frequency dependent complex permittivity and permeability showed large variation between the two systems. Reflection losses at multiple frequencies were observed in exchange-coupled composites and maximum loss of -23.9 dB was obtained at 15.3 GHz frequency. These magnetic and microwave analysis suggests that single-step method is appropriate to prepare exchange-coupled system.

- Second, exchange-coupled BaM/NZFO composite in 70/30 weight ratio were prepared and effect of annealing temperature (950 °C–1150 °C) has been investigated. The X-ray diffraction pattern confirms co-existence of both BaM and NZFO phases for all studied temperature. TEM micrographs showed well distinguished particles of BaM and NZFO with different symmetry in the composites. Magnetic measurement confirmed the existence of exchange coupling between hard and soft phases. Higher *M*

and low $H_c$ than theoretical calculated values suggested that phases were well exchange-coupled. For 1050 °C; $M$ increased from 58 emu/g to 65 emu/g with drastic decrease in coercivity $H_c$. A sharp $T_c$ (473 °C) for exchange-coupled composite was observed, however, in non-exchange coupled system independent values of $T_c$ for NZFO (347 °C) and BaM (527 °C) were observed. The variation in $M$ and $H_c$ demonstrated that annealing temperature has strong influence on exchange coupling. Reflection losses in $K_u$-band were found to increase with a maximum value of −38 dB for the composite annealed at 1050 °C. Loss frequency also shifted toward lower values as a consequence of annealing temperature and exchange coupling.

- Series of exchange-coupled nanocomposites of BaM/NZFO were prepared and the effect of relative weight fraction has been investigated. Co-existence of BaM and NZFO phases in all composites were confirmed by XRD patterns. Well distinguished hexagonal BaM platelets along with small NZFO grains were observed in composite system. Coherent demagnetization curve for all studied composition demonstrated that BaM and NZFO phases were well exchange coupled. The drastic increase in $M$ with corresponding sharp decrease in $H_c$ for 70/30 weight ratio was observed. Complex permeability and permittivity in $K_u$-band showed oscillatory behaviour for higher weight fraction of NZFO. Reflection loss frequency also found to depends on NZFO content and maximum loss of -41 dB was observed for 70/30 weight ratio at 13.8 GHz frequency.

- Series of exchange-coupled BaM/CFO and BaM/CZFO composites were synthesized and effect of soft (CFO/CZFO) phase weight fraction on the properties of composites has been investigated and compared. Phase identification and microstructural analysis confirmed the presence of BaM and CFO/CZFO phases in the composites. Existence of interfacial coupling was verified by smooth demagnetization behavior and single peak in corresponding d$M$/d$H$ curves. $M$ and $H_c$ showed strong dependence on relative weight fraction and nature of soft phase. Parallel existence of high permeability ($\mu$) as well as high permittivity ($\varepsilon$) was obtained in these exchange-coupled composite systems. Such exchange-coupled composite could be a promising magnetodielectric material for microwave applications.

- Composite of BaM and $Ni_{1-x}Zn_xFe_2O_4$ ($x$ = 0.0, 0.1, 0.2, 0.3, 0.4, 0.5) in the weight ratio of 70/30 were prepared and effect of soft phase magnetization on exchange coupling were explained. Different values of soft phase magnetization were induced by substituting non magnetic $Zn^{2+}$ ions. The diffraction patterns confirmed the coexistence of BaM and spinel phases in all the composites. $M$ and $H_c$ showed strong dependence on nature of soft phase. Composites with $x$ =0.1 and 0.5 soft phase showed reflection losses at multiple frequencies. Permittivity and permeability spectra also varied with soft phase magnetization.
- A successful attempt has been made to deposit bilayer thin film of $NiFe_2O_4$ /$BaFe_{12}O_{19}$. Smooth demagnetization and single peak in respective SFD curve confirms the exchange coupling between $NiFe_2O_4$ and $BaFe_{12}O_{19}$ layer.

Obtained properties from different series are shown in Table 5.1.

Table 1.1 Comparative properties of studied composite systems.

| **Composite** | ***M*** (emu/g) | $H_c$ (Oe) | **Reflection loss** | **Dielectric properties** |
|---|---|---|---|---|
| $BaFe_{12}O_{19}(70)/NiFe_2O_4(30)$ | 57.7 | 1068 | -23.9 dB at 15.3 GHz<br>-21.2 dB at 16.3 GHz | ε =11<br>$\mu$= 1.26 |
| $BaFe_{12}O_{19}(70)/Ni_{0.7}Zn_{0.3}Fe_2O_4(30)$ | 60 | 679 | -5 dB at 15.5 GHz | ε =18.7<br>$\mu$= 1.9 |
| $BaFe_{12}O_{19}(70)/Ni_{0.6}Zn_{0.4}Fe_2O_4(30)$ | 62 | 665 | -4 dB at 15.6 GHz | ε =27.2<br>$\mu$= 1.8 |
| $BaFe_{12}O_{19}(70)/Ni_{0.5}Zn_{0.5}Fe_2O_4(30)$ | 64.5 | 690 | -41 dB at 13.8 GHz | ε =11<br>$\mu$= 1.26 |
| $BaFe_{12}O_{19}(50)/CoFe_2O_4(50)$ | 63.9 | 498 | -41 dB at 18 GHz | ε =47<br>$\mu$= 1.7 |
| $BaFe_{12}O_{19}(50)/Co_{0.5}Zn_{0.5}Fe_2O_4(50)$ | 71.8 | 146 | ----- | ε =24<br>$\mu$= 1.2 |

**Future Scope**

The result indicates that exchange coupling between hard and soft phases, remarkably affect it magnetodielectric properties in microwave region. It was concluded that both permittivity and permeability can be simultaneously enhanced in the microwave frequency bands (12.4 - 18 GHz) for exchange coupled ferrites.

Such exchange-coupled composite are widely explored as microwave absorber, however their realization as magnetodielectric material operable in GHz range need an attention. For instance, exchange-coupled magnetodielectric with high permittivity and permeability could be exploited as antenna substrate for miniaturization.

## References


[1] R. Coehoorn, D.B. de Mooij, C. de Waard, Meltspun permanent magnet materials containing $Fe_3B$ as the main phase, J. Magn. Magn. Mater. 80 (1989) 101–104. https://doi.org/10.1016/0304-8853(89)90333-8.

[2] E.F. Kneller, R. Hawig, The exchange-spring magnet: A new material principle for permanent magnets, IEEE Trans. Magn. 27 (1991) 3588–3600. https://doi.org/10.1109/20.102931.

[3] R. Skomski, J.M.D. Coey, Giant energy product in nanostructured two-phase magnets, Phys. Rev. B. 48 (1993) 15812–15816. https://doi.org/10.1103/PhysRevB.48.15812.

[4] J.M.D.Coey, R. Skomski, Nucleation field and energy product of aligned two-phase magets- progress towards the "$1MJ/m^3$" magnet, IEEE Trans. Magn. 29 (1993) 2860–2862.

[5] C. J. Yang, E.B. Park, The effect of magnetic field treatment on the enhanced exchange coupling of a $Nd_2Fe_{14}B/Fe_3B$ magnet, J. Magn. Magn. Mater. 166 (1997) 243–248. https://doi.org/10.1016/S0304-8853(96)00421-0.

[6] Y. Gao, J.H. Zhu, C.J. Yang, E.B. Park, Thermomagnetic behaviors of $Nd_2Fe_{14}B/Fe_3B$ based nanocomposite magnets, J. Magn. Magn. Mater. 186 (1998) 97–103. https://doi.org/10.1016/S0304-8853(98)00056-0.

[7] A. V. Khvalkovskii, K.A. Zvezdin, A.A. Zvezdin, V.S. Gornakov, D.G. Skachkov, P. Perlo, Micromagnetic investigation of reversal processes in SmCo/Fe exchange-coupled magnets, Phys. B Condens. Matter. 372 (2006) 358–361. https://doi.org/10.1016/j.physb.2005.10.085.

[8] T. Schrefl, H. Forster, R. Dittrich, D. Suess, W. Scholz, J. Fidler, Reversible magnetization processes and energy density product in Sm-CoFe and Sm-Co/Co bilayers, J. Appl. Phys. 93 (2003) 6489–6491. https://doi.org/10.1063/1.1558245.

[9] J.M.D. Coey, R. Skomski, New magnets from interstitial intermetallics, Phys. Scr. 1993 (1993) 315–321. https://doi.org/10.1088/0031-8949/1993/T49A/055.

[10] L.H. Lewis, D.O. Welch, V. Panchanathan, L.H. Lewis, D.O. Welch, " Exchange-spring " Nd–Fe–B alloys : Investigations into reversal mechanisms and their temperature dependence, J. Appl. Phys. 81 (1997) 4422–4424. https://doi.org/10.1063/1.364789.

[11] V.M. Chakka, Z.S. Shan, J.P. Liu, Effect of coupling strength on magnetic properties of exchange spring magnets, J. Appl. Phys. 94 (2003) 6673–6677. https://doi.org/10.1063/1.1621712.

[12] E.E. Fullerton, J.S. Jiang, S.D. Bader, Hard/soft magnetic heterostructures: model exchange-spring magnets, J. Magn. Magn. Mater. 200 (1999) 392–404. https://doi.org/10.1016/S0304-8853(99)00376-5.

[13] C.L. Platt, A.E. Berkowitz, S. David, E.E. Fullerton, J.S. Jiang, S.D. Bader, Reversal

modes of exchange-spring magnets revealed by torque magnetometry, Appl. Phys. Lett. 79 (2001) 3992–3994. https://doi.org/10.1063/1.1425432.

[14] V.G. Harris, A. Geiler, Y. Chen, S.D. Yoon, M. Wu, A. Yang, Z. Chen, P. He, P. V. Parimi, X. Zuo, C.E. Patton, M. Abe, O. Acher, C. Vittoria, Recent advances in processing and applications of microwave ferrites, J. Magn. Magn. Mater. 321 (2009) 2035–2047. https://doi.org/10.1016/j.jmmm.2009.01.004.

[15] M. Pardavi-Horvath, Microwave applications of soft ferrites, J. Magn. Magn. Mater. 215 (2000) 171–183. https://doi.org/10.1016/S0304-8853(00)00106-2.

[16] V.G. Harris, Modern microwave ferrites, IEEE Trans. Magn. 48 (2012) 1075–1104. https://doi.org/10.1109/TMAG.2011.2180732.

[17] J. L. Snoek, Non-metallic magnetic materials for high frequencies, Philips Tech. Rev. 8 (1946) 353–360.

[18] J.L. Snoek, Magnetic and electrical properties of the binary systems $MO.Fe_20_3$, Physica. (1936).

[19] J.Y. Shin, J.H. Oh, The Microwave Absorbing Phenomena of Ferrite Microwave Absorbers, IEEE Trans. Magn. 29 (1993) 3437–3439. https://doi.org/10.1109/20.281188.

[20] H.J. Kwon, J.Y. Shin, J.H. Oh, The microwave absorbing and resonance phenomena of Y-type hexagonal ferrite microwave absorbers, J. Appl. Phys. 75 (1994) 6109–6111. https://doi.org/10.1063/1.355476.

[21] A.J.B. Fuller, Ferrites at Microwave frequencies, Peter Peregrinud(Ltd.), 1987.

[22] V. Sunny, P. Kurian, P. Mohanan, P.A. Joy, M.R. Anantharaman, A flexible microwave absorber based on nickel ferrite nanocomposite, J. Alloys Compd. 489 (2010) 297–303. https://doi.org/10.1016/j.jallcom.2009.09.077.

[23] T. Giannakopoulou, L. Kompotiatis, A. Kontogeorgakos, G. Kordas, Microwave behavior of ferrites prepared via sol-gel method, J. Magn. Magn. Mater. 246 (2002) 360–365. https://doi.org/10.1016/S0304-8853(02)00106-3.

[24] H. Kojima, Chapter 5 Fundamental properties of hexagonal ferrites with magnetoplumbite structure, (1982).

[25] J. J. A. Kohn, D. W. Eckart, C. F. Cook, Crystallography of the hexagonal ferrites, Science (80). 172 (1971) 519–525.

[26] J.C.J. X. Obradors, A. Collomb, M. Pernet, D. Samaras, X-ray analysis of the structural and dynamic properties of $BaFe_{12}O_{19}$ hexagonal ferrite at room temperature, J. Solid State Chem. 56 (1985) 171–181.

[27] Y.J. Kim, S.S. Kim, Magnetic and microwave absorbing properties of Ti and Co substituted M-hexaferrites in Ka-band frequencies (18-26.5̃4 GHz), J. Electroceramics. 24 (2010) 314–318. https://doi.org/10.1007/s10832-009-9575-x.

[28] C.V. J. Wang, A. Geiler, P. Mistry, D.R. Kaeli, V.G. Harris, Design and simulation of self-biased circulators in the ultrahigh frequency band, J. Magn. Magn. Mater. 324 (2012) 991–994.

[29] R.C. Pullar, Hexagonal ferrites : A review of the synthesis , properties and applications of hexaferrite ceramics, J. Prog. Mater. Sci. 57 (2012) 1191–1334. https://doi.org/10.1016/j.pmatsci.2012.04.001.

[30] R.C. Pullar, Hexagonal ferrites: A review of the synthesis, properties and applications of hexaferrite ceramics, Prog. Mater. Sci. 57 (2012) 1191–1334. https://doi.org/10.1016/j.pmatsci.2012.04.001.

[31] G. Feng, W. Zhou, C.H. Wang, Y. Qing, D. Chen, L. Gao, F. Luo, D. Zhu, Microwave absorption of M-type hexaferrite $Ba_{1-x}Ca_xFe_{12}O_{19}$ ($x \leq 0.4$) ceramics in 2.6–18 GHz, Ceram. Int. 45 (2019) 7102–7107. https://doi.org/10.1016/j.ceramint.2018.12.214.

[32] H. Sözeri, Z. Mehmedi, H. Erdemi, A. Baykal, U. Topal, B. Aktaş, Microwave properties of $BaFe_{11}Mg^{2+}_{0.25}X^{2+}_{0.25}Ti^{4+}_{0.25}O_{19}$ ($X^{2+}$=Cu, Mn, Zn, Ni and Co) nanoparticles in 0-26.5 GHz range, Ceram. Int. 42 (2016) 2611–2625. https://doi.org/10.1016/j.ceramint.2015.10.065.

[33] A. Baykala, Eryiğit, M. Amir, H. Güngüneş, H. Sözeri, S.E. Shirsath, M. Sertkol, S.M. Asiri, Magnetic Properties and Cation Distribution of Bimetallic (Mn–Co) Doped $NiFe_2O_4$ Nanoparticles, J. Inorg. Organomet. Polym. Mater. 27 (2017) 1893–1900. https://doi.org/10.1007/s10904-017-0659-9.

[34] A. Baykal, S. Ünver, U. Topal, H. Sözeri, Pb substituted Ba,Sr-hexaferrite nanoparticles as high quality microwave absorbers, Ceram. Int. 43 (2017) 14023–14030. https://doi.org/10.1016/j.ceramint.2017.07.134.

[35] G. Albanese, A. Deriu, E. Lucchini, G. Slokar, Mössbauer investigation of In and Sc substituted barium hexaferrite, Appl. Phys. A Solids Surfaces. 26 (1981) 45–50. https://doi.org/10.1007/BF01197677.

[36] T. Perekalina, M. Vinnik, R. Zvereva, A. Shchurova, Magnetic Properties of Hexagonal Ferrites with Weak Exchange Coupling between Sublattices, Sov. J. Exp. Theor. Phys. 32 (1971) 813.

[37] G. Albanese, A. Deriu, Magnetic properties of Al, Ga, Sc, In substituted barium ferrites: A comparative analysis, Ceramurg. Int. 5 (1979) 3–10. https://doi.org/10.1016/0390-5519(79)90002-4.

[38] L.G. Van Uitert, F.W. Swanekamp, Permanent magnet oxides containing divalent metal ions. II, J. Appl. Phys. 28 (1957) 482–485. https://doi.org/10.1063/1.1722776.

[39] K. Haneda, H. Kojima, Intrinsic Coercivity of $BaFe_{12-x}Cr_xO_{19}$, Phys. Status Solidi. 6 (1971) 259–264. https://doi.org/10.1002/pssa.2210060129.

[40] A.H. Mones, E. Banks, Cation substitutions in $BaFe_{12}O_{19}$, J. Phys. Chem. Solids. 4 (1958) 217–222. https://doi.org/10.1016/0022-3697(58)90119-7.

[41] P.C. Dorsey, P. Lubitz, D.B. Chrisey, J.S. Horwitz, $CoFe_2O_4$ thin films grown on (100) MgO substrates using pulsed laser deposition, J. Appl. Phys. 79 (1996) 6338. https://doi.org/10.1063/1.361991.

[42] Y.B.L. K.P. Chae, J.G. Lee, W.K. Kim, Magnetic properties of Ti-doped $CoFe_2O_4$ films, J. Magn. Magn. Mater. 248 (2002) 236–240.

[43] Liu C., Zou B., Rondinone A. J., Zhang Z. J., Chemical Control of Superparamagnetic Properties of Magnesium and Cobalt Spinel Ferrite Nanoparticles through Atomic Level Magnetic Couplings, J. Am. Chem. Soc. 122 (2000) 6263–6267.

[44] K.T.Han, The origin of FMR parameter shift in pollycrystalline $MgFe_2O_4$ ferrite spheres, Phys. Status Solidi. 155 (1996) 215–222.

[45] H. How, P. Shi, C. Vittoria, L.C. Kempel, K.D. Trott, Single-crystal YIG phase shifter using composite stripline structure at X band , J. Appl. Phys. 87 (2000) 4966–4968. https://doi.org/10.1063/1.373217.

[46] Y. Chen, T. Sakai, T. Chen, S.D. Yoon, C. Vittoria, V.G. Harris, Screen printed thick self-biased, low-loss, barium hexaferrite films by hot-press sintering, J. Appl. Phys. 100 (2006) 1–9. https://doi.org/10.1063/1.2221527.

[47] A. Ataie, I.R. Harris, C.B. Ponton, Magnetic properties of hydrothermally synthesized strontium hexaferrite as a function of synthesis conditions, J. Mater. Sci. 30 (1995) 1429–1433. https://doi.org/10.1007/BF00375243.

[48] S.D. Yoon, C. Vittoria, Microwave and magnetic properties of barium hexaferrite films having the c-axis in the film plane by liquid phase epitaxy technique, J. Appl. Phys. 93 (2003) 8597–8599. https://doi.org/10.1063/1.1557791.

[49] F. Licci, G. Turilli, T. Besagni, Phase Analysis and Single Domain Detection in Hexaferrite Powders for Magnetic Recording., IEEE Trans. Magn. 24 (1987) 593–597. https://doi.org/10.1109/20.43989.

[50] J.F. Wang, C.B. Ponton, I.R. Harris, Ultrafine SrM particles with high coercivity by chemical coprecipitation, 245 (2002) 1464–1467.

[51] R.C. Pullar, A.K. Bhattacharya, The synthesis and characterisation of $Co_2X$ ($Ba_2Co_2Fe_{28}O_{46}$) and $Co_2U$ ($Ba_4Co_2Fe_{36}O_{60}$) ferrite fibres, manufactured from a sol-gel process, J. Mater. Sci. 36 (2001) 4805–4812. https://doi.org/10.1023/A:1017947625940.

[52] Z.H.M. G.Xiong, Preparation and magnetic properties of $Ba_2Co_2Fe_{28}O_{46}$ nanocrystals, J. Appl. Phys. 88 (2000) 519–523.

[53] K.N. Rozanov, Z.W. Li, L.F. Chen, M.Y. Koledintseva, Microwave permeability of $Co_2Z$ composites, J. Appl. Phys. 97 (2005) 013905–1 – 013905–7. https://doi.org/10.1063/1.1827911.

[54] C.K.O. Z.W. Li, L. Chen, High-frequency magnetic properties of W-type barium-ferrite

$BaZn_{2-x}Co_xFe_{16}O_{27}$ composites, J. Appl. Phys. 94 (2003) 5918–5924.

[55] M. Obol, X. Zuo, C. Vittoria, Oriented Y-type hexaferrites for ferrite device, J. Appl. Phys. 91 (2002) 7616–7618. https://doi.org/10.1063/1.1446113.

[56] S.E. Jacobo, P.G. Bercoff, C.A. Herme, L.A. Vives, Sr hexaferrite/Ni ferrite nanocomposites: Magnetic behavior and microwave absorbing properties in the X-band, Mater. Chem. Phys. 157 (2015) 124–129. https://doi.org/10.1016/j.matchemphys.2015.03.026.

[57] S. Tyagi, H.B. Baskey, R.C. Agarwala, V. Agarwala, T.C. Shami, Development of hard/soft ferrite nanocomposite for enhanced microwave absorption, Ceram. Int. 37 (2011) 2631–2641. https://doi.org/10.1016/j.ceramint.2011.04.012.

[58] A. Saini, K. Rana, A. Thakur, P. Thakur, J.L. Mattei, P. Queffelec, Low loss composite nano ferrite with matching permittivity and permeability in UHF band, Mater. Res. Bull. 76 (2016) 94–99. https://doi.org/10.1016/j.materresbull.2015.12.002.

[59] N. Poudyal, C. Rong, V.V. Nguyen, J.P. Liu, Hard-phase engineering in hard/soft nanocomposite magnets, Mater. Res. Express. 1 (2014). https://doi.org/10.1088/2053-1591/1/1/016103.

[60] A. Saini, A. Thakur, P. Thakur, Effective Permeability and Miniaturization Estimation of Ferrite-loaded Microstrip Patch Antenna, J. Electron. Mater. 45 (2016) 4162–4170. https://doi.org/10.1007/s11664-016-4634-y.

[61] R. Skomski, Nanomagnetics, J. Phys. Condens. Matter. 15 (2003). https://doi.org/10.1088/0953-8984/15/20/202.

[62] D. Suess, T. Schrefl, S. Fähler, M. Kirschner, G. Hrkac, F. Dorfbauer, J. Fidler, Exchange spring media for perpendicular recording, Appl. Phys. Lett. 87 (2005). https://doi.org/10.1063/1.1951053.

[63] T. Schrefl, H. Kronmüller, J. Fidler, Exchange hardening in nano-structured two-phase permanent magnets, J. Magn. Magn. Mater. 127 (1993) L273–L277. https://doi.org/10.1016/0304-8853(93)90042-Z.

[64] T. Schrefl, R. Fischer, J. Fidler, H. Kronmüller, Two- and three-dimensional calculation of remanence enhancement of rare-earth based composite magnets (invited), J. Appl. Phys. 76 (1994) 7053–7058. https://doi.org/10.1063/1.358026.

[65] T. Schrefl, J. Fidler, Modelling of exchange-spring permanent magnets, J. Magn. Magn. Mater. 177–181 (1998) 970–975. https://doi.org/10.1016/S0304-8853(97)00653-7.

[66] T. Schrefl, J. Fidler, H. Kronmüller, Remanence and coercivity in isotropic nanocrystalline permanent magnets, Phys. Rev. B. 49 (1994) 6100–6110. https://doi.org/10.1103/PhysRevB.49.6100.

[67] E.H. Feutrill, P.G. McCormick, R. Street, Simulation of magnetization reversal in two-

phase exchange coupled nanocrystalline materials, J. Appl. Phys. 75 (1994) 5701–5703. https://doi.org/10.1063/1.355588.

[68] R. Fischer, T. Schrefl, H. Kronmüller, J. Fidler, Phase distribution and computed magnetic properties of high-remanent composite magnets, J. Magn. Magn. Mater. 150 (1995) 329–344. https://doi.org/10.1016/0304-8853(95)00298-7.

[69] W.C. Feng, R.W. Gao, S.S. Yan, W. Li, M.G. Zhu, Effects of phase distribution and grain size on the effective anisotropy and coercivity of nanocomposite $Nd_2Fe_{14}B$/α-Fe magnets, J. Appl. Phys. 98 (2005). https://doi.org/10.1063/1.2009078.

[70] C.J. Yang, E.B. Park, The effect of magnetic field treatment on enhanced exchange coupling of $Nd_2Fe_{14}B/Fe_3B$ magnet, IEEE Trans. Magn. 32 (1996) 4428–4430. https://doi.org/10.1109/20.538890.

[71] D.H. Ping, Y.Q. Wu, K. Hono, Microstructure and magnetic properties of microalloyed α-Fe/$Nd_2Fe_{14}B$ nanocomposites, J. Magn. Magn. Mater. 239 (2002) 437–440. https://doi.org/10.1016/S0304-8853(01)00615-1.

[72] Z.H. Cheng, H. Kronmüller, B.G. Shen, Microstructure refinement and improvements of magnetic properties of two-phase exchange-coupled $Sm_2Fe_{15}Ga_2Cx$/α-Fe nanocomposites by additional Zr, Appl. Phys. Lett. 73 (1998) 1586–1588. https://doi.org/10.1063/1.122212.

[73] R.W. Gao, W.C. Feng, H.Q. Liu, B. Wang, W. Chen, G.B. Han, P. Zhang, H. Li, W. Li, Y.Q. Guo, W. Pan, X.M. Li, M.G. Zhu, X. Li, Exchange-coupling interaction, effective anisotropy and coercivity in nanocomposite permanent materials, J. Appl. Phys. 94 (2003) 664–668. https://doi.org/10.1063/1.1581380.

[74] Y.J. Tang, F.T. Parker, H. Harper, A.E. Berkowitz, K. Vecchio, A. Rohatgi, B.M. Ma, Microstructure and exchange coupling in nanocrystalline $Nd_2(FeCo)_{14}B$α-FeCo particles produced by spark erosion, Appl. Phys. Lett. 86 (2005) 1–3. https://doi.org/10.1063/1.1890474.

[75] M.F. Hansen, K.S. Vecchio, F.T. Parker, F.E. Spada, A.E. Berkowitz, Exchange-spring permanent magnet particles produced by spark-erosion, Appl. Phys. Lett. 82 (2003) 1574–1576. https://doi.org/10.1063/1.1560559.

[76] V. Neu, P. Crespo, R. Schäfer, J. Eckert, L. Schultz, High remanence Nd-Fe-B-X (X = Cu, Si, Nb, Cu, Zr) powders by mechanical alloying, J. Magn. Magn. Mater. 157–158 (1996) 61–62. https://doi.org/10.1016/0304-8853(95)01151-X.

[77] T. Hopfinger, A.R. Yavari, D. Negri, J. Alonso, A. Hernando, Nanocrystallization reactions in the fabrication of $Fe_{14}Nd_2B$ + Fe hard-soft magnets, J. Magn. Magn. Mater. 164 (1996). https://doi.org/10.1016/S0304-8853(96)00655-5.

[78] T. Maeda, S. Sugimoto, T. Kagotani, N. Tezuka, K. Inomata, Effect of the soft/hard exchange interaction on natural resonance frequency and electromagnetic wave absorption of the rare earth-iron-boron compounds, J. Magn. Magn. Mater. 281 (2004) 195–205. https://doi.org/10.1016/j.jmmm.2004.04.105.

[79] N.V.R. Rao, R. Gopalan, M.M. Raja, V. Chandrasekaran, D. Chakravarty, Structural and magnetic studies on spark plasma sintered $SmCo_5$/Fe bulk nanocomposite magnets, 312 (2007) 252–257. https://doi.org/10.1016/j.jmmm.2006.10.057.

[80] Y. Hou, S. Sun, C. Rong, J.P. Liu, $SmCo_5$ Fe nanocomposites synthesized from reductive annealing of oxide nanoparticles, Appl. Phys. Lett. 91 (2007) 1–4. https://doi.org/10.1063/1.2799170.

[81] X.Y. Xiong, C.B. Rong, S. Rubanov, Y. Zhang, J.P. Liu, Atom probe study on the bulk nanocomposite SmCo/Fe permanent magnet produced by ball-milling and warm compaction, J. Magn. Magn. Mater. 323 (2011) 2855–2858. https://doi.org/10.1016/j.jmmm.2011.06.035.

[82] M. Shindo, M. Ishizone, A. Sakuma, H. Kato, T. Miyazaki, Magnetic properties of exchange-coupled α-Fe/Nd–Fe–B multilayer thin-film magnets, J. Appl. Phys. 81 (1997) 4444–4446. https://doi.org/10.1063/1.364970.

[83] J.S. Jiang, J.E. Pearson, Z.Y. Liu, B. Kabius, S. Trasobares, D.J. Miller, S.D. Bader, D.R. Lee, D. Haskel, G. Srajer, J.P. Liu, A new approach for improving exchange-spring magnets, J. Appl. Phys. 97 (2005) 10K311. https://doi.org/10.1063/1.1855032.

[84] J.E. Davies, O. Hellwig, E.E. Fullerton, J.S. Jiang, S.D. Bader, G.T. Zimányi, K. Liu, Anisotropy dependence of irreversible switching in Fe/SmCo and FeNi/FePt exchange spring magnet films, Appl. Phys. Lett. 86 (2005) 1–3. https://doi.org/10.1063/1.1954898.

[85] D.R. Cornejo, F.P. Missell, Preisach analysis of reversible magnetization in SmCo/Fe films, J. Appl. Phys. 87 (2000) 4741–4743. https://doi.org/10.1063/1.373144.

[86] X.H. Liu, L.Y. Cui, S.X. Zhou, C.Y. Wang, B.Y. Quan, L.J. Wang, W. Zheng, A.L. Wang, J.C. Chen, Magnetic properties of SmCo/Fe/SmCo trilayer films, Mater. Sci. Eng. A. 304–306 (2001) 969–971. https://doi.org/10.1016/S0921-5093(00)01585-9.

[87] V. Neu, K. Häfner, A.K. Patra, L. Schultz, Fully epitaxial, exchange coupled $SmCo_5$/Fe/$SmCo_5$ trilayers, J. Phys. D. Appl. Phys. 39 (2006) 5116–5120. https://doi.org/10.1088/0022-3727/39/24/003.

[88] Y. Choi, J.S. Jiang, J.E. Pearson, S.D. Bader, J.J. Kavich, J.W. Freeland, J.P. Liu, Controlled interface profile in Sm-CoFe exchange-spring magnets, Appl. Phys. Lett. 91 (2007). https://doi.org/10.1063/1.2769755.

[89] Y. Choi, J.S. Jiang, J.E. Pearson, S.D. Bader, J.P. Liu, Origin of recoil hysteresis loops in Sm-CoFe exchange-spring magnets, Appl. Phys. Lett. 91 (2007) 1–4. https://doi.org/10.1063/1.2752534.

[90] Y. Liu, Y.Q. Wu, M.J. Kramer, Y. Choi, J.S. Jiang, Z.L. Wang, J.P. Liu, Microstructure analysis of a SmCo/Fe exchange spring bilayer, Appl. Phys. Lett. 93 (2008). https://doi.org/10.1063/1.2978325.

[91] S. Sawatzki, R. Heller, C. Mickel, M. Seifert, L. Schultz, S. Sawatzki, R. Heller, C.

Mickel, M. Seifert, L. Schultz, V. Neu, Largely enhanced energy density in epitaxial $SmCo_5/Fe/SmCo_5$ exchange spring trilayers, 123922 (2013). https://doi.org/10.1063/1.3596756.

[92] W. Bin Cui, Y.K. Takahashi, K. Hono, $Nd_2Fe_{14}B$/FeCo anisotropic nanocomposite films with a large maximum energy product, Adv. Mater. 24 (2012) 6530–6535. https://doi.org/10.1002/adma.201202328.

[93] J. Zhang, Y.K. Takahashi, R. Gopalan, K. Hono, $Sm(Co,Cu)_5$/Fe exchange spring multilayer films with high energy product, Appl. Phys. Lett. 86 (2005) 1–3. https://doi.org/10.1063/1.1889238.

[94] X.J. Weng, L.C. Shen, H. Tang, G.P. Zhao, J. Xia, F.J. Morvan, J. Zou, Change of coercivity mechanism with the soft film thickness in hard-soft trilayers, J. Magn. Magn. Mater. 475 (2019) 352–358. https://doi.org/10.1016/j.jmmm.2018.10.118.

[95] W. Si, G.P. Zhao, N. Ran, Y. Peng, F.J. Morvan, X.L. Wan, Deterioration of the coercivity due to the diffusion induced interface layer in hard/soft multilayers, Sci. Rep. 5 (2015) 1–9. https://doi.org/10.1038/srep16212.

[96] and Z.X. HAN Zhidong, DONG Limin, ZHANG Dawei, WU Ze, Synthesis of $BaFe_{12}O_{19}/MFe_2O_4$(M= Co, Mn) by sol-gel method, Rare Met. 25 (2006) 462–464.

[97] K.W. Moon, S.G. Cho, Y.H. Choa, K.H. Kim, J. Kim, Synthesis and magnetic properties of nano Ba-hexaferrite/NiZn ferrite composites, Phys. Status Solidi Appl. Mater. Sci. 204 (2007) 4141–4144. https://doi.org/10.1002/pssa.200777228.

[98] D. Roy, C. Shivakumara, P.S. Anil Kumar, Observation of the exchange spring behavior in hard-soft-ferrite nanocomposite, J. Magn. Magn. Mater. 321 (2009) 12–15. https://doi.org/10.1016/j.jmmm.2008.09.017.

[99] D. Roy, P.S.A. Kumar, Enhancement of (BH)max in a hard-soft-ferrite nanocomposite using exchange spring mechanism, J. Appl. Phys. 106 (2009) 1–5. https://doi.org/10.1063/1.3213341.

[100] D. Roy, C. Shivakumara, P.S. Anil Kumar, On the magnetization reversal of the oxide-based exchange spring magnet, J. Appl. Phys. 109 (2011) 2011–2014. https://doi.org/10.1063/1.3568813.

[101] D. Roy, K. V. Sreenivasulu, P.S. Anil Kumar, Investigation on non-exchange spring behaviour and exchange spring behaviour: A first order reversal curve analysis, Appl. Phys. Lett. 103 (2013). https://doi.org/10.1063/1.4836015.

[102] V. Harikrishnan, R. Ezhil Vizhi, A study on the extent of exchange coupling between $(Ba_{0.5}Sr_{0.5}Fe_{12}O_{19})_{1-x}(CoFe_2O_4)_x$ magnetic nanocomposites synthesized by solgel combustion method, J. Magn. Magn. Mater. 418 (2016) 217–223. https://doi.org/10.1016/j.jmmm.2016.03.037.

[103] V. Harikrishnan, R. Ezhil Vizhi, Temperature-dependent phase transition: Structural and magnetic properties of $Ba_{0.5}Sr_{0.5}Fe_{12}O_{19}$-$CoFe_2O_4$ nanocomposites, J. Phys. Chem.

Solids. 127 (2019) 35–42. https://doi.org/10.1016/j.jpcs.2018.12.004.

[104] S. Hazra, M.K. Patra, S.R. Vadera, N.N. Ghosh, A novel but simple "one-Pot" synthetic route for preparation of $(NiFe_2O_4)_x$-$(BaFe_{12}O_{19})_{1-x}$ composites, J. Am. Ceram. Soc. 95 (2012) 60–63. https://doi.org/10.1111/j.1551-2916.2011.04958.x.

[105] R. Xiong, W. Li, C. Fei, Y. Liu, J. Shi, Exchange-spring behavior in $BaFe_{12}O_{19}$-$Ni_{0.5}Zn_{0.5}Fe_2O_4$ nanocomposites synthesized by a combustion method, Ceram. Int. 42 (2016) 11913–11917. https://doi.org/10.1016/j.ceramint.2016.04.114.

[106] F. Song, X. Shen, M. Liu, J. Xiang, Magnetic hard/soft nanocomposite ferrite aligned hollow microfibers and remanence enhancement, J. Colloid Interface Sci. 354 (2011) 413–416. https://doi.org/10.1016/j.jcis.2010.11.020.

[107] M. Liu, X. Shen, F. Song, J. Xiang, X. Meng, Microstructure and magnetic properties of electrospun one-dimensional $Al^{3+}$ substituted $SrFe_{12}O_{19}$ nanofibers, J. Solid State Chem. 184 (2011) 871–876. https://doi.org/10.1016/j.jssc.2011.02.010.

[108] S. Torkian, A. Ghasemi, R.S. Razavi, Magnetic properties of hard-soft $SrFe_{10}Al_2O_{19}/Co_{0.8}Ni_{0.2}Fe_2O_4$ ferrite synthesized by one-pot sol-gel auto-combustion, J. Magn. Magn. Mater. 416 (2016) 408–416. https://doi.org/10.1016/j.jmmm.2016.05.050.

[109] S. Torkian, A. Ghasemi, Energy product enhancement in sufficiently exchange-coupled nanocomposite ferrites, J. Magn. Magn. Mater. 469 (2019) 119–127. https://doi.org/10.1016/j.jmmm.2018.07.018.

[110] J. Xia, Y. Shen, C. Xiao, W. Chen, X. Wu, W. Wu, Q. Wang, J. Li, Structural and Magnetic Properties of Soft/Hard $Mn_{0.6}Zn_{0.4}Fe_2O_4$@$Sr_{0.85}Ba_{0.15}Fe_{12}O_{19}$ Core/Shell Composite Synthesized by the Ball-Milling-Assisted Ceramic Process, J. Electron. Mater. 47 (2018) 6811–6820. https://doi.org/10.1007/s11664-018-6584-z.

[111] J. Xia, X. Wu, Y. Huang, W. Wu, J. Liang, Q. Li, Enhancements of saturation magnetization and coercivity in $Ni_{0.5}Zn_{0.5}Fe_2O_4/SrFe_{12}O_{19}$ composite powders by exchange-coupling mechanism, J. Mater. Sci. Mater. Electron. 30 (2019) 11682–11693. https://doi.org/10.1007/s10854-019-01527-2.

[112] W. Chen, C. Xiao, C. Huang, X. Wu, W. Wu, Q. Wang, J. Li, K. Zhou, Y. Huang, Exchange-coupling behavior in soft/hard $Li_{0.3}Co_{0.5}Zn_{0.2}Fe_2O_4/SrFe_{12}O_{19}$ core/shell composite synthesized by the two-step ball-milling-assisted ceramic process, J. Mater. Sci. Mater. Electron. 30 (2019) 1579–1590. https://doi.org/10.1007/s10854-018-0429-7.

[113] M.A. Almessiere, Y. Slimani, A. Baykal, Exchange spring magnetic behavior of $Sr_{0.3}Ba_{0.4}Pb_{0.3}Fe_{12}O_{19}/(CuFe_2O_4)_x$ nanocomposites fabricated by a one-pot citrate sol-gel combustion method, J. Alloys Compd. 762 (2018) 389–397. https://doi.org/10.1016/j.jallcom.2018.05.232.

[114] J.N. Dahal, D. Neupane, T.P. Poudel, Synthesis and magnetic properties of 4:1 hard-soft $SrFe_{12}O_{19}$-$La_{1-x}Sr_xMnO_3$ nanocomposite prepared by auto-combustion method,

AIP Adv. 9 (2019) 1–7. https://doi.org/10.1063/1.5096530.

[115] D. Li, F. Wang, A. Xia, L. Zhang, T. Li, C. Jin, X. Liu, A facile way to realize exchange coupling interaction in hard/soft magnetic composites, J. Magn. Magn. Mater. 417 (2016) 355–358. https://doi.org/10.1016/j.jmmm.2016.05.094.

[116] L. Zhao, Y. Wang, Y. Liu, Y. Zhu, Q. Cheng, L. Zheng, Q. Wang, Enhanced magnetic properties of $xSrFe_{12}O_{19}/(1-x)CoFe_2O_4$ composites, Mater. Res. Express. 4 (2017). https://doi.org/10.1088/2053-1591/aa9030.

[117] F. Tavakolinia, M. Yousefi, S.S.S. Afghahi, S. Baghshahi, S. Samadi, Synthesis of novel hard/soft ferrite composites particles with improved magnetic properties and exchange coupling, Process. Appl. Ceram. 12 (2018) 248–256. https://doi.org/10.2298/PAC1803248T.

[118] S. Manjura Hoque, C. Srivastava, V. Kumar, N. Venkatesh, H.N. Das, D.K. Saha, K. Chattopadhyay, Exchange-spring mechanism of soft and hard ferrite nanocomposites, Mater. Res. Bull. 48 (2013) 2871–2877. https://doi.org/10.1016/j.materresbull.2013.04.009.

[119] H. Yang, M. Liu, Y. Lin, Y. Yang, Simultaneous enhancements of remanence and $(BH)_{max}$ in $BaFe_{12}O_{19}/CoFe_2O_4$ nanocomposite powders, J. Alloys Compd. 631 (2015) 335–339. https://doi.org/10.1016/j.jallcom.2015.01.012.

[120] H. Yang, T. Ye, Y. Lin, M. Liu, G. Zhang, P. Kang, Giant enhancement of $(BH)_{max}$ in $BaFe_{12}O_{19}/Y_3Fe_5O_{12}$ nanocomposite powders, Mater. Lett. 145 (2015) 19–22. https://doi.org/10.1016/j.matlet.2015.01.080.

[121] Y. Wang, Y. Huang, Q. Wang, Preparation and magnetic properties of $BaFe_{12}O_{19}/Ni_{0.8}Zn_{0.2}Fe_2O_4$ nanocomposite ferrite, J. Magn. Magn. Mater. 324 (2012) 3024–3028. https://doi.org/10.1016/j.jmmm.2012.04.059.

[122] A. Xia, C. Zuo, L. Zhang, C. Cao, Y. Deng, W. Xu, M. Xie, S. Ran, C. Jin, X. Liu, Magnetic properties, exchange coupling and novel stripe domains in bulk $SrFe_{12}O_{19}/(Ni,Zn)Fe_2O_4$ composites, J. Phys. D. Appl. Phys. 47 (2014). https://doi.org/10.1088/0022-3727/47/41/415004.

[123] A. Xia, Y. Li, T. Li, S. Su, C. Jin, X. Liu, The availability of Henkel plots for sintered hard/soft magnetic composite ferrites, Phys. B Condens. Matter. 493 (2016) 14–16. https://doi.org/10.1016/j.physb.2016.04.013.

[124] A. Xia, S. Ren, J. Lin, Y. Ma, C. Xu, J. Li, C. Jin, X. Liu, Magnetic properties of sintered $SrFe_{12}O_{19}$-$CoFe_2O_4$ nanocomposites with exchange coupling, J. Alloys Compd. 653 (2015) 108–116. https://doi.org/10.1016/j.jallcom.2015.08.252.

[125] H. Yang, M. Liu, Y. Lin, Y. Yang, Simultaneous enhancements of remanence and $(BH)_{max}$ in $BaFe_{12}O_{19}/CoFe_2O_4$ nanocomposite powders, J. Alloys Compd. 631 (2015) 335–339. https://doi.org/10.1016/j.jallcom.2015.01.012.

[126] N.A. Algarou, Y. Slimani, M.A. Almessiere, A. Baykal, S. Guner, A. Manikandan, I.

Ercan, Enhancement on the exchange coupling behavior of $SrCo_{0.02}Zr_{0.02}Fe_{11.96}O_{19}/MFe_2O_4$ (M = Co, Ni, Cu, Mn and Zn) as hard/soft magnetic nanocomposites, J. Magn. Magn. Mater. 499 (2020) 166308. https://doi.org/10.1016/j.jmmm.2019.166308.

[127] N.A. Algarou, Y. Slimani, M.A. Almessiere, S. Güner, A. Baykal, I. Ercan, P. Kögerler, Exchange-coupling effect in hard/soft $SrTb_{0.01}Tm_{0.01}Fe_{11.98}O_{19}/AFe_2O_4$ (where A = Co, Ni, Zn, Cu and Mn) composites, Ceram. Int. (2019). https://doi.org/10.1016/j.ceramint.2019.11.201.

[128] A. Hilczer, K. Kowalska, E. Markiewicz, A. Pietraszko, B. Andrzejewski, Dielectric and magnetic response of $SrFe_{12}O_{19}$-$CoFe_2O_4$ composites obtained by solid state reaction, Mater. Sci. Eng. B Solid-State Mater. Adv. Technol. 207 (2016) 47–55. https://doi.org/10.1016/j.mseb.2016.02.003.

[129] R.K. Kotnala, S. Ahmad, A.S. Ahmed, J. Shah, A. Azam, Investigation of structural, dielectric, and magnetic properties of hard and soft mixed ferrite composites, J. Appl. Phys. 112 (2012). https://doi.org/10.1063/1.4752030.

[130] S.F. Mansour, O.M. Hemeda, M.A. Abdo, W.A. Nada, Improvement on the magnetic and dielectric behavior of hard/soft ferrite nanocomposites, J. Mol. Struct. 1152 (2018) 207–214. https://doi.org/10.1016/j.molstruc.2017.09.089.

[131] N. Chen, G. Mu, X. Pan, K. Gan, M. Gu, Microwave absorption properties of $SrFe_{12}O_{19}/ZnFe_2O_4$ composite powders, Mater. Sci. Eng. B Solid-State Mater. Adv. Technol. 139 (2007) 256–260. https://doi.org/10.1016/j.mseb.2007.02.002.

[132] L. Zhang, Z. Li, Synthesis and characterization of $SrFe_{12}O_{19}/CoFe_2O_4$ nanocomposites with core-shell structure, J. Alloys Compd. 469 (2009) 422–426. https://doi.org/10.1016/j.jallcom.2008.01.152.

[133] M. Mehdipour, H. Shokrollahi, Comparison of microwave absorption properties of $SrFe_{12}O_{19}$, $SrFe_{12}O_{19}/NiFe_2O_4$, and $NiFe_2O_4$ particles, J. Appl. Phys. 114 (2013). https://doi.org/10.1063/1.4816089.

[134] S. Tyagi, H.B. Baskey, R.C. Agarwala, V. Agarwala, T.C. Shami, Development of hard/soft ferrite nanocomposite for enhanced microwave absorption, Ceram. Int. 37 (2011) 2631–2641. https://doi.org/10.1016/j.ceramint.2011.04.012.

[135] S. Hazra, B.K. Ghosh, M.K. Patra, R.K. Jani, S.R. Vadera, N.N. Ghosh, A novel "one-pot" synthetic method for preparation of $(Ni_{0.65}Zn_{0.35}Fe_2O_4)_x$-$(BaFe_{12}O_{19})_{1-x}$ nanocomposites and study of their microwave absorption and magnetic properties, Powder Technol. 279 (2015) 10–17. https://doi.org/10.1016/j.powtec.2015.03.046.

[136] S. Hazra, B.K. Ghosh, M.K. Patra, R.K. Jani, S.R. Vadera, N.N. Ghosh, One-pot synthesis of $(NiFe_2O_4)_x$-$(SrFe_{12}O_{19})_{1-x}$ nanocomposites and their microwave absorption properties, J. Nanosci. Nanotechnol. 15 (2015) 6559–6567. https://doi.org/10.1166/jnn.2015.10491.

[137] S.R. Saeedi Afshar, M. Hasheminiasari, S.M. Masoudpanah, Structural, magnetic and

microwave absorption properties of $SrFe_{12}O_{19}/Ni_{0.6}Zn_{0.4}Fe_2O_4$ composites prepared by one-pot solution combustion method, J. Magn. Magn. Mater. 466 (2018) 1–6. https://doi.org/10.1016/j.jmmm.2018.06.061.

[138] V. Sharma, S. Kumari, B.K. Kuanr, Exchange-coupled hard-soft ferrites; A new microwave material, J. Alloys Compd. 736 (2018) 266–275. https://doi.org/10.1016/j.jallcom.2017.11.113.

[139] Y. Lin, X. Liu, T. Ye, H. Yang, F. Wang, C. Liu, Preparation and microwave absorption property of graphene-supported $CoFe_2O_4/Y_3Fe_5O_{12}$ nanocomposite, J. Mater. Sci. Mater. Electron. 27 (2016) 8177–8182. https://doi.org/10.1007/s10854-016-4821-x.

[140] Y. Liu, Z. Wang, L. Zhao, J. Zhou, Y. Wang, Improved magnetic and electromagnetic absorption properties of $xSrFe_{12}O_{19}/(1-x)NiFe_2O_4$ composites, J. Am. Ceram. Soc. 102 (2019) 6680–6687. https://doi.org/10.1111/jace.16506.

[141] K. Pubby, P. Sharma, S.B. Narang, Structural, magnetic, dielectric, microwave absorption, and optical characterization of $Ni_{0.1}Co_{0.9}(MnZr)_xFe_{2-2x}O_4/Ba_ySr_{1-y}Fe_{12}O_{19}$ nanocomposites, J. Mater. Sci. Mater. Electron. 31 (2020) 599–609. https://doi.org/10.1007/s10854-019-02564-7.

[142] Y. Lin, Y. Liu, J. Dai, L. Wang, H. Yang, Synthesis and microwave absorption properties of plate-like $BaFe_{12}O_{19}@Fe_3O_4$ core-shell composite, J. Alloys Compd. 739 (2018) 202–210. https://doi.org/10.1016/j.jallcom.2017.12.086.

[143] S.C. Sahoo, N. Venkataramani, S. Prasad, M. Bohra, R. Krishnan, Magnetic properties of nanocrystalline $CoFe_2O_4/ZnFe_2O_4$ bilayers, J. Supercond. Nov. Magn. 25 (2012) 2653–2657. https://doi.org/10.1007/s10948-011-1237-y.

[144] B.N. Sahu, S.C. Sahoo, N. Venkataramani, S. Prasad, R. Krishnan, M. Kostylev, R.L. Stamps, Magnetic and FMR study on $CoFe_2O_4/ZnFe_2O_4$ bilayers, IEEE Trans. Magn. 49 (2013) 4200–4203. https://doi.org/10.1109/TMAG.2013.2251327.

[145] A. V. Ramos, S. Matzen, J.B. Moussy, F. Ott, M. Viret, Artificial antiphase boundary at the interface of ferrimagnetic spinel bilayers, Phys. Rev. B - Condens. Matter Mater. Phys. 79 (2009) 1–8. https://doi.org/10.1103/PhysRevB.79.014401.

[146] J.M.P. and R.J.F. Y.Suzuki, R.B. van Dover, E.M. Gyorgy, Exchange-coupling in single-crystalline spinel-structure $(Mn,Zn)Fe_2O_4/CoFe_2O_4$ bilayers, Phys. Rev. B. 53 (1996) 14016–14019.

[147] J. Dong, Y. Zhang, X. Zhang, Q. Liu, J. Wang, Improved magnetic properties of $SrFe_{12}O_{19}$/FeCo core-shell nanofibers by hard/soft magnetic exchange-coupling effect, Mater. Lett. 120 (2014) 9–12. https://doi.org/10.1016/j.matlet.2014.01.022.

[148] X. Xu, J. Park, Y.K. Hong, A.M. Lane, Magnetically self-assembled $SrFe_{12}O_{19}$/Fe-Co core/shell particles, Mater. Chem. Phys. 152 (2015) 9–12. https://doi.org/10.1016/j.matchemphys.2014.11.061.

[149] M. Kahnes, J. Töpfer, Synthesis and magnetic properties of hard/soft $SrAl_2Fe_{10}O_{19}$ /Fe($FeCo_2$) nanocomposites, J. Magn. Magn. Mater. 480 (2019) 40–46. https://doi.org/10.1016/j.jmmm.2019.02.065.

[150] P. Veverka, E. Pollert, K. Závěta, S. Vasseur, E. Duguet, Sr-hexaferrite/maghemite composite nanoparticles - Possible new mediators for magnetic hyperthermia, Nanotechnology. 19 (2008). https://doi.org/10.1088/0957-4484/19/21/215705.

[151] T. Caillot, G. Pourroy, D. Stuerga, Microwave hydrothermal flash synthesis of nanocomposites Fe-Co alloy/cobalt ferrite, J. Solid State Chem. 177 (2004) 3843–3848. https://doi.org/10.1016/j.jssc.2004.06.009.

[152] N. Viart, R.S. Hassan, C. Ulhaq-Bouillet, C. Mény, P. Panissod, J.L. Loison, G. Versini, F. Huber, G. Pourroy, J. Verbeeck, G. Van Tendeloo, Oxidation processes at the metal/oxide interface in $CoFe_2/CoFe_2O_4$ bilayers deposited by pulsed laser deposition, Acta Mater. 54 (2006) 191–196. https://doi.org/10.1016/j.actamat.2005.08.041.

[153] G.C.P. Leite, E.F. Chagas, R. Pereira, R.J. Prado, A.J. Terezo, M. Alzamora, E. Baggio-Saitovitch, Exchange coupling behavior in bimagnetic $CoFe_2O_4/CoFe_2$ nanocomposite, J. Magn. Magn. Mater. 324 (2012) 2711–2716. https://doi.org/10.1016/j.jmmm.2012.03.034.

[154] J. Xiang, X. Zhang, J. Li, Y. Chu, X. Shen, Fabrication, characterization, exchange coupling and magnetic behavior of $CoFe_2O_4/CoFe_2$ nanocomposite nanofibers, Chem. Phys. Lett. 576 (2013) 39–43. https://doi.org/10.1016/j.cplett.2013.05.020.

[155] J. Liang, Z. Li, K. Ma, X. Wu, W. Wu, J. Xia, Y. Huang, Y. Huang, Improved magnetic properties of $Co_{0.5}LaxFe_{2.5-x}O_4$/FeCo composite powders by magnetic exchange–coupling effect, J. Magn. Magn. Mater. 491 (2019). https://doi.org/10.1016/j.jmmm.2019.165596.

[156] J. Sravani, S. V. Kummari, A. Dhole, V.V.S.S. Srikanth, C. Bansal, A. Rajanikanth, Synthesis of a novel rare earth free $Co_3C$-$Co_{0.35}Fe_{0.65}$ exchange spring magnet, Mater. Lett. 255 (2019) 126576. https://doi.org/10.1016/j.matlet.2019.126576.

[157] R. Safi, A. Ghasemi, R. Shoja-Razavi, The role of shell thickness on the exchange spring mechanism of cobalt ferrite/iron cobalt magnetic nanocomposites, Ceram. Int. 43 (2017) 617–624. https://doi.org/10.1016/j.ceramint.2016.09.203.

[158] F. Fabris, E. Lima, C. Quinteros, L. Neñer, M. Granada, M. Sirena, R.D. Zysler, H.E. Troiani, V. Leborán, F. Rivadulla, E.L. Winkler, Tunnel Magnetoresistance in Self-Assemblies of Exchange-Coupled Core/Shell Nanoparticles, Phys. Rev. Appl. 11 (2019) 1. https://doi.org/10.1103/PhysRevApplied.11.054089.

[159] A. Quesada, G. Delgado, L. Pascual, A.M. Aragón, P. Marín, C. Granados-Miralles, M. Foerster, L. Aballe, J.E. Prieto, J. De La Figuera, J.F. Fernández, P. Prieto, Exchange-spring behavior below the exchange length in hard-soft bilayers in multidomain configurations, Phys. Rev. B. 98 (2018) 1–7. https://doi.org/10.1103/PhysRevB.98.214435.

[160] N. Viart, R.S. Hassan, C. Ḿny, P. Panissod, C. Ulhaq-Bouillet, J.L. Loison, G. Versini, F. Huber, G. Pourroy, Diversity of the magnetic coupling behaviors in the $CoFe_2/CoFe_2O_4$ system, Appl. Phys. Lett. 86 (2005) 1–3. https://doi.org/10.1063/1.1923763.

[161] N. Imaoka, E. Kakimoto, K. Takagi, K. Ozaki, M. Tada, T. Nakagawa, M. Abe, Exchange coupling between soft magnetic ferrite and hard ferromagnetic $Sm_2Fe_{17}N_3$ in ferrite/$Sm_2Fe_{17}N_3$ composites, AIP Adv. 6 (2016) 2–8. https://doi.org/10.1063/1.4944519.

[162] H. Zeng, J. Li, J.P. Liu, Z.L. Wang, S. Sun, Exchange-coupled nanocomposite magnets by nanoparticle self-assembly, Nature. 420 (2002) 395–398. https://doi.org/10.1038/nature01208.

[163] R.A. Griffiths, J.L. Warren, C.W. Barton, J.J. Miles, P.W. Nutter, T. Thomson, Temperature-Dependent Studies of Coupled $Fe_{55}Pt_{45}/Fe_{49}Rh_{51}$ Thin Films, Phys. Rev. Appl. 10 (2018) 1. https://doi.org/10.1103/PhysRevApplied.10.054015.

[164] J.U. Thiele, S. Maat, E.E. Fullerton, FeRH/FePt exchange spring films for thermally assisted magnetic recording media, Appl. Phys. Lett. 82 (2003) 2859–2861. https://doi.org/10.1063/1.1571232.

[165] J.L. Tsai, H. Te Tzeng, G. Bin Lin, Magnetization reversal process in Fe/FePt films, Appl. Phys. Lett. 96 (2010) 20–23. https://doi.org/10.1063/1.3293444.

[166] G.B.G. Stenning, G.J. Bowden, S.A. Gregory, J.M.L. Beaujour, P.A.J. De Groot, G. Van Der Laan, L.R. Shelford, P. Bencok, P. Steadman, A.N. Dobrynin, T. Hesjedal, Magnetic reversal in a $YFe_2$ dominated $DyFe_2/YFe_2$ multilayer film, Appl. Phys. Lett. 101 (2012) 1–5. https://doi.org/10.1063/1.4746749.

[167] S. Sabet, A. Moradabadi, S. Gorji, M.H. Fawey, E. Hildebrandt, I. Radulov, D. Wang, H. Zhang, C. Kübel, L. Alff, Correlation of Interface Structure with Magnetic Exchange in a Hard/Soft Magnetic Model Nanostructure, Phys. Rev. Appl. 11 (2019) 32–37. https://doi.org/10.1103/PhysRevApplied.11.054078.

[168] S. Sabet, A. Moradabadi, S. Gorji, M. Yi, Q. Gong, M.H. Fawey, E. Hildebrandt, D. Wang, H. Zhang, B.X. Xu, C. Kübel, L. Alff, Impact of interface structure on magnetic exchange coupling in MnBi/FexCo1-x bilayers, Phys. Rev. B. 98 (2018) 1–8. https://doi.org/10.1103/PhysRevB.98.174440.

[169] M.R. Corfield, A.J. Williams, I.R. Harris, Effects of long term annealing at 1000 °C for 24 h on the microstructure and magnetic properties of Pr-Fe-B/Nd-Fe-B magnets based on $Nd_{16}Fe_{76}B_8$ and $Pr_{16}Fe_{76}B_8$, J. Alloys Compd. 296 (2000) 138–147. https://doi.org/10.1016/S0925-8388(99)00506-X.

[170] B.D. Cullity, Elements of X–ray Powder Diffraction, 1978.

[171] S. Bindra Narang, P. Kaur, S. Bahel, C. Singh, Microwave characterization of Co-Ti substituted barium hexagonal ferrites in X- band, J. Magn. Magn. Mater. 405 (2016) 17–21. https://doi.org/10.1016/j.jmmm.2015.12.044.

[172] P. Sharma, R.A. Rocha, S.N. de Medeiros, A. Paesano, Structural and magnetic studies on barium hexaferrites prepared by mechanical alloying and conventional route, J. Alloys Compd. 443 (2007) 37–42. https://doi.org/10.1016/j.jallcom.2006.10.022.

[173] H.L. Zhigang Zhang, Guangchun Yao, Xiao Zhang, Junfei Ma, Synthesis and characterization of nickel ferrite nanoparticles via planetary ball milling assisted solid-state reaction, Ceram. Int. 41 (2015) 4523-4530.

[174] A.M. Nicolson, G.F. Ross, Measurement of the Intrinsic Properties Of Materials by Time-Domain Techniques, IEEE Trans. Instrum. Meas. 19 (1970) 377–382. https://doi.org/10.1109/TIM.1970.4313932.

[175] Y.J. Kim, S.S. Kim, Magnetic and microwave absorbing properties of Ti and Co substituted M-hexaferrites in Ka-band frequencies (26.5̃40 GHz), J. Electroceramics. 24 (2010) 314–318. https://doi.org/10.1007/s10832-009-9575-x.

[176] R.B. Jotania, R.A. Nandotaria, C.C. Chauhan, M. Hashim, S. Singh Meena, S.E. Shirsath, Structural phases and Maxwell-Wagner relaxation in magnetically soft-$ZnFe_2O_4$ and hard-$Sr_2Cu_2Fe_{12}O_{22}$ nanocomposites, Ceram. Int. 42 (2016) 2289–2298. https://doi.org/10.1016/j.ceramint.2015.10.023.

[177] S. Mahadevan, C. Pahwa, S.B. Narang, P. Sharma, Structural, dielectric and magnetic properties of $BaFe_{12-x}Al_xO_{19}$ hexaferrite thick films, J. Magn. Magn. Mater. 441 (2017) 465–474. https://doi.org/10.1016/j.jmmm.2017.05.087.

[178] A. Hajalilou, S.A. Mazlan, K. Shameli, A comparative study of different concentrations of pure Zn powder effects on synthesis, structure, magnetic and microwave-absorbing properties in mechanically-alloyed Ni-Zn ferrite, J. Phys. Chem. Solids. 96–97 (2016) 49–59. https://doi.org/10.1016/j.jpcs.2016.05.001.

[179] L.M. Silber, E. Tsantes, P. Angelo, Ferromagnetic resonance in a uniaxial anisotropic ferrite: $BaFe_{12}O_{19}$, J. Appl. Phys. 38 (1967) 5315–5318. https://doi.org/10.1063/1.1709321.

[180] N.N. Jiang, Y. Yang, Y.X. Zhang, J.P. Zhou, P. Liu, C.Y. Deng, Influence of zinc concentration on structure, complex permittivity and permeability of Ni-Zn ferrites at high frequency, J. Magn. Magn. Mater. 401 (2016) 370–377. https://doi.org/10.1016/j.jmmm.2015.10.003.

[181] S.S. Jadhav, S.E. Shirsath, S.M. Patange, K.M. Jadhav, Effect of Zn substitution on magnetic properties of nanocrystalline cobalt ferrite, J. Appl. Phys. 108 (2010). https://doi.org/10.1063/1.3499346.

[182] C. Srinivas, B. V. Tirupanyam, S.S. Meena, S.M. Yusuf, C.S. Babu, K.S. Ramakrishna, D.M. Potukuchi, D.L. Sastry, Structural and magnetic characterization of co-precipitated $Ni_xZn_{1-x}Fe_2O_4$ ferrite nanoparticles, J. Magn. Magn. Mater. 407 (2016) 135–141. https://doi.org/10.1016/j.jmmm.2016.01.060.

Journal of Alloys and Compounds 725 (2017) 1175–1181

Contents lists available at ScienceDirect

Journal of Alloys and Compounds

journal homepage: http://www.elsevier.com/locate/jalcom

# Structural, magnetic and microwave properties of exchange coupled and non-exchange coupled $BaFe_{12}O_{19}/NiFe_2O_4$ nanocomposites

Chhavi Pahwa [a], Santhoshkumar Mahadevan [a], Sukhleen Bindra Narang [b], Puneet Sharma [a, *]

[a] School of Physics and Materials Science, Thapar University, Patiala, 147004, Punjab, India
[b] Department of Electronics Technology, Guru Nanak Dev University, Amritsar, Punjab, India

ARTICLE INFO

*Article history:*
Received 6 June 2017
Received in revised form
21 July 2017
Accepted 22 July 2017
Available online 26 July 2017

*Keywords:*
Exchange coupled ferrites
Barium hexaferrite
Nickel ferrite
Magnetic properties
Microwave properties

ABSTRACT

In the present work, exchange coupled and non-exchange coupled $BaFe_{12}O_{19}$ (BaM)/$NiFe_2O_4$ (NiF) nanocomposites with varying composition were prepared by adopting two different processing methods. Phase formation and microstructural changes were analyzed by X-ray diffraction (XRD) and Scanning electron microscopy (SEM) respectively. Effect of exchange coupling on magnetic and microwave properties (in Ku-band) were studied by vibrating sample magnetometer and vector network analyzer respectively. XRD patterns confirmed the co-existence of BaM and NiF phases in composites without any secondary phase. SEM micrographs showed the well distinguished BaM and NiF grains in exchange coupled composites. Smooth hysteresis loops were observed for exchange coupled composites in contrast to non-exchanged coupled, which showed stepped-loops for all studied compositions. Higher saturation magnetization ($M_s$) was also found in exchange coupled composites. Whereas, $M_s$ showed a linear decrease with NiF content in non-coupled composites. Coercivity found to decrease with NiF content with distinct trend among the two systems. Frequency dependent complex permittivity and permeability showed large variation between the two systems. Reflection losses at multiple frequencies were observed in exchange coupled composites.



## 1. Introduction

Recently, magnetic ferrites including hexagonal, spinel and garnets has gained a considerable attention for microwave frequency applications due to their moderate magnetization, high permeability, high permittivity and low losses [1–3]. Among the hexagonal ferrites, M-type hard ferrite such as $BaFe_{12}O_{19}$ (BaM) is unique for its high magnetocrystalline anisotropic field $H_A$ (~17 kOe), and high natural ferromagnetic resonance (FMR) frequency (~36 GHz) [1]. Moreover, suitable cations substitution for $Fe^{3+}$ ion, remarkably affect it's $H_A$ with a subsequent shift in its FMR, and hence the operational frequency band. For example, the substitution of $Sc^{3+}$ or $In^{3+}$ for $Fe^{3+}$ ions reduces its operable frequency to X-band [4,5], while the substitution of $Al^{3+}$, $Cr^{3+}$ and $Ga^{3+}$ increase the device operational frequency up to W-band [6–9]. In summary, devices based on BaM and its substitution systems can be operable from 1 to 100 GHz. In contrast to BaM, the operation frequencies of magnetically soft spinel and garnets with cubic symmetry are limited to 3 GHz due to low $H_A$ [2]. However, the presence to biased field can further increase their operational frequencies upto X-band with an implication of large device size.

In addition, composite ferrites with high and low $H_A$ could be an alternative methodology to develop tunable microwave devices. Moreover, wide flexibility of composition variation as compared to substitution may further provide a broad operating frequency band. It is well reported that hard/soft magnetic composite shows size dependent exchange coupling, which is predominantly an interface phenomenon [10]. In 1991, E. F. Kneller first proposed the idea of exchange coupled composite magnets consisted of two mutually exchange coupled phases [11]. After this, large data were reported on exchange coupled alloy composites based permanent magnets like $SmCo_5$, $Nd_2Fe_{14}B$, FePt and hard/soft thin films like SmCo/Fe, SmCo/Co and FeNi/FePt etc [12–17]. Later, the exchange coupling behavior in ferrite base nanocomposites bilayer was also reported [18,19]. Irrespective to the form of composite, one common observation is that the exchange coupling vanishes above a critical size of

* Corresponding author.
*E-mail address:* puneet.sharma@thapar.edu (P. Sharma).

http://dx.doi.org/10.1016/j.jallcom.2017.07.220
0925-8388/

the powder or the film thickness. With respect to composite nanopowders, the processing methods strongly influence the exchange coupling and well differentiated by the nature of magnetic hysteresis loop. A well exchange coupled composite shows smooth demagnetization behavior with coherent rotation of spins, while non-coupled system shows a stepped-curve which indicates non coherent rotation of spins [20].

In last few years, tremendous work has been done to investigate the magnetic behavior of exchange coupled ferrites adopting different processing methodologies and reported accordingly [21–23]. However, role of exchange coupling in the view of its magnetic and microwave properties needs an attention. A systematic comparison based on composition and processing may paved the way to exploit them for a better magnetic and microwave applications. In the present work, exchange coupled and non-exchange coupled composite ferrites of BaM and $NiFe_2O_4$ (NiF) with varying composition were prepared. The effect of coupling on the magnetic and microwave properties are systematically studied and compared. It is observed the exchange coupled composite shows better magnetic properties as compared to non-exchange coupled ferrites. The microwave reflection losses at multiple frequencies are observed in Ku band in exchange coupled composite, while non-exchange coupled system showed losses at single frequency. Such exchange coupled ferrites could be potential candidate for microwave absorber for wide working frequency range.

## 2. Experimental details

In the present work, BaM/NiF nanocomposite ferrites with different weight ratio i.e. 90/10, 80/20, 70/30, 60/40 and 50/50 were prepared by two different processing methods.

In the first method, stoichiometric amount of analytical grade metal nitrates $Fe(NO_3)_3 \cdot 9H_2O$, $Ba(NO_3)_2$, $Ni(NO_3)_2 \cdot 6H_2O$ and citric acid ($C_6H_8O_7$) were weighed and dissolved in deionized water in the single step. A pH of ~7 was maintained by adding $NH_3$ solution during stirring. The solution was heated at 70–80 °C to turn into viscous gel. This gel was ignited in air resulting in the formation of black color powder. As obtained composite powder were calcined at 1050 °C for 3 h in a resistance furnace. The composite powders were further pressed into pellets and sintered at 1100 °C for one hour in ambient atmosphere. Hence, composites with different composition prepared by this method are named as single step method (SS) and labelled as SS90/10, SS80/20 and SS70/30 and so on.

In the second method, BaM and NiF were individually prepared as mentioned above. The desired compositions were physically mixed and wet milled in a planetary ball for one hour. Further the powder were pressed and sintered at 1100 °C in resistance furnace for one hour. Composites prepared by this method is named as physically mixed (PM) and labelled as PM90/10, PM80/20 and PM70/30 and so on.

The phase analysis of pure BaM, NiF and composites were carried out by X-ray diffraction (XRD) (PANalytical), using Cu-$K_{\alpha 1}$ radiation. Room temperature (*R-T*) magnetic hysteresis (*M-H*) loops and Magnetization vs temperature (*M-T*) measurements were performed by vibrating sample magnetometer (VSM) using Lake Shore model 7404 with maximum applied field of 1 T. Microstructure analysis was carried out by scanning electron microscope (SEM) model JEOL (JSM-IT100). The reflection losses ($R_L$), permeability ($\mu$) and permittivity ($\varepsilon$) of the pure BaM and composites were measured by vector network analyzer (Agilent N5225A PNA series) in the frequency range of 12–18 GHz ($K_u$-band).

## 3. Results and discussion

### 3.1. XRD analysis

X-ray diffraction (XRD) patterns of pure BaM, NiF and BaM/NiF nanocomposites prepared by SS and PM methods are shown in Fig. 1(a–c). In pure BaM and NiF, all the diffraction peaks correspond to single phase without any impurity. Representative XRD patterns of composite confirmed the co-existence of BaM and NiF phases. From the figure, it is clear that the intensity of the NiF increases with the NiF content. Crystallite size for BaM (~45 nm) and NiF (~38 nm) phase was calculated by Scherrer equation in pure and composite samples, and found nearly same irrespective to processing method. Since crystallite size primarily depends upon the calcination temperatures, which are kept same (1050 °C) for both the methods.

### 3.2. Magnetic measurements

Fig. 2 (a–f) shows the *M-H* behavior of pure BaM, NiF and nanocomposite samples prepared by SS and PM methods. Pure BaM and NiF shows characteristic *M-H* loop of hard and soft magnetic materials respectively. BaM phase shows higher saturation magnetization compared to NiF and in agreement with the previously reported one [24,25]. *M-H* behavior of nanocomposites prepared by SS and PM methods are well distinct. In PM samples, stepped *M-H* loops were observed while SS composite shows a smooth curve without any step. Stepped *M-H* loops corresponds to the individual switching of hard and soft phases which is a

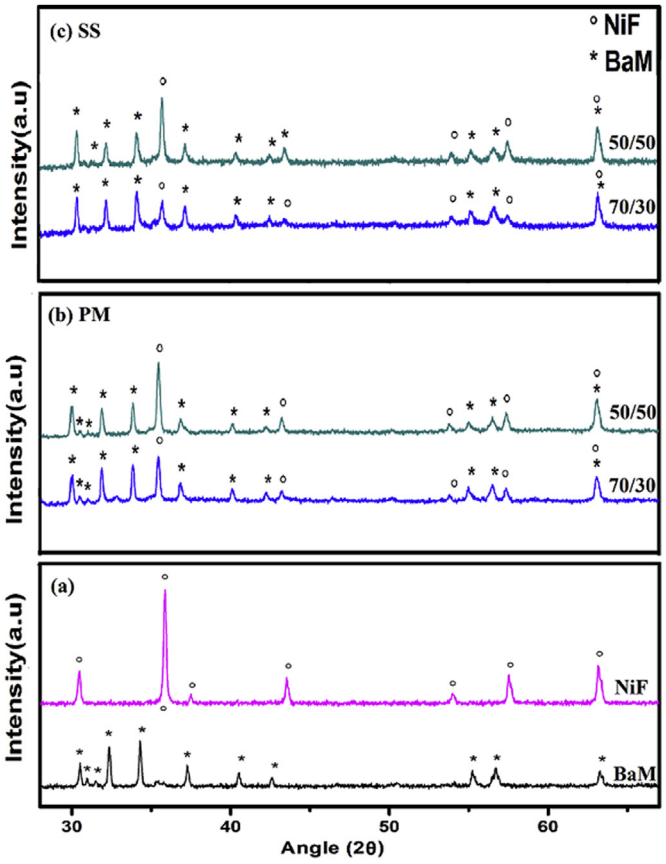


**Fig. 1.** X-ray diffraction patterns of (a) BaM and NiF (b) PM, & (c) SS nanocomposites with different composition.

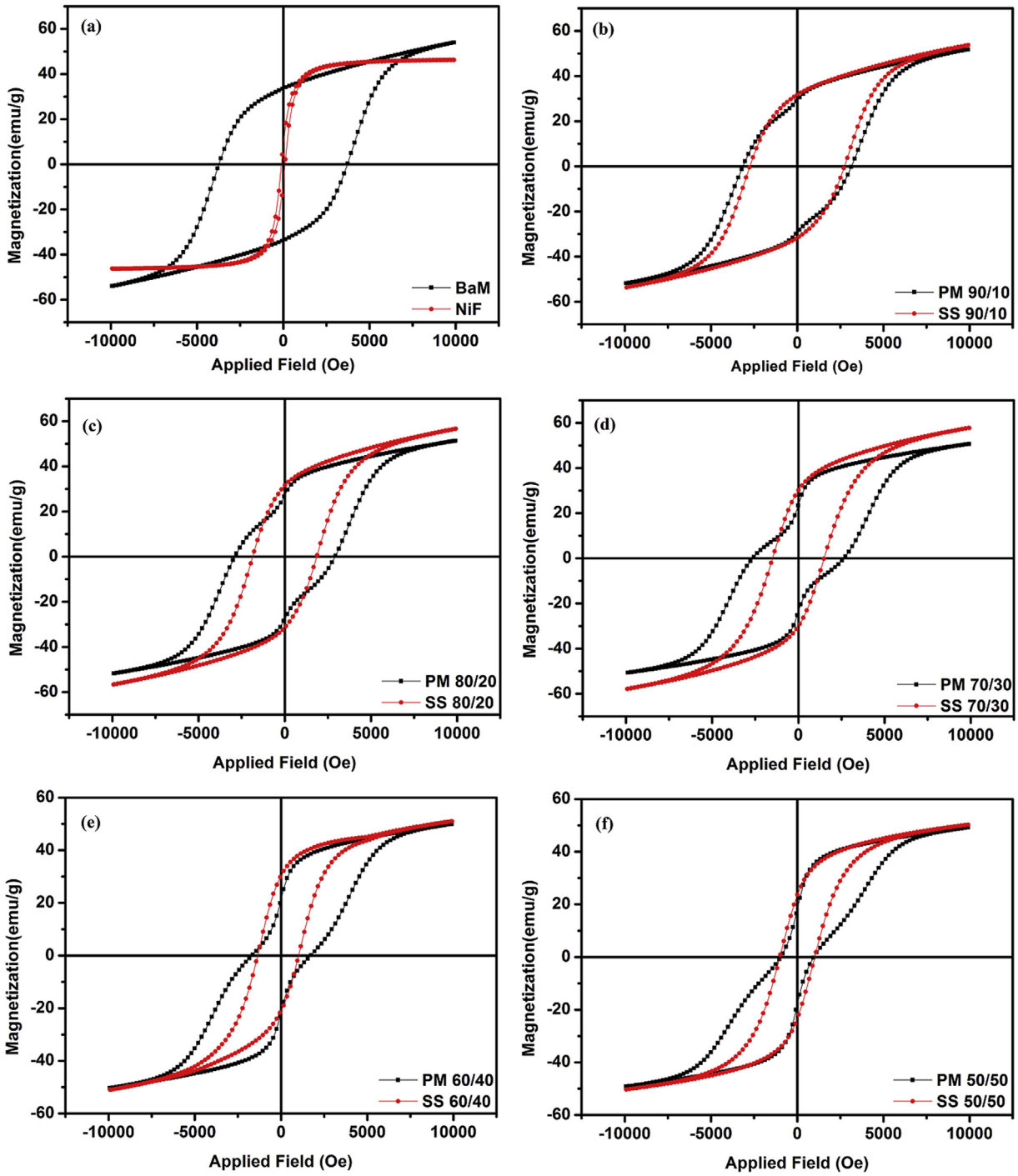


**Fig. 2.** Comparative *M-H* loops of (a) BaM & NiF, (b–f) SS & PM nanocomposites with different composition.

characteristic behavior of uncoupled hard and soft phases. While the simultaneously switching of BaM and NiF suggest the existence of exchange coupling among the phases. The difference in the demagnetization behavior is interplay of three types of spin interactions in the composites i.e. between soft-soft phase, hard-hard phase and hard-soft phases. For exchange couple systems, the interfacial interaction between hard and soft phases should be dominating. And grain size of soft phase should not be larger than the domain wall width of the hard phase [26,27]. If the spin interactions of individual phases are stronger than interfacial interaction, the independent switching of soft phase occurs at relatively lower field than that of hard phase. The observed step in demagnetization curve is consequence of spin torque effect of the soft phase on to hard phase [28]. The step is more pronounced in the composite with higher NiF content.

Variation in $M_s$, $M_r$ and $H_c$ with NiF content in SS and PM composites is shown in Fig. 3(a–c). It is well evident that $M_s$ and $M_r$ behavior are different for SS and PM samples. $M_s$ found to increase initially with the NiF content and then decrease, while a continuous decrease is observed for PM samples. For 70/30 composition, the $M_s$ and $M_r$ for SS composites are 57.7 emu/g and 30.1 emu/g respectively. While for PM composites low values of $M_s$ (50.6 emu/g) and

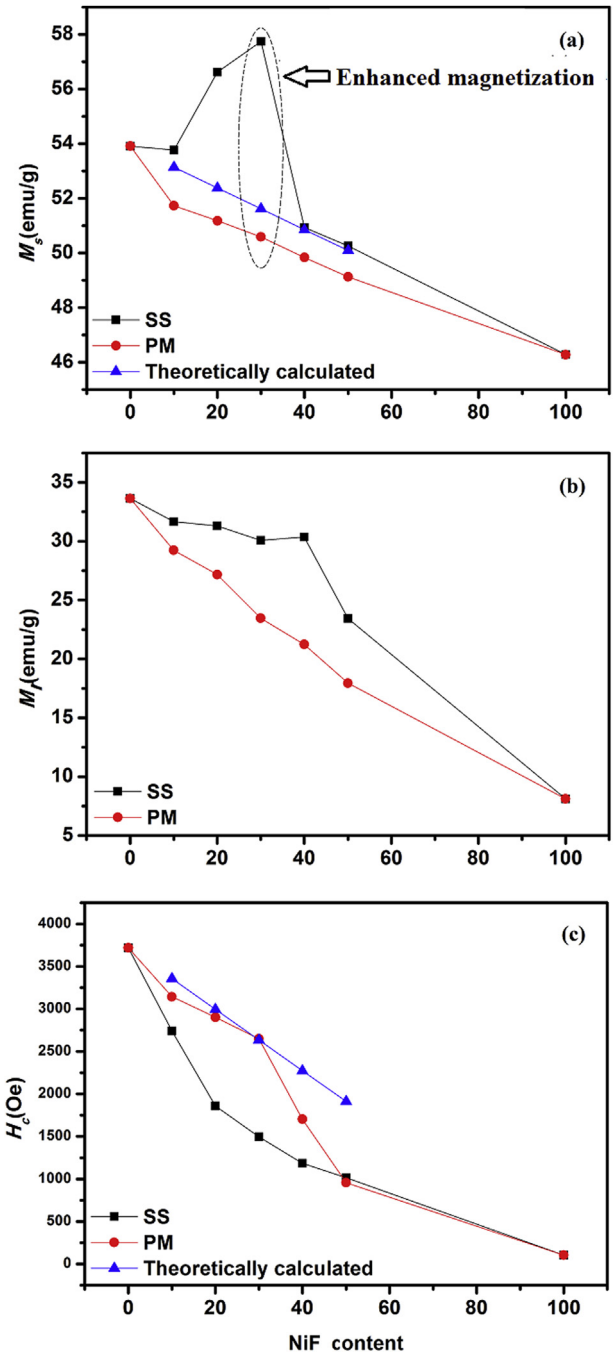


**Fig. 3.** (a–c) Variation in $M_s$, $M_r$ and $H_c$ with NiF content in SS and PM nanocomposites.

$M_r$ (23.5 emu/g) are obtained. The high $M_s$ and $M_r$ of SS composites is a consequence of interfacial coupling driven alignment of more magnetic moments. Further, decrease in $M_s$ and $M_r$ is due to the higher NiF content which dominates over the exchange coupling dependent magnetization enhancement. On other hand, a linear decrease in $M_s$ and $M_r$ is observed in PM composites as it is well reported that non-exchange coupled system follows the rule of mixture [29,30]. Employing it in a present system, $M_s$ of composite can be expressed as:

$$M_c = (1-x)M_{BaM} + xM_{NiF} \quad (1)$$

where, $M_{BaM}$ and $M_{NiF}$ are the measured $M_s$ of BaM and NiF respectively and $x$ is the weight fraction of NiF. Similarly, the $M_r$ and $H_c$ of composites can also be calculated. Therefore, the decrease in magnetic parameters ($M_s$, $M_r$) of PM composites is merely due to the low $M_s$ of NiF and decreases linearly with its content. $H_c$ is found to decrease with NiF content in both the samples due to its soft magnetic nature. However, exchange-coupled sample shows an asymptotic decrease in $H_c$ compared to linear decrease in non-coupled samples. This depicts that SS method is more appropriate for well exchange coupled system [23].

Fig. 3 represent the experimentally observed and theoretically calculated values of $M_s$, $M_r$ and $H_c$. It is clear that experimentally observed magnetic properties for non-coupled composites are very close to theoretically calculated values while wide deviation is observed in exchange-coupled samples. In summary, exchange coupling among the BaM and NiF, strongly effect the magnetic properties of nanocomposite. Further, composites prepared by SS and PM were sintered, and their magnetic behavior was observed. Fig. 4 shows the representative *M-H* loops of PM70/30 and SS70/30 with a confirmation of distinct loop in the sintered composite magnets.

Fig. 5 shows the magnetization *vs* temperature (*M-T*) behavior of pure BaM, SS70/30 and SS50/50 at 1000 Oe. The decrease in *M* with temperature is due to thermal effect. Curie temperature ($T_c$) is measured by plotting derivative of *M* ($dM/dT$) with respect to *T* (Fig. 5(b)). The $T_c$ was also found to increase from 497 °C to 517 °C which also confirms the existence of exchange coupling between hard and soft phases [31].

### 3.3. SEM analysis

Fig. 6 (a–d) shows the SEM micrographs of pure BaM, NiF and SS70/30, PM70/30 composites sintered at 1100 °C. Microstructure of pure BaM shows large elongated grains with an aspect ratio ~3.0. Elongated grains are characteristic property of sintered BaM as observed earlier [32]. NiF grains are nearly spherical in shape with an average size of ~2 μm. On comparing the microstructural features of SS70/30 and PM70/30 composites (Fig. 6(c–d)); the SS70/30 shows the well distinguished grains of BaM and NiF. The larger grain corresponds to the BaM, while smaller represents the NiF phase. On other hand no well distinguished particles are observed in PM 70/30 composite. This shows that the processing method plays an important role in defining the microstructure of composite. The crystallite size of BaM and NiF in sintered composites are also calculated by debye-scherrer formula, and found ~50 nm and

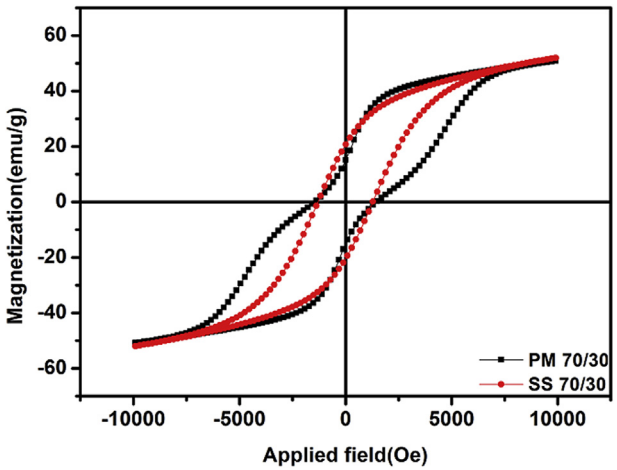


**Fig. 4.** *M-H* loops of PM 70/30 & SS 70/30 sintered composite magnets.

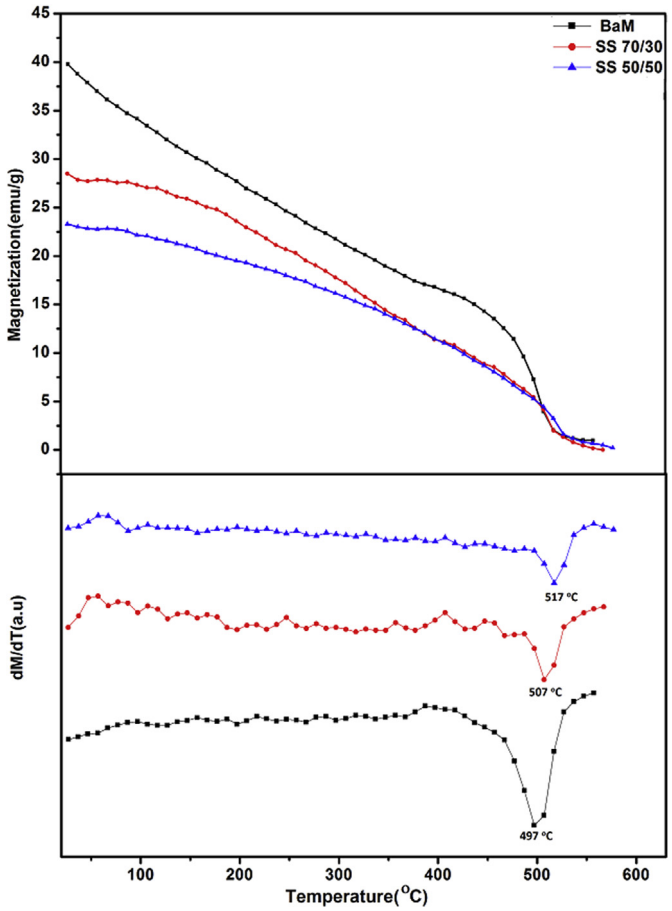


**Fig. 5.** High temperature *M-T* plots for BaM and SS 70/30 & SS50/50 nanocomposites.

~45 nm respectively. A slight increase in crystallite size, as compared to powder, is due to the higher sintering temperature (1100 °C). Hence, the larger grains as observed by SEM in sintered samples are basically the agglomerates of several nanosize crystallites.

### 3.4. Microwave absorption study

*R-T* microwave absorption properties of BaM, SS70/30, SS50/50, PM70/30 and PM 50/50 were investigated by VNA in the frequency range of $K_u$-band (12–18 GHz). Permittivity (ε) and permeability (μ) were calculated using Nicolson and Ross technique [33]. The variation of ε and μ with frequency were plotted in Fig. 7(a–b). From Fig. 7 (a) it is clear that the ε of pure BaM is high as compared to the nanocomposites because of high uniaxial anisotropy and large $H_c$ of hexaferrite [34]. Nearly constant ε is observed for PM composites in the measured frequency range and found to decreases with NiF content. On other hand, the large fluctuations in ε spectra are observed in the SS composites. The SS50/50 composition shows more variation in ε between 13–16 GHz frequencies range. As in exchange coupled system, the spin-spin interaction or interfacial dipoles may exist and in phase at a particular applied field frequency, which are responsible for the observed peaks in permittivity spectra. Fig. 7(b) shows the permeability spectra of BaM and nanocomposite samples. It is clear from the figure that permeability spectra for BaM, PM 70/30 and SS 70/30 is nearly same (1.18–1.25 at 12.4 GHz) and shows the similar behavior with frequency. However, a slight variation in permeability with composition and processing is ascribed to different magnetization behavior PM and SS composites.

Reflection loss curves were simulated using electromagnetic properties for 1.3 mm thick BaM and nanocomposites pellet using:

$$RL = 20 \log \left| \frac{(Z_{in} - Z_0)}{(Z_{in} + Z_0)} \right| \quad (2)$$

$Z_{in}$ is given by

$$Z_{in} = Z_0 \sqrt{\frac{\mu_r}{\varepsilon_r}} \tanh \left\{ j \left( \frac{2\pi f t}{c} \right) \sqrt{\mu_r \varepsilon_r} \right\} \quad (3)$$

where, f is the frequency, t is the thickness of sample, $\mu_r = \mu' - j\mu''$ and $\varepsilon_r = \varepsilon' - j\varepsilon''$ are the complex relative permeability and

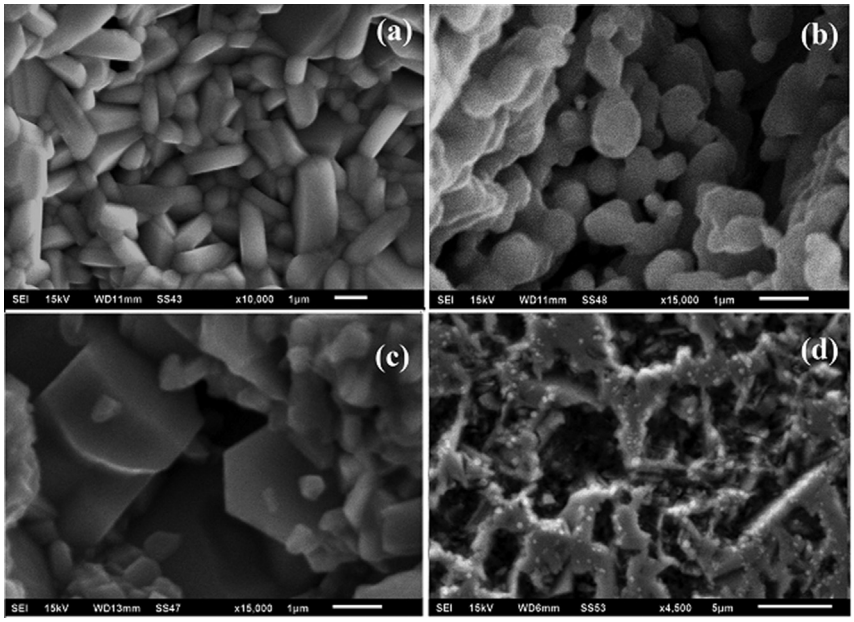


**Fig. 6.** SEM micrographs of (a) BaM, (b) NiF (c) SS 70/30 composite, and (d) PM 70/30 composite.

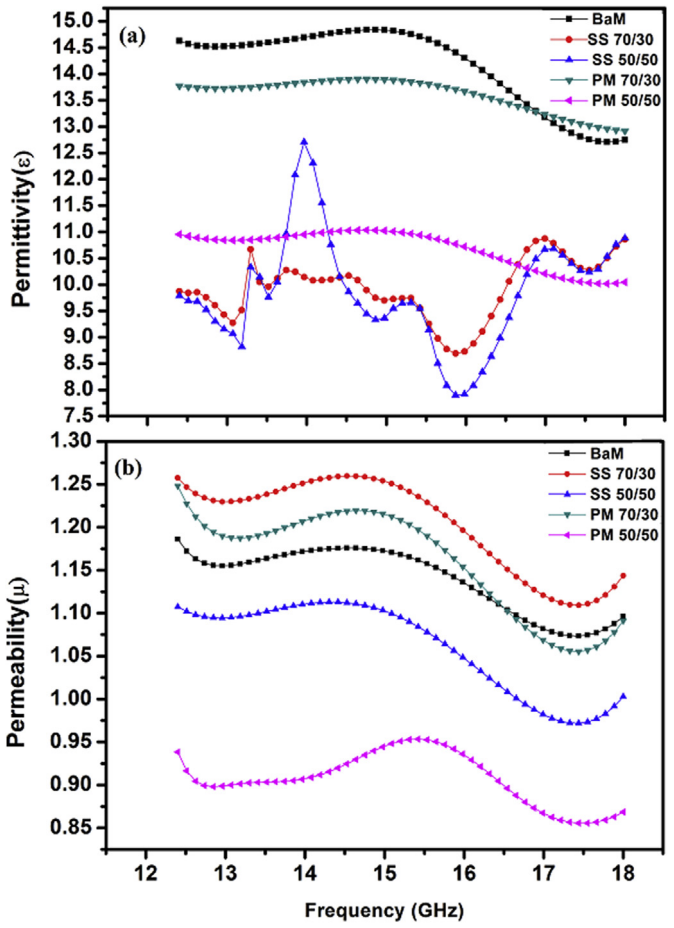


**Fig. 7.** (a) Complex permittivity & (b) Complex permeability of BaM, SS 70/30, SS 50/50, PM 70/30 & PM 50/50 nanocomposite.

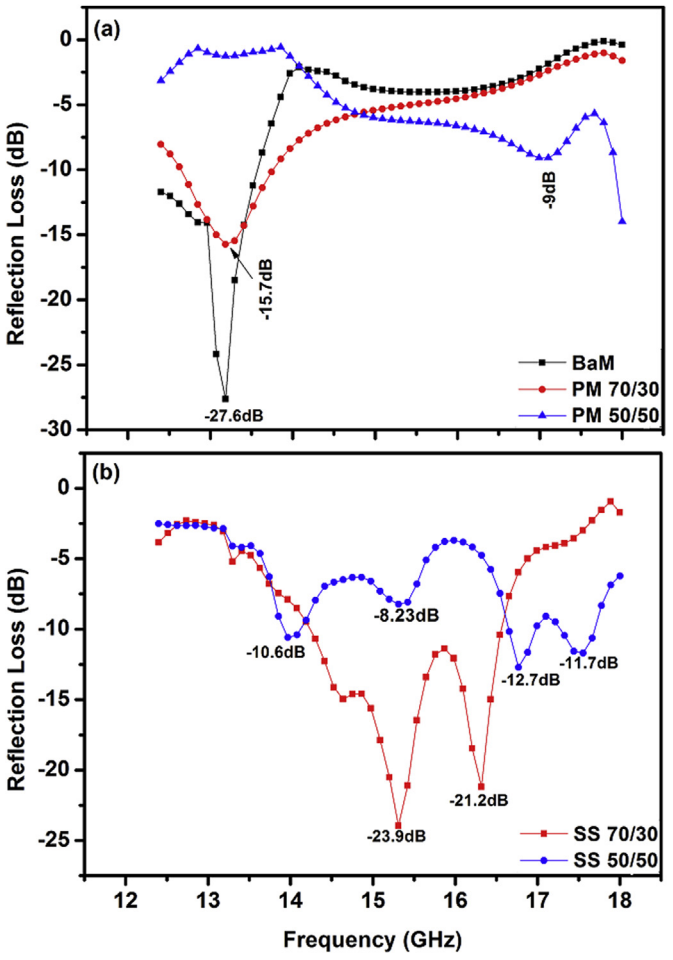


**Fig. 8.** Reflection loss *vs* frequency plots for (a) BaM, PM 70/30, PM50/50 & (b) SS 70/30, SS50/50 nanocomposites.

permittivity of the sample, c is the velocity of the light, $Z_0$ is the impedance of air and $Z_{in}$ is the input impedance at the absorber surface [35].

Fig. 8 shows reflection loss curves for pure BaM and nanocomposite samples. The dip of the plots demonstrates the minimum reflection loss and maximum absorption. It was observed that with increasing the NiF content, microwave absorption properties were decreased in the studied frequency range. The observed minimum reflection loss of pure BaM was −27.6 dB at 13.2 GHz frequency. For composite SS 70/30, reflection losses are found at 5.3 GHz and 16.3 GHz, whereas PM70/30 shows loss at only 13.2 GHz. The SS 50/50 composite exhibits reflection losses at 13.9 GHz, 16.7 GHz and 17.5 GHz. PM 50/50 composites exhibits reflection loss at 17 GHz. The observed reflection loss peaks for the SS composites gets shifted to the higher frequency bands as compared to the pure BaM and PM nanocomposites. This enhancement in matching frequency in nanocomposites prepared by SS method might be due to the exchange coupling between hard and soft ferrite. The reflection loss and absorption loss can further be improved by varying the thickness of the sample [36].

## 4. Conclusion

Exchange coupled and non-exchange coupled $BaFe_{12}O_{19}$/$NiFe_2O_4$ nanocomposite ferrites were prepared by SS and PM method and their structural, magnetic and microwave properties have been investigated. XRD patterns confirm the co-existence of both hard and soft phases in the composite systems. Magnetic measurement confirms the existence of exchange coupling between hard and soft phases in composite prepared by SS method. *M-H* loops confirm that interfacial interaction is predominant in exchange coupled nanocomposites. Exchange coupled composites shows enhanced $M_s$ compared to non-exchange coupled system. $T_c$ is found to increase with the soft NiF content, which confirms the exchange coupling. SEM shows well distinguished BaM and NiF grains in SS nanocomposite. These magnetic and microwave analysis suggests that SS method is appropriate to prepare exchange coupled system. Reflection losses in $K_u$—band found to depends on NiF content. Also exchange coupled nanocomposites shows reflection losses at multiple frequencies. These exchange coupled composite can be used for tunable microwave device applications.

## Acknowledgments

This work has been carried out under the financial support provided by DST (SERB/F/2947/2014-2015).

## References

[1] V.G. Harris, Modern microwave ferrites, IEEE Trans. Magn. 48 (3) (2012) 1075–1104.
[2] M. Pardavi-Horvath, Microwave applications of soft ferrites, J. Magn. Magn. Mater. 215 (2000) 171–183.
[3] V.G. Harris, Anton Geiler, Yajie Chen, Recent advances in processing and applications of microwave ferrites, J. Magn. Magn. Mater. 321 (2009)

2035–2047.
[4] G. Albanese, A. Deriu, E. Lucchini, G. Slokar, Mossbauer investigation of in and Sc substituted barium hexaferrite, Appl. Phys. A 26 (1981) 45–50.
[5] T.M. Perekalina, M.A. Vinnik, R.I. Zvereva, A.D. Shchurova, Magnetic properties of hexagonal ferrites with weak exchange coupling between sublattices, Sov. J. Exp. Theor. Phys. 32 (5) (1971) 813–814.
[6] G. Albanese, A. Deriu, Magnetic properties of Al, Ga, Sc, in substituted barium ferrites: a comparative analysis, Ceramargia Int. 5 (1) (1979) 3–10.
[7] L.G. Van Uitert, F.W. Swanekamp, Permanent magnet oxides containing divalent metal ions. 11, J. Appl. Phys. 28 (Apr. 1957) 482–485.
[8] K. Haneda, H. Kojima, Intrinsic coercivity of substituted $BaFe_{12}O_{19}$, Jpn. J. Appl. Phys. 12 (3) (1973) 355.
[9] A.H. Mones, E.J. Banks, Cation substitutions in $BaFe_{12}O_{19}$, Phys. Chem. Solids 4 (3) (1958) 217.
[10] Debangsu Roy, K.V. Sreenivasulu, P.S. Anil Kumar, Investigation on non-exchange spring behaviour and exchange spring behaviour: a first order reversal curve analysis, Appl. Phys. Lett. 103 (2013) 22406.
[11] E.F. Kneller, R. Hawig, The exchange–spring magnets: a new materials principle for permanent magnets, IEEE Trans. Magn. 27 (4) (1991) 3588–3600.
[12] V. Neu, K. Hafner, A.K. Patra, L. Schultz, Fully epitaxial, exchange coupled $SmCo_5$/Fe/$SmCo_5$ trilayers, J. Phys. D. Appl. Phys. 39 (2006) 5116–5120.
[13] M. Shindo, M. Ishizone, A. Sakuma, H. Kato, T. Miyazaki, Magnetic properties of exchange-coupled α-Fe/Nd–Fe–B multilayer thin-film magnets, J. Appl. Phys. 81 (1997) 4444.
[14] Hao Zeng, Jing Li, J.P. Liu, Shouheng Sun, Exchange-coupled nanocomposite magnets by nanoparticles self-assembly, Nature 420 (2002) 396–398.
[15] J.S. Jiang, J.E. Pearson, Z.Y. Liu, B. Kabius, S. Trasobares, D.J. Miller, S.D. Bader, D.R. Lee, D. Haskel, G. Srajer, J.P. Liu, A new approach for improving exchange-spring magnets, J. Appl. Phys. 97 (2005) 10K311.
[16] Y. Choi, J.S. Jiang, J.E. Pearson, S.D. Bader, Origin of recoil hysteresis loops in Sm–Co/Fe exchange-spring magnets, Appl. Phys. Lett. 91 (2007) 022502.
[17] Joseph E. Davies, Olav Hellwig, Eric E. Fullerton, J.S. Jiang, S.D. Bader, G.T. Zimányi, Kai Liu, Anisotropy dependence of irreversible switching in Fe/SmCo and FeNi/FePt exchange spring magnet films, Appl. Phys. Lett. 86 (2005) 262503. Y. Suzuki, R. B. van Dover, E. M. Gyorgy, Julia M. Phillips, and R. J. Felder," Exchange coupling in single-crystalline spinel-structure Mn,Zn.Fe2O4/CoFe2O4 bilayers," Physica Review B, vol. 53, no.21. pp. 14016–14019, 1996.
[18] Xiansong Liu, Wei Zhong, Benxi Gu, Youwei Du, Exchange-coupling interaction in nanocomposites $SrFe_{12}O_{19}$/γ-$Fe_2O_3$ permanent ferrites, J. Appl. Phys. 92 (2) (2002) 1028–1032.
[19] Vamsi M. Chakka, Z.S. Shan, J.P. Liu, Effect of coupling on magnetic properties of exchange spring magnets, J. Appl. Phys. 94 (10) (2002) 6673–6677.
[20] Yan Wang, Ying Huang, Qiufen Wang, Preparation and magnetic properties of $BaFe_{12}O_{19}$/$Ni_{0.8}Zn_{0.2}Fe_2O_4$ nanocomposite ferrite, J. Magn. Magn. Mater. 324 (2012) 3024–3028.
[21] R.K. Kotnana, Shabad Ahmad, Arham S. Ahmad, Jyoti Shah, Ameer Azam, Investigation of structural, dielectric, and magnetic properties of hard and soft mixed ferrite composites, J. Appl. Phys. 112 (2012) 054323.
[22] Subhenjit Hazra, Barun Kumar Ghosh, Manoj Kumar Patra, Raj Kumar Jani, Sampat Raj Vadera, Narendra Nath Ghosh, One-pot synthesis of $(NiFe_2O_4)_x$–$(SrFe_{12}O_{19})_{1-x}$Nanocomposites and their microwave absorption properties, J. Nanosci. Nanotechnol. 15 (9) (2015) 6559–6567.
[23] P. Sharma, R.A. Rocha, S.N. de Medeiros, A. Paesano Jr., Structural and magnetic studies on barium hexaferrites prepared by mechanical alloying and conventional route, J. Alloys Compd. 443 (2007) 37–42.
[24] Zhigang Zhang, Guangchun Yao, Xiao Zhang, Junfei Ma, Hao Lin, Synthesis and characterization of nickel ferrite nanoparticles via planetary ball milling assisted solid-state reaction, Ceram. Int. 41 (3) (2015) 4523–4530.
[25] T. Schrefl, H. Kronmiiller, J. Fidler, Exchange hardening in nano-structured two-phase permanent magnets, J. Magn. Magn. Mater. 127 (1993) L27–L277.
[26] Debangsu Roy, C. Shivakumara, P.S. Anil Kumar, Observation of the exchange spring behavior in hard–soft-ferrite nanocomposite, J. Magn. Magn. Mater. 321 (2009) L11–L14.
[27] Eric E. Fullerton, J.S. Jiang, S.D. Bader, Hard/Soft magnetic heterostructures: model exchange-spring magnets, J. Magn. Magn. Mater. 200 (1999) 392–404.
[28] K.W. Moon, S.G. Cho, Y.H. Cho, K.H. Kim, J. Kim, Synthesis and magnetic properties of nano Ba-hexaferrite/NiZn ferrite composites, Phys. Stat. Sol. 204 (12) (2007) 4141–4144. M.Dhlgren, R.Grissin.
[29] Ralph Skomski, J.M.D. Coey, Gaint energy product in nanostructured two-phase magnets, Phys. Rev. B 48 (1993) 15812–15816.
[30] M. Dhlgren, R. Grössinger, Enhancement of curie temperature for exchange coupled Nd-Fe-Band Pr-Fe-B magnets, IEEE Trans. Magn. 33 (5) (1997) 3895–3897.
[31] S. Mahadevan, C. Pahwa, S.B. Narang, P. Sharma, Structural, dielectric and magnetic properties of $BaFe_{12-x}Al_xO_{19}$ hexaferrite thick films, J. Magn. Magn. Mater. 441 (2017) 465–474.
[32] A.M. Nicolson, G.F. Ross, Measurement of the intrinsic properties of materials by time-domain techniques, IEEE Trans. Magn. 19 (4) (1970) 377–382.
[33] Yong-Jin Kim, Sung-Soo Kim, Magnetic and microwave absorbing properties of Ti and Co substituted M-hexaferrites in Ka-band frequencies, J. Electroceram. 24 (2010) 314–318.
[34] S. Sugimoto, S. Kondo, K. Okayama, D. Book, T. Kagotani, M. Homma, M-type ferrite composite as a microwave absorber with wide bandwidth in the GHz range, IEEE Trans. Magn. 33 (5) (1979) 377–382.
[35] Subhenjit Hazraa, Barun Kumar Ghosha, Manoj Kumar Patrab, Raj Kumar Janib, Sampat Raj Vaderab, Narendra Nath Ghosha, A novel 'One-Pot' synthetic method for preparation of $(Ni_{0.65}Zn_{0.35}Fe_2O_4)$x- $(BaFe_{12}O_{19})_{1-x}$ nanocomposites and study of their microwave absorption and magnetic properties, Powder Technol. 279 (2015) 10–17.

Journal of Magnetism and Magnetic Materials 484 (2019) 61–66

Contents lists available at ScienceDirect

Journal of Magnetism and Magnetic Materials

journal homepage: www.elsevier.com/locate/jmmm

Research articles

# Interfacial exchange coupling driven magnetic and microwave properties of $BaFe_{12}O_{19}/Ni_{0.5}Zn_{0.5}Fe_2O_4$ nanocomposites

Chhavi Pahwa[a], Sukhleen Bindra Narang[b], Puneet Sharma[a,*]

[a] School of Physics & Materials Science, Thapar Institute of Engineering & Technology, Patiala 147004, Punjab, India
[b] Department of Electronics Technology, Guru Nanak Dev University, Amritsar, Punjab, India

ARTICLE INFO

*Keywords:*
Barium hexaferrite
Nickel zinc ferrite
Exchange coupled composites
Magnetic properties
Microwave properties

ABSTRACT

Exchange coupled hard/soft nanocomposite ferrites consist of $BaFe_{12}O_{19}$/ $Ni_{0.5}Zn_{0.5}Fe_2O_4$ (BaM/NZFO) in 70/30 wt ratio were prepared by sol–gel auto combustion method. Effect of annealing temperature (950 °C–1150 °C) on structural, magnetic and microwave properties have been investigated. The X-ray diffraction pattern confirms co-existence of both BaM and NZFO phases without any secondary phase. TEM micrographs showed well distinguished particles of BaM and NZFO with different symmetry. Saturation magnetization ($M_s$) increased from 58 emu/g to 65 emu/g with drastic decrease in coercivity ($H_c$). Higher $M_s$ and low $H_c$ than theoretical calculated values suggested that phases are well exchange coupled. A sharp Curie temperature (473 °C) for the composite was observed. The variation in $M_s$ and $H_c$ demonstrated that annealing temperature has strong influence on exchange coupling. Reflection losses in $K_u$-band were found to increase with a maximum value of −38 dB for the composite annealed at 1050 °C. Loss frequency also shifted toward lower values as a consequence of annealing temperature and exchange coupling.

## 1. Introduction

Exchange coupling between hard and soft magnetic phases at nanometric scale has gained considerable attention due to associated intriguing physics in the system and their application in high energy product magnets [1–4]. In early 1990s, Kneller and Hawing first proposed the concept of exchange-spring magnets in suitably dispersed hard and soft magnetic materials [5]. The studies on such system were largely focused on hard/soft magnetic bilayer thin films and oxide based nanopowders. Reportedly, exchange coupling between the phases is predominantly interfacial in nature; primarily governed by film thickness and size of powders [6–8]. A strongly coupled system shows coherent rotation of hard/soft magnetic spins and represent smooth demagnetization curve [9]. Hard/soft bilayer films also depicted a kink in demagnetization curve which referred as exchange-spring magnets. The observed kink was due to pinning of soft magnetic spins by hard magnetic spins at the interface [10]. In similar concept, exchange-spring behavior was well demonstrated in Sm-Co/Fe, FeNi/FePt, Fe/Nd-Fe-B, $SrFe_{12}O_{19}/\gamma$-$Fe_2O_3$ systems [11–13].

Contrary to films, kinked and smooth demagnetization curves of hard/soft magnetic composite powders were referred as non-exchange and exchange coupled systems respectively [14,15]. Exchanged coupled nanocomposites also showed high energy product upto a certain composition and could be used for permanent magnets [3,16,17]. Such composite systems are also potential materials for microwave absorbing materials [18,19]. The magnetization reversal behavior of hard/soft composite nanopowders is strongly governed by processing methods which consequently affects particle size and exchange coupling. It is well reported that individually mixed nano-powders does not show exchange coupling, whereas powders prepared by one pot chemical method, reflects exchange coupling with smooth hysteresis loop [20–22]. Among the various processing parameters, annealing of ferrite nanopowders strongly influence their magnetic and structural properties. Accordingly, in hard/soft magnetic nanocomposites, the magnetization of individual phase and their particle size can be varied with annealing temperature, which may directly affect the interfacial coupling.

In the present work, exchange coupled $BaFe_{12}O_{19}/Ni_{0.5}Zn_{0.5}Fe_2O_4$ nanocomposite powders were prepared by sol–gel auto combustion route. The effect of annealing temperature on structural, magnetic and microwave properties were systematically investigated. The focus of the study is to develop exchange coupled composite ferrites with varied coupling for microwave device application.

* Corresponding author.
*E-mail address:* puneet.sharma@thapar.edu (P. Sharma).

https://doi.org/10.1016/j.jmmm.2019.03.127
Received 18 February 2019; Received in revised form 29 March 2019; Accepted 30 March 2019
Available online 01 April 2019

## 2. Experimental details

In the present work, nanocomposite ferrite of $BaFe_{12}O_{19}$ (BaM)/$Ni_{0.5}Zn_{0.5}Fe_2O_4$ (NZFO) in weight ratio of 70/30 were prepared by sol–gel auto combustion method. Analytical grade metal nitrates; $Fe(NO_3)_3{\cdot}9H_2O$, $Ba(NO_3)_2$, $Ni(NO_3)_2{\cdot}6H_2O$, $Zn(NO_3)_2{\cdot}6H_2O$ and citric acid ($C_6H_8O_7$) of 99.9% purity were used. The precursors were weighed in the stoichiometric ratio and dissolved in deionized water. $NH_3$ solution was added during stirring to maintain pH ~7 of the solution. The solutions were heated at 70–80 °C to turn into viscous gel till ignited in air resulting powder formation. The powders of BaM, NZFO and BaM/NZFO were annealed at 950 °C, 1000 °C, 1050 °C, 1100 °C and 1150 °C for three hours in a resistance furnace. The annealed powders were further pressed into rectangular pellets (21 mm × 11 mm) and sintered at 1200 °C for one hour in ambient atmosphere. The phase analysis of BaM, NZFO and composite powders were carried out by X-ray diffraction (XRD) (PANalytical) using Cu-$K_{\alpha1}$ radiation. Room temperature (*R–T*) magnetic hysteresis (*M−H*) loops and Magnetization *vs* temperature (*M−T*) measurements were performed by vibrating sample magnetometer (VSM) using Lake Shore model 7404 with maximum applied field of 1 T. Microstructure analysis was carried out by scanning electron microscope (SEM) model JEOL (JSM-IT100) and Transmission electron microscope (TEM) model (Tecnai G3, F30). Prior to SEM, surface was made conducting by Au sputtering to avoid any charging during measurement. For magnetic and reflection losses; sintered pellets were ground to the size of wave guide cavity (15.74 mm × 7.96 mm) and measured by vector network analyzer (Agilent N5225A PNA series) in the frequency range of 12–18 GHz ($K_u$-band).

## 3. Results and discussion

### 3.1. Phase analysis

X-ray diffraction (XRD) patterns of BaM/NZFO nanocomposites annealed at 950 °C, 1050 °C and 1150 °C are shown in Fig. 1. The XRD peaks confirm co-existence of both BaM and NZFO phases. The average crystallite size for BaM & NZFO peaks in composites was calculated by Scherrer equation [23]. The minimum crystallite size of NZFO and BaM in the nanocomposite was 28 nm and 21 nm at 1050 °C respectively. The variation in crystallite size with the annealing temperature is shown in Table 1.

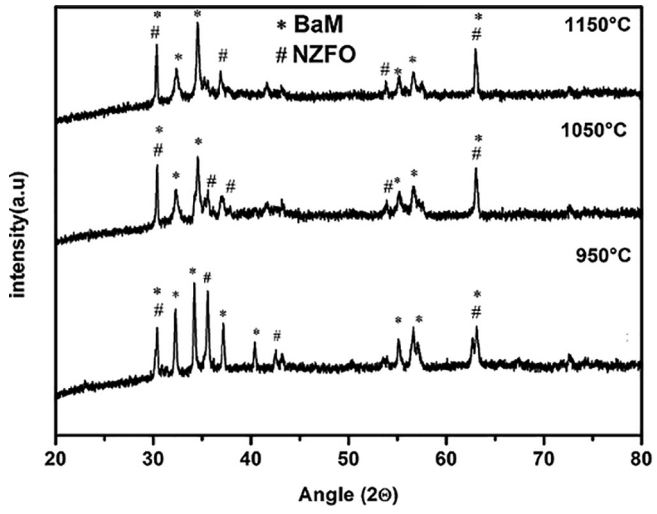


**Fig. 1.** X-ray diffraction patterns of BaM/NZFO nanocomposite annealed at 950 °C, 1050 °C and 1150 °C.

**Table 1**
Crystallite size of BaM and NZFO in composite with annealing temperature.

| Temperature (°C) | Crystallite Size (nm) | |
|---|---|---|
| | NZFO | BaM |
| 950 | 36.7 | 40.1 |
| 1050 | 29.4 | 20.7 |
| 1150 | 34.0 | 29.3 |

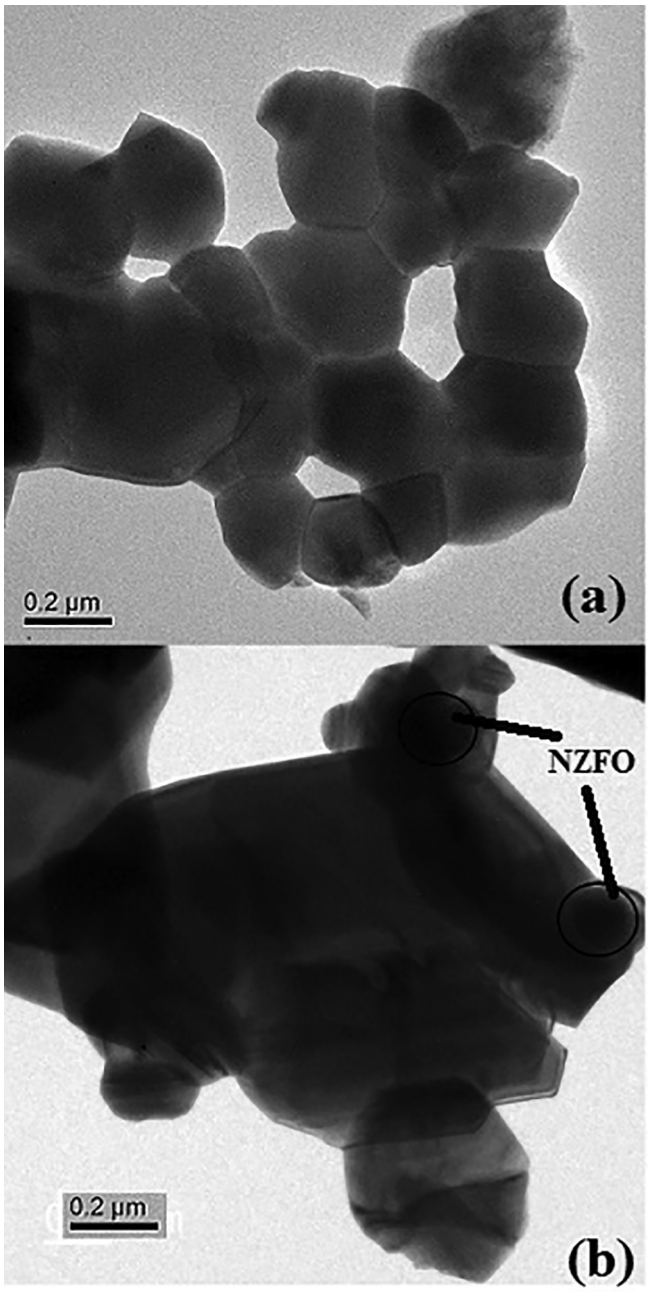


**Fig. 2.** TEM micrographs of (a) BaM (b) BaM/NZFO nanocomposite powders annealed at 1050 °C.

### 3.2. Microstructure analysis

Fig. 2(a & b) shows TEM micrographs of BaM and BaM/NZFO nanocomposite powders. In BaM; all particle shows hexagonal morphology. In composite (Fig. 2(b)) smaller NZFO particles are coagulated with larger BaM particles. The stacking of particles is due to their

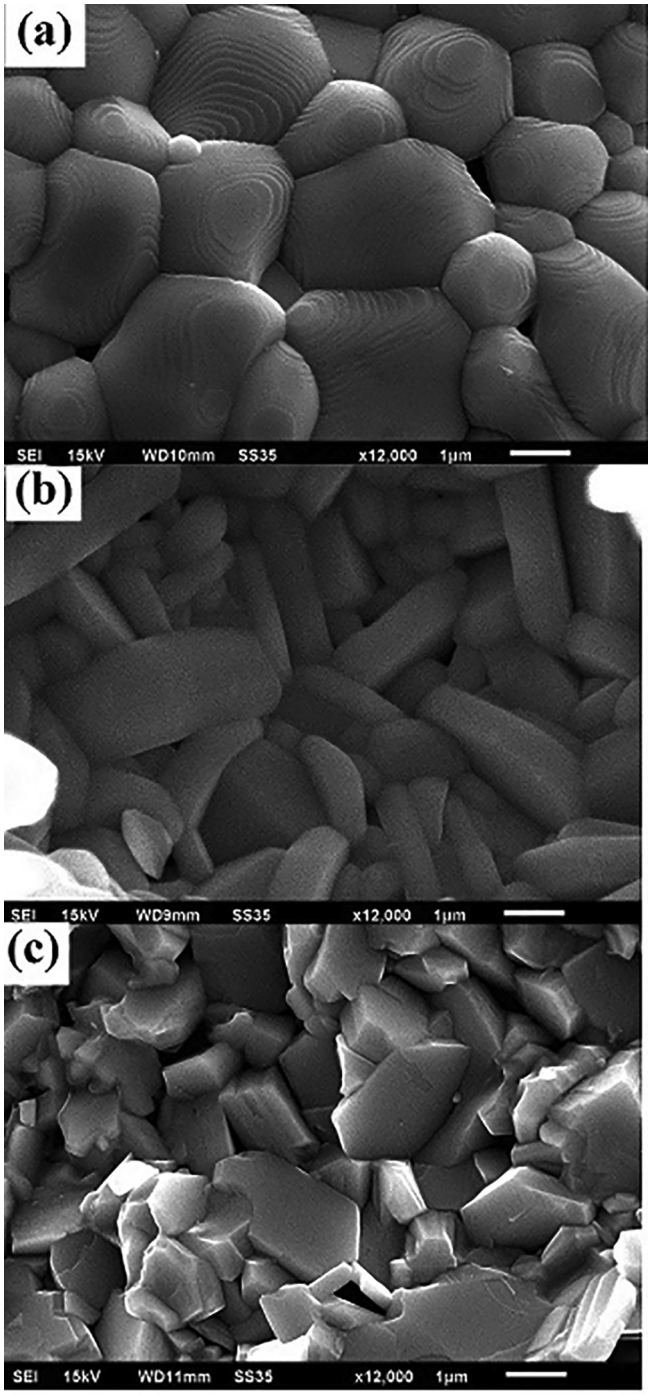


**Fig. 3.** SEM micrographs of (a) BaM, (b) NZFO & (c) BaM/NZFO nanocomposite annealed at 1050 °C and sintered at 1200 °C.

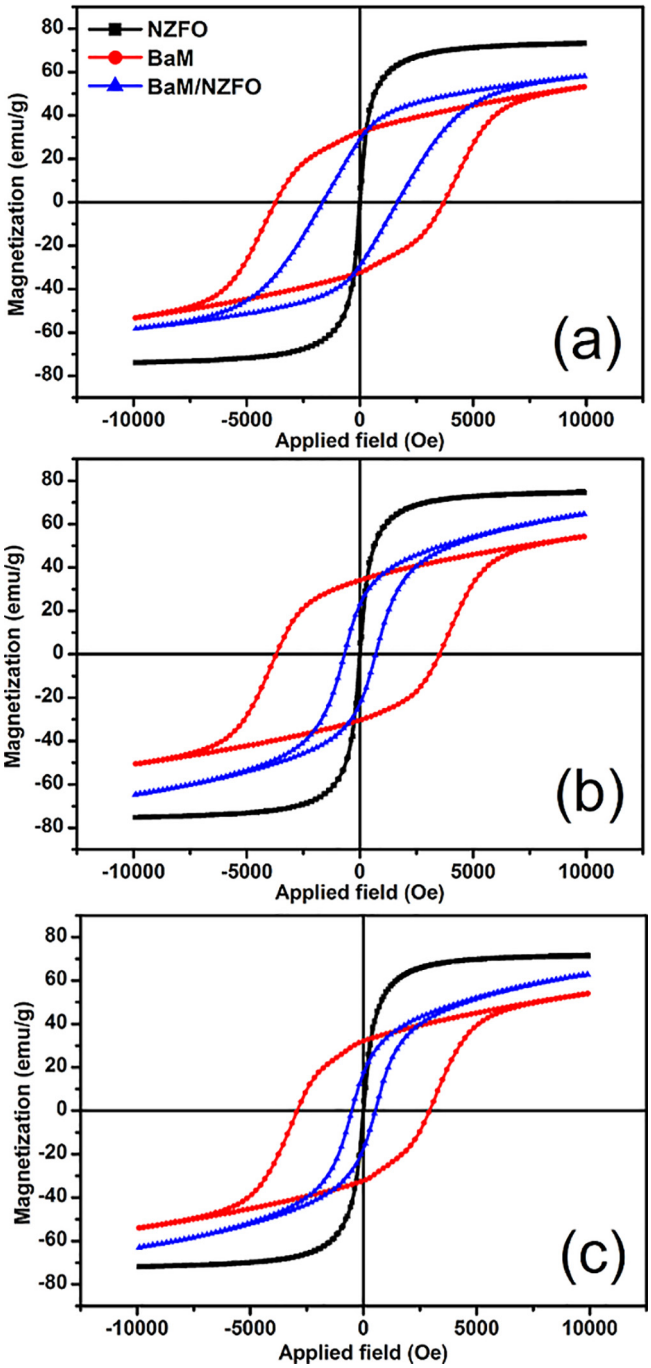


**Fig. 4.** Comparative $M-H$ loops of BaM, NZFO and BaM/NZFO nanocomposite powders annealed at (a) 950 °C, (b) 1000 °C and (c) 1150 °C.

mutual magnetic attraction [24].

Fig. 3(a–c) shows the fractured surface micrographs of NZFO, BaM and BaM/NZFO composite sintered at 1200 °C. Microstructure of NZFO shows well distinguished equiaxed grains whereas, BaM shows randomly oriented elongated grains. The microstructure of composite shows distinct feature from BaM and NZFO with cleavage fracture and smaller grains. All microstructure shows dense morphology without any measurable porosity.

### 3.3. Magnetic measurements

Fig. 4(a–c) shows the representative $M-H$ plots of NZFO, BaM and BaM/NZFO composite powders annealed at 950 °C, 1050 °C and 1150 °C. $M-H$ loops of BaM and NZFO shows the characteristic behavior of hard and soft magnetic materials respectively. Higher saturation magnetization ($M_s$) of NZFO compared to BaM is in agreement with previous studies [25,26].

$M-H$ loops of nanocomposites showed coherent demagnetization due to simultaneous switching of NZFO and BaM spins. The observed switching suggests that the system is well exchange coupled in the studied temperature range. It is well reported that non-exchange coupled system shows a kink or shoulder in demagnetization curve [21].

Variation in $M_s$ and $H_c$ for BaM, NZFO and BaM/NZFO nanocomposite as a function of annealing temperature are shown in Fig. 5(a & b). $M_s$ and $H_c$ were also theoretically calculated by the rule of mixture

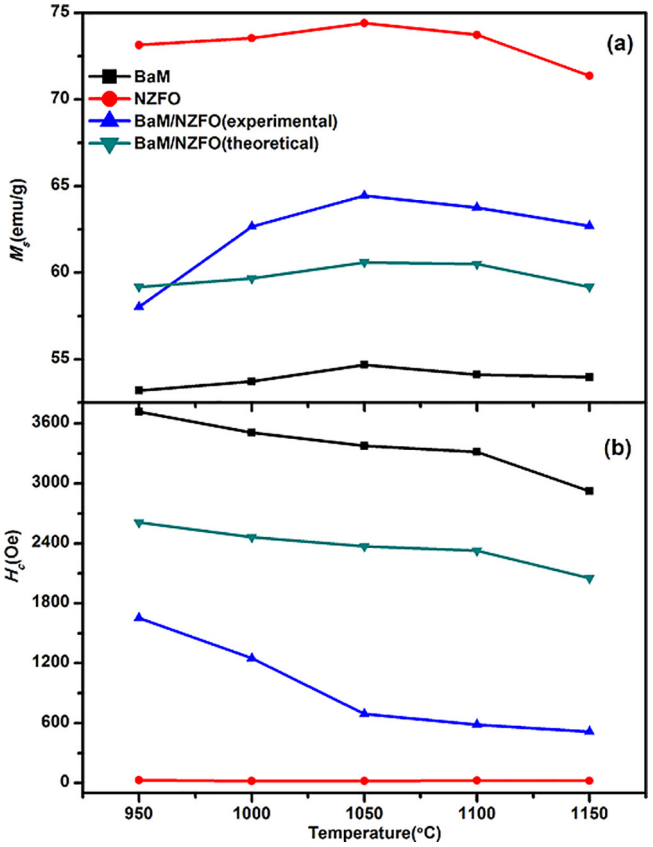


**Fig. 5.** Variation in theoretical and experimentally observed (a) $M_s$ and (b) $H_c$ of BaM, NZFO and BaM/NZFO powders with annealing temperature.

using Eq. (1) [21].

$$M = 0.7M_{BaM} + 0.3M_{NZFO} \quad (1)$$

where, $M_{BaM}$ and $M_{NZFO}$ are the measured $M_s$ of BaM and NZFO respectively. Similarly, theoretical $H_c$ was calculated and compared to experimental values. In our previous work, we have shown that non-exchange coupled system nearly follows the rule of mixture [21]. The $M_s$ of BaM and NZFO increase with annealing temperature and then decrease (Fig. 5(a)). The maximum observed values for BaM and NZFO at 1050 °C is 54.7 emu/g and 74.4 emu/g respectively. The increase in $M_s$ with temperature is due to the distribution of cations at ferromagnetically favourable sites. A drastic increase in $M_s$ of BaM/NZFO nanocomposite has been observed with temperature from 950 °C to 1050 °C (58 emu/g to 65 emu/g) followed by slight decrease. It is well evident that experimentally observed $M_s$ of nanocomposites are higher than theoretically calculated, which suggests that system is well exchange coupled. Also, the variation in $M_s$ with temperature reflects that extent of exchange coupling is temperature dependent. Since the coupling between phases is interfacial in nature; therefore powders with optimum crystallite size may prevail higher exchange coupling. The high $M_s$ of nanocomposite at 1050 °C is ascribed to higher coupling associated with minimum crystallite size of BaM and NZFO phase (Table 1).

Contrary to $M_s$ behavior, the $H_c$ values of nanocomposite are well below the theoretically calculated values for studied temperatures. The $H_c$ is primarily governed by crystal anisotropy and particle/crystallite size of magnetic phases. Since the composition of BaM/NZFO is constant, hence the role of crystal anisotropy of the composite on $H_c$ can be ignored. A sharp decrease in $H_c$ of nanocomposite with temperature may ascribe to variation in crystallite size (Table 1). However, a minimum $H_c$ value is observed for the composite with lower crystallite size suggests the dominance of exchange coupling over structural

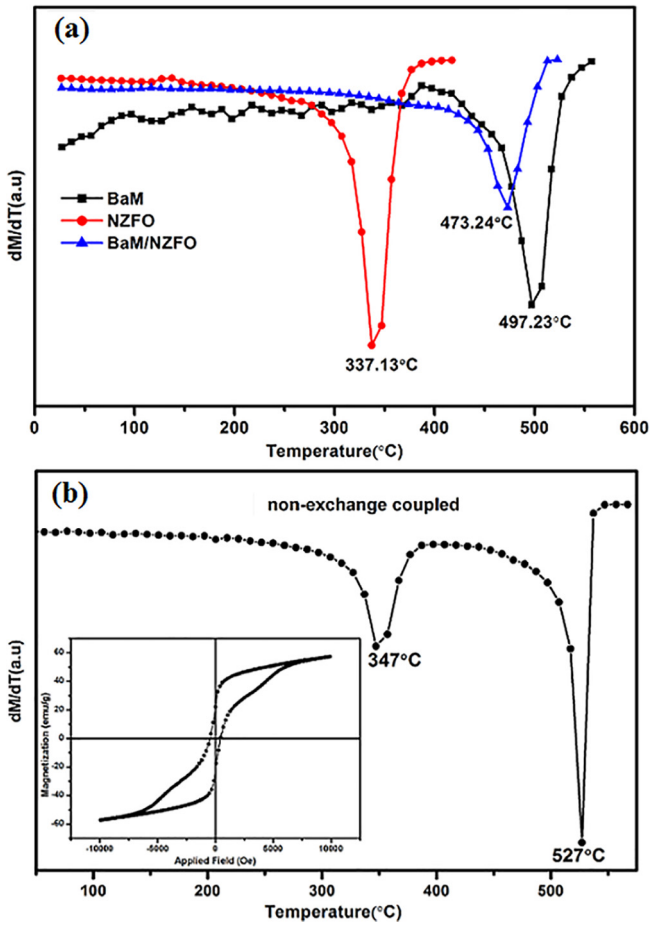


**Fig. 6.** (a) High temperature $M-T$ plots for BaM, NZFO and BaM/NZFO annealed at 1050 °C, (b) $M-T$ plot and $M-H$ loop (inset) for non-exchange coupled BaM/NZFO.

parameters. Therefore, low $H_c$ of nanocomposites than the theoretically calculated values may due to strong intervening coupling between the phases where switching of soft magnetic spins at low nucleation field drive away the hard magnetic spins.

The Curie temperature of BaM, NZFO and BaM/NZFO nanopowders annealed at 1050 °C was measured by plotting derivative of $M$ ($dM/dT$) with respect to temperature. The sharp dips in Fig. 6(a) represents the $T_c$ of respective phases. The $T_c$ for BaM and NZFO was found to be 497 °C [21] and 337 °C respectively. The observed $T_c$ for exchange coupled nanocomposite is 473 °C which is close to BaM due to its higher weight fraction. For non-exchange coupled system independent values of $T_c$ for NZFO (347 °C) and BaM (527 °C) were observed as shown in Fig. 6 (b). The inset in Fig. 6(b) depicts the representative $M-H$ loop of non-exchange system. A single $T_c$ value for BaM/NZFO nanocomposite also demonstrates that the phases are well exchange coupled.

### 3.4. Microwave absorption studies

Microwave absorption studies for BaM and BaM/NZFO composite annealed at 950 °C, 1050 °C and 1150 °C were measured by vector network analyzer in $K_u$-band. Fig. 7 shows the variation of magnetic loss tangent (tan $\delta_\mu$) with frequency. For BaM, tan $\delta_\mu$ remains constant in studied frequency range, however, low losses were observed for the samples annealed at higher temperature. For BaM/NZFO composite; variation in tan $\delta_\mu$ along with resonance peaks at different frequency were observed. Sample annealed at 950 °C showed a sharp resonance peak at 16 GHz. However, composites annealed at 1050 °C and 1150 °C showed resonance peaks in broad frequency range. In the composite

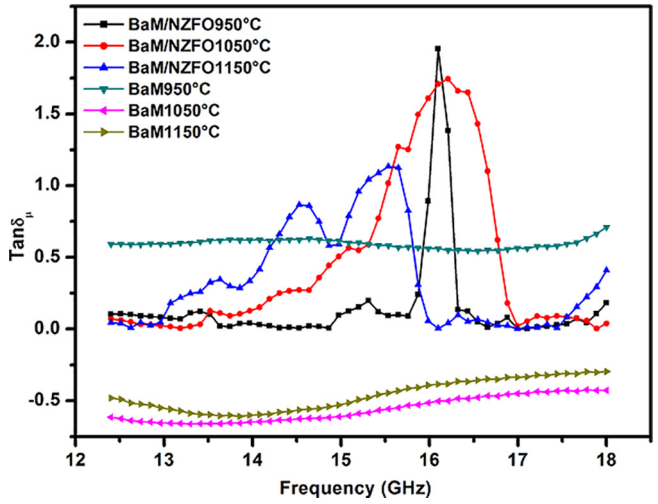


**Fig. 7.** Frequency dependent magnetic losses of BaM and BaM/NZFO nanocomposites annealed at 950 °C, 1050 °C and 1150 °C.

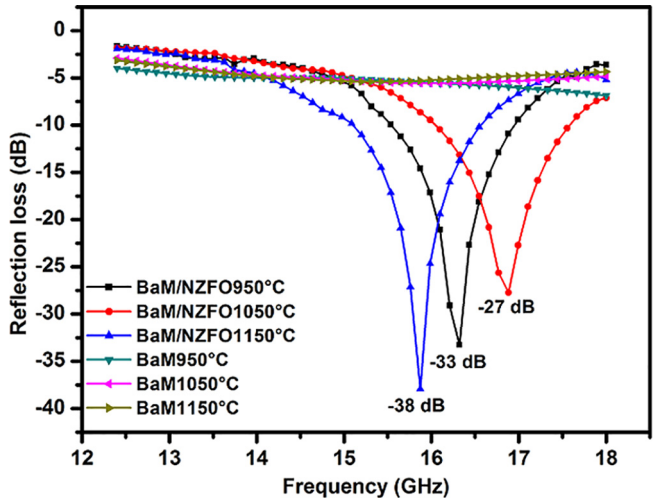


**Fig. 8.** Reflection loss *vs* frequency plots for BaM and BaM/NZFO nanocomposites annealed at 950 °C, 1050 °C and 1150 °C.

system, spin–spin interaction and interfacial dipole may exist and are in phase at a particular applied field, which are responsible for peaks in loss tangent. Also, resonance peaks found to shift towards lower frequency with annealing temperature. The observed variation in tan $\delta_\mu$ may arise due to varied exchange coupling between hard/soft phases.

To evaluate microwave absorption, reflection loss curves were simulated for 2.2 mm thick BaM and BaM/NZFO composites (calcined at 950 °C, 1050 °C and 1150 °C) pellets (sintered at 1200 °C) using following equations:

$$RL = 20 \log \left| \frac{(Z_{in} - Z_0)}{(Z_{in} + Z_0)} \right| \quad (2)$$

$Z_{in}$ is given by

$$Z_{in} = Z_0 \sqrt{\frac{\mu_r}{\varepsilon_r}} \tanh\left\{ j\left(\frac{2\pi f t}{c}\right)\sqrt{\mu_r \varepsilon_r} \right\} \quad (3)$$

where, f is the frequency, t is the thickness of sample, $\varepsilon_r = \varepsilon' - j\varepsilon''$ and $\mu_r = \mu' - j\mu''$ are the complex relative permittivity and permeability of the sample, c is the velocity of the light, $Z_0$ is the impedance of air and $Z_{in}$ is the input impedance at the absorber surface.

Fig. 8 shows the reflection loss *vs* frequency plots for BaM and BaM/NZFO composite sintered at 1200 °C. For BaM, no reflection losses were observed in the studied frequency band (12–18 GHz) irrespective to annealing temperature. The absence of reflection dip may ascribe to higher ferromagnetic resonance frequency of BaM (36–43 GHz) [27,28]. The composites annealed at 950 °C, 1050 °C and 1150 °C showed well defined reflection loss dips at 16.9 GHz, 15.8 GHz and 16.3 GHz respectively. The reflection losses are well above −10 dB (absorption more than 90%) with a maximum value of −38 dB for composite annealed at 1050 °C. It is also evident that the reflection loss frequency depends upon the coupling, since sample with higher exchange coupling (annealed at 1050 °C) shows losses at lower frequency. The results suggest that the extent of exchange coupling depends on annealing temperature and hence affect absorption losses. Compared to BaM, the reflection loss peaks for composites system observed at lower frequencies as a consequence of lower ferromagnetic frequency of NZFO. Such composite could play a dominant role in microwave device application with tunable frequency.

## 4. Conclusion

Exchange coupled $BaFe_{12}O_{19}$(BaM)/$Ni_{0.5}Zn_{0.5}Fe_2O_4$(NZFO) nanocomposite ferrites were prepared by sol–gel auto combustion method followed by annealing. Their structural, magnetic and microwave properties have been investigated. XRD patterns confirmed the co-existence of BaM and NZFO phases. TEM micrographs for composite demonstrated that NZFO particles were coagulated with BaM particles. Magnetic measurement confirmed the existence of exchange coupling between hard and soft phases. The extent of coupling found to vary with annealing temperature. A sharp Curie temperature was observed for exchange coupled composite. Microwave studies in $K_u$–band suggested that the exchange coupling significantly affect microwave absorption losses which can be suitably tuned with annealing temperature for microwave application. In summary, exchange coupled composites with tunable magnetic and microwave property can be used as microwave absorption materials.

## Acknowledgment

The author gratefully acknowledges the financial support provided by CSIR under grant no. 03(1449)/18/EMR-II and SRF 09/677(0032)/2018-EMR-I.

## References

[1] R. Coehoorn, D.B. DE Mooij, C. DE Waard, Meltspun permanent magnet materials containing $Fe_3B$ as the main phase, J. Magn. Magn. Mater. 80 (1989) 101–104.
[2] T. Schrefl, H. Kronmiiller, J. Fidler, Exchange hardening in nano-structured two-phase permanent magnets, J. Magn. Magn. Mater. 127 (1993) L273–L277.
[3] Debangsu Roy, P.S. Anil Kumar, Enhancement of $(BH)_{max}$ in a hard-soft-ferrite nanocomposite using exchange spring mechanism, J. Appl. Phys. 106 (2009) 073902.
[4] D. Suess, T. Schrefl, S. Fähler, M. Kirschner, G. Hrkac, F. Dorfbauer, J. Fidler, Exchange spring media for perpendicular recording, Appl. Phys. Lett. 87 (2005) 012504.
[5] E.F. Kneller, R. Hawig, The exchange spring magnets: a new materials principle for permanent magnets, IEEE Trans. Magn. 27 (4) (1991) 3588–3600.
[6] Y. Choi, J.S. Jiang, J.E. Pearson, S.D. Bader, Origin of recoil hysteresis loops in SmeCo/Fe exchange-spring magnets, Appl. Phys. Lett. 91 (2007) 022502.
[7] Y. Suzuki, R.B. van Dover, Julia M. Phillips, R.J. Felder, Exchange coupling in single-crystalline spinel-structure (Mn, Zn)$F_e2_O4$/$CoF_e2_O4$ bilayers, Phys. Rev. B 53 (1996) 14016–14019.
[8] Hao Zeng, Jing Li, J.P. Liu, Shouheng Sun, Exchange-coupled nanocomposite magnets by nanoparticles self-assembly, Nature 420 (2002) 396–398.
[9] Eric E. Fullerton, J.S. Jiang, S.D. Bader, Hard/soft magnetic heterostructures: model exchange-spring magnets, J. Magn. Magn. Mater. 200 (1999) 392–404.
[10] K.V. Debangsu Roy, P.S. Sreenivasulu, Anil Kumar, Investigation on non exchange spring behaviour and exchange spring behaviour: a first order reversal curve analysis, Appl. Phys. Lett. 103 (2013) 22406.
[11] Joseph E. Davies, Olav Hellwig, Eric E. Fullerton, J.S. Jiang, S.D. Bader, G.T. Zimi, Kai Liu, Anisotropy dependence of irreversible switching in Fe/SmCo and FeNi/FePt exchange spring magnet films, Appl. Phys. Lett. 86 (2005) 262503.
[12] M. Shindo, M. Ishizone, Magnetic properties of exchange-coupled α-Fe/Nd-Fe-B multilayer thin-film magnets, J. Appl. Phys. 81 (8) (1997) 4444–4446.

[13] Xiansong Liu, Wei Zhong, Benxib Gu, Youwei Du, Exchange-coupling interaction in nanocomposites $SrFe_{12}O_{19}/\gamma$-$Fe_2O_3$ permanent ferrites, J. Appl. Phys. 92 (2) (2002) 1028–1032.
[14] Rui Xiong, Weiwei Li, Chunlong Fei, Yong Liu, Jing Shi, Exchange-spring behavior in $BaFe_{12}O_{19}$-$Ni_{0.5}Zn_{0.5}Fe_2O_4$nanocomposites synthesized by a combustion method, Ceram. Int. 42 (10) (2016) 11913–11917.
[15] K.W. Moon, S.G. Cho, Y.H. Choa, K.H. Kim, J. Kim, Synthesis and magnetic properties of nano Ba-hexaferrite/NiZnferrite composites, Phys. Stat. Sol. (a) 204 (2007) 4141–4144.
[16] Miao Liu, Haibo Yang, Ying Lin, Yanyan Yang, Simultaneous enhancements of remanence and $(BH)_{max}$ in $BaFe_{12}O_{19}/CoFe_2O_4$ nanocomposite powders, J. Alloys Compd. 631 (2015) 335–339.
[17] Haibo Yang, Ting Ye, Ying Lin, Miao Liu, Ge Zhang, Pan Kang, Giant enhancement of $(BH)_{max}$ in $BaFe_{12}O_{19}/Y_3Fe_5O_{12}$ nanocomposite powders, Mater. Lett. 145 (2015) 19–22.
[18] Haibo Yang, Ting Ye, Ying Lin, Miao Liu, Preparation and microwave absorption property of graphene/$BaFe_{12}O_{19}/CoFe_2O_4$nanocomposite, Appl. Surf. Sci. 357 (2015) 1289–1293.
[19] Haibo Yang, Ting Ye, Ying Lin, Miao Liu, Excellent microwave absorption property of ternary composite: polyaniline-$BaFe_{12}O_{19}$-$CoFe_2O_4$ powders, J. Alloys Compd. 653 (2015) 135–139.
[20] S. Hazra, M.K. Patra, S.R. Vadera, N.N. Ghosh, A novel but simple “One-Pot Synthetic Route for Preparation of $(NiFe_2O_4)_x$-$(BaFe_{12}O_{19})_{1-x}$ Composites”, J. Am. Ceram. Soc. 95 (2012) 60–63.
[21] Chhavi Pahwa, Santhoshkumar Mahadevan, Sukhleen Bindra, Puneet Sharma, Structural magnetic and microwave properties of exchange coupled and non-exchange coupled $BaFe_{12}O_{19}/NiFe_2O_4$ nanocomposites, J. Alloys Compd. 725 (2017) 1175–1181.
[22] Debangsu Roy, C. Shiva kumara, P.S. Anil Kumar, Observation of the exchange spring behavior in hard–soft-ferrite nanocomposite, J. Magn. Magn. Mater. 321 (2009) L11–L14.
[23] B.D. Cullity, Elements of X–ray Powder Diffraction, Addison-Wesley Publishing Company Inc, USA, 1978.
[24] Rajshree B. Jotania, Reshma A. Nandotaria Chetna, C. Chauhan Mohd. Hashim, Structural phases and Maxwell-Wagner relaxation in magnetically soft-$ZnFe_2O_4$ and hard-$Sr_2Cu_2Fe_{12}O_{22}$ nanocomposites, Ceram. Int. 42 (2) (2016) 2289–2298.
[25] S. Mahadevan, C. Pahwa, S.B. Narang, P. Sharma, Structural, dielectric and magnetic properties of $BaFe_{12}$-$xAlxO_{19}$ hexaferrite thick films, J. Magn. Magn. Mater. 441 (2017) 465–474.
[26] Abdollah Hajalilou, Saiful Amri Mazlan, Kamyar Shameli, A comparative study of different concentrations of pure Zn powder effects on synthesis, structure, magnetic and microwave-absorbing properties in mechanically-alloyed Ni–Zn ferrite, J. Phys. Chem. Solids 96–97 (2016) 49–59.
[27] L.M. Silber, E. Tsantes, P. Angelo, Ferromagnetic resonance in a uniaxial anisotropic ferrite: $BaFe_{12}O_{19}$, J. Appl. Phys. 38 (1967) 5315–5318.
[28] R.C. Pullar, Hexagonal ferrites: a review of the synthesis, properties and applications of hexaferrite ceramics, Prog. Mater. Sci. 57 (2012) 1191–1334.

Journal of Alloys and Compounds 815 (2020) 152391

Contents lists available at ScienceDirect

Journal of Alloys and Compounds

journal homepage: http://www.elsevier.com/locate/jalcom

# Composition dependent magnetic and microwave properties of exchange-coupled hard/soft nanocomposite ferrite

Chhavi Pahwa [a], Sukhleen Bindra Narang [b], Puneet Sharma [a, *]

[a] School of Physics & Materials Science, Thapar Institute of Engineering & Technology, Patiala, 147004, India
[b] Department of Electronics Technology, Guru Nanak Dev University, Amritsar, India

ARTICLE INFO

*Article history:*
Received 22 July 2019
Received in revised form
19 September 2019
Accepted 20 September 2019
Available online 21 September 2019

*Keywords:*
Barium hexaferrite
Nickel–zinc ferrite
Exchange-coupled composites
Magnetic properties
Microwave properties

ABSTRACT

In the present work, exchange-coupled $BaFe_{12}O_{19}$ (BaM)/$Ni_{0.5}Zn_{0.5}Fe_2O_4$ (NZFO) nanocomposites with different weight ratio were prepared by sol-gel autocombustion method. The effect of relative weight fraction on structural, morphological, magnetic and microwave properties were investigated. X-ray diffraction patterns of composites confirmed the co-existence of BaM and NZFO phases without any secondary phase. Smooth hysteresis loops without kink confirmed that BaM/NZFO phases were well exchange-coupled. Non linear change in magnetization ($M_s$) and coercivity ($H_c$) with NZFO content were observed. The drastic increase in $M_s$ with corresponding sharp decrease in $H_c$ for 70/30 wt ratio was observed. The change in $M_s$ and $H_c$ was explained with the schematic model of interfacial spin interactions. Complex permeability and permittivity in $K_u$-band showed oscillatory behaviour for higher weight fraction of NZFO. Reflection loss frequency found to depends on NZFO content and maximum loss (−41 dB) was observed for 70/30 wt ratio at 13.8 GHz frequency.



## 1. Introduction

Exchange-coupled hard/soft magnetic nanocomposite has gained attention in permanent magnet and microwave device application due to large compositional flexibility and wide variation in magnetic properties [1–5]. In early 1990s, Kneller and Hawing proposed the concept of exchange-coupled composite system consisted of two mutually exchange coupled phases [6]. The studies on such system were focused on hard/soft magnetic bilayer thin films and oxide based nanopowders [7,8]. The coupling between hard/soft phases is primarily interfacial in nature and greatly affected by processing methods [9,10]. A well exchange-coupled composite shows smooth demagnetization behaviour with coherent rotation of spins, while non-coupled system shows a stepped hysteresis curve due to individual switching of hard-soft spins [11–13]. Interfacial coupling has been largely investigated for alloy based composite magnets, thin films and nanopowders i.e. SmCo/Co, SmCo/Fe, Fe/Nd-Fe-B, and FeNi/FePt etc. [14,15]. The existing coupling were strongly depends on film thickness, and powder/grain size which vanishes beyond a critical size [16,17]. A well exchange-coupled nanocomposite permanent magnets showed higher energy product in many systems [1,5]. Later, exchange coupling in ferrite based bilayer system and nanocomposite powders such as (Mn, Zn) $Fe_2O_4/CoFe_2O_4$, $SrFe_{12}O_{19}/\gamma Fe_2O_3$, $SrFe_{12}O_{19}/NiFe_2O_4$ etc. were also investigated [18–20]. Comparing with alloy based composite magnets; the exchange-coupled ferrites are also used for microwave devices operable in wide frequency range.

Hard ferrite such as $BaFe_{12}O_{19}$ can be operable upto W- band due to its high magneto-crystalline anisotropy and high ferromagnetic resonance frequency (~35 GHz) [21]. On contrary, low anisotropic soft spinel ferrite limits their microwave application upto 1 GHz [22]. Therefore, combination of high anisotropic hard ferrite and low anisotropic soft ferrite can be an alternate for various microwave device applications. The studies on exchange-coupled nanocomposite ferrites for microwave absorbers were already reported [23,24]. Apart from the microwave application; the magneto-dielectric nature with high permittivity ($\varepsilon_r$) and permeability ($\mu_r$) of exchange-coupled composite ferrites could replace dielectric only substrates for antenna miniaturization. The dielectric studies on such composites were studied at low frequencies (upto 1 GHz) [25,26]. However, the magneto-dielectric behavior of such composites on high frequencies (12–18 GHz) is scarcely investigated.

* Corresponding author.
*E-mail address:* puneet.sharma@thapar.edu (P. Sharma).

https://doi.org/10.1016/j.jallcom.2019.152391
0925-8388/

In the present work, exchange-coupled nanocomposite ferrites of $BaFe_{12}O_{19}$ (BaM)/$Ni_{0.5}Zn_{0.5}Fe_2O_4$ (NZFO) with varying composition were prepared by sol-gel autocombustion method. The effect of BaM/NZFO weight ratio on magnetic and microwave properties was systematically investigated.

## 2. Experimental details

Exchange-coupled nanocomposite ferrites of $BaFe_{12}O_{19}$ (BaM)/$Ni_{0.5}Zn_{0.5}Fe_2O_4$ (NZFO) with different weight ratio (90/10, 80/20, 70/30, 60/40, and 50/50) were prepared by sol-gel auto combustion method. Stoichiometric amount of analytical grade metal nitrates; $Fe(NO_3)_3\cdot 9H_2O$, $Ba(NO_3)_2$, $Zn(NO_3)_2\cdot 6H_2O$, $Ni(NO_3)_2\cdot 6H_2O$ and citric acid ($C_6H_8O_7$) of 99.9% purity were used as precursors. The detailed description of powder processing is described earlier [27]. The obtained powders were calcined at 1050 °C for 3 h in the resistance furnace. The calcined powders were further pressed into pellets (21 mm × 11 mm) and sintered at 1200 °C for 1 h in ambient atmosphere.

The phase analysis of BaM, NZFO and BaM/NZFO composites were carried out by X-ray diffraction (XRD) (PANalytical), using Cu-$K_{\alpha 1}$ radiation. Microstructures of sintered pellets were examined by scanning electron microscope (SEM) model JEOL (JSM-IT100). Magnetic hysteresis (*M-H*) loops were measured by vibrating sample magnetometer (VSM) using Lake Shore model 7404 with maximum applied field of 1 T. The permeability (μ), permittivity (ε) and reflection losses (RL) in $K_u$-band were measured by vector network analyzer (Agilent N5225A PNA series).

## 3. Results and discussion

### 3.1. XRD analysis

XRD patterns of BaM, NZFO and BaM/NZFO composite powders in the weight ratio of 70/30 and 50/50 are shown in Fig. 1(a–d). All diffraction peaks of BaM and NZFO corresponds to hexagonal BaM (space group $P6_3/mmc$) and cubic NZFO (space group Fd3m) phase. Representative XRD patterns of BaM/NZFO nanocomposites confirmed the co-existence of both the phases. No intermediate phase was formed during calcination and sintering of composites. The NZFO peak intensity found to increase with its content. The average crystallite size was calculated by Debye Scherrer equation [28]. All individual peaks of BaM and NZFO were considered for crystallite size calculations. Table 1 shows the average crystallite size calculated for different composition. It is clear that the crystallite size is independent to the relative weight ratio. Since the annealing temperature is constant (1050 °C), therefore no obvious changes in crystallite size were on expected lines.

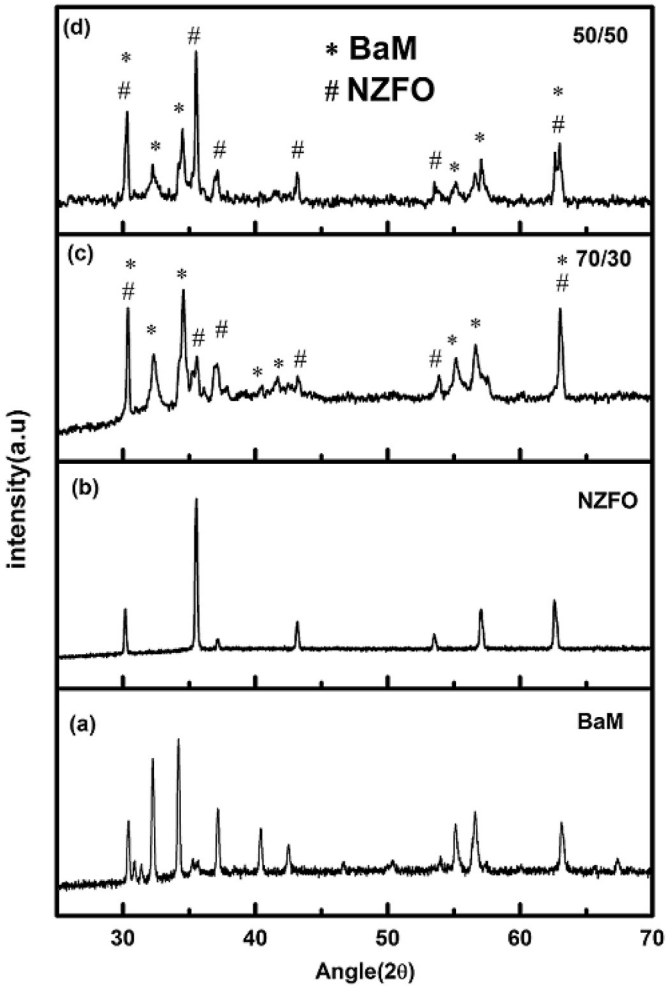


**Fig. 1.** X-ray diffraction patterns of (a) BaM, (b) NZFO, (c) 70/30, (d) 50/50 nanocomposite powders.

**Table 1**
Crystallite size of BaM and NZFO in the composite samples.

| Composition (BaM/NZFO) | Crystallite Size (nm) | |
|---|---|---|
| | NZFO | BaM |
| 100/0 | – | 37.4 |
| 70/30 | 37.6 | 38.5 |
| 50/50 | 39.5 | 38.6 |
| 0/100 | 38.0 | – |

### 3.2. Microstructure analysis

Fig. 2(a–c) shows the fractured surface micrographs of BaM, NZFO and BaM/NZFO (70/30) composite sintered at 1200 °C. Randomly oriented elongated grains were observed in BaM whereas; NZFO grains posses equiaxed morphology. In BaM/NZFO composite; well distinguished hexagonal BaM platelets along with small NZFO grains were observed. The corresponding EDS spectrum (Fig. 2(d)) confirms the presence of all elements (Ba, O, Fe, Ni and Zn) in the composite.

### 3.3. Magnetic measurements

Fig. 3(a and b) shows magnetization curves (*M-H* loop) of BaM, NZFO and their -nanocomposite (90/10, 80/20, 70/30, 60/40, 50/50) powders respectively. The *M-H* loops of BaM and NZFO (Fig. 3(a)) confirmed the hard and soft magnetic nature respectively. Smooth demagnetization curve without any kink (Fig. 3(b)) suggests that hard/soft phases are well exchange coupled in composites. It is also well reported that the smooth demagnetization of exchange-coupled composite is a consequence of coherent rotation of hard and soft spins with applied magnetic field. Composite of BaM and NZFO was also prepared by physical mixing method where a kink in demagnetization behavior was observed inset Fig. 3(b). The signature kink is a characteristic feature depicting individual switching of hard and soft magnetic spins. Such systems are termed as non-exchange system [12]. We have also observed similar kind of behavior in our previously reported studies [29].

To confirm exchange-coupling between hard and soft phases, switching field distribution (SFD) i.e. d*M*/d*H* *vs* applied field were

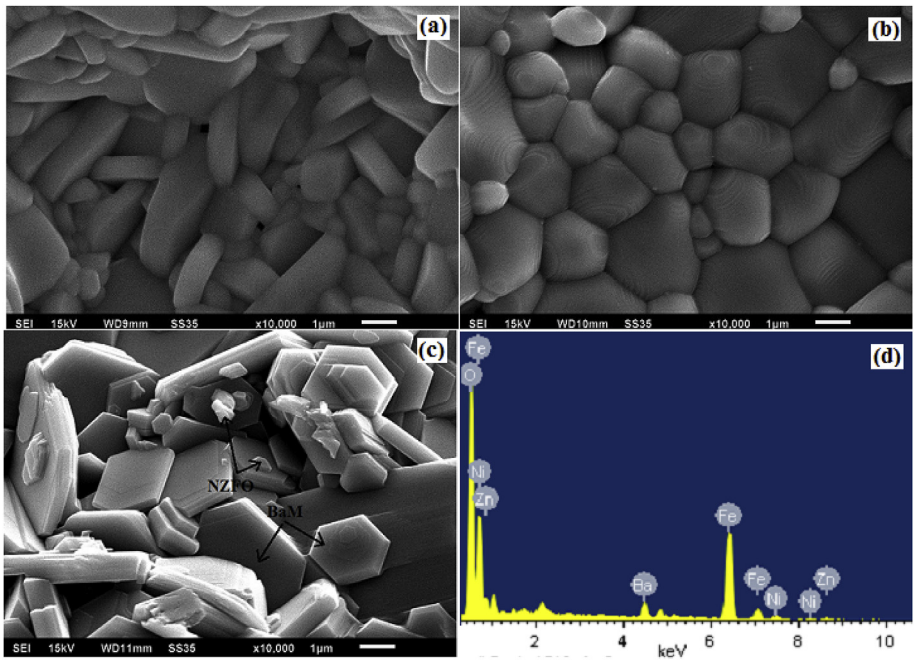


**Fig. 2.** SEM micrographs of (a) BaM, (b) NZFO, (c) BaM/NZFO (70/30), and (d) EDS of sintered composite.

plotted (Fig. 4). Single peak in d$M$/d$H$ for nanocomposites indicates the strong exchange-coupling between hard and soft phases. The SFD of non-exchange coupled composite shows two distinct peaks, which corresponds to individual switching of hard and soft magnetic spins (inset Fig. 4).

The measured magnetization ($M_s$) and coercivity ($H_c$) of BaM, NZFO and their respective composites are shown in Table 2. The $M_s$ and $H_c$ of composites lies between their constituents magnetic properties.

Fig. 5(a and b) shows the variation in measured and theoretical calculated $M_s$ and $H_c$ of composites with NZFO content. The theoretical $M_s$ and $H_c$ were calculated using Eq. (1) [30].

$$X = (1 - x)\, X_{BaM} + xX_{NZFO} \quad (1)$$

where, $X_{BaM}$ and $X_{NZFO}$ are experimentally measured $M_s$/$H_c$ of BaM and NZFO respectively and x is the weight fraction of NZFO.

The $M_s$ of nanocomposites drastically increased from 53.63 emu/g (x = 10) to 64.44 emu/g (x = 30). Further, $M_s$ found to be nearly constant for higher NZFO content (Fig. 5(a)). Contrary to $M_s$ behavior, sharp decrease in $H_c$ was observed for x = 30 (Fig. 5 (b)) followed by marginal decrease. It is to be noted that, the change in $M_s$ and $H_c$ is nonlinear and vastly deviates from theoretical calculated values. This anomalous behaviour suggest that spin interactions between hard-soft phases were maximum for certain composition (x = 30). Reportedly, any change in $M_s$ and $H_c$ of the composite is a consequence of three types of spin interactions i.e. between soft-soft phase, hard-hard phase and hard-soft phases [31]. In the present case, enhancement in magnetization was dominated by interfacial spin interaction of soft and hard phase.

To understand the anomalous increase in $M_s$, the spin alignment behaviour of BaM in exchange-coupled composites with different NZFO content was compared. The schematic (Fig. 6) represents interfacial surface spins of composites with and without magnetic field. In the absence of field, both hard and soft magnetic spins are randomly oriented. At H = 10 KOe, it is shown that the fraction of aligned spins in BaM are increasing with NZFO content.

Schematic represents that in pure BaM; major fraction of spins is aligned in the field direction. The remaining spins are not able to align (hindered spins) due to grain boundary hindrance to spin alignment in polycrystalline materials. Such hindered spins may require larger field or an additional driving force to align. With addition of NZFO, the interfacial spin interactions between hard-soft phases occurs, which increases with its content. Owing to soft magnetic nature of NZFO, spins get swiftly align at much lower magnetic field and provide a torque to hard hindered spins. As a result, higher fraction of spin alignment increases the magnetization (53.6 emu/g to 64.5 emu/g). In schematic, it is also depicted that interfacial interactions are optimal for 70/30 wt ratio where all possible spins of BaM are aligned. As a consequence of optimum spins orientation causes an abrupt increase in magnetization. However, further increase in NZFO content $M_s$ remains nearly same, which suggests that hard-soft interfacial interactions reached to its saturation. The torque due to soft magnetic spins and coherent demagnetization caused a corresponding sharp decrease in $H_c$ of composites (Fig. 5(b)).

### 3.4. Microwave studies

Fig. 7(a–d) shows the real and imaginary parts of complex permittivity and permeability of BaM, NZFO and BaM/NZFO composites in $K_u$-band (12.4–18 GHz). The real part (ε' and μ') shows the storage capacity and imaginary part (ε" and μ") represents the loss of electric and magnetic energy respectively. It is clear that ε' and μ' found to increase initially with the NZFO content and then decreases. For higher NZFO content large fluctuations were observed. The similar variation was also observed for ε" and μ". To understand the effective loss mechanism in the composite; complex permittivity (ε = ε'- jε") and permeability (μ = μ'- jμ") of BaM, NZFO and BaM/NZFO composites were plotted as shown in Fig. 8(a and b).

It is clear that ε and μ remains constant for BaM, NZFO and 90/10, 80/20 & 70/30 composites. However, oscillatory behaviour of ε and μ were observed for higher weight ratio of NZFO as in real and

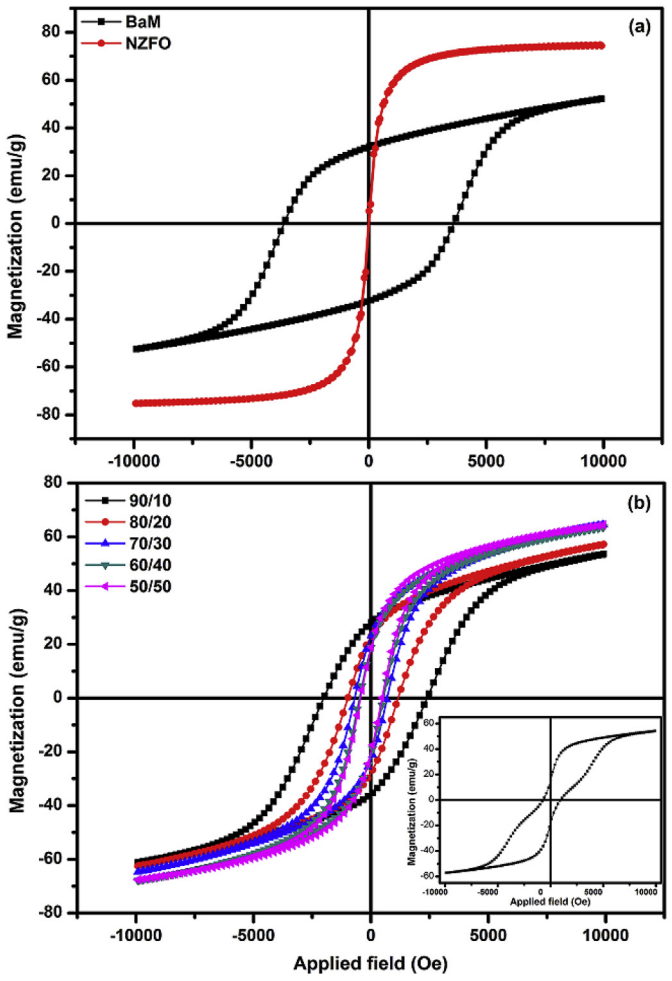


**Fig. 3.** Comparative *M-H* loops of (a) BaM & NZFO and (b) BaM/NZFO nanocomposite with different weight ratio and inset represent *M-H* loop of non exchange-coupled system.

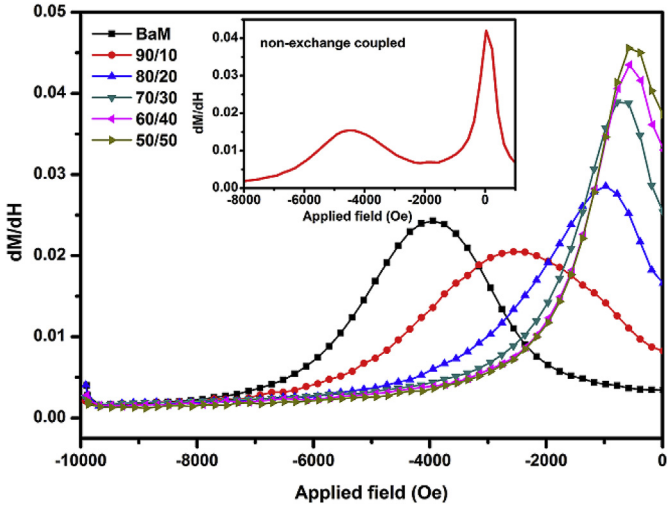


**Fig. 4.** d*M*/d*H* *vs* applied field curves of BaM and BaM/NZFO nanocomposites.

**Table 2**
Magnetic properties of BaM, NZFO and BaM/NZFO nanocomposites.

| Magnetic properties | BaM/NZFO weight ratio | | | | | | |
|---|---|---|---|---|---|---|---|
| | BaM | 90/10 | 80/20 | 70/30 | 60/40 | 50/50 | NZFO |
| $M_s$ (emu/g) | 52.14 | 53.63 | 57.21 | 64.44 | 63.62 | 64.31 | 74.40 |
| $H_c$ (Oe) | 3615.38 | 2204.9 | 1079 | 691.18 | 522.3 | 481.6 | 22.5 |
| $M_r$ (emu/g) | 32.16 | 27.97 | 22.79 | 22.81 | 17.98 | 18.39 | 3.3 |

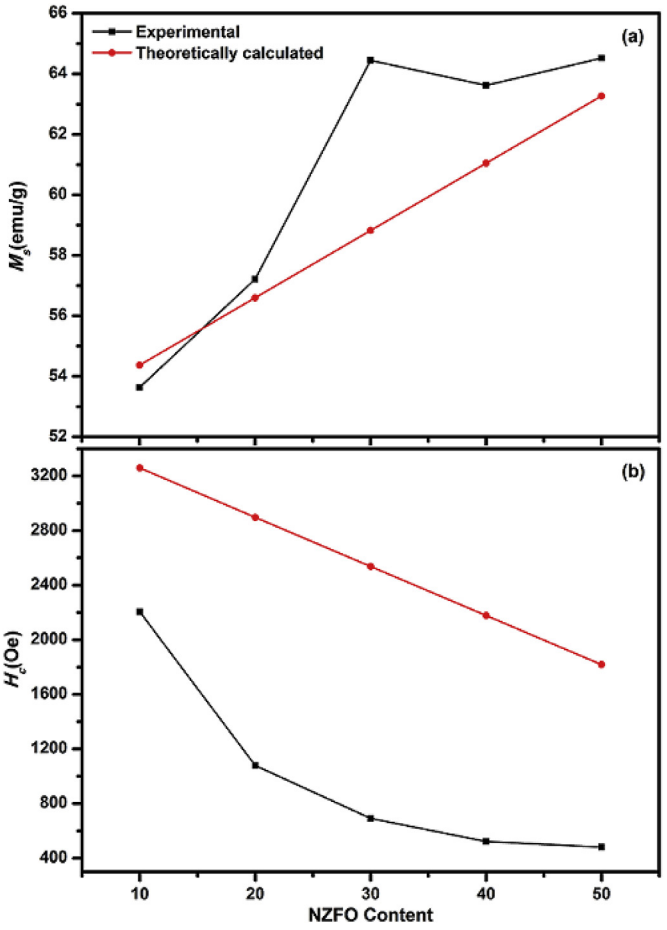


**Fig. 5.** Variation in theoretical and experimentally observed (a) $M_s$, and (b) $H_c$ of BaM/NZFO composite with NZFO content.

imaginary part. The large variations in ε between 13 and 16 GHz frequency range may ascribe to the resonance of interfacial dipolar interaction with applied field frequency (14.8 GHz and 15.4 GHz). For low NZFO content, the μ found to be nearly constant. This may due to the overlapping of precession motion of different magnetization vector. However, fluctuation in μ may correspond to individual precession of the magnetic vectors of hard and soft phases, which dominates for higher NZFO content.

The variation in ε and μ with the NZFO content at 12.5 GHz frequency is shown in Fig. 9. Both ε and μ found to increase initially with the NZFO content. The initial increase in ε of the composite is due to the hindrance to charge motion caused by NZFO particles. Also, capacitive action caused by low resistive NZFO phase separated by high resistive BaM; results in higher ε. At higher NZFO content, low resistive continuous channels forms that facilitate charge conduction with a subsequent decrease in ε.

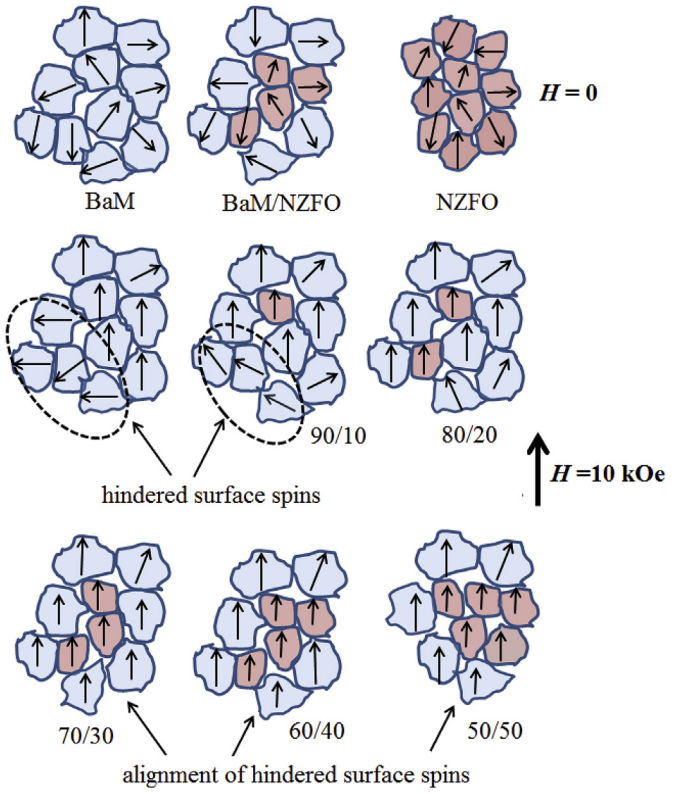


**Fig. 6.** Schematic representation of surface spins interactions of exchange-coupled BaM/NZFO composites.

The measured permeability of NZFO and BaM at 12.5 GHz are 0.6 and 1.5 respectively which are in agreement with the previously reported data [10,32]. The maximum value of μ is observed for 70/30 wt ratio. Strong exchange-coupling between high and low permeable phases might be the reason for high μ of composite.

Reflection losses of BaM, NZFO and BaM/NZFO composites were calculated using following equations:

$$RL = 20 \log \left| \frac{(Z_{in} - Z_0)}{(Z_{in} + Z_0)} \right| \quad (2)$$

$Z_{in}$ is given by

$$Z_{in} = Z_0 \sqrt{\frac{\varepsilon}{\mu}} \tanh \left\{ j \left( \frac{2\pi f t}{c} \right) \sqrt{\mu\varepsilon} \right\} \quad (3)$$

where, f is the applied frequency, t is thickness of specimen, c is velocity of the light, $Z_0$ is the impedance of air and $Z_{in}$ is the input impedance at the absorber surface.

Fig. 10 shows the reflection loss plots for BaM/NZFO composites and compared with individual BaM and NZFO phases. For BaM, reflection loss of −27 dB was observed at 13 GHz, whereas no losses were seen for NZFO due to its low ferromagnetic resonance frequency (FMR) [22]. In the composite, reflection losses were observed at higher frequencies. The maximum reflection loss of -41 dB (absorption > 99%) was obtained for 70/30 wt ratio. The results suggest that reflection losses and their loss frequency strongly depend upon the exchange coupling. Such composites could play a dominant role in tunable microwave device application.

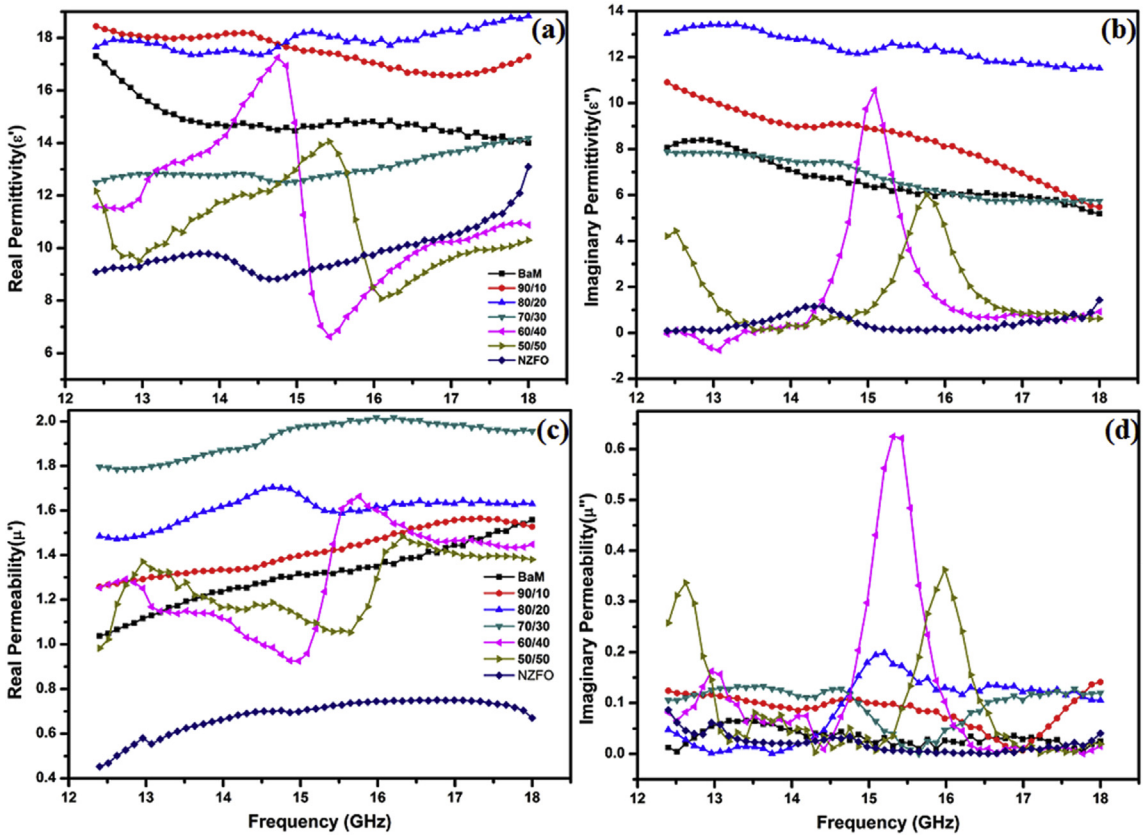


**Fig. 7.** (a) Real (ε'), imaginary (ε") part of complex permittivity and (c) real (μ'), (d) imaginary (μ") part of complex permeability of BaM, NZFO & BaM/NZFO composite.

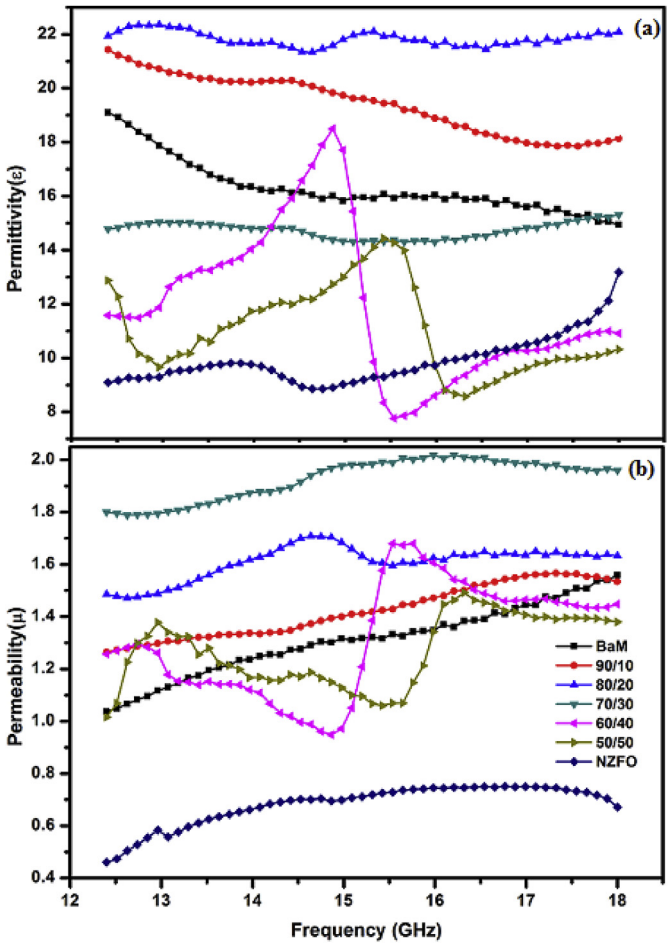


**Fig. 8.** Frequency dependent (a) Complex permittivity (ε) & (b) Complex permeability (μ) of BaM, NZFO & BaM/NZFO composite.

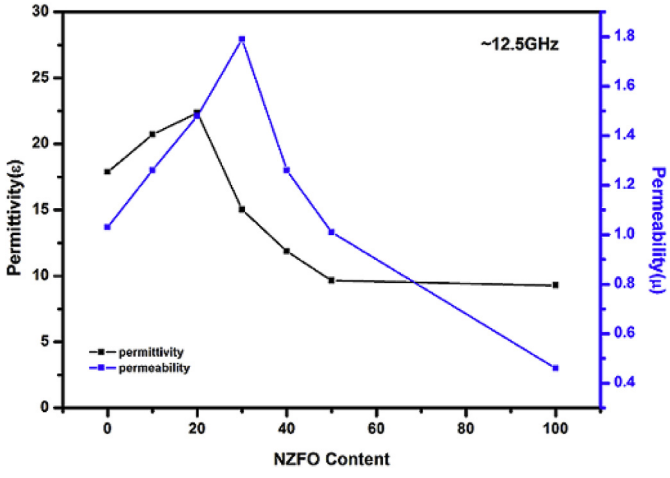


**Fig. 9.** Permittivity (ε) and permeability (μ) of the composite with NZFO content.

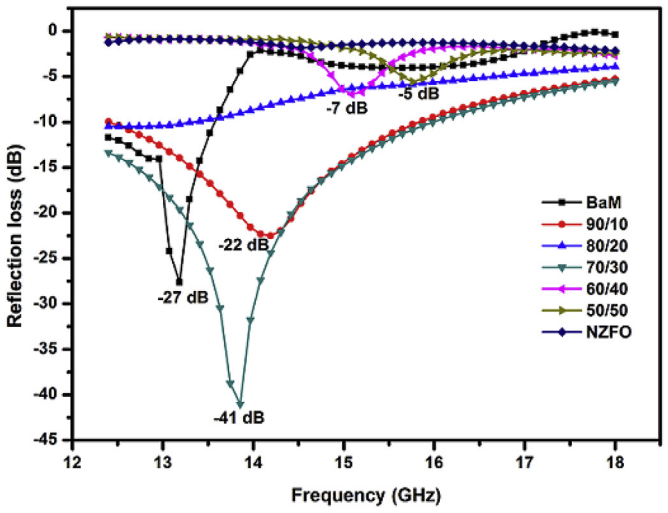


**Fig. 10.** Reflection loss *vs* frequency plots for BaM, NZFO and BaM/NZFO nanocomposites for different NZFO content.

## 4. Conclusion

Exchange-coupled nanocomposites of $BaFe_{12}O_{19}$ (BaM)/$Ni_{0.5}Zn_{0.5}Fe_2O_4$ (NZFO) in different weight ratio were prepared by sol-gel autocombustion method. Their structural, morphological, magnetic and microwave properties has been investigated. Co-existence of BaM and NZFO phases in composites was confirmed by XRD patterns. Coherent demagnetization curve for all studied composition demonstrated that BaM and NZFO phases were well exchange coupled. Magnetization ($M_s$) found to increase with NZFO content. Maximum $M_s$ was obtained for 70/30 nanocomposite. On contrary, coercivity ($H_c$) of the composites found to decrease. Large variation in complex permeability and permittivity were observed for composites with high NZFO content. Reflection losses found to vary with NZFO content and maximum (−41 dB) was observed for 70/30 wt ratio. In conclusion magnetic and microwave property strongly depends upon interfacial exchange coupling and such composites can be used for tunable microwave application.

## Acknowledgment

The author gratefully acknowledge the financial supports provided by CSIR under grant no. 03(1449)/18/EMR-II and SRF 09/677(0032)/2018-EMR-I.

## References

[1] Debangsu Roy, P.S. Anil Kumar, Enhancement of $(BH)_{max}$ in a hard-soft-ferrite nanocomposite using exchange spring mechanism, J. Appl. Phys. 106 (2009), 073902.
[2] Miao Liu, Haibo Yang, Ying Lin, Yanyan Yang, Simultaneous enhancements of remanence and $(BH)_{max}$ in $BaFe_{12}O_{19}/CoFe_2O_4$ nanocomposite powders, J. Alloy. Comp. 631 (2015) 335–339.
[3] Vamsi M. Chakka, Z.S. Shan, J.P. Liu, Effect of coupling strength on magnetic properties of exchange spring magnets, J. Appl. Phys. 94 (10) (2003), 073902.
[4] Haibo Yang, Ting Ye, Ying Lin, Miao Liu, Ge Zhang, Pan Kang, Giant enhancement of $(BH)_{max}$ in $BaFe_{12}O_{19}/Y_3Fe_5O_{12}$ nanocomposite powders, Mater. Lett. 145 (2015) 19–22.
[5] D. Suess, T. Schrefl, S. Fähler, M. Kirschner, G. Hrkac, F. Dorfbauer, J. Fidler, Exchange spring media for perpendicular recording, Appl. Phys. Lett. 87 (2005), 012504.
[6] E.F. Kneller, R. Hawig, The exchange spring magnets: a new materials principle for permanent magnets, IEEE Trans. Magn. 27 (4) (1991) 3588–3600.

[7] J.S. Jiang, J.E. Pearson, Z.Y. Liu, B. Kabius, S. Trasobares, D.J. Miller, S.D. Bader, A new approach for improving exchange-spring magnets, J. Appl. Phys. 97 (2005) 10K311.
[8] Debangsu Roy, C. Shiva kumara, P.S. Anil Kumar, Observation of the exchange spring behavior in hard–soft-ferrite nanocomposite, J. Magn. Magn. Mater. 321 (2009) L11–L14.
[9] T. Schrefl, H. Kronmiiller, J. Fidler, Exchange hardening in nano-structured two-phase permanent magnets, J. Magn. Magn. Mater. 127 (1993) L273–L277.
[10] Subhenjit Hazra, Barun Kumar Ghosha, Manoj Kumar Patrab, Raj Kumar Janib, Sampat Raj Vaderab, Narendra Nath Ghosha, A novel 'One-Pot' synthetic method for preparation of $(Ni_{0.65}Zn_{0.35}Fe_2O_4)_x$- $(BaFe_{12}O_{19})_{1-x}$ nanocomposites and study of their microwave absorption and magnetic properties, Powder Technol. 279 (2015) 10–17.
[11] Rui Xiong, Weiwei Li, Chunlong Fei, Yong Liu, Jing Shi, Exchange-spring behavior in $BaFe_{12}O_{19}$-$Ni_{0.5}Zn_{0.5}Fe_2O_4$ nanocomposites synthesized by a combustion method, Ceram. Int. 42 (10) (2016) 11913–11917.
[12] Debangsu Roy, K.V. Sreenivasulu, P.S. Anil Kumar, Investigation on non exchange spring behaviour and exchange spring behaviour: a first order reversal curve analysis, Appl. Phys. Lett. 103 (2013) 22406.
[13] Yan Wang, Ying Huang, Qiufen Wang, Preparation and magnetic properties of $BaFe_{12}O_{19}/Ni_{0.8}Zn_{0.2}Fe_2O_4$ nanocomposite ferrite, J. Magn. Magn. Mater. 324 (2012) 3024–3028.
[14] Joseph E. Davies, Olav Hellwig, Eric E. Fullerton, J.S. Jiang, S.D. Bader, G.T. Zimi, Kai Liu, Anisotropy dependence of irreversible switching in Fe/SmCo and FeNi/FePt exchange spring magnet films, Appl. Phys. Lett. 86 (2005) 262503.
[15] M. Shindo, M. Ishizone, Magnetic Properties of exchange-coupled α-Fe/Nd-Fe-B multilayer thin-film magnets, J. Appl. Phys. 81 (8) (1997) 4444–4446.
[16] Hao Zeng, Jing Li, J.P. Liu, Shouheng Sun, Exchange-coupled nanocomposite magnets by nanoparticles self-assembly, Nature 420 (2002) 396–398.
[17] Eric E. Fullerton, J.S. Jiang, S.D. Bader, Hard/soft magnetic heterostructures: model exchange-spring magnets, J. Magn. Magn. Mater. 200 (1999) 392–404.
[18] Y. Suzuki, R.B. van Dover, Julia M. Phillips, R.J. Felder, Exchange coupling in single-crystalline spinel-structure $(Mn,Zn)Fe_2O_4/CoFe_2O_4$ bilayers, Phys. Rev. B 53 (1996) 14016–14019.
[19] Xiansong Liu, Wei Zhong, Benxi Gu, Youwei Du, Exchange-coupling interaction in nanocomposites $SrFe_{12}O_{19}/\gamma$-$Fe_2O_3$ permanent ferrites, J. Appl. Phys. 92 (2) (2002) 1028–1032.
[20] Sachin Tayagi, Himanshu B. Baskey, Ramesh Chandra Agarwala, Vijaya Agarwala, Development of hard/soft ferrite nanocomposite for enhanced microwave absorption, Ceram. Int. 37 (2011) 2631–2641.
[21] V.G. Harris, Modern microwave ferrites, IEEE Trans. Magn. 48 (2012) 31075–31104.
[22] M. Pardavi-Horvath, Microwave applications of soft ferrites, J. Magn. Magn. Mater. 215 (2000) 171–183.
[23] M. Mehdipour, H. Sholrollahi, Comparison of microwave absorption properties of $SrFe_{12}O_{19}$, $SrFe_{12}O_{19}/NiFe_2O_4$ and $NiFe_2O_4$ particles, J. Appl. Phys. 113 (2013), 043906.
[24] Andrzej Hilczer, Katarzyna Kowalska, Ewa Markiewicz, Pietraszko Adam, Dielectric and magnetic response of $SrFe_{12}O_{19}$-$CoFe_2O_4$ composites obtained by solid state reaction, Mater. Sci. Eng., B 207 (2016) 47–55.
[25] Ashish Saini, Atul Thakur, Preeti Thakur, Effective permeability and miniaturization estimation of ferrite-loaded microstrip patch antenna, J. Electron. Mater. 45 (8) (2016) 4162–4170.
[26] Ashish Saini, Kush Rana, Atul Thakur, Preeti Thakur, Jean Luc, Mattei Patrick, P. Queffelec, Low loss Composite nano ferrite with matching permittivity and permeability in UHF band Materials, Res. Bull. 76 (2016) 94–99.
[27] Chhavi Pahwa, Sukhleen Bindra Narang, Puneet Sharma, Interfacial exchange coupling driven magnetic and microwave properties of $BaFe_{12}O_{19}/Ni_{0.5}Zn_{0.5}$-$Fe_2O_4$ nanocomposites, J. Magn. Magn. Mater. 484 (2019) 61–66.
[28] B.D. Cullity, Elements of X–Ray Powder Diffraction, Addison-Wesley Publishing Company Inc, USA, 1978.
[29] Chhavi Pahwa, Santhoshkumar Mahadevan, Sukhleen Bindra, Puneet Sharma, Structural magnetic and microwave properties of exchange coupled and non-exchange coupled $BaFe_{12}O_{19}/NiFe_2O_4$ nanocomposites, J. Alloy. Comp. 725 (2017) 1175, 117118.1.
[30] M. Li, M.G. Zhu, X. Li Ralph Skomski, J.M.D. Coey, Gaint energy product in nanostructured two phase magnets, Phys. Rev. B 48 (1993) 15812–15816.
[31] R.W. Gao, W.C. Feng, H. Q, B. Wang, W. Chen, G.B. Han, P. Zhang, H. Li, W. Li, Y.Q. Guo, W. Pan, X. Li, Exchange-coupling interaction, effective anisotropy and coercivity in nanocomposite permanent materials, J. Appl. Phys. 94 (2003) 664–668.
[32] Nan-Nan Jiang, Yang Yang, YU-Xiang Zhang, Jian-Ping Zhou, Chao-Yong Deng, Influence of zinc concentration on structure, complex permittivity and permeability of Ni-Zn ferrite at high frequency, J. Magn. Magn. Mater. 401 (2016) 370–377.

Gmail **Chhavi Pahwa <chhavipahwa09@gmail.com>**

# Transmag: Revision Submitted - TMAG-20-02-0120.R2

**IEEE Transactions on Magnetics** <onbehalfof@manuscriptcentral.com> Mon, Oct 5, 2020 at 6:05 PM
Reply-To: transmag@ieee.org
To: puneet.sharma@thapar.edu
Cc: chhavipahwa09@gmail.com, santhosh.kumar@thapar.edu, sukhleen2@yahoo.com, puneet.sharma@thapar.edu

Dear Dr.Sharma:

This note is to let you know that IEEE Transactions on Magnetics acknowledges receipt of the following revised manuscript, of which you are listed as an author:

Title: Studies on exchange-coupled magnetodielectric ceramics for microwave application in Ku-band
ID: TMAG-20-02-0120.R2

It is understood that this manuscript is entirely original; that is has not been copyrighted, published, submitted or accepted for publication elsewhere; and that you have obtained all necessary clearances and releases. If any of that is not the case, please inform us immediately.

Since the paper is at the revision stage, if you have questions about it please get in touch directly with the editor who issued the decision on the earlier version. If you did not keep his e-mail, there is a copy in your Author Center, under "Manuscripts with Decisions". In any emails about your manuscript, please refer to it by the ID number above.

Sincerely,
Editorial Office
transmag@ieee.org